MICROEARTHQUAKE AND BACKGROUND SEISMIC NOISE STUDIES OF MOUNT ETNA, SICILY

Thesis

submitted by

MOHAMMED MUNIRUZZAMAN, B.Sc., M.Sc., D.I.C.

for the

Degree of Doctor of Philosophy

of the

University of London

Department of Geophysics

Imperial College of Science and Technology

London SW7

December 1977

"If the facts are correctly observed there must be some means of explaining and co-ordinating them ....." .

Bullard, 1965

to my

Mother

ABSTRACT

Mount Etna is a very complex volcano, famous for its persistent eruptions through the ages. However, very little is known about the mechanism of these eruptions. In an attempt to improve the situation, two microearthquake and background seismic noise surveys were carried out in the late summer of 1974 and the early summer of 1975, respectively.

The 1974 survey was conducted with a high-gain, high-sensitivity, seismograph. During the 30-day sampling period, an average of about seven microearthquakes were recorded per day. Study of the signatures of these events revealed three broad groupings, the first having an impulsive P arrival and a distinguishable P-S phase, and the second and third having impulsive and emersion arrivals respectively, and no distinguishable P and S phases. The cumulative frequency versus magnitude relationship for the first group produced a b-value (recurrence curve slope) of 0.99 . This agrees well with the only other value available for the area, 1.01. The b-value for the second and third groups combined was found to be 1.78. No other value is available for comparison. The first group is thought to be of the class known as volcano-tectonic microearthquakes, and to be tectonic in origin, resulting from the re-distribution of stress due to the movement of magma, and the second and third to be volcanic microearthquakes resulting from the activity of the volcano itself.

Four high-gain portable seismographs were operated during the 1975 survey, and recorded an average of about two events per day. As the recorded microearthquakes were small (with estimated magnitudes ranging between 0 and 1.5), hypocentres could be located for only two tectonic and one volcanic microearthquake. The results are consistent with the tectonic event being deep-seated, at an estimated depth of not more than 20 km, and the volcanic event shallow and

probably arising from the summit area.

No conclusion could be reached regarding magmatic reservoirs beneath Etna, due mainly to the paucity of recorded microearthquakes.

Spatial and temporal analysis of the background seismic noise revealed a dominant frequency range of between about 1.2 and 2.9 Hz, with very little variation in the recorded amplitudes. The source of the disturbance was located between the Northeast Crater and a point about 3 km NW of the Central Crater. Using the constraints of the present seismic survey, a possible mechanism of tremor, based on elementary thermodynamic considerations, is examined.

Spectra of the tectonic microearthquakes appear to be spikey, with important peaks up to about 10 Hz. Volcanic microearthquakes, on the other hand, have smoother spectra, with dominant peaks between 1 and 5 Hz. It is, however, difficult to distinguish between these types of microearthquakes on their frequency contents alone.

CONTENTS

ABSTRACT 3

CONTENTS 5

ACKNOWLEDGEMENTS 9

CHAPTER I INTRODUCTION

1.1 Introduction 11
1.2 Method of Investigation 13
1.3 Scope of Thesis 17

CHAPTER II BACKGROUND INFORMATION ON MOUNT ETNA

2.1 Introduction 19
2.2 Geological Features of Sicily 24
2.3 Geological Setting of Mount Etna 28
2.3.1 Tectonic Control of Mount Etna 31
2.4 A Brief Tectonic History 33

CHAPTER III SEISMIC INVESTIGATIONS OF MOUNT ETNA DURING AUG. - SEPT. 1974

3.1 Introduction 39
3.2 The Seismic Equipment 42
3.2.1 The Smoked Drum Microearthquake Recorder 42
3.2.2 Optimization of Signal-to-Noise Ratio 46
3.2.3 Handling of Records 47
3.3 The Recording Sites 49
3.4 Analysis of Data 53
3.4.1 Classification of Microearthquakes 54
3.4.2 Distribution of S-P Intervals 60
3.4.3 Microearthquake Occurrence Rate 63
3.5 Microearthquakes and the Problem of Magnitude Determination 69
3.5.1 Magnitude and Cumulative Frequency of Earthquakes Originating from Volcanoes 72

3.5.2 Derivation of b-value from Maximum Trace Amplitudes 74

3.6 Determination of the b-value from the 1974 Data 75

(1) A-type Microearthquakes 76

(2) B-type Microearthquakes 83

3.7 Energy Considerations 86

CHAPTER IV SEISMIC INVESTIGATIONS OF MOUNT ETNA DURING MAY - JUNE 1975

4.1 Introduction 89

4.2 The Recording System 91

(1) The Geostore Tape Recorder 95

(2) The Seismometers 99

(3) The Amplifier-Modulator 99

(4) The Field Test Box 100

4.2.1 The Equipment Setting up and Operating Procedure 101

4.2.2 The Analogue Playback System 103

4.2.3 Playing Back Geostore Tapes 104

4.2.4 The Store 4 Tape Recorder 112

4.3 Analysis of Data 113

4.3.1 Seismic Activity of the Volcano 115

4.3.2 Distribution of S-P Intervals 121

4.3.3 Magnitudes 122

4.3.4 b-values 122

4.3.5 Seismic Method of Locating Magma Chambers 123

4.4 Review of Techniques used to Locate Local Earthquakes 126

4.4.1 Other Location Techniques 131

4.4.2 A Brief Discussion of Programme HYPO 135

4.4.3 Location of Microearthquakes on Etna Using Programme HYPO 137

CHAPTER V SPECTRAL CHARACTERISTICS OF MICROEARTHQUAKES AND BACKGROUND SEISMIC NOISE

5.1	Introduction	145
5.2	Selection of Data for Digitization	151
5.2.1	Digitization of Seismic Data	154
5.2.2	Conversion of Punched Paper-Tape	160
5.3	Introduction to Power Spectral Analysis	160
5.3.1	Power Spectrum via the Auto-correlation Function	165
5.3.2	Pre-Whitening	170
5.3.3	Some Practical Aspects of Spectral Estimation	171
5.4	Data Analysis and Results	174
5.4.1	Part I: Background Seismic Record	174
5.4.1.1	Station 1: Serra La Nave	175
5.4.1.2	Station 2: IC Bench Mark	182
5.4.1.3	Station 3: Forestale Hut	184
5.4.1.4	Station 4: Monte S. Maria	184
5.4.2	Inter-Station Comparison and Source Location	188
5.4.3	Mechanics of Volcanic Tremor	197
5.4.4	Part 2: Microearthquake Analysis	203
5.4.4.1	A-type Microearthquake	204
5.4.4.2	B-type Microearthquake	209
5.4.5	Comparison Between the two Types of Microearthquakes	215

CHAPTER VI DISCUSSIONS

6.1	Comparative Study of the 1974 and 1975 Field Investigations	217
6.2	A Brief Description of the Activity of Mount Etna During the Two Recording Periods	219
6.3	Significance of the Present Findings	221
6.4	Predicting Eruptions on Mount Etna	228

CHAPTER VII SUMMARY OF CONCLUSIONS AND RECOMMENDATIONS FOR FURTHER STUDY

7.1 Summary of Conclusions 234

7.2 Recommendations for Further Study 237

REFERENCES 239

APPENDICES 249

ACKNOWLEDGEMENTS

The author would like to take this opportunity to thank all those contributors without whom the investigation described would not have been possible.

I am especially grateful to my supervisor Professor R.G. Mason for his critical suggestions, comments and the final reading of the manuscript.

Thanks are due to Burmah Eastern Oil Company for providing much of the financial assistance for the research, when the author was on leave of absence from the Jahangir Nagar University, Dacca, Bangladesh.

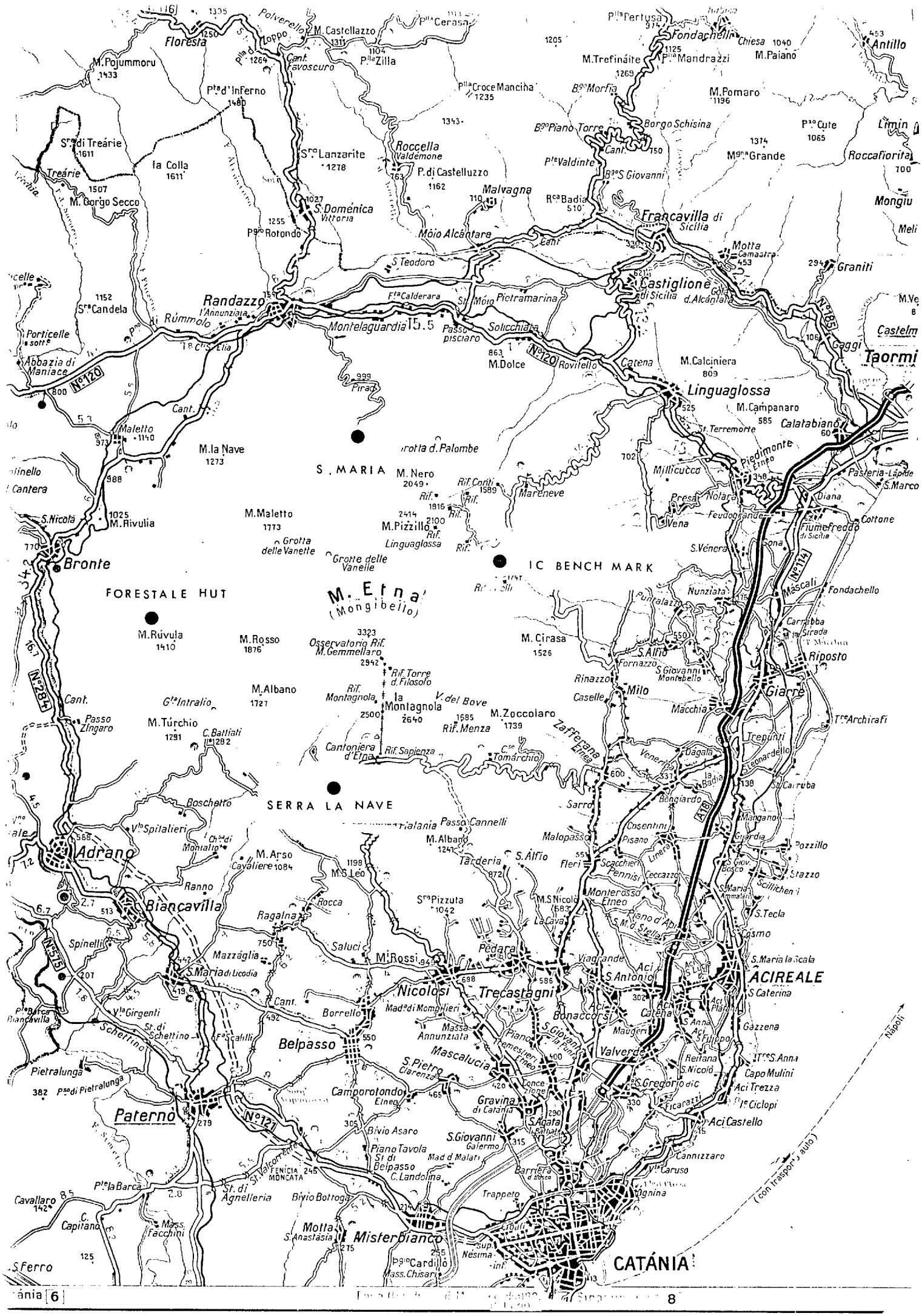
I am greatly indebted to the United Kingdom Natural Environment Research Council, for meeting the field work expenses and also providing the Geostore recording equipment. I am also grateful to the personnel, especially Mr. K. Chappel and Mr. G. McGonnegall, of the Seismological Observatory at Eskdalemuir for providing the Geostore reproduction facilities and assisting me in their efficient handling.

Special thanks are due to Mr. M.G. Bill for helping the author with the field work, and Mr. K. O'Hara for help in smoothing out some of the electronics difficulties.

Thanks are also extended to the Imperial College Computer Centre for the use of their excellent computing facilities, the University of Catania for letting the author use the seismic vault at Serra La Nave, the personnel at the

Institute of Volcanology, Catania, and my friends and colleagues in the Department for many useful discussions.

Finally my deep appreciation to my parents for their encouragement during the course of my research, and to Miss M.T.M. Chock for the final typing of the thesis.


Floresta
M. Pojummoru 1433
Pta d'Inferno 1480
M. Castellazzo
P.lla Cerasa
P.lla Zilla
P.lla Croce Manciha 1235
Fondachelli
Chiesa 1040
Antillo
M. Trefináite 1269
P.lla Mandrazzi 1125
M. Paiano
M. Pomaro 1196
B.go Morfia
B.go Piano Torre
Borgo Schisina
P.ta Cute 1065
Limin
Mgna Grande 1374
Roccafiorita 700
Mongiu
Meli
S.ta di Treárie 1611
Treárie 1507
M. Gorgo Secco
la Colla 1611
S.ta Lanzarite 1278
Roccella Valdémone
P. di Castelluzzo 1162
Malvagna
P.te Valdinte
B.go S. Giovanni
Rca Badia 510
Francavilla di Sicilia
S. Domenica Vittoria 1027
P.go Rotondo 1255
Móio Alcántara
Motta Camastra 453
Graniti
S. Teodoro
S.ta Candela 1152
Randazzo
Ftta Calderara
St. Móio
Pietramarina
Castiglione di Sicilia
Gola d. Alcántara
Porticelle sotto
Abbazia di Maniace
Rúmmolo
Montelaguardia 15.5
Passo pisciaro
Solicchiata
M. Dolce 863
Rovitello
Catena
M. Calciniera 869
Gaggi
Taormi
Castelm
Linguaglossa
M. Campanaro 525
Calatabiano 60
St. Terremorte 585
Maletto 1140
M. la Nave 1273
Grotta d. Palombe
S. MARIA
M. Nero 2049
Rif. Coniti 1589
Mareneve
Millicucco 702
Piedimonte Etneo 348
Pasteria-Lapide
S. Marco
Presa
Nolara
Diana
Feudogrande
Vena
Cottone
Fiumefreddo di Sicilia
S. Vénera
Sona
Bronte
S. Nicolà
M. Rivulia 1025
M. Maletto 1773
M. Pizzillo 2414
Rif. Linguaglossa 2100
Grotta delle Vanette
Grotte delle Vanelle
IC BENCH MARK
FORESTALE HUT
M. Etna (Mongibello)
Nunziata
Mascali
Fondachello
Puntalazza
Carrabba
M. Rúvula 1410
M. Rosso 1876
Osservatorio M. Gemmellaro 2942
M. Cirasa 1526
S. Alfio
Fornazzo
S. Giovanni Montebello
Riposto
Rif. Torre d. Filosofo
Rinazzo
Milo
Giarre
M. Albano 1727
Rif. Montagnola
la Montagnola 2640
V. del Bove
Caselle
Macchia
M. Túrchio 1291
C. Battiati 1282
M. Zoccolaro 1739
Rif. Menza 1585
Zaffarana Etnea
Trepunti
Tre Archirafi
Cantoniera d'Etna
Rif. Sapienza
C.se Tomárchio
Venerina
Dagala
Leonardello
la Badia
S. Caruba
SERRA LA NAVE
Boschetto
Sarro
Bongiardo
Mangano
Adrano
V.le Spitalieri
M. Albano 1241
Passo Cannelli
Malopasso
Cosentini
Pisano
Guardia
Pozzillo
M. Arso Cavaliere 1084
M. S. Leo 1198
Tarderia
S. Alfio 872
Fleri
Scacchieri
Pennisi
Ceccazzo
Linera
Stazzo
Ranno
Biancavilla
Rocca
Ragalna
Sra Pizzuta 1042
M. S. Nicolò 683
Monterosso Etneo
S. Tecla
Cosmo
Spinelli
Saluci
Pedara
M. Rossi 944
Viagrande
Aci S. Antonio
S. Maria la Scala
ACIREALE
Mazzáglia
S. Maria di Licodia
Nicolosi
Trecastagni
S. Caterina
Borrello
Mad.a di Mompilieri
Bonaccorsi
Aci Catena
Gazzena
Schettino
Belpasso
Massa Annunziata
Piano Tremestieri Etneo
S. Giovanni la Punta
Valverde
Aci S. Filippo
Mascalucia
S. Pietro Clarenza
Reitana
S. Nicolò
Tre S. Anna
Capo Mulini
Pietralunga
Camporotondo Etneo
Gravina di Catania
S. Gregorio di C.
Aci Trezza
I Ciclopi
Paternò
Bivio Asaro
S. Agata
Aci Castello
S. Giovanni Galermo
Piano Tavola
Mad.a di Malati
Cannizzaro
Cavallaro
C. Capitano
Mass. Facchini
Bivio Bottoga
Trappeto
Misterbianco
Motta S. Anastasia
Barriera
Ognina
CATÁNIA
S. Ferro
Napoli
(con trasporto auto)
Scala di 1:200 000 1 cm 2 km

CHAPTER I

INTRODUCTION

1.1 INTRODUCTION

Volcanoes and earthquakes are confined to the same worldwide belts. This has been known for a long time. Aristotle thought earthquakes were caused by the rumblings of pent up wind whose outlets were volcanoes. A more modern concept would be that the seismicity and volcanicity are related to the interactions at major plate boundaries.

There are numerous volcanoes around the world which remain dormant for most of their active lives; sometimes however, perhaps not very often during their lifetime, volcanoes erupt. Catastrophic volcanic eruptions are one of the most formidable of natural phenomena, which sometimes take the lives of hundreds of people and lead directly to enormous losses of material and property.

There have been a large number of reported eruptions in the historical record, some of them extremely large, but there must have been many others that passed unnoticed because they occurred in uninhabited areas. For example, the eruption of Vesuvius in A.D.74, which lasted for only two days, completely obliterated both the ancient cities of Pompeii and Herculaneum, and killed thousands of people. The 1883 eruptions of Krakatoa lasted for about 100 days killing as many as 36,000 people, though not by the direct effects of

explosions, suffocating gases and lava flows, but indirectly through the tsunamis, or tidal waves, triggered off by the eruptions. And in the present century, the 1902 eruption of Mount Pelee in the Carribbean Island of Martinique "burned, boiled and suffocated to death 30,000 people" of the island, and completely destroyed the thriving town of St. Pierre.

Not all volcanoes have such a violent history. Thus Mount Etna, one of the world's most prolific volcanoes, has had more eruptions in historical times than any other volcano, according to MacDonald (1972), the first recorded Etnean eruption dating back to about 394 B.C. However, few eruptions on Etna have resulted in any great loss of life, despite the high density of population on its slopes. That is probably why Etna on the whole is often regarded as a benefactor rather than something to be feared. These factors, combined with the fact that during the last century only four eruptions destroyed human habitations, is the main reason why so little geophysical interest has been taken in the possibility of forecasting eruptions on Etna.

The most fundamental geophysical approach to the study of a volcano is through its seismicity, which can be expected to yield information about dynamic aspects of its mechanism. The very little seismic work that has been done in the area of Etna has been either in the form of volcanic tremor studies (Shomozuru, 1971; Schick and Riuscetti, 1973; Riuscetti and Schick, 1977) or short-period microearthquake studies (Latter, 1966; Lo Bascio et al., 1976; Guerra et al., 1976). This thesis is an attempt at establishing the

'relative activity' of the volcano by studying the micro-earthquakes as well as background noise conditions around it.

1.2 METHOD OF INVESTIGATION

The seismic investigation of volcanic phenomena is a very recent and newly found branch of volcanology. Before the beginning of the twentieth century, volcanology depended on eye-witness observations, and consisted mainly in geological and petrological investigations. But at the turn of the century instrumental recording of earthquakes and volcanic tremor became possible, temporarily at first, but soon developing into continuous observations at permanent observatories. The Americans pioneered the work of volcano observation on the Kilauea and Mauna Loa volcanoes in the island of Hawaii. In other countries, Japan and the U.S.S.R. being the foremost amongst them, studies are being conducted to investigate the connection between earthquakes and other seismic phenomenoa associated with volcanoes, and other volcanic activity in general.

Strong earthquakes have been known to occur prior to a major eruption (Shimozuru, 1971), but it would take tens or hundreds of years to gather reliable data to predict the activity of a volcano based on such information. It was Asada (1957) and Asada et al. (1958) who showed that in an active region, orders of magnitude increase in the number of recorded earthquakes could be obtained by the use of ultra-

sensitive seismographs capable of recording the small earthquakes generally known as microearthquakes. In regions where the total seismicity is relatively low, it becomes more important to use high-gain seismographs in order to obtain a useful sample of earthquakes in a reasonably short time. The use of such equipment to record microearthquake is now fairly common (Oliver et al., 1966; Matumoto and Ward, 1967; Ward et al., 1969) in the investigation of both tectonic and volcanic type seismicity. Although a single small shock does not have the significance of a major shock, microearthquakes are important because of their high rate of occurrence and wide spatial distribution. Microearthquakes have been used by various authors (e.g. Oliver et al., 1966; Crosson, 1972; Hadley and Combs, 1974) to delineate active structures that might otherwise have taken a long time to discover.

The seismic research of volcanoes at the present time seems to have developed along two broad lines: (1) Classification of microearthquakes on the basis of their cumulative frequency versus magnitude relationship (Minakami, 1960) or attempts to characterize the source of certain seismic events that have peculiar or strange signatures (Koyanagi, 1968) and (2) Changes in (a) the occurrence rate, and (b) the location, of microearthquakes with time, and their relationship with the observed volcanic activity or surface deformation around the volcano (Eaton, 1962; Kubotera and Yoshikawa, 1963).

As mentioned before, very few studies of either of the above two general types have previously been attempted on Mount Etna. It might also be mentioned that no serious attempt has yet been made to study the broad underlying structure of Etna using seismic techniques.

In undertaking the study of microearthquakes associated with Mount Etna it was decided to begin the investigation by making a reconnaissance survey of the area. The aims were to determine the frequency of occurrence of microearthquakes and compare them with similar events observed with high-gain seismographs in other volcanic areas (e.g. Matumoto and Ward, 1967; Unger, 1969; Westhusing, 1974; Wood, 1974). If the results obtained were encouraging, it was intended to select various sites around the volcano for a more detailed survey the following year.

The reconnaissance survey produced good results. It was then decided to carry out a more detailed survey using a four-station array of three-component seismographs. This was a much more ambitious programme and one of the most detailed ever to be attempted on Etna so far. In particular, it was intended to (1) locate the origin of as many microearthquakes as possible in order to establish their spatial relationship within the volcano, (2) study the signature of these events for comparison with microearthquakes recorded on volcanoes elsewhere, (3) make a simple compilation of the 'activity and seismicity' of the volcano based on the cumulative frequency of microearthquakes versus their magnitude (or

amplitude) relationship and (4) map the magma chamber by recording the attenuation of the S-wave from sites around the volcano. This method of seismic mapping of the magma chamber has been successfully employed by Kubota and Berg (1967) in studying the Katmai Volcanic Range. Some success was met in achieving the first three of these aims, but insufficient data was obtained for the location of magma chambers.

There is a general agreement among seismologists investigating volcanic processes, about the importance of the study of volcanic tremors for a deeper understanding of the mechanism of volcanic activity in general, and for predicting eruptions in particular (see for instance Sassa, 1935; Dibble, 1969; Clacy, 1972; Decker, 1973). Unlike microearthquakes, volcanic tremor is a more or less continuous oscillating ground motion found in association with nearly all active volcanoes. It is a unique phenomenon in that it has no correspondence with any other phenomenon being studied by seismic methods, except possibly geyser fields and regions of geothermal activity (Rinehart, 1965; Nicholls and Rinehart, 1967; Goforth et al., 1972; Douze and Sorrels, 1972; Iyer and Hitchcock, 1974).

In order, thus, to gain a better understanding of the generation of volcanic tremor on Etna, and its variation in space and time, it was decided to spectrally analyse selected sections of tremor records. Spectral analyses of volcanic tremor on Etna were previously carried out by Shimozuru (1971),

Schick and Riuscetti (1973), Lo Bascio et al. (1976), Guerra et al. (1976) and Riuscetti and Schick (1977). To complete the study of Mount Etna it was also decided to spectrally analyse selected microearthquakes, to gain more information about their nature and source mechanism.

1.3 SCOPE OF THESIS

A brief introduction to the objectives of this thesis and the present state of the seismic investigation of volcanic phenomena has already been presented.

An introduction to Mount Etna is given in Chapter II, which deals also with the geology of Sicily, current views on the evolution of, and tectonic control on, Mount Etna, and briefly with the tectonic history of the area.

Chapter III deals with the first of the two microearthquake surveys carried out on Etna. Brief accounts are given of sites, and the recording instrument. Various statistical studies of the recorded microearthquakes are presented and comparisons made with recordings on other volcanoes.

Chapter IV is in effect an extension of Chapter III, dealing with the second survey, in which simultaneous recordings were made at two or more stations. Apart from the usual statistical studies of microearthquakes, the screening effect of the shear waves and the location of these events are also discussed.

Seismic background noise studies are thought to be

very important for a better understanding of the workings of a volcano. Chapter V deals with the spectral analysis of background seismic noise, and a tentative interpretation is presented to explain the source and mechanism of their generation. Spectral characteristics of selected micro-earthquakes are also described, and comparisons made with background seismic noise recordings.

Results obtained during the two surveys are presented in Chapter VI. Attempts have then been made to explain these findings in terms of the known activity of the volcano.

Chapter VII, the final chapter, includes a summary of the conclusions reached and suggestions for further work on Mount Etna.

CHAPTER II

BACKGROUND INFORMATION ON MOUNT ETNA

2.1 INTRODUCTION

Mount Etna is the largest volcano in Europe. It is essentially a central volcano, and its summit is at a height of 3323m. The central part of the latter is located at $37^{o}45'N$, $15^{o}01'E$ of Greenwich, towering over the eastern slopes of Sicily.

Etna covers an area of nearly five hundred square miles and has a circumference of over ninety miles. Its base is roughly eliptical, with a major-axis (north-south) of approximately thirty miles and a minor axis (east-west) of nearly twenty-five miles. Unlike the steep-sided volcanoes such as Stromboli and Vesuvius, Etna has a gently dipping slope and a much broader profile.

The summit of Etna is flat and truncated and has a large terminal crater. It is irregular in shape, for it represents the coalescing of the true summit cone and the lesser neighbouring cones of the North-eastern crater (Fig. 2.1). The diameter of the base of the summit proper is about 1000m and the crater is about 550m in diameter. The crater of the summit cone is called the Central Crater, and within it are two smaller cones. They are called the 1964 crater, or the Chasm, and the Bocca Nuova - a collapse crater. The Chasm at present is connected to the central conduit and is about 270m in

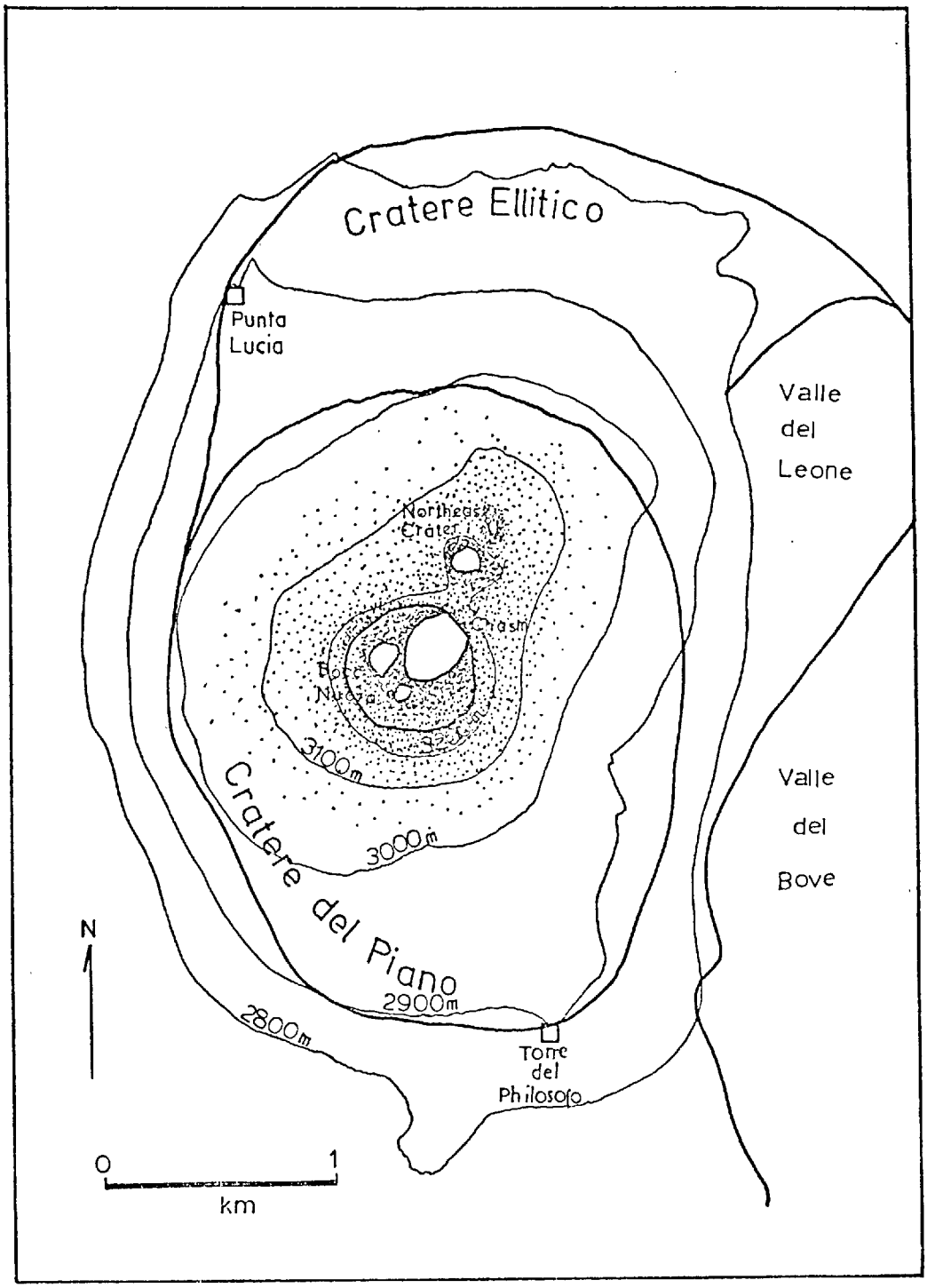


Figure 2.1 Probable outline of the summit region.

diameter at the surface (Murray et al., 1974). Guest (1973) gives a good description of the geology of the summit region as it was in 1971,which is essentially the same as today.

The Central Crater dates back about three hundred years or more, while the Chasm is about fifteen years old. During the last twenty years there have been two major eruptions from the Central Crater, the 1956 and the 1964 eruptions, while the majority of the rest were from the North-east Crater. Despite the large number of recorded eruptions of Mount Etna over the centuries, very little is known about the mechanics of its eruptions, the chief reason being its complex nature, which is well reflected in Rittmann's (1962) classification of it as a "composite - volcano ..... a shield volcano overlain by a stratovolcano (predominantly trachyandesite)".

On the eastern flank of the volcano is the impressive Valle del Bove. This deep valley has a width of about five kilometres and its steep walls rise between 600 and 1100m above the bottom of the valley. These walls consist of alternating layers of lava and tuff,which are cut by numerous dykes, thus allowing the study of the internal structures of the volcano.

Looking at Etna, one is impressed by the number of parasitic eruption centres scattered over its flanks. In fact, (mainly) between the 2500 metre and the 800 metre contour lines there are as many as 200 flank eruption sites, (Rittmann, 1963) which are generally located along radial fissures (Wilcoxson, 1967). (See Figure 2.2).

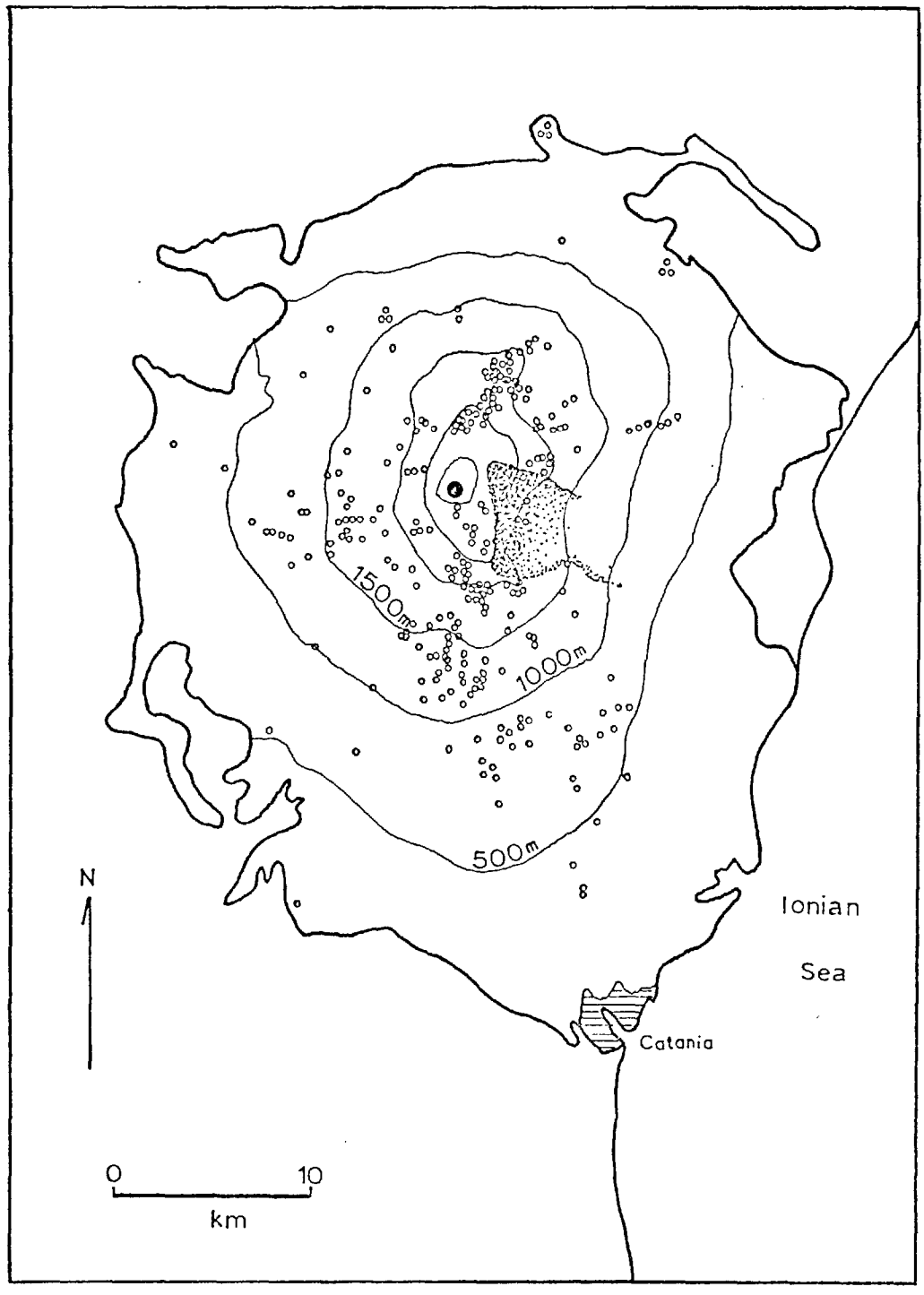


Figure 2.2. Addentive cones and sites of major flank eruptions. Heavy lines indicate the boundary of Etnean volcanic formations, and the dotted area indicates the rim of the caldera of the Valle del Bove. (After Rittmann, 1973).

There is no obvious progressive phase of preliminary action through which Etna must pass before a full-scale eruption occurs, as is the case with Vesuvius, and predictions of eruptions have so far been based more on tumescence and other secondary effects. As with most repeatedly erupting volcanoes, there obviously is some sort of cyclic pattern of activity on Etna,but this is not sufficiently well understood for eruptions to be predicted with any degree of accuracy.

Once the activity has begun, and a fissure has opened, however, Etna follows a typical pattern. Along the trend of the flank fissure a series of craters are formed. The type of activity in each depends primarily on its position in an elevation sequence. The highest and first-formed vents on the fissures are explosive outlets discharging little else but excess volatiles and the pulverised fragments of older materials. Proceeding downwards in elevation, the next crater forcibly expels small pyroclastic ejecta, such as incandescent lava blobs and solid fragments, which form small cones of cinder, ash and lapilli. The next vents eject somewhat larger volcanic bombs, less explosively, and form spatter cones, and finally the lowest craters are responsible for copious lava flows. From the top to the bottom of the fissure there is a decided diminution of explosive activity.

The size and persistent active nature of Etna has inspired awe and admiration in many Greek and Roman scholars of the past. The volcano was considered to be the origin of fire, and the house of the fire-God Vulcan. It was also

identified with the giant Typhon, as well as the site of the fight of Zeus and the giants. There is also the well-known legend of Empedocles (fifth century B.C.) committing suicide in the crater of Etna. Today, however, Etna arouses more interest amongst the scientific community than among poets and classical scholars of the present time.

2.2 GEOLOGICAL FEATURES OF SICILY

For a proper understanding of the evolution and the tectonic history of Etna it is important to understand how it fits into the geological structure of Sicily. Geologically, Sicily can be divided into four major structural units (Caire, 1970). From south to north, they are:

1. Foreland of the Sicilian Alpine Chain

The most southerly unit is represented by the stable Ragusan-Iblei Carbonate platform (Fig. 2.3). This carbonate formation is not affected by Alpine folding, and can be considered as a prolongation (or the equivalent) of the Sahara beyond the Sicilian - Tunisian Basin.

The Ragusan platform is broken up by a network of normal faults striking SSW and SSE. It is separated from the Caltanisetta Basin (see 2 below) by a system of faults and flexures which extend to the NNE into the Iblean mountains. These were the passages during the early Miocene of basaltic extrusions that underlie the Quaternary volcano of Mount Etna.

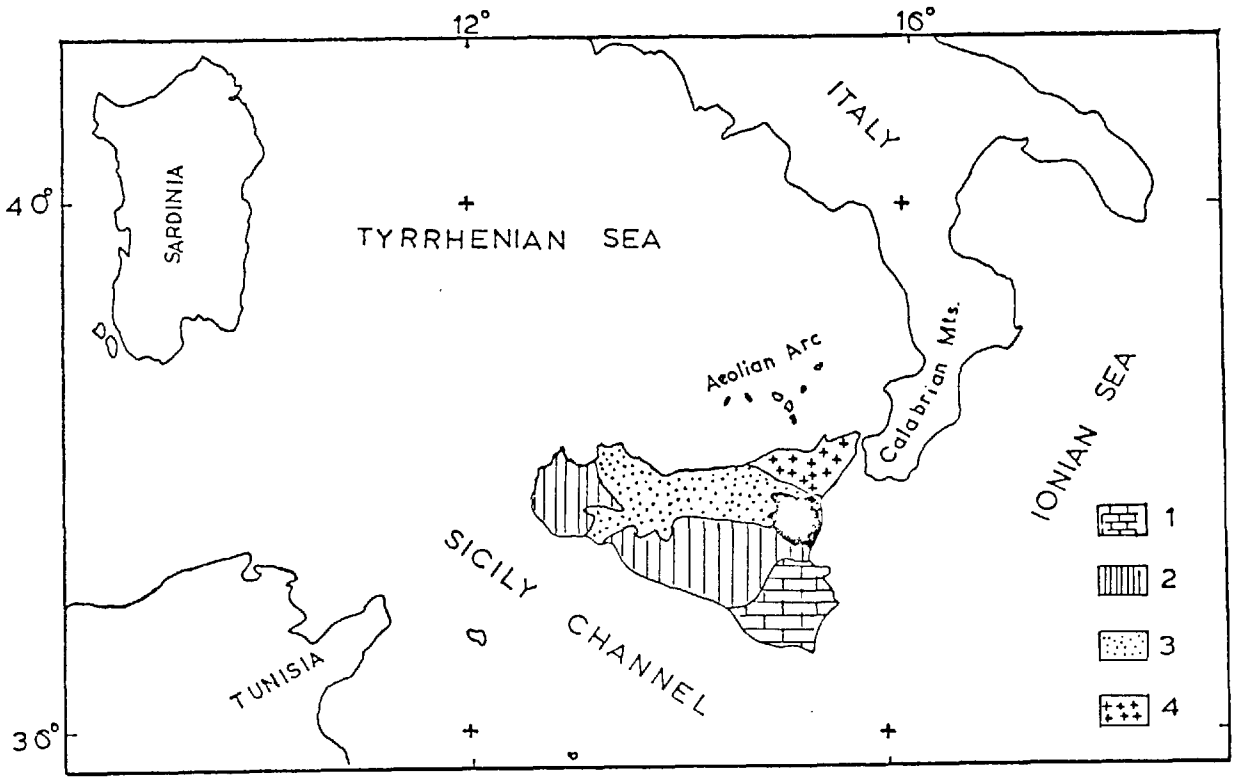


Figure 2.3. Geological sketch map of Sicily. 1=Ragusa-Iblei carbonate platform; 2=Neogene sedimentary basin; 3=different nappe units; 4=Peloritani crystalline domain. (After Barberi et al., 1974)

2. Middle Sicily and the Basin of Re-sedimentation

Middle Sicily includes all of western Sicily and ends towards the east in the region of Catania, between the Ragusa Plateau to the south and the Nebrodi and the Peloritani Massifs to the north. The structural unit is here represented by Mio-Pliocene basins, where fragments and debris from different facies zones have been deposited. One of these basins, the most important, is the Central Sicilian or Caltanissetta Basin. Due to the tectonic uplift of Sicily during the lower Pliocene times, upper Pliocene and lower Quaternary deposits are now to be found in this basin up to a height of several hundred metres above sea level.

3. The Flysch Nappes

The northern half of Sicily, except for the northwestern and northeastern extremities, is occupied by a sequence of Cretaceous to Miocene flysch nappes. This is a term applied to the widespread deposits of sandstones, shales and clays which lie on the northern and southern borders of the Alps in association with large bodies of rocks that have moved forwards for considerable distances from their original positions, either by overthrusting or by recumbent folding. These nappes are similar to, or even identical with, their corresponding equivalents in North Africa. They appear as a structural edifice similar to that in Algeria. From Sicily to Calabria they show, in plan view, curving boundaries concave to the northwest, and overthrusts which moved from the insides to the outsides of these arcs.

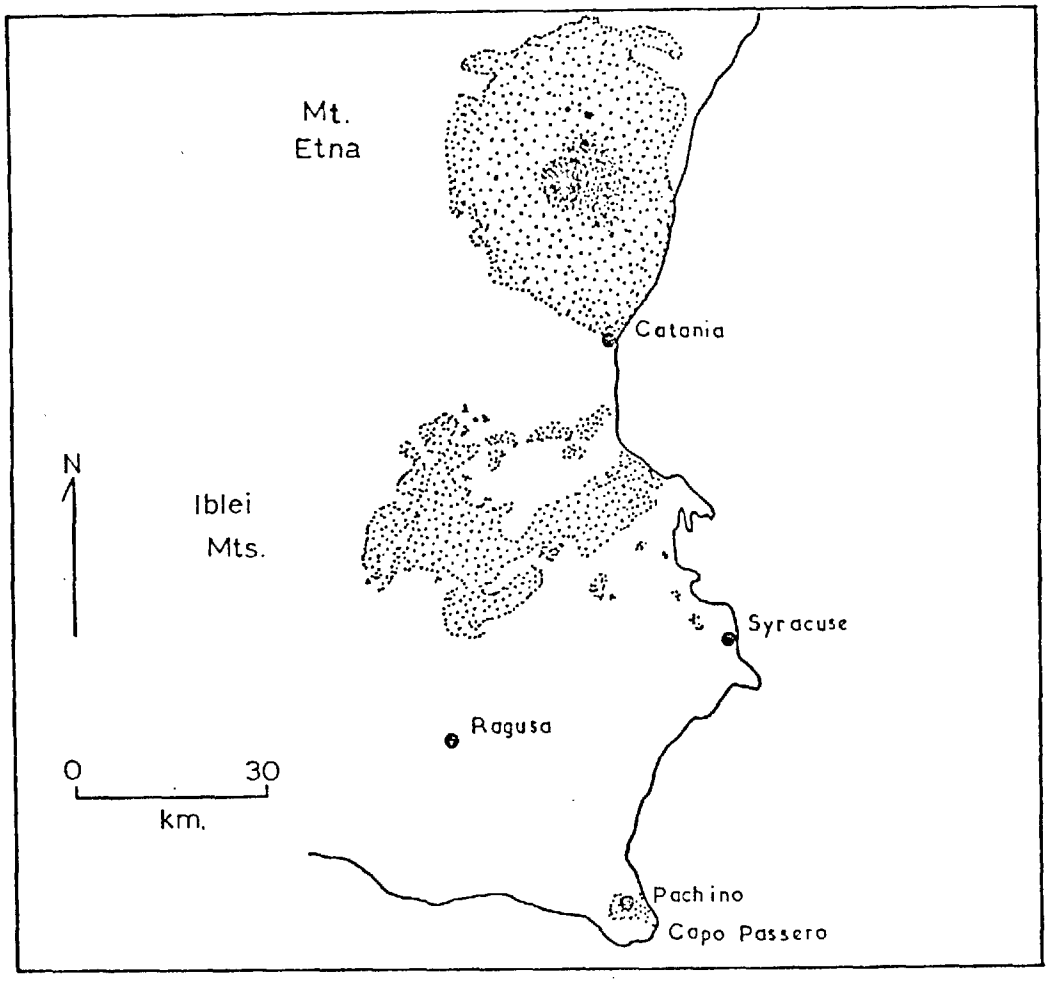


Figure 2.4. Volcanic rocks of eastern Sicily, Capo Passero and Pachino (Cretaceous); Iblean mountains (Neogene to lower Pleistocene); Mount Etna (lower Quarternary to Recent). (After Rittmann, 1973).

4. The Peloritani Massif

To the northeast is the uppermost unit, the Peloritani Massif, which is the Sicilian continuation of the Calabrian arc. It includes a metamorphic basement with granite intrusions affected by reversal and overthrusting towards the south. With these geological features of Sicily in mind, let us try and explain the present tectonic setting of Mount Etna.

2.3 GEOLOGICAL SETTING OF MOUNT ETNA

The south-eastern part of Sicily has been the site of volcanism of a dominantly basaltic nature since the middle Triassic period (Cristofolini, 1973). This volcanism occurred in a submarine environment, giving rise to pillow-lavas and hyaloclastites through fissures cutting a carbonate platform. The oldest exposed rocks in the area are the Cretaceous Volcanics of Pachino and Capo Passero (Fig. 2.4). Further north, in the Iblean mountains, volcanic rocks of Miocene, Pliocene and Pleistocene age occur. Much older volcanic rocks have, however, been found in drillings for petroleum in Ragusa.

In the middle Quaternary period the area presently occupied by Mount Etna was a gulf in which clays of Sicilian origin were deposited. It appears that at some point during this time submarine fissure eruptions of basaltic magma broke out on the floor of this shallow gulf. These eruptions produced mostly spilitized pillow lavas and hyaloclastites, exposed at present on the coast north of Catania. The

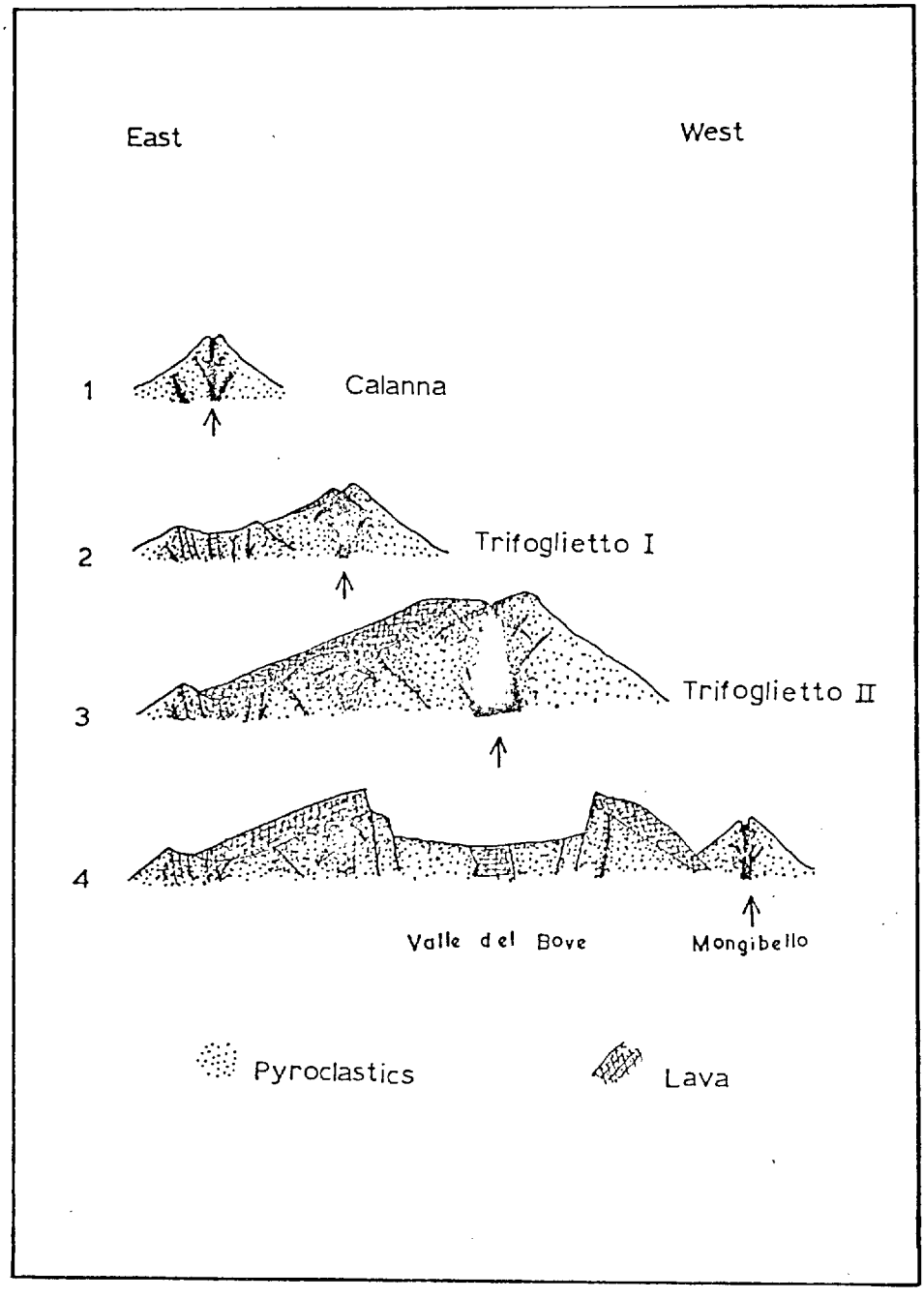


Figure 2.5. Hypothetical profiles at the various stages in the evolution of the volcano that occupied the Valle del Bove. Stage 4 represents the destruction of the Trifoglietto volcano before the formation of the post-Trifoglietto cones, arrows indicate migration of active vents. (After Klerx, 1970).

initial submarine eruptions gradually became sub-aerial as a result of the tectonic uplift of Sicily. These sub-aerial volcanoes later on built up the complex of Mount Etna. Figure 2.4 illustrates this northward migration of volcanic activity in time, from the Cretaceous volcanics of Capo Passero in the south to Mount Etna itself in the north.

The sedimentary basin upon which Mount Etna rests consists broadly of flysch type deposits of Cretaceous to Miocene age in the north, Miocene sandstones in the west, and Pleistocene alluvial deposits in the Plain of Catania to the south.

The huge caldera-like feature on the eastern slope of Mount Etna offers us some insight into the complex tectonic processes the volcano underwent. This depression is known as the Valle del Bove, and its walls reveal at least three significant stages of its development before the present time (Klerx, 1968). The first position occupied by the volcano was at the Valle del Calanna, and then the two subsequent stages of the Trifoglietto volcano in the Valle del Bove. These volcanoes maintained a pattern of westward migrating activity, resulting in the present volcanic centre, Mongibello. Figure 2.5 shows a hypothetical profile at four stages in the evolution of this volcano. Various theories have been proposed to explain the origin of the Valle del Bove, among which Kieffer's (1969) 'explosive-origin' theory seems to be the most quoted. Kieffer proposes that the Valle del Bove dates from about 5000 years B.P. and that most of the material

after the explosion was transported to the east to form the large detrital fan which overlies the lava in the coastal area to the east of Etna.

Klerx and Evrard (1970) made a gravity survey of the Valle del Bove and came out with a positive anomaly of 27 mgals situated over the site Kieffer had earlier proposed as the centre of the Trifoglietto. This was interpreted by them as being the now solidified small basic or ultra-basic magma chamber at the root of the Trifoglietto. Yokoyama (1963), however, showed that a negative anomaly is associated with pumiceous calderas. If his findings are true, it is difficult to reconcile Kieffer's pumice eruption theory with Yokoyama's gravity results.

2.3.1 TECTONIC CONTROL OF MOUNT ETNA

Mount Etna is very strongly controlled by a system of faults (Rittmann, 1973; Romano, 1970). Figure 2.6 shows that the two major fault systems south of the volcano trend roughly NNE and NNW, while a WNW trend is dominant to the north. To the west of the volcano the fissural trends are less obvious and it is almost impossible to find evidence of any fault in that region. However, the ENE sinistral strike slip faults (Ritsema, 1969) have considerable influence on the basement of Etna, as is reflected by the distribution of various eruptive centres (see Section 2.1 and Fig. 2.3).

The major structural feature of eastern Sicily is however the Messina Fault, an active normal fault striking NE through the Straits of Messina. The 1783 Calabrian earthquake,

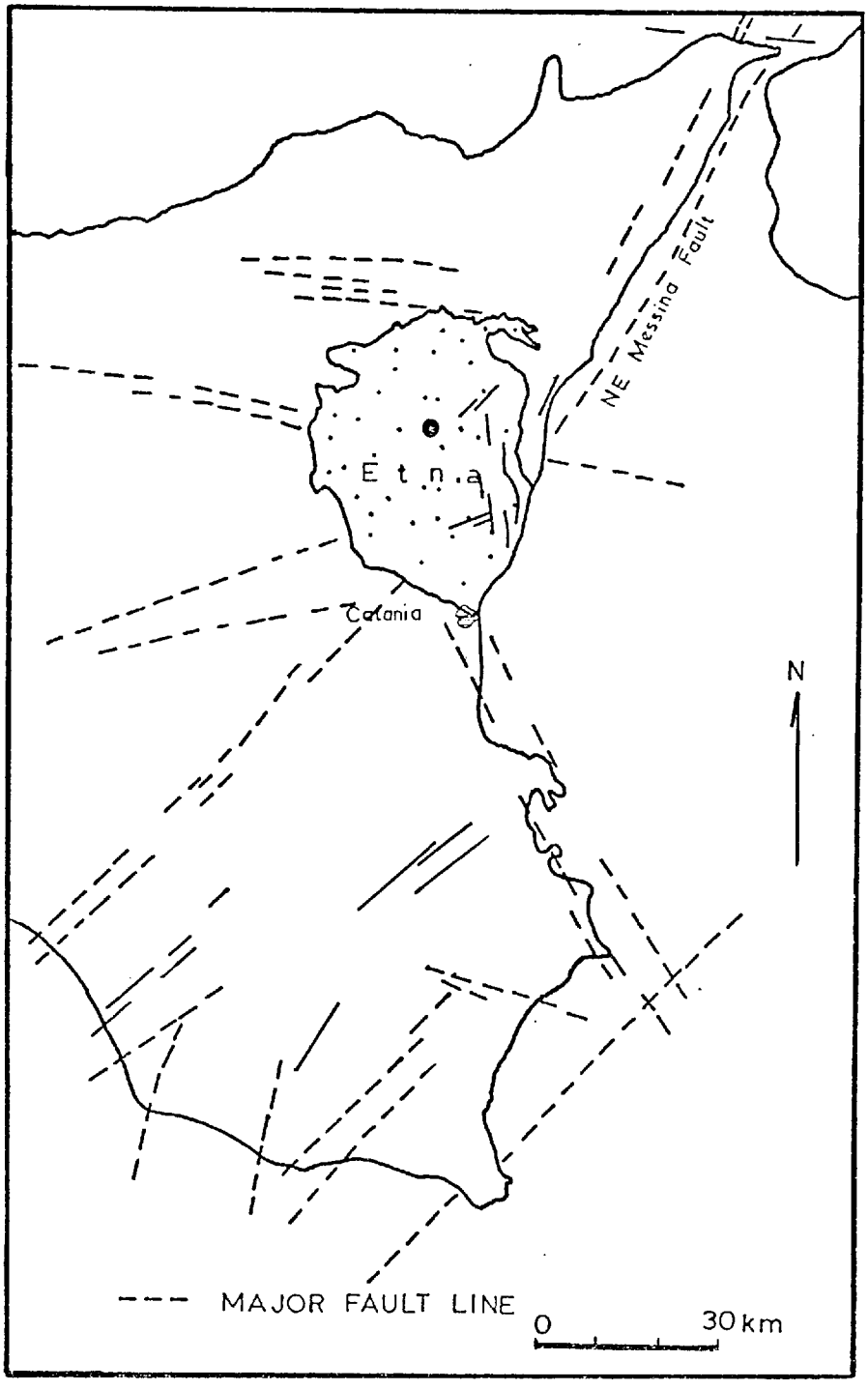


Figure 2.6. Tectonic frame - work of eastern Sicily.

and the Messina earthquake of 1908, emphasize the tectonically active nature of this fault. The realization of this has prompted Italian workers to initiate distance measurements across the Straits of Messina, to establish any differential movement between mainland Italy and Sicily (Caputo et al., 1974).

There is some evidence that the Etnean region is rising isostatically. The uplift of the sedimentary basement of Etna is proved by the outcrop of Sicilian clay (Quaternary) at an altitude of 800 m on the eastern, and at 1050 m on the western slope of the volcano (Rittmann, 1973). The rate of uplift has been calculated by Grindley (1973), to be of the order of 1 mm/yr. Francavigalia (1959) and Ogniben (1963) think of the uplifted basement as a WNW-ESE trending anticline, and Rittmann (1963) favours a horst-like feature controlled by a N-S trending normal fault parallel to the Ionian graben.

2.4 A BRIEF TECTONIC HISTORY

In order to understand the present structural setting of Mount Etna, it is essential to construct the past movements of Sicily relative to Africa and Europe. In this section an attempt has been made to reconstruct this movement on the basis of various geophysical data as well as on the distribution, age and nature of volcanism in eastern Sicily.

Paleomagnetic data from the outcrops of volcanic rocks of Capo Passero dykes in the Ragusan platform indicate that, at least since the upper Cretaceous time, Sicily has been part of the African plate. The Plio- Pleiostocene pole for Sicily evaluated from the Mount Iblei lavas, is also con-

sistent with the upper Tertiary-Quaternary pole for Europe (Barberi et al., 1974). The conclusion that can be be drawn from this result is that Sicily, as part of the African plate, collided with the European plate towards the end of the Oligocene, producing the island-arc volcanism of the Aeolian Islands. In the lower Miocene, the thrusting nappes and metamorphic belt of the Peloritanian mountains to the north of Mount Etna were formed (Grindley, 1973) and since the late Miocene times Sicily has been part of the European continent (Barberi et al., 1974).

The Aeolian Island arc is located at the boundary between the converging African and European plates, and the volcanism is considered to be in a senile state (Belderson et al., 1974). The Aeolian arc displays a transition in lava composition from calc-alkaline to shoshonitic suite, over a period of less than one million years. This rapid variation is thought to be suggestive of a deepening Benioff zone (Barberi et al., 1974a). Both shallow and deep focus seismicity occur in the area. Shallow focus seismicity characterizes the Sicilian-Calabrian fold belt, whereas much of the deep-seismic activity occurs in the SE Tyrrhenian basin, at a depth of 200-350 km (Ninkovich and Hayes, 1972). Ritsema (1969) and Caputo et al. (1972) have shown that this WNW seismic plane has a limited lateral extent of about 225 km and dips at 50^{o}-60^{o} beneath the Tyrrhenian Sea. Focal solutions of these earthquakes (McKenzie, 1970 and 1972) show a thrust mechanism on the E-W plane. This mechanism is consistent with the Gibraltar Morocco-Algeria line, and the north Sicily

seismic line seems to be its prolongation.

Despite the close proximity of Mount Etna to the Aeolian Islands there is no close relationship between the two. Mount Etna volcanic rocks have a low $^{87}Sr/^{86}Sr$ ratio (0.7033) compared with the average for Aeolian rocks (0.7045). This shows that Etna's source magma has not been contaminated by crustal assimilation. The volcanic rocks of the Sicily Channel on the other hand have the same $^{87}Sr/^{86}Sr$ ratio as those of Mount Etna, which suggests a similar tectonic setting for the two volcanic regions.

An E-W seismic sounding was recently carried out by Giese et al. (1973) across North Sicily, and their analysis showed a crustal thickness of 38 km in the Etna region. Barberi et al. (1973) showed that the crustal thickness increases from the Sicily Channel in the south to the northern edge of Sicily ($\simeq$ 40 km), and that the crust/mantle interface is very diffused in this region. The crustal thickness however remains constant along the northern part of Sicily but sharply decreases to the north, where the plate is subducted under the Tyrrhenian Sea. Recent echo-soundings in the Ionian Sea have shown that a poorly developed ridge system (Beldersen et al., 1974) exists concentric to the Calabrian arc. The existence of the Calabrian ridge implies crustal shortening related to the compression which is associated with the Benioff zone beneath the Calabrian arc. The compression is probably a result of the south-easterly motion of the Tyrrhenian region.

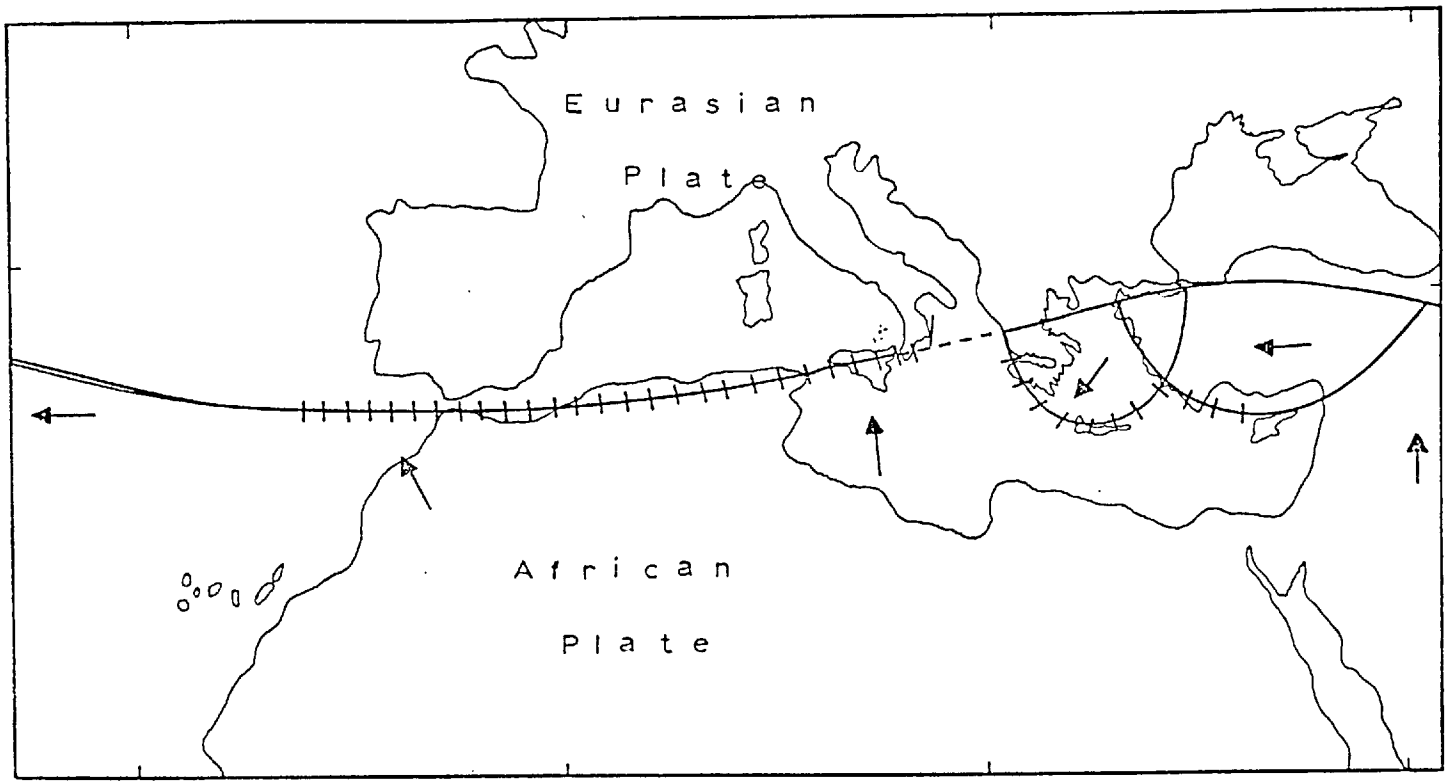


Figure 2.7. Probable positions of plate boundaries at the present time. Direction of arrows indicate relative motion of the African and Eurasian plates. Boundaries at which lithosphere is being created are shown by double lines and boundaries at which plates are being consumed, by lines at right angles. (After McKenzie, 1970; and Barberi et al., 1974).

To sum up, we see that Mount Etna lies just south of a diffuse plate boundary, with a ridge system running ENE in the Ionian Sea. These relationships are shown in Figure 2.7.

Many investigators have tried to explain the peculiar structural position of Etna. Mount Etna not only is situated in what would normally be expected to be a non-volcanic zone, but is active and producing magma. In order to produce an integrated picture of the area, Barberi et al. (1974) relate the fluctuations of the geochemistry of the volcanic products to the compressional and distentional tectonics of the area, thought to have been brought about by the changing nature of the African and European plate interactions since the Triassic period. Eastern Sicily, however, has been the border zone of the colliding continental plates since the upper Miocene. This gave rise to a local distensive tectonics related to the stress field directed normally to the motion of the oceanic lithosphere. Barberi et al. (1974), however, do not explain how "distensive tectonics" exist on top of a subducting plate. Grindley (1973) overcomes the problem by proposing a high rate of arc migration for the plate and, indeed "rates of arc migration are sufficiently rapid" even though eastern Sicily is being uplifted at the rate of 1 mm/year, to allow crustal dilatation normal to the Calabrian arc.

These features of the plate tectonic setting of Mount Etna have attracted special attention in the region and at present there are several geological and geophysical

programmes in the area other than the work described in this study. It is hoped that as more data becomes available we shall be able to understand these peculiarities of Mount Etna more fully.

CHAPTER III

SEISMIC INVESTIGATIONS OF MOUNT ETNA DURING AUG - SEPT 1974

3.1 INTRODUCTION

The 1974 reconnaissance seismic survey of Mount Etna was inspired by the fact that for several years the Geophysics Department of the Imperial College had been involved in geophysical studies of Mount Etna, with NERC support, aimed at investigating its changing shape during the various phases of eruptive activity. One aspect of this problem is the location of magma chambers, for which seismic methods might be particularly useful. It was thus hoped that a seismic survey in the form of microearthquake and background seismic noise recordings would add a new dimension to the understanding of this complex volcano.

The instrument used for the survey was a Sprengnether MEQ 800 microearthquake recorder with a MK I Willmore seismometer (Fig. 3.1). The MEQ 800 has proved to be highly satisfactory for recording tectonic microearthquakes and had earlier been used for seismic studies in Iran (Mohajer - Ashjai, 1975; Hedayati, 1976). No published information was available concerning its suitability for studying volcanic microearthquakes,though it was thought likely that it had been used elsewhere for the purpose.

There are, in various respects essential differences



Figure 3.1. The Sprengnether MEQ 800 portable seismograph.

between observations of volcanic, as opposed to tectonic, earthquakes. Firstly, volcanic earthquakes are, in general, shallower in origin and have much smaller magnitudes. Secondly, in most cases it is very difficult to observe the high-frequency waves of volcanic earthquakes, because of absorption. As a consequence, seismographs of high magnification have to be used. On the other hand, the seismic background noise of volcanoes is normally very high, due mainly to the continuous volcanic tremors. This thus sets a limit to the maximum usable magnification of seismographs on volcanoes, which in turn sets a limit on the smallest micro-earthquake detectable at each site.

At the present time, seismic observations of volcanoes are usually made via telemetering system. This avoids the problem of installing heavy and expensive equipment near active craters, fissure zones and so on, where most of the volcanic earthquakes originate. Telemetering systems were first used at the Hawaiian and Asama (Japan) volcano observatories. There are two systems in common use, (1) telemetering by cable, in which the seismometer (sometimes with a pre-amplifier) is connected to the observatory by cable, and (2) telemetering by radio. The former has limited applications, as there is always the risk of damage to the cables, transducers and amplifiers, and recording equipment by lightning. In addition, there is the problem of laying the cables, sometimes over long distances and over obstructions of various kinds. The second method has the advantage of range, but the cost of setting up such a telemetering system is very

high, and provision of the necessary power is sometimes a problem. A radio-linked system has been successfully used by the Japanese on Sakura-Zima volcano, and on Etna itself such a system is in use by the University of Catania.

Telemetering systems (had they been available) were obviously not appropriate for the reconnaissance survey. In fact, the Sprengnether seismograph proved highly satisfactory for the purpose, being reasonably portable, not too difficult to provide with power, and producing an easily appraisable record. Between 6 August and September 4th 1974, nine sites were investigated, eight of which were on compact lavas, volcanic agglomerate or re-worked volcanics, at elevations of between 1500m and 2500m. The ninth site was situated at an altitude of about 800m on a sedimentary basement near Bronte (for description of sites and their locations refer to Section 3.5). At some sites, recordings were terminated after only a few hours, while at others they extended over several weeks, depending on the suitability of the site, particularly as regards the background noise level.

3.2 THE SEISMIC EQUIPMENT

3.2.1 THE SMOKED-DRUM MICROEARTHQUAKE RECORDER

The Sprengnether MEQ 800 is a self-contained portable smoked-drum seismic recording system with a high gain, wide-sensitivity range. It was used with a single component vertical Willmore MK I seismometer having a natural frequency of 1 Hz.

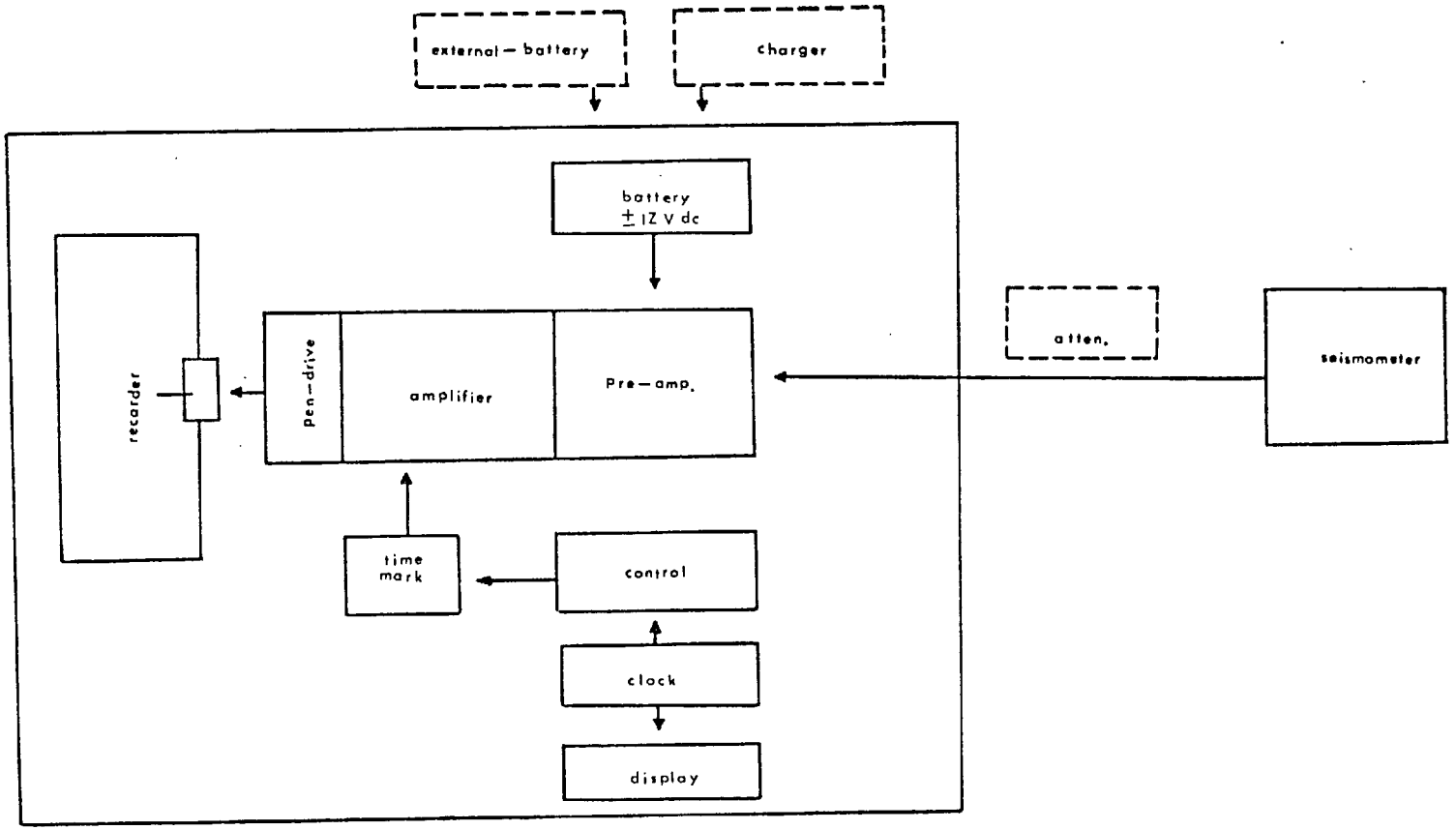


Figure 3.2. Block diagram of the Sprengnether MEQ 800.

The Sprengnether has incorporated in it the following essential units (1) Variable gain amplifier; (2) Adjustable filters; (3) The Drum Recorder, i.e. Drum Pen-motor with associated drives; (4) Timing system, and (5) Power supply (see Fig. 3.2).

(1) The gain is adjustable in 6 dB steps from 60 dB minimum to 120 dB maximum. The corresponding system voltage sensitivity range is 0.33 millivolt/mm pen deflection to 0.33 microvolt/mm pen deflection.

(2) The adjustable filters include a switch that controls a 12 dB/octave high-pass filter to regulate the systems low-frequency response, and a similar switch that controls a low-pass filter and regulates the systems high-frequency response. Low and high filter settings of 'out', 5 and 10 Hz and 'out', 30, 10 and 5 Hz, respectively, are available. Typical response curves are shown in Figure 3.3. With filters 'out' the gain is substantially flat from 0.5 to 30 Hz.

(3) The drum around which the recording paper is wound is about 343x190 mm in diameter the record being about 340x600mm. It is rotated by an electric motor via a friction drive. It can be set at either 10 or 20 min/rev. The record is scratched on the smoked paper by a sapphire-tipped stylus driven by a pen-motor. The latter is translated parallel to the axis of rotation of the drum via a lead-screw driven by a second electric motor, whose rate of rotation can be adjusted so that it traverses the drum in 48, 24 or 12 hrs.

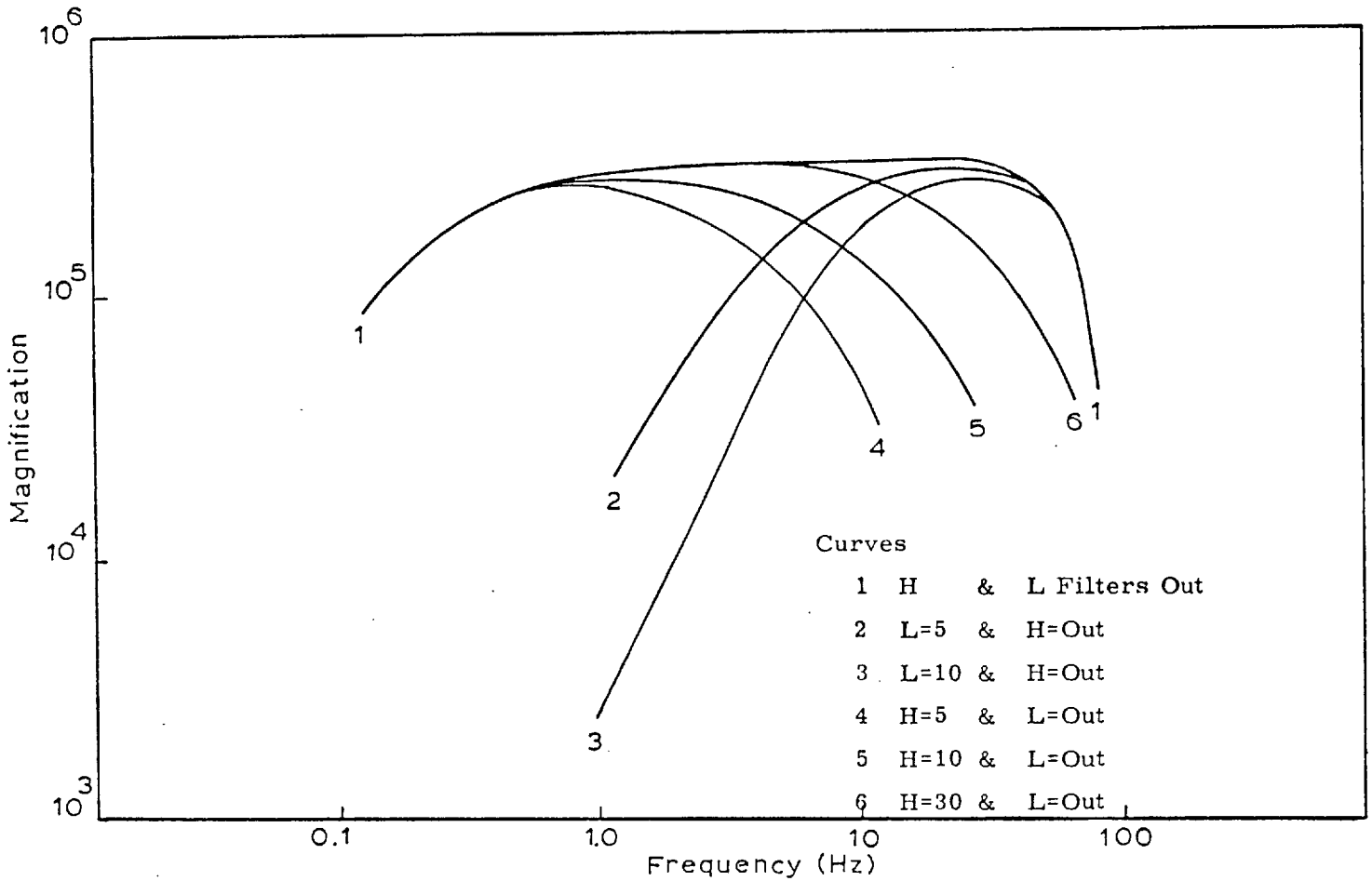


Figure 3.3. Response curve for the Sprengnether MEQ 800 seismograph system. Settings at different combinations of high- and low-pass filters.

Depending on the combination of rotation and traverse rates used, the separation between the adjacent lines may be 1, 2 or 4 mm.

(4) Precision timing is provided by a crystal oscillator which drives a digital clock. The latter is made to deflect the trace for 2.0 sec in every minute and for 4.0 sec at the hour. The crystal clock also provides an accurate 60 Hz output, which is used to stabilize the rate of rotation of the drive motors. The clock is accurate to ±0.1 sec/month within the temperature range 0^{o} - 50^{o}C.

(5) The necessary ±12V power supply is derived from four internal 12 volt, 1.5 AH rechargeable sealed lead-acid batteries arranged in a series/parallel combination. This enables the batteries to be replaced one at a time without interrupting the power supply (and the quartz clock). Provision is made for changing the batteries while the instrument is in operation, also for operating it from external batteries.

3.2.2 OPTIMIZATION OF SIGNAL-TO-NOISE RATIO

As the magnitudes of volcanic microearthquakes are usually small, seismographs of relatively high magnification must be used. The usual magnification of the seismograph depends of course on the background noise level. The main contributions to the background noise are the wind-induced noise, microseisms, and the continuous volcanic tremor. The wind, the microseisms and the volcanic tremor set a lower limit below which microearthquakes cannot be detected.

Because of the difference in spectral content between the wanted signal and the unwanted noise, some improvement in the signal-to-noise ratio can be obtained by suitable adjustment of the filters. Various combinations of low and high cut filters were used to give at each site what was judged to be the best result. The final result, i.e. the ability to distinguish characteristics of the wanted signal against the background noise, could also be optimized by appropriate adjustment of the gain. In practice, the amplifier gains were normally set between 60 and 90 dB, giving an effective overall magnification of between 1×10^3 and 3.2×10^4.

3.2.3 HANDLING OF RECORDS

The paper used for the smoked records was a non-absorbent, 80 pound heavy enamelled paper, that was fixed to the recording drum by rubber cement and adhesive tape. It was smoked by means of a kerosine burner, the drum being rotated slowly over the large smokey flame until it was uniformly blackened. When the stylus has traversed the drum, the latter is removed from the recorder and replaced by a second drum, previously smoked. This record is then fixed while still on the drum, by rotating it in a shellac/alcohol solution, after which it is removed and dried in the air for an hour or two before storage. Surplus shellac is removed from the drum by wiping it with a rag soaked in alcohol.

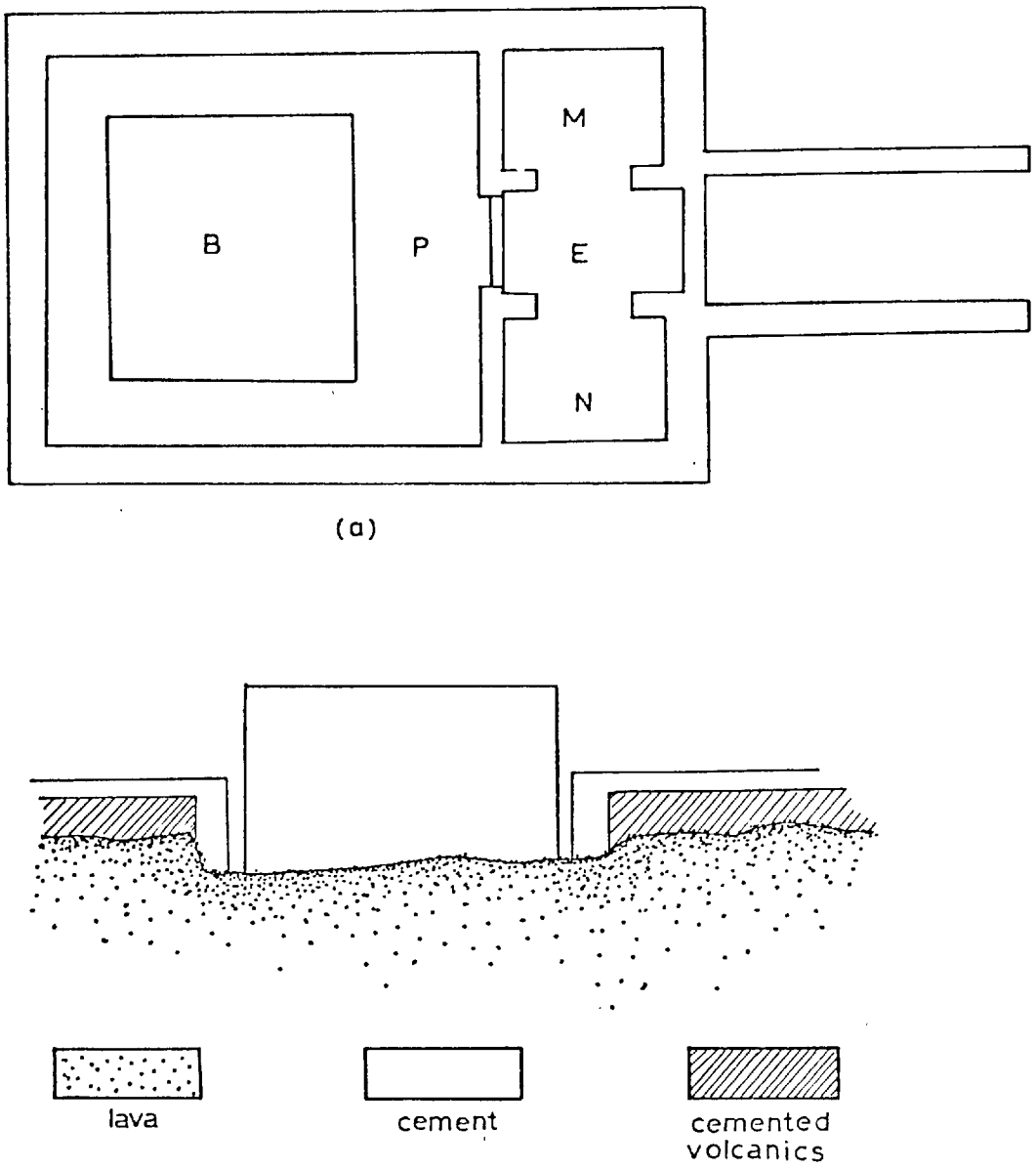


Figure 3.4. Serra La Nave seismic vault, (a) plan of station (b) construction of basement. (After Bottari and Riuscetti, 1967).

3.3 THE RECORDING SITES

It was intended in the 1974 survey to evaluate as many sites around the volcano as time permitted, to aid in the planning of more detailed microearthquake surveys in the future. The reason for looking for sites on the less accessible northern side of the volcano was that mapping of the magma chambers may be possible in the future by studying the relative attenuation of S-waves that have travelled by various paths through the volcano. It is necessary, therefore, that future recording sites should be as widely distributed around the volcano as possible.

Two important factors usually governed where a station can be located. Firstly, it must be relatively easy of access to delicate scientific equipment, and secondly, it must be sited on the most suitable available bedrock. The first station occupied was the seismic vault at Serra La Nave, in the grounds of the Astrophysical Observatory at an elevation of 1732 m about 5 km south of the summit. A detailed description of this station is given by A. Bottari and M. Riuscetti (1967). The main features of the vault are shown in Figure 3.4a. B is the basement, consisting of a concrete block founded on the compact lava that underlies the site, and insulated from the main room P of the vault, by an air gap. The seismometer and the recorder were placed on B. M and N are small adjacent rooms for accessories. E is the entrance. Figure 3.4b is a cross-section through B and P.

The various other sites that were occupied were

Table 3.1

Site Descriptions

Station	Latitude (N)	Longitude (E)	Elevation (m)	Foundation	Remarks
Serra La Nave (1)	37° 41' 40"	14° 58' 26"	1732	Lava flow	Serra La Nave Observatory
Basement of Ski Club (2)	37° 42' 32"	14° 59' 58"	2100	Uncompact Lava flow	Midway between Rifugio Sapienza and Piccolo Rifugio
Torre del Philosofo (3)	37° 44' 13"	15° 00' 05"	2913	Lava flow	On the basement inside the Torre del Philosofo
Rifugio Citelli (4)	37° 45' 56"	15° 03' 36"	1743	Lava flow	On the basement inside the Rifugio Citelli
IC Bench Mark Site near Rifugio Citelli (5)	37° 46' 02"	15° 03' 30"	1690	Lava flow	On an exposed bedrock near Rifugio Citelli (IC levelling site, u)
Inside a '71 lava cave (6)	37° 44' 13"	14° 59' 44"	2900	Inside a Lava cave	500 m west of Torre del Philosofo, inside '71 lava cave

...../contd

Station	Latitude (N)	Longitude (E)	Elevation (m)	Foundation	Remarks
Inside a '74 lava cave (7)	37° 44' 37"	14° 55' 48"	1680	Lava flow	Inside a small lava cave near the '74 eruption site
Near Monte Nero (8)	37° 42' 57"	14° 59' 19"	2250	Lava flow	Inside a small lava cave near Monte Nero
Bronte (9)	37° 46' 03"	14° 59' 35"	800	Sedimentary rock	On an exposure of sedimentary rock before entering Bronte

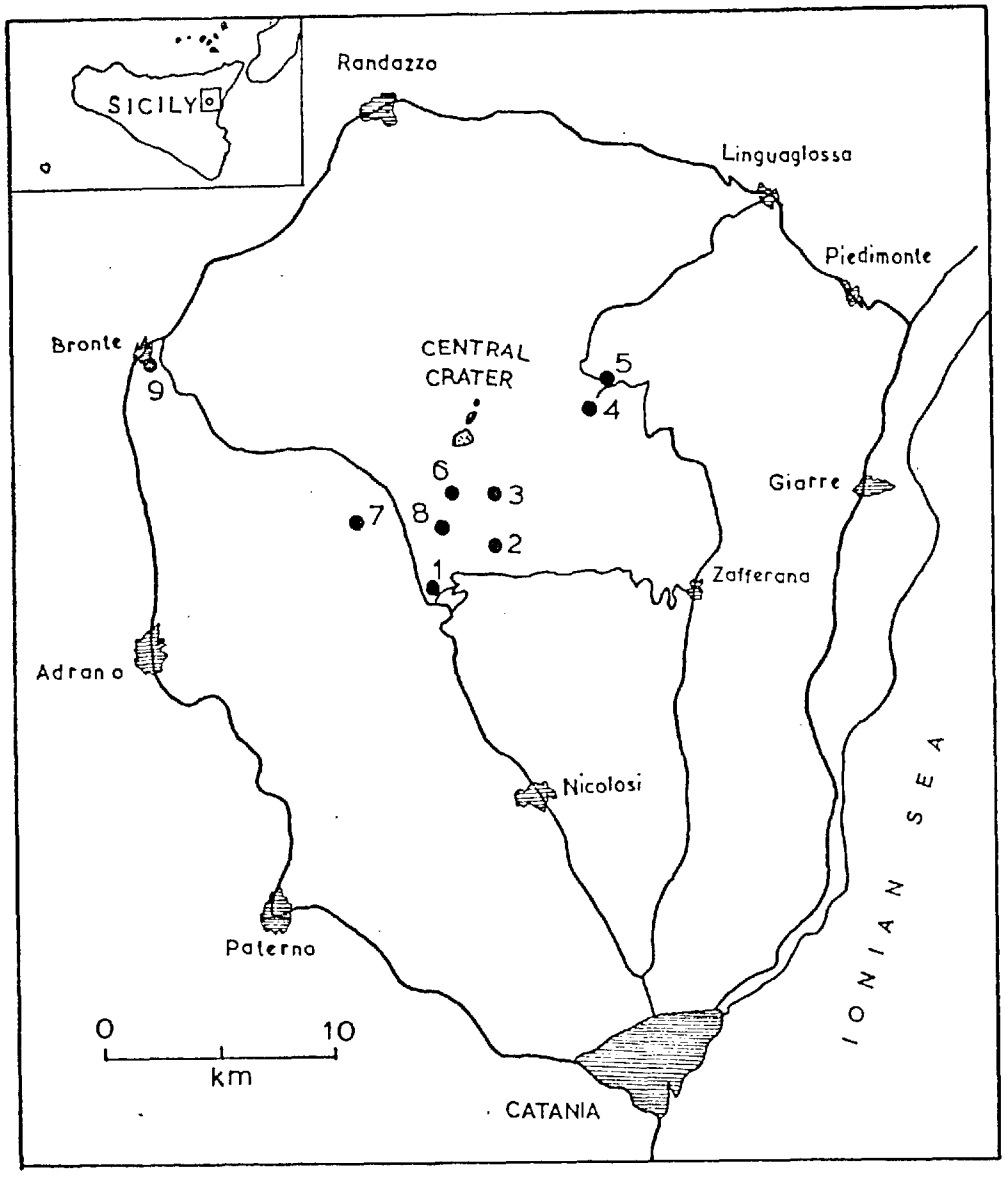


Figure 3.5. Sketch map around Mount Etna showing all the nine sites occupied during the 1974 investigation. (The lines connecting the various towns indicate motorable roads).

either on exposed bedrock, tuff, compact lava, or in the basement of some abandoned building. Seismograms obtained from exposed bedrocks were of very good quality, showing very little background disturbances. One such site was near the Rifugio Citelli (IC bench mark site, Wadge, 1974). It was decided to use it for future work. The lava caves near the '74 eruption, and the Monte Nero site, also produced good quality recordings, but very small earthquakes were masked by high background noise. This was particularly true for the Monte Nero site. The basement sites at the Rifugio Citelli, Ski Club and Torre del Philosofo were considered to be unsuitable for future work because of the constant presence of tourists and vehicles.

Table 3.1 gives a brief description of the various characteristics of the recording sites, and their relative locations, and Figure 3.5 shows the sites occupied in the 1974 study of Etna. All the stations occupied during the course of the 1974 investigations lie within the altitude range of 1500 and 2500m. except the one site at Bronte, which was at a much lower elevation (~ 800m).

3.4 ANALYSIS OF DATA

The seismograms obtained from the Sprengnether MEQ 800 are smoked paper records, and with the recording parameters used in the 1974 survey cover a period of 24 hrs. These seismograms present ground velocity for a given site, as a function of time within the frequency limits as indicated in Section 3.3 and Figure 3.3.

Figures 3.6 and 3.7 show examples of recordings taken at the Serra La Nave seismic observatory. The first shows a record taken during a period of high background noise, and Figure 3.7a is a record taken at the same site during a quiet period.

The 1974 investigation resulted in records for all or part of 30 days, representing samples from nine different sites. No attempt was made at detailed analysis in the field, though the records were of course appraised with a view to deciding for how long the instrument should be left at a particular site.

With the help of a magnifying glass records can be read to about 0.1 sec. Although the time resolution is adequate to pick the arrival times of the P-Waves to an accuracy of 0.1 sec, S-wave arrivals are more difficult to pick and are accurate to no better than about 0.5 sec.

The determination of magnitude raises various problems, when a portable system is employed on a survey, where very little seismic data is available. Various methods were tried in an attempt to get around those problems, but met with limited success. A brief discussion of the present available methods of magnitude determination, and problems involved, are discussed in a separate section.

3.4.1 CLASSIFICATION OF MICROEARTHQUAKES

Microearthquakes are identified as high-frequency envelopes of short duration ($\simeq$ 1 min) superimposed on a con-

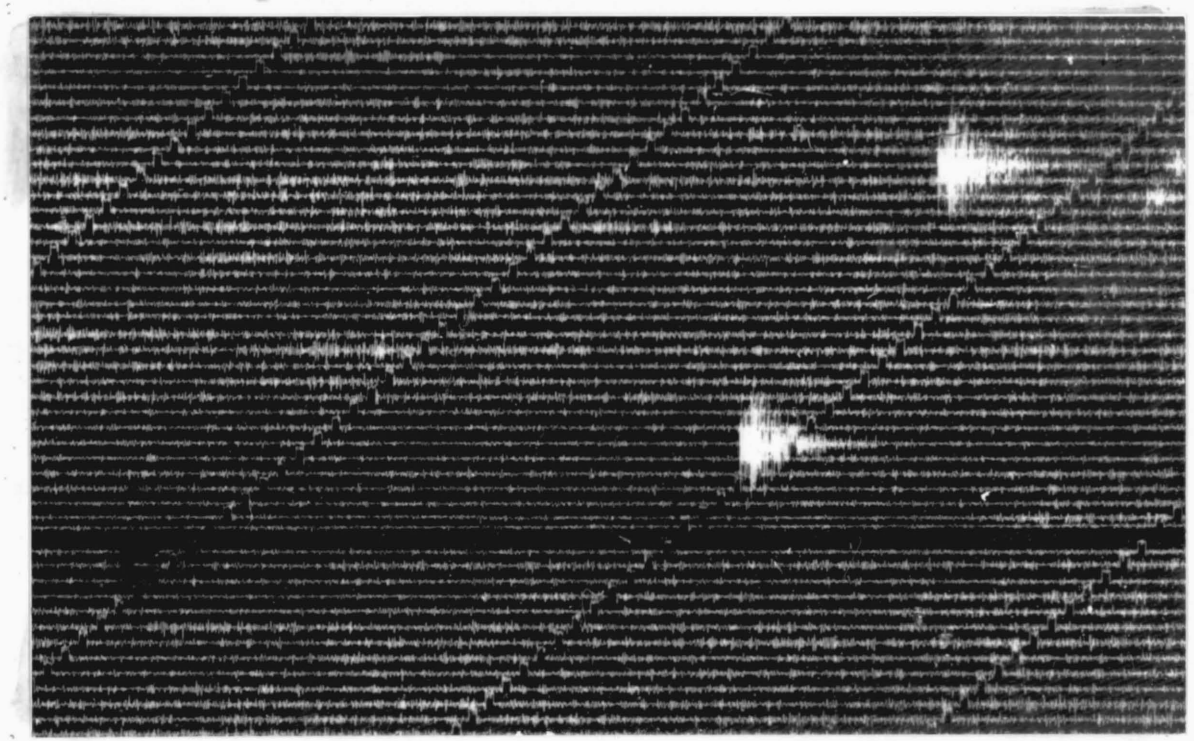


Figure 3.6. Seismogram of A-type microearthquakes recorded at Serra La Nave . Note the impulsive first arrival and the small S-P interval.

tinuous low-frequency background noise. Figure 3.6 shows some very well-defined events recorded at the Serra La Nave seismic vault. In the event of shocks much smaller than those shown in Figure 3.6 it is difficult to distinguish them from the background noise. In order to be on the safe side many doubtful events were thus eliminated from final consideration.

The background volcanic tremor appears to have frequencies below about 5 Hz. The microearthquakes on the other hand have frequencies above 5 Hz. These frequency ranges are in general agreement with results obtained elsewhere.

Three groups of microearthquakes can be broadly distinguished on the seismograms. The first are characterized by a sharp and impulsive arrival, and appear to have distinguishable P and S phases. The recorded amplitude of the S phase is in almost all cases greater than the first cycle of the P wave, and S-P times are typically in the region of 2.5 sec or less. The first motion (P arrival), whenever it was possible to distinguish it, showed both compressional and dilatational arrivals. The total duration of these microearthquakes is normally in the region of 10 to 50 sec. Figure 3.6 shows several examples of this kind of shock. About 18% of the total recorded microearthquakes fall in this category. These kind of events seem to resemble tectonic microearthquakes, and will be discussed further in a subsequent section.

The second kind of event is also characterized by

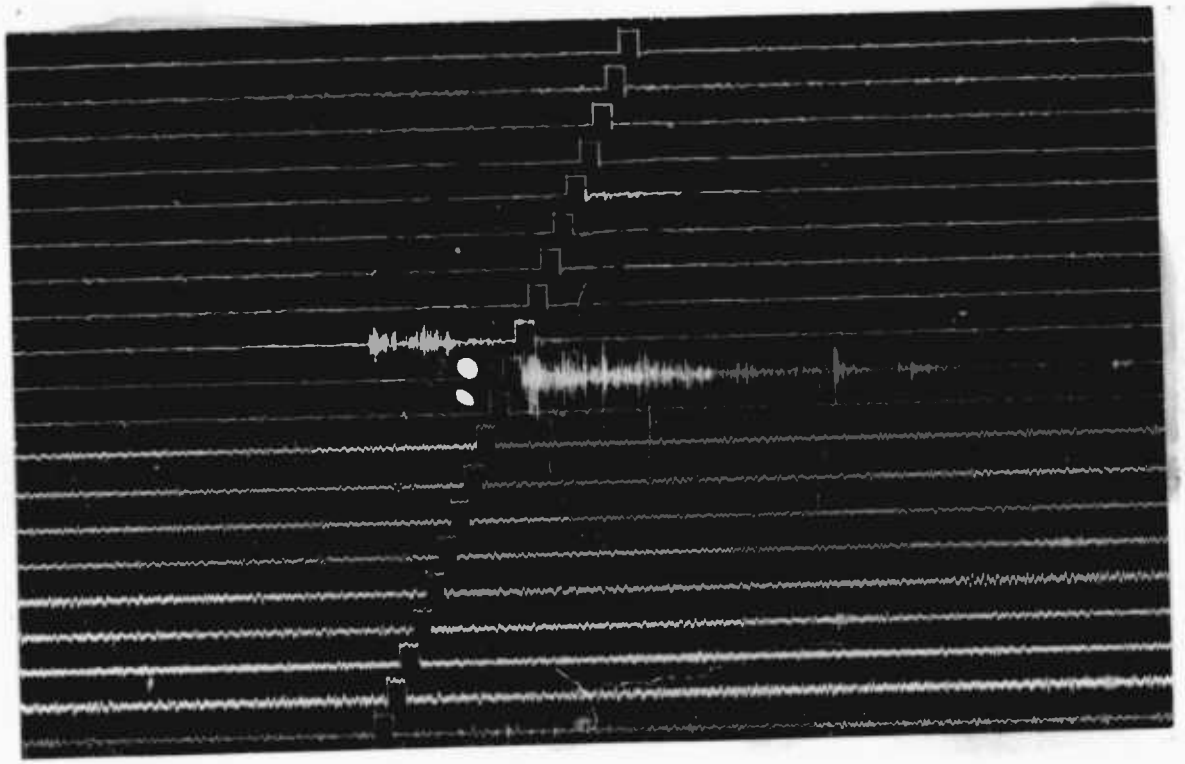


Figure 3.7a. Seismogram of B-type microearthquakes showing impulsive first arrival and no distinguishable P-S phases (recorded at Serra La Nave).

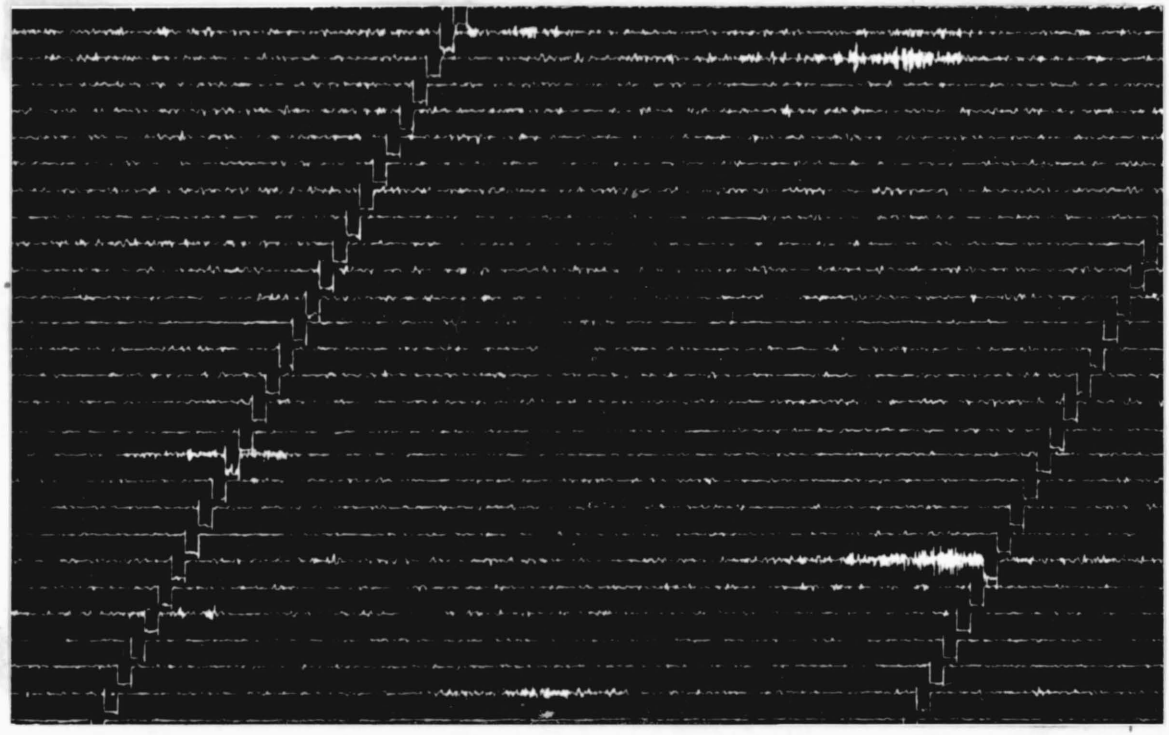


Figure 3.7b. Seismogram of B-type microearthquakes showing emersion arrival and no distinguishable P-S phases (recorded at IC bench mark).

a sharp and impulsive arrival, but appears to have no distinguishable P or S phases. The maximum amplitude in some of these events appears within the first few cycles, and the signal decays slowly before finally merging into the background volcanic noise. The duration of these events is not more than about 15 sec. On very quiet (background noise) days, shocks of very short duration and trace amplitude could also be identified. Figure 3.7a shows some typical examples of such events.

The third kind of events are best characterized by what is sometimes referred to as their 'emersion-type' arrival, unique signature, and short duration. These shocks, as with the second kind, have no clear P or S phases (Fig. 3.7c) and seem to attain their maximum amplitude about half-way through the oscillation. Many other investigators have reported similar kinds of events near active volcanoes (e.g. Minakami, 1960; Matumoto and Ward, 1967; Koyanagi and Endo, 1965; Unger, 1969; Wood, 1973; Lo Bascio et al., 1976; Guerra et al., 1976). These three types of microearthquakes appear to fall into the general classification scheme of Minakami (1960). The first kind is what Minakami designated A-type microearthquakes. They have focal depths of between 1 and 10 km, and are associated with all active volcanoes. They increase in frequency prior to and in the initial stages of an eruption. The signatures of this kind of microearthquake cannot be distinguished from those of shallow tectonic earthquakes. The P and S phases are clearly evident in both types.

The second and third types appear to be similar to Minakami's (1960) B-type volcanic microearthquakes. They have hypocentres limited to an area about one kilometer in radius around the active craters. In almost all cases the hypocentres are much shallower than the A-type volcanic microearthquakes, and they commonly occur in swarms. Since surface waves are predominant, the S phase is not clearly defined.

However, the critical criterion for defining both the A and B-type volcanic microearthquakes are their b-values, determined from the magnitude/frequency relationship, discussed more fully in Section 3.6.

The above described microearthquakes are very different from the other principal type of event, not recorded during the present survey. These are teleseisms from distant earthquakes. Teleseisms are characterized by a low frequency P phase and a long S-P interval. The duration of such shocks is generally measured in terms of minutes, and they involve long-period surface waves with relatively low amplitudes.

3.4.2 DISTRIBUTION OF S-P INTERVALS

Figure 3.8 shows the normalized frequency distribution of S-P times at two recording stations, Serra La Nave and Monte Nero. The distribution has been normalized for 1000 hrs of continuous recording at both stations. It is seen from the diagram that 68% of all the recorded shocks at Serra La Nave have S-P times of between 1.1 and 2.0 sec while, at the

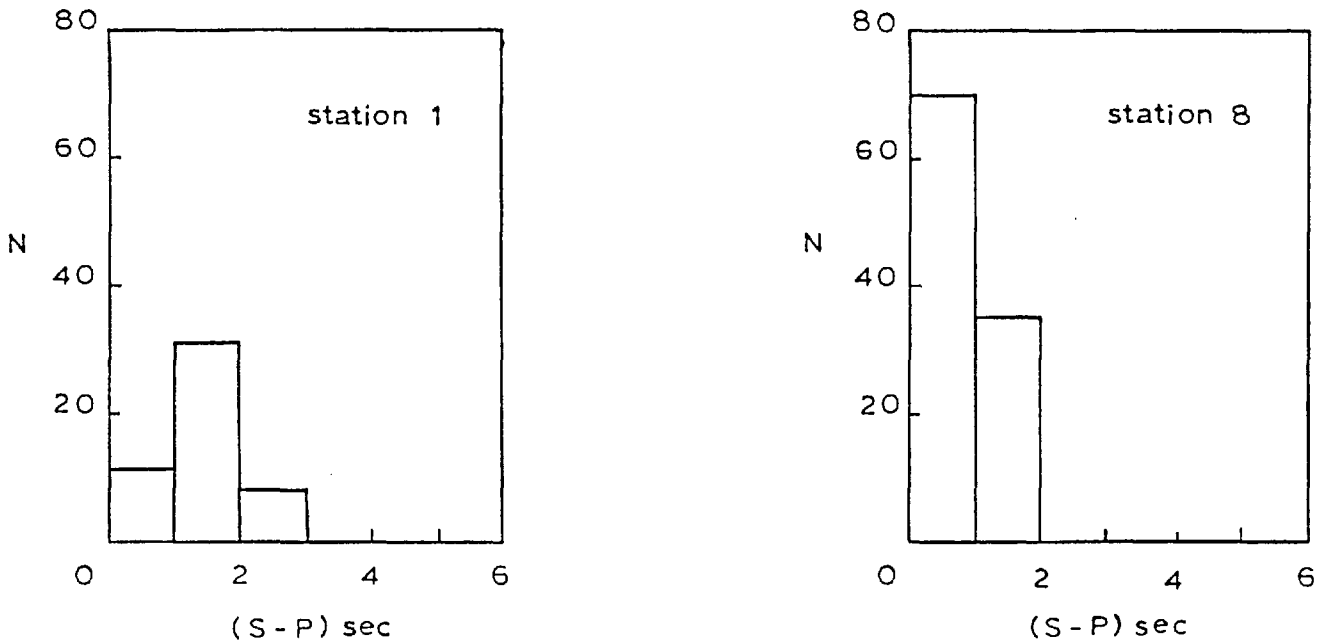


Figure 3.8. Normalized frequency distribution (for 1000 hrs.) of microearthquakes versus distance from the recording stations. Distances are in terms of S-P intervals.

other station approximately 70% of all the shocks have S-P times of less than 1.0 sec. These figures appear to indicate that the source of the seismic disturbance is much nearer to Monte Nero than to Serra La Nave (assuming of course that they originate from the same place).

In order to make an estimate of the epicentral distribution of these microearthquakes, an average P-wave velocity (V_p) of 5.0 km/sec was assumed (based on the seismic velocity studies of Cassinis et al., 1969). Taking Poissons ratio (σ) as 0.25, the shear wave velocity (V_s) is $0.59V_p$ or 2.95 km/sec. Now the P-wave travel time (t_p) for an epicentral distance d is d/V_p, and the corresponding S-wave travel time (t_s) is d/V_s. Thus:

$$t_s - t_p = d\left(\frac{1}{V_s} - \frac{1}{V_p}\right) = d\frac{V_p - V_s}{V_p V_s}$$

$$\text{Thus} \qquad d = \frac{V_p V_s}{V_p - V_s} \times (t_s - t_p) \qquad (3.1)$$

For $V_p = 5.0$ and $V_s = 2.95$ km/sec, this becomes

$$d = 7.2(t_s - t_p)\text{km}$$

As the maximum observed travel time in the present survey was rather less than 3 sec, this sets an upper limit to epicentral distance of about 22 km.

3.43 MICROEARTHQUAKE OCCURRENCE RATE

As explained in the introduction, the main purpose of the 1974 field survey was to gain experience of handling equipment at the sub-zero temperatures on Mount Etna, prior to the making of a more detailed survey the following year, also to obtain a measure of the level of seismic activity of the volcano.

During this 30 days of recording, nine stations were occupied (Fig. 3.5). The total recording time at each station, the number of hours of useable record, the number of microearthquakes of each type recorded, and the average daily rate are given in Table 3.2. In calculating the occurrence rate (shocks/day) the figures were in some cases derived from recording periods of less than a day, and in others more. The results are thus to be interpreted with caution. Obviously, the shorter the recording time the less reliable will be the average daily rate. These results indicate that, seismically, the most active area was the IC bench mark site (station 5). This site is approximately 2.0 km from the 1971 eruption site. Although this result was arrived at from only two days of recording, it is interesting to note the proximity of this, the most active recording site, to the '71 eruption. It might also be noted that all the events recorded at station 5 are of the B-type, a kind of shock that is believed to be connected with the active part of a volcano. The other two sites that show comparable activity are Serra La Nave (maximum $\simeq$ 22 shocks/day) and Monte Nero (maximum $\simeq$ 9 shocks/day). The microearthquakes recorded

Table 3.2

Microearthquake Activity

August/September 1974

Station	Recording time (hrs)		No. of microearthquakes			Number per day
	Total	Usable	A-type	B-type	Total	
Serra La Nave	269.00	261.00	13	63	76	7
Basement of Ski Club	5.30	0	-	-	-	-
Torre del Philosofo	18.50	0	-	-	-	-
Rifugio Citelli	6.20	0	-	-	-	-
IC Bench Mark (near Rifugio Citelli)	44.00	43.50	0	55	55	30
Inside a '71 Lava Cave	12.00	0	-	-	-	-
Inside a '74 Lava Cave	12.50	12.25	-	-	-	-
Near Monte Nero	143.50	143.0	15	10	25	4
Near Bronte	9.0	8.30	1	-	1	3

at Serra La Nave are a mixture of both A and B-type events, with the latter predominating. At Monte Nero, on the other hand, over 50% of all the recorded shocks are of the first kind. Unlike Serra La Nave, however, no small events could be identified at this station because of the constant presence of high amplitude background noise. At other locations the recording times were too short for any conclusion to be drawn. These microearthquake occurrence-rates give some indication of the seismic activity of an area and have the advantage of being derivable from recordings extending over short periods of time (though of course the shorter the period the less the certainty of obtaining a fair sample).

In order to determine the pattern of occurrence of microearthquakes in space and time, plots were made of the cumulative hours of recording time versus cumulative number of shocks. Figure 3.9a shows the result for station 1, where recordings were made continuously from the 6 - 14 Aug. a total of 175 hours, and from the 31 Aug. - 5 Sept. for 86 hours. Figure 3.9b is a similar plot for station 5 (for 44 hours) and 8 (for 143 hours).

From the nature of such graphs, if the seismic activity was constant with time the points would fall on a straight line. This is not the case; certain intervals of time are less active than others.

A straight line was fitted to the data by the method of least-squares, the slope of which gives the average activity of the site in question. It is seen from these

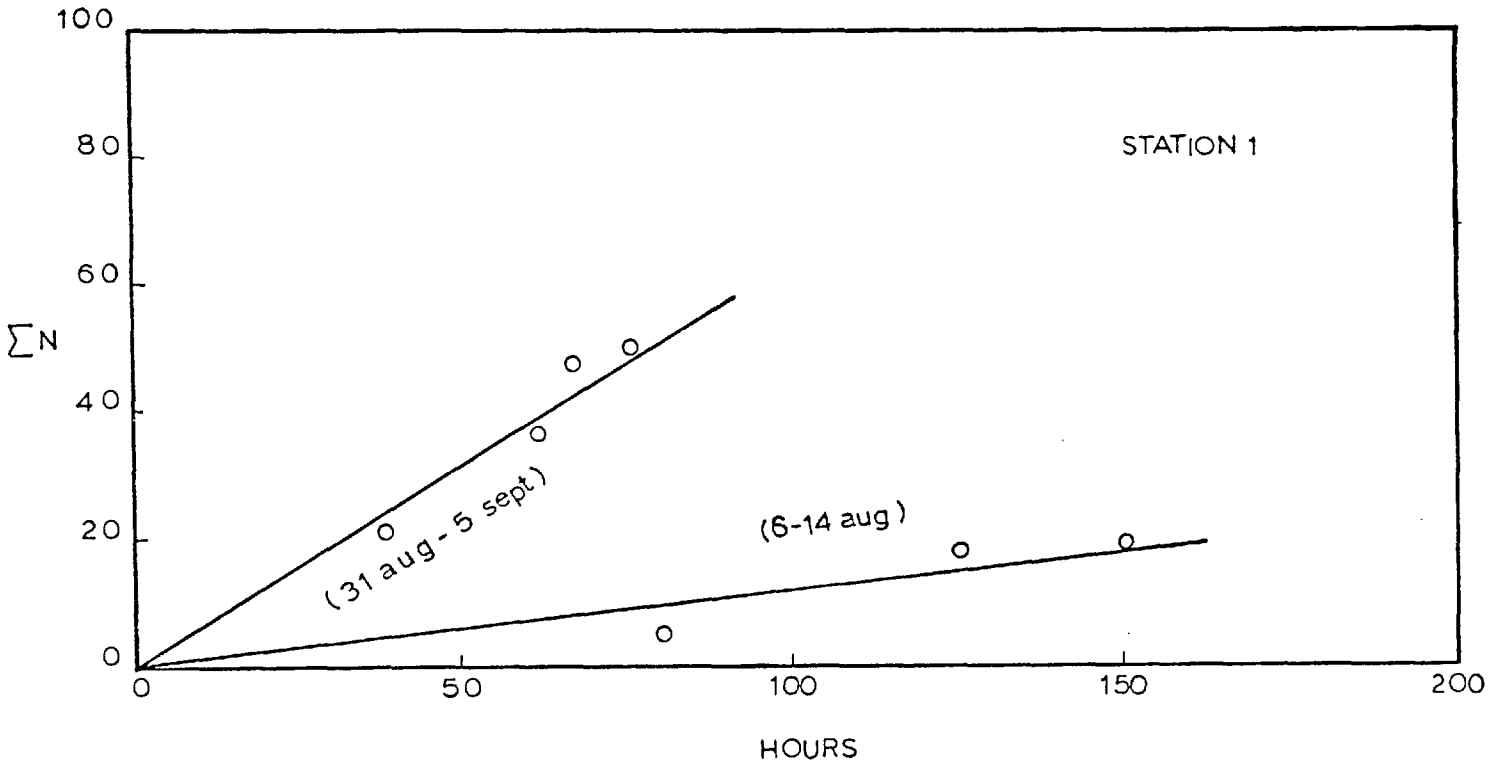


Figure 3.9a. Cumulative number of microearthquakes versus cumulative noise free recording time, for Serra La Nave during the two periods (as indicated). The straight lines are least-square fits for the respective periods.

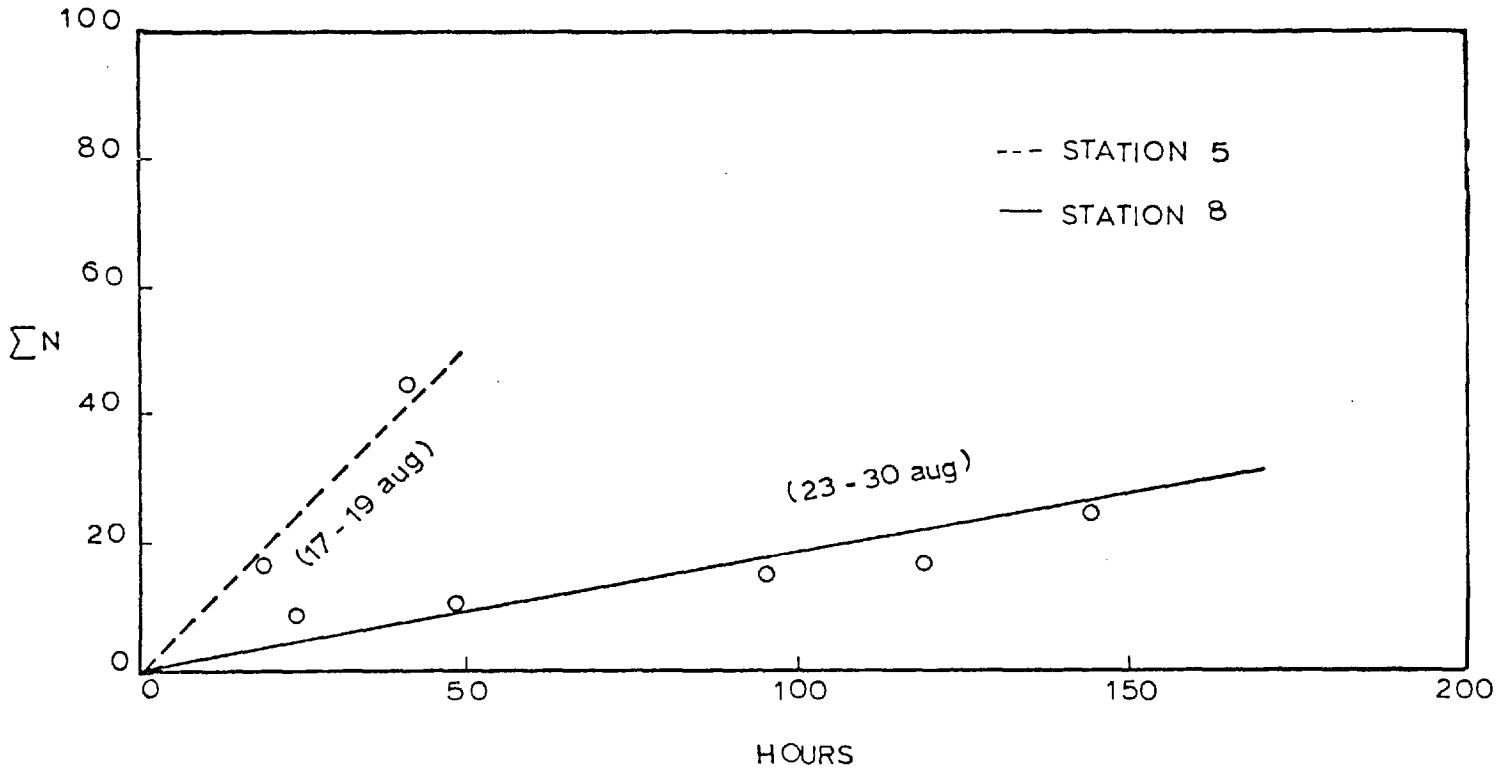


Figure 3.9b. Cumulative number of microearthquakes recorded versus cumulative noise free recording time, for IC bench mark and Monte Nero. The straight lines are least-square fit to the data, at the respective sites.

graphs that at station 1 the rate was very much greater in early September than it was three weeks earlier.

Another quantity, called the 'average activity' of the volcano, was calculated. This was defined as the total number of microearthquakes divided by the total number of days of usable record, and was found to be approximately 7 shocks/day. It is interesting to compare this figure with the results obtained in other volcanic regions. Matumoto and Ward (1967) investigating Mount Katmai and vicinity in Alaska quote a normal rate of between 40 and 80 shocks per day, with as many as 190 shocks on an exceptionally active day. At Mount Tsukuba Japan, Asada (1957) recorded 200 events per day. At Kilauea volcano the average activity ranges from 50-100 per day (Moore and Krivoy, 1964). Wood (1974), during a microearthquake survey of various Central American volcanoes, recorded from as few as 7 events/day at Masaya volcano to more than 1500 events/day at San Cristobal volcano. Del Pezzo et al. (1974) investigating Mount Stromboli recorded as many as 212 events/day. On Mount Etna itself Guerra et al. (1976) recorded up to 3 events/day. These numbers and comparisons, however, must be interpreted qualitatively, as these observations are very much dependent on the interpreter and the type of equipment used. If any conclusions can be drawn from these results, it is that at the time of the reconnaisance survey of Etna the microearthquake activity, though low by comparison with some volcanoes, was not exceptionally so.

3.5 MICROEARTHQUAKES AND THE PROBLEM OF MAGNITUDE DETERMINATION

The concept of magnitude was first introduced by Richter (1935) to measure the size of shallow earthquakes in California. For this purpose he defined magnitude as the logarithm of the maximum recorded (trace) amplitude (expressed in microns) by a Wood-Anderson torsion seismograph with specified constants (free period = 0.8 sec, maximum magnification = 2800, damping factor = 0.8) when the seismograph was at an epicentral distance of 100 km. This quantity is now known as the local magnitude, M_L, but has never been very much used outside California. However, the basic idea was later extended for use at greater distances (still for shallow depth) by defining the magnitude M_s, which is based on the maximum amplitude (A) of surface waves having a period (T) of about 20 ± 2 seconds. Another magnitude m_b, known as the body wave magnitude, makes use of the amplitude (A) of the body waves at large distances from the epicentre and for events at any depth. M_s and M_b are the two magnitude measures now in common use.

In practice, M_L, can be determined for local earthquakes, but in applying it to microearthquakes modifications have to be made, for the following reasons:

(1) Because microearthquakes are so local, the amplitudes of the shocks depend more on the hypocentral distance than on the epicentral distance.

(2) The high-frequency, high-sensitivity, seismograph used

in this study differs considerably from the Wood-Anderson seismograph, which is the reference standard on the Richter scale.

(3) Crustal structure affects significantly the attenuation of near events.

In addition, some workers e.g. Mohajer-Ashjai (1975) and Hedayati (1976), have found that the small dynamic range of smoked-drum microearthquake recorders limits the use of magnitude relations based on record amplitude. Thus, if the gain is set so that the minimum detectable amplitude is 1 mm, and the pen excursion limited to $\pm$ 12.5 mm, to avoid undue interference between adjacent traces, then the seismograph can only deal with an amplitude range of 12.5 to 1 (or a magnitude range of little more than 1) without saturating the record. Fortunately, this was not a serious problem in the present case, as only a few A-type microearthquakes and no B-type had large enough trace amplitudes to reach saturation level. This indicates that in general (as was pointed out in Section 3.1) volcanic microearthquakes have much smaller magnitudes than (non-volcanic) tectonic microearthquakes.

To overcome these problems (especially 1, 2 and 3) recourse is often taken to a method developed by Tsumura (1967). Tsumura's method evolved from a study of the microearthquakes recorded at the Wakayama network in Japan, which showed that a relationship exists between the magnitude of a local earthquake and the duration of its recorded signal

above the background noise level. Tsumura found that for earthquakes whose epicentral distances were less than 200 km, and which occurred at depths of less than 60 km, the magnitude could be related to the signal duration by the expression

$$M = \alpha + \beta \log D \qquad (3.2)$$

where M = local magnitude

D = signal duration of the microearthquake in sec

and α and β are constants.

For epicentral distances of up to 1000 km, the expression is still valid, except for the addition of what is known as a time term (strictly speaking a distance term) Tsumura (1967). The final expression is then

$$M = \alpha + \beta \log D + \gamma(\Delta)$$

For the Wakayama region $\gamma(\Delta) \simeq 0.001$, where Δ (the epicentral distance) is in units of kilometers.

The first requirement of the method is thus a measurement of the signal duration for a number of microearthquakes (recorded in the portable system) whose magnitudes have been assigned by conventional methods. A least-square fit to these points give values of α and β. It is interesting to note that α in Eqn. (3.2) is the magnitude corresponding to a signal duration of 1 sec.

Tsumura's (1967) method has the advantage that it is simple and easy to use when α and β are available. As magnitude determined this way is dependent on the logarithm of the

signal duration, the method is relatively insensitive to uncertainties in the latter.

However, one big disadvantage of the method is that α depends upon the instrument being used and also upon local geological factors. As a result, the instrument has to be calibrated for each microearthquake survey.

The method has been used, apparently with success, in various parts of the world. Thus Tsumura (1967) used it to study the Wakayama region of Japan, and Crosson (1972), the Puget Sound region of Washington state. Others who have used the method are Lee et al. (1972) for Central Californian microearthquakes, Real and Teng (1974) for Southern California, and Langenkamp and Combs (1974) for the Elsinore Fault zone, also in Southern California. More recently, Mohajer-Ashjai (1975) and Hedayati (1976) applied it to their seismotectonic studies of Iran.

It is interesting to note that for the same region e.g. Southern California, Real and Teng (1974) and Langenkamp and Combs (1974) quote results which vary in their α values by as much as 88%. The β values are, however, more consistent.

3.5.1 MAGNITUDE AND CUMULATIVE FREQUENCY OF EARTHQUAKES ORIGINATING FROM VOLCANOES

An important fact first noted by Gutenberg and Richter (1954) is that, considering the earthquakes occurring in a given area within a given time, the number having a

magnitude greater than a given value decreases logarithmically with magnitude. This can be expressed by the relation:

$$\log N = a - bM$$

where N is the number of earthquakes of magnitude greater than M, and a and b are constants. a may have any value, since it represents the total number of earthquakes of magnitude greater than zero, and hence depends on the seismicity of the area and the length of the period under consideration. b, however, which is the slope of what is generally referred to as the recurrence curve, and represents the magnitude distribution of the earthquakes, is relatively constant for a given region, though varying from region to region, and generally lies between 0.5 and 3.5 (Isacks and Oliver, 1964). The important fact about b is that its value depends on the nature of the earthquake and it therefore has diagnostic value in distinguishing, for example, between tectonic and volcanic events.

Regarding microearthquakes originating from volcanoes, the most important study of cumulative frequency versus magnitude was made by Minakami (1960), who explains how to distinguish between the various types of microearthquakes from their b-values. From his investigations of the A-type volcanic microearthquakes originating from Hawaii and Aso-San volcanoes he concluded that the slope, or b-value, of these earthquakes lies between 0.8 and 1.2, about the same as for normal tectonic earthquakes in may parts of the world. As to the B-type volcanic microearthquakes, his data from Asama-Yama, Sukra-Zima and Usu-San seems to indicate b-values of from about 1.8 to

3.5, generally very much larger than the b-values of A-type microearthquakes. Thus the two types of microearthquakes can be distinguished not only by their visual characteristics but also by their quite different b-values.

3.5.2 DERIVATION OF b-VALUE FROM MAXIMUM TRACE AMPLITUDES

If it is assumed that the number $\delta N(A)$ of microearthquakes whose trace amplitude lies between A and $A+\delta A$ is inversely proportional to some power $m(>1)$ of A, then

$$\delta N(A) = kA^{-m}\delta A$$

where k is a constant.

Integrating from $A = \infty$ to A

$$N(A) = \frac{kA^{-(m-1)}}{-(m-1)}$$

or $$\log N(A) = \text{const} - (m-1)\log A$$

Replacing $\log A$ by M, this is seen to be equivalent to the expression for the number of shocks of magnitude > M ,

$$\log N = a - bM$$

the b being equal to m-1 i.e. $m = b+1$.

Attention was first drawn to this relationship by Ishimoto and Iida (1939) while studying the earthquakes occurring in the Kanto District of Japan. It was subsequently investigated by Suzuki (1953, 1954, 1958, 1959) who confirmed that Ishimoto-Iida's formula holds good irrespective of the

place of observation and of the magnification, as well as the response characteristics, of the recording instruments. Suzuki (1959) found that this relation sometimes holds also for aftershocks sequences of great earthquakes, but it was Asada et al. (1951) who found that the relation holds also for microearthquakes.

As can be seen from the above discussion, the frequency distribution of A is equivalent to the frequency distribution of magnitude. Thus the objective of investigating the magnitude versus occurrence frequency relationship in the microearthquake case can be accomplished through studying the frequency distribution of the maximum trace amplitude.

3.6 DETERMINATION OF THE b-VALUE FROM THE 1974 DATA

Determination of the b-value in the expression $\log N = a - bM$, requires some means for determining the magnitudes of the microearthquakes being studied. There are basically two ways of doing this, by using Tsumura's (1967) relation between magnitude and signal duration

$$M = \alpha + \beta \log D$$

or by using an amplitude relation of the form

$$M = \log A + k$$

(since we were not using the Wood-Anderson seismograph, the uncertainty in estimating M will then lie in the constant k).

The first method is used here to study A-type, and the second method to study B-type, microearthquakes.

(1) A-type Microearthquakes

In using Tsumura's relation

$$M = \alpha + \beta \log D$$

as a means for obtaining the M in the recurrence formula

$$\log N = a - bM$$

and hence enabling the b-value to be determined, it is not necessary to actually calculate the α or the M, though it is necessary to determine β as an intermediate step. The procedure is as follows:

Eliminating M separately from the recurrence formula and Tsumura's relation and from the Tsumura's formula and the relation

$$M = \log A + k$$

we obtain, respectively,

$$\log N = Q - b\beta \log D$$

and

$$\log A = R + \beta \log D$$

where $Q = a - b\alpha$ and $R = \alpha - k$, both of which are constants. N, A and D are all measurable quantities. Thus, by plotting log N against log D, a value can be found for $b\beta$. Similarly, by plotting log A against log D, a value can be obtained for β, and hence for b.

Two possible reading errors will however have to be taken into account in the determination of R and β. Firstly, the trace amplitude A cannot be read to an accuracy of better than 0.3 mm. Secondly, the estimated values of the signal duration (D) in the present case are perhaps accurate to no better than ± 5.0 seconds. Fortunately, both quantities appear as logarithms in the expressions, and in the present analysis the effects due to the errors in reading A were considered small in comparison with the reading errors in D, and hence were neglected. The signal duration was based on the time interval from the initial P arrival until, as far as can be judged, the recorded seismic signal falls to the same level as prior to the arrival of the micro-earthquake.

Twenty-one well-recorded A-type microearthquakes were selected for this study from two adjacent stations (Serra La Nave and Monte Nero). β was first found from a plot of logA versus logD (Fig. 3.10), using seven of the twenty-one events whose amplitudes could be read with the necessary accuracy (Table 3.3). The fit is good but is of course based on a small amount of data. β was found to be +0.62, and R, -0.08. No independent estimate of β is available in the area for comparison.

Figure 3.11 is a least-square fit to the plot of logN versus βlogD, using the above value of β. The b-value (based on all the twenty-one events, Table 3.4) in this case is found to be 0.99 ± 0.03. This lies within the range commonly found for volcano-

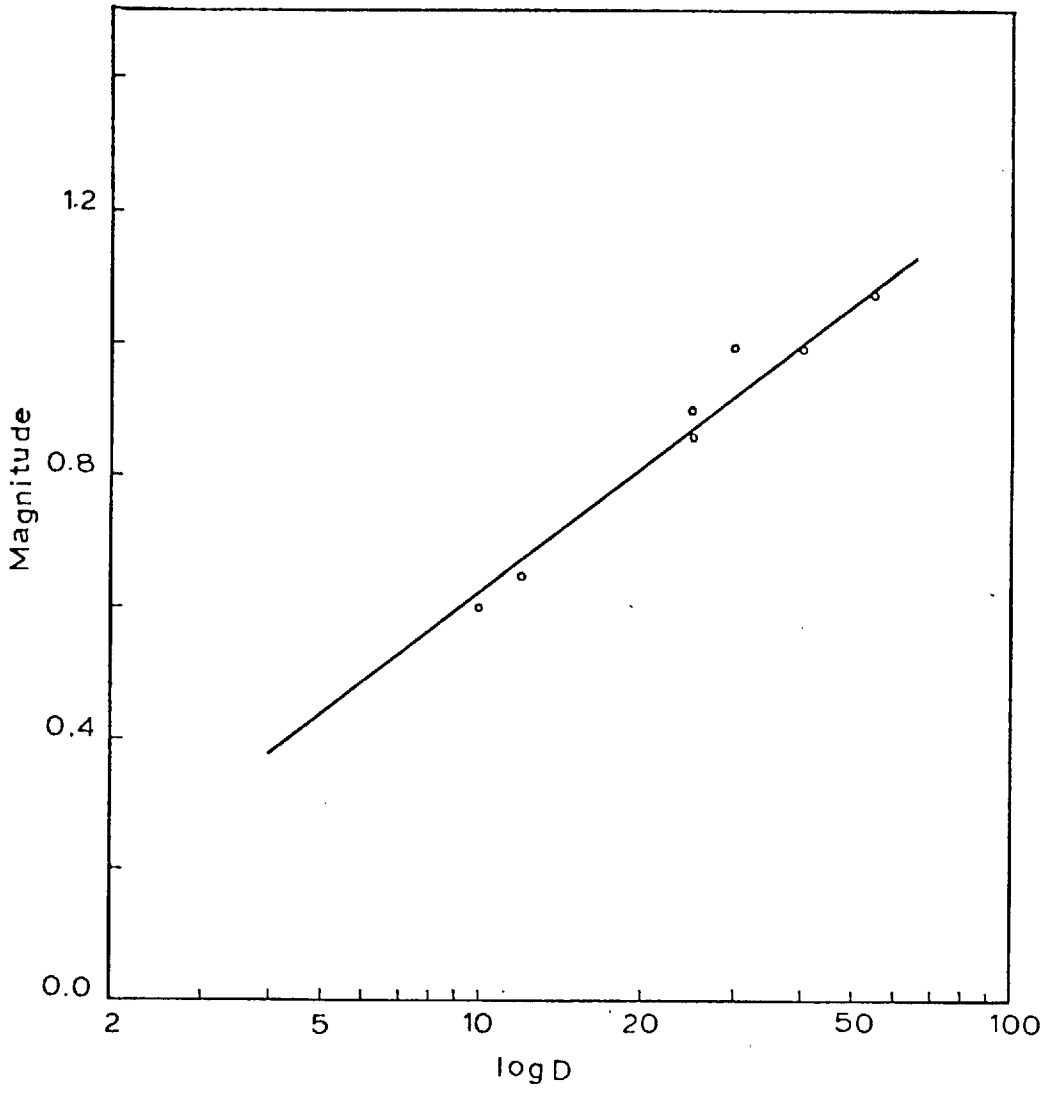


Figure 3.10. Plot of magnitude versus signal duration of volcano-tectonic microearthquakes recorded on Mount Etna (at Serra La Nave). The solid line indicates the least-square fit to the data.

Table 3.3

List of A-type Microearthquakes Used to Determine the β-value

Signal Duration (D) (sec)	Trace Amplitude (A) (mm)
10	4.0
12	4.5
25	8.0
25	7.5
30	9.0
40	10.0
55	12.0

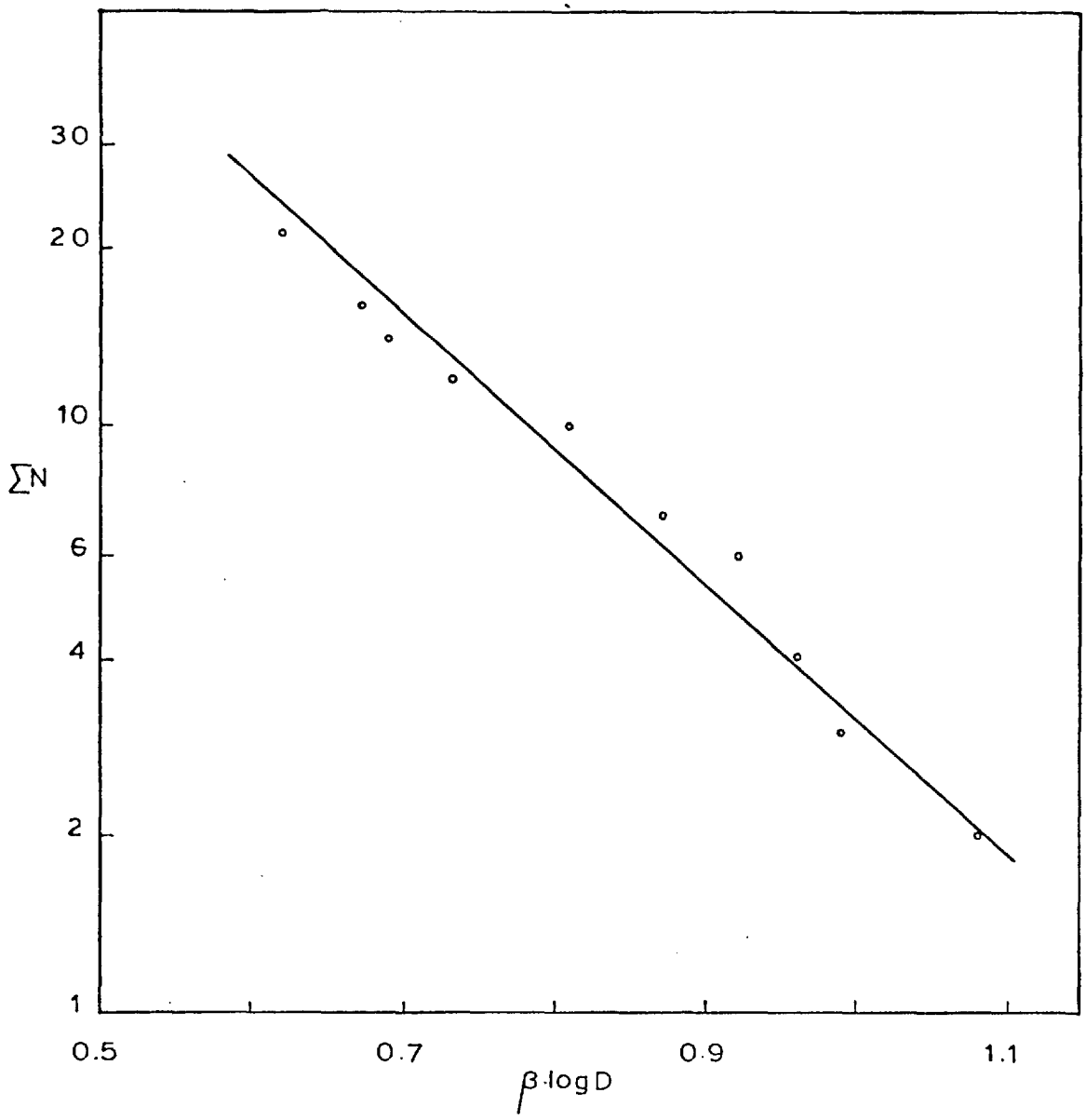


Figure 3.11. Plot of cumulative number of volcano-tectonic microearthquakes versus magnitude (the recurrence curve) recorded on Mount Etna. The solid line is the least-square fit to the data.

Table 3.4

List of A-type Microearthquakes Used to Determine the b-value

Signal Duration (D) (sec)	βlogD	ΣN
10	0.62	21
12	0.67	16
13	0.69	13
15	0.73	12
20	0.81	10
25	0.87	7
30	0.92	5
35	0.96	4
40	0.99	3
55	1.08	2

tectonic microearthquakes. It would be interesting to perform this analysis on a large sample of microearthquakes whose magnitudes are well known. If we accept the above analysis, the b-value for these shocks seem to support the previous belief that these microearthquakes are tectonic, or A-type volcanic, microearthquakes. Various other investigators have reported recording this kind of shock. Unger (1969) in an investigation of the microearthquake activity of Mount Rainier, Washington, obtained a b-value of 0.82. Westhusing (1974) made a reconnaissance survey of the seismic activity in the volcanoes of the Cascade Range, Oregon, and obtained a b-value of 0.80. On Mount Etna itself Guerra et al. (1976) calculated a b-value of 1.01 $\pm$ 0.05 during and after the 1974 eruption. Matumoto and Ward (1967) during a 39 day recording period in Mount Katmai and vicinity, Alaska, recorded 1800 events. A log-log plot of cumulative frequency versus the maximum trace amplitude produced a b-value of 1.42. This b-value is thought to represent a mixture of tectonic and volcanic type seismicity.

Large b-values have also been found elsewhere for supposedly tectonic earthquakes. Thus Sykes (1970) estimated the b-value of two earthquake swarms originating from the Mid-Atlantic Ridge. In both cases his b-values (1.3) are higher than would have been expected had the earthquakes been tectonic in origin. His conclusion was that along rift zones, where the temperature is high, earthquakes occur as a cataclastic process, hence the large b-value.

(2) B-type Microearthquakes

Fifty-five volcanic microearthquakes recorded at the IC bench mark site were selected for the analysis. The recorded trace amplitude A in this case ranged from 0.5 to 3.0 mm. The probable reading errors in the amplitude is about $\pm$ 0.3 mm.

Figure 3.12 shows a plot of the cumulative number of microearthquakes versus the logarithm of trace amplitude (the trace amplitudes of the fifty-five microearthquakes have been divided into six groups, each with an interval of 0.5 mm, see Table 3.5). It is seen that in the amplitude range between 1.0 mm and 3.0 mm the curve can be approximated by a straight line. A least square fit to the data gives a b-value of 1.78 $\pm$ 0.04. Departure of the points from a straight line for amplitudes less than about 1 mm suggests that this is the approximate detection threshold for the microearthquakes in this survey.

Thus the determination of the recurrence slope agrees well, at least within the calculated limits of uncertainty, with those of Minakami's (1960) B-type microearthquakes in Hawaii and Japan. Del Pezzo et al. (1974) made a similar survey of Stromboli, and their b-value shows good agreement with the present findings. Microearthquakes recorded at St. Augustine volcano, Alaska, by Mauk and Kienle (1973) yielded b-values mostly between 1.7 and 2.5.

The significance of the b-value for both the volcano and volcano-tectonic microearthquakes recorded in this in-

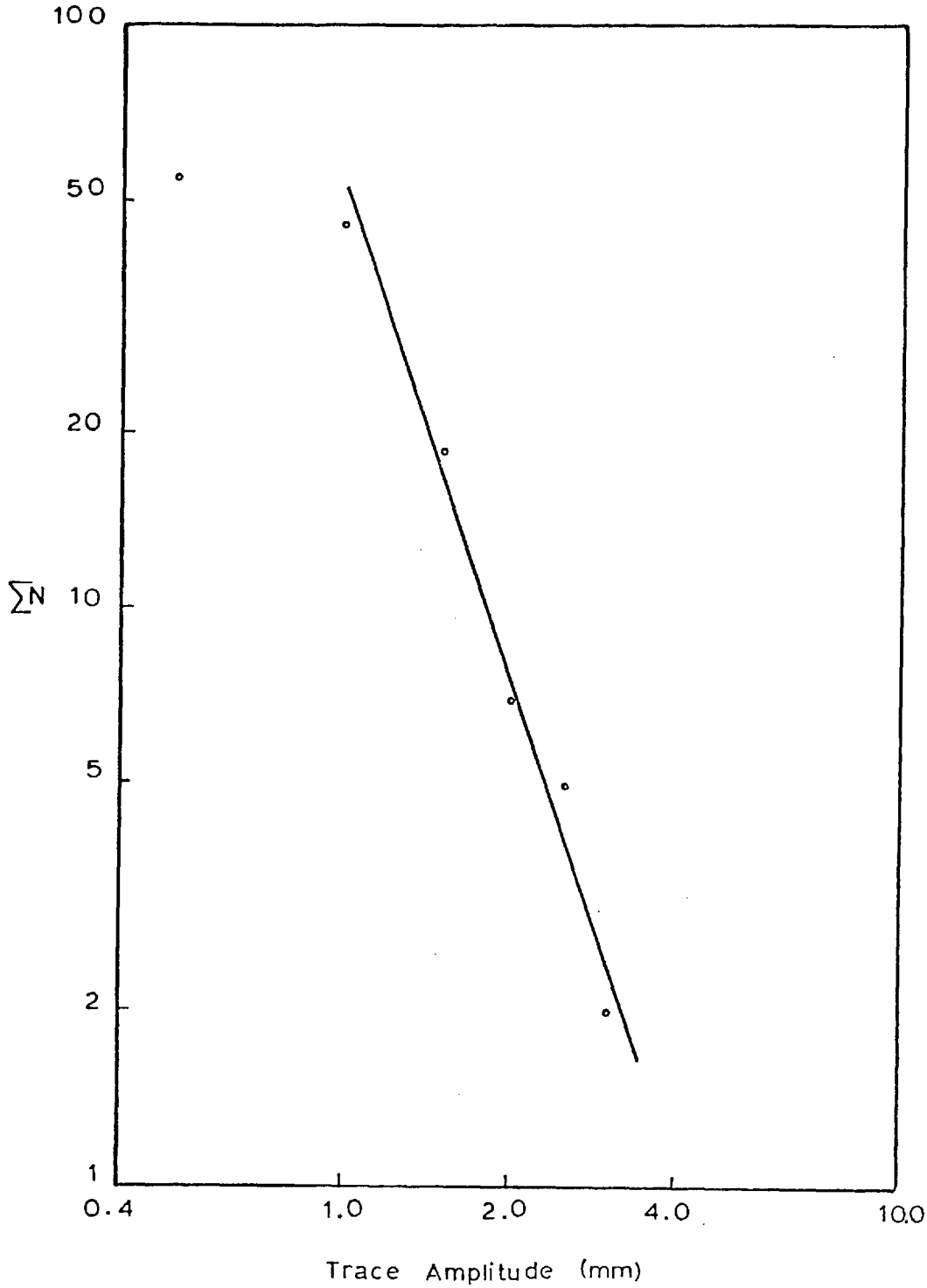


Figure 3.12. Cumulative number of recorded volcanic-microearthquakes versus maximum trace amplitude (the recurrence curve) for Mount Etna (at IC bench mark). The straight line is the least-square fit to the linear part of the curve.

Table 3.5

List of B-type Microearthquakes Used to Determine the b-value

Trace Amplitude (A) (min)	ΣN
A_{min} - 0.5	55
0.6 - 1.0	46
1.1 - 1.5	19
1.6 - 2.0	7
2.1 - 2.5	5
2.6 - 3.0	2

vestigation will be discussed in detail in Chapter 6.

3.7 ENERGY CONSIDERATIONS

The magnitude of an earthquake, as was shown in an earlier section (3.5), is a quantitative measure of its size determined from the amplitudes of the elastic wave it generates. The scale of magnitude now almost universally accepted was first developed by Richter. It was later modified to take into account earthquakes of any size and at any distance. The main significance of the magnitude lies in the fact that it permits a classification of earthquakes based upon the energy released. When an earthquake occurs, the original potential energy of strain stored in the rock is dissipated in the following ways:

(1) Part of the original potential energy goes into mechanical work, as in raising crustal blocks against gravity, or in crushing material in the fault zone.

(2) Part is dissipated as heat.

(3) Some is stored in other places as potential energy.

(4) The rest is radiated as seismic elastic waves.

It is thought that in the Californian earthquake of 1906 as much as 1.75×10^{24} ergs of energy was released, mainly in displacing crustal blocks. The Pamir earthquake of 1911 (magnitude 7.6) was calculated by Jeffreys (as reported by Richter, 1958) to have released about 10^{21} ergs. Sagisaka (also reported by Richter, 1958) estimated that about 3.1×10^{20}

ergs were released by a Japanese earthquake of magnitude 7.1 at a depth of 360 km.

In theory, the energy of an elastic wave of given period is proportional to the square of its amplitude. Thus if seismograms of different earthquakes at a fixed distance differed only in amplitude, their frequency content being the same, then their energy should be related to their maximum amplitude by the expression

$$\log E = c + 2 \log A$$

where c is a constant, or in terms of magnitude

$$\log E = c + dM$$

where c and d are constants. Various estimates have been made of c and d. Recent values, given by Bath (1973) are

$$\log E = 12.24 + 1.44M \quad \text{where E is in ergs.}$$

If the above equation is used to estimate the energy of the largest recorded earthquake ($M \simeq 8.7$), a value of 5×10^{24} ergs is obtained. This is about 0.05% of the annual energy of heat flow from the entire earth, which is taken to be 10^{28} ergs/year (Stacy, 1969). A further point of interest is the comparison sometimes made between a large earthquake and an atomic bomb. The energy released by a 'Hiroshima type' atomic bomb is about 8×10^{20} ergs. The largest earthquake ($M \simeq 8.7$) is thus seen to be equivalent to about 10^4 atomic bombs of that size.

The energy released in a microearthquake is obviously a very small fraction of that of a large earthquake, but the same physical principles might be expected to hold for both.

If the above equation is used to calculate the energies of the A-type microearthquakes recorded in 1974, we obtain values of the order of 10^{13} ergs. The energy released by the B-type microearthquakes is about one order less, i.e. around 10^{12} ergs.

It must however be remembered that since the microearthquake recorder could not be calibrated in the field against magnitudes determined independently by properly standardized permanent observatories, the estimated magnitudes, and hence the energy values quoted above, are very approximate.

CHAPTER IV

SEISMIC INVESTIGATIONS OF MOUNT ETNA DURING MAY - JUNE 1975

4.1 INTRODUCTION

In December 1974, analysis of the microearthquake data on Etna showed the volcano to be in a moderately seismically active state, and that the signature and characteristics of the microearthquakes were not fundamentally different from those recorded on other volcanoes around the world. This provided the impetus to carry out a more detailed study in May - June 1975. For this survey, four stations were operated simultaneously using Geostore magnetic tape recorders, borrowed fromthe NERC pool (Fig. 4.1), the Sprengnether microearthquake recorder being used to monitor the seismic signal at one of them. The various seismic phenomena observed from this study, and their volcanological significance, are discussed in this and the following chapters.

The first station occupied during the 1975 investigation was the Serra La Nave seismic vault (a brief description of which was given in Section 3.3). The station became operational on the 30th May. Apart from the routine check-up of instruments and changing of batteries, the recorder gave no trouble. This station operated continuously until the 16th of June, when a violent thunderstorm struck the area. Although the instrument otherwise continued to operate satisfactorily, the Geostore clock was completely upset, probably

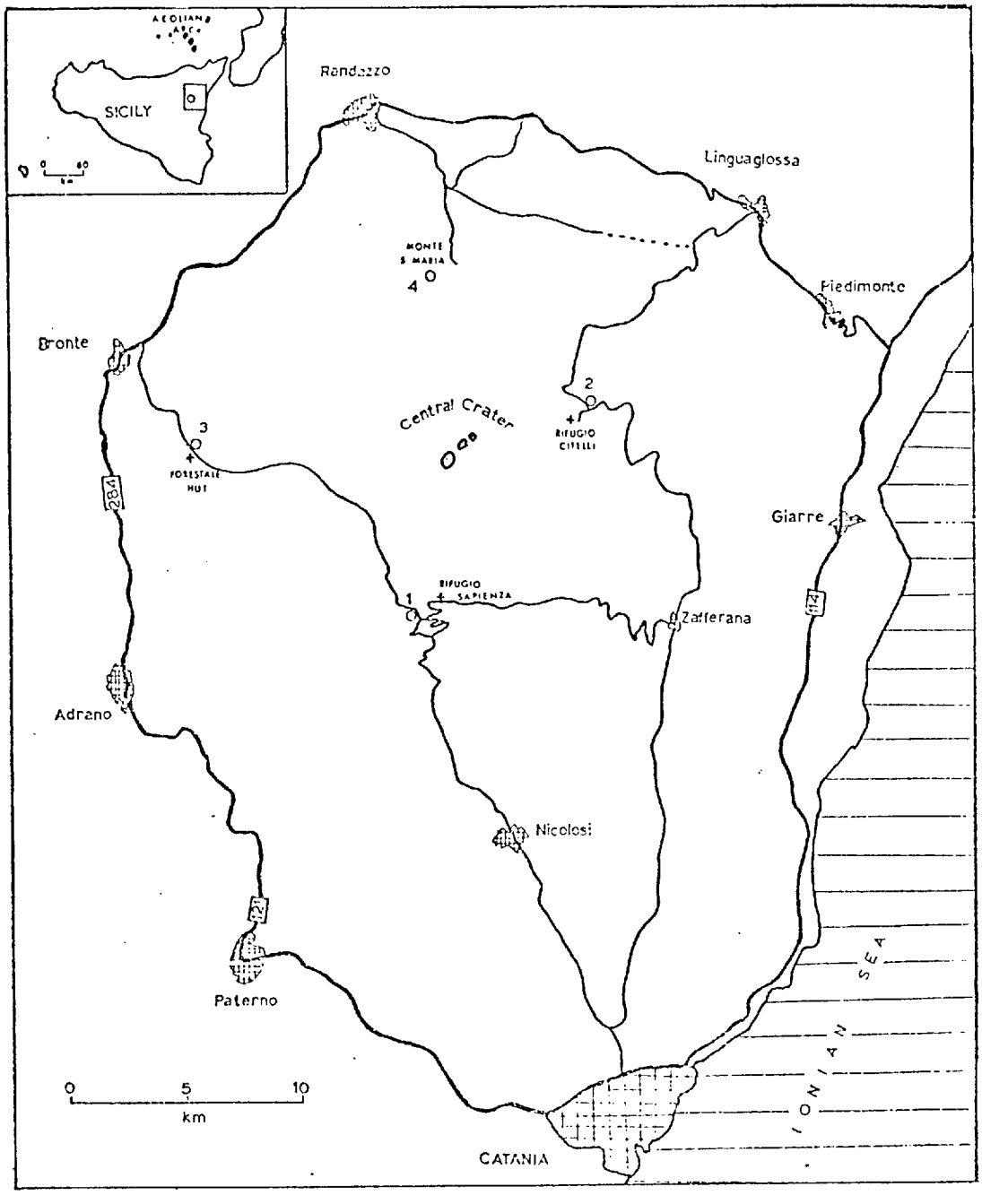


Figure 4.1. Sketch map around Mount Etna area showing the sites occupied in the present study. (The thick lines with numbers indicate highways and thin lines motorable roads. The dotted line is road under construction).

because of induction effects. The time of occurrence of microearthquakes subsequent to the storm could no longer be determined from the timing pulses, and the instrument was finally dismantled on the 19th June.

The second station, at the IC bench mark site near the Rifugio Citelli (see Fig. 4.1), worked continuously from the 2nd to 18th June '75 and gave no trouble whatsoever.

The third station, in the Forestale area, could not be set up before the 7th June, and proved to be the most troublesome of all. A new site had to be found for this station because the necessary permission could not be procured for re-occupation of the 1974 site. When the instrument started operating, it was discovered that the clock was malfunctioning. The fault was corrected but the clock worked for a short while only and broke down again. The seismograph then worked intermittently for the next few days, when finally after the thunderstorm of June 16th it stopped altogether.

The fourth station, below Monte S. Maria, became operational on the 8th June and worked intermittently until the 11th. From then onwards it recorded continuously until the 18th June.

Table 4.1 lists the station parameters.

4.2 THE RECORDING SYSTEM

The Geostore recording system consists of four basic units: (1) Geostore Magnetic Tape Recorder, (2) Seismometer,

Table 4.1

Network Station Data

Station	Latitude (N)	Longitude (E)	Elevation (m)	Foundation	Remarks
Serra La Nave (1)	37° 41' 40"	14° 58' 26"	1732	Lava flow	Same station as occupied in 1974.
IC Bench Mark (2)	37° 46' 02"	15° 03' 30"	1690	Lava flow	Displaced 5m to the NE of the 1974 site.
Forestale Hut (3)	37° 44' 45"	14° 51' 43"	1150	Lava flow	On a river bed about 10m NW of the hut.
Monte S. Maria (4)	37° 49' 23"	14° 59' 53"	1675	Lava flow	Same site as was inspected last year.



Figure 4.2. The Geostore portable seismograph.

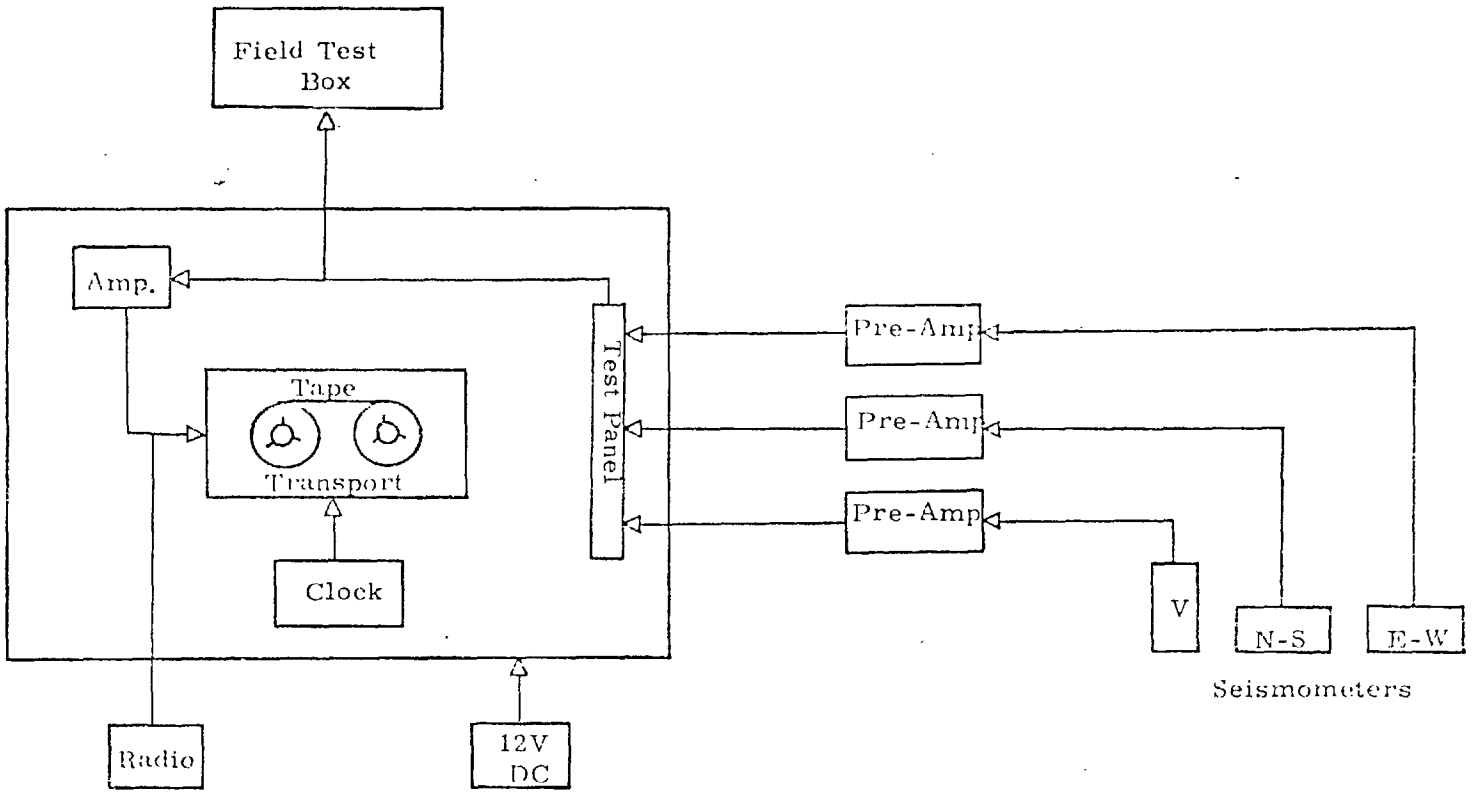


Figure 4.3. Block diagram of Geostore portable seismograph showing how the various components were connected in the field.

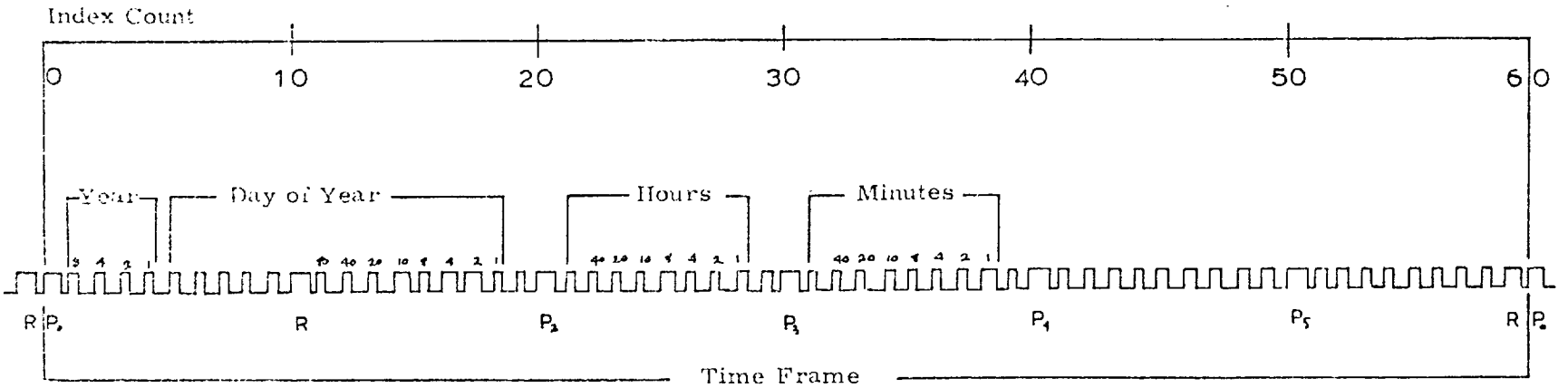
(3) Amplifier-Modulator and (4) Field Test Box. The various units are shown in Figure 4.2 and illustrated diagrammatically in Figure 4.3.

The Geostore system has not been used in volcanic environments before, although it was successfully used earlier by Hedayati (1976) in Iran.

A brief description of the different recording units used in the present study is given below.

(1) The Geostore Tape Recorder

The Geostore is a precision recording system for the acquisition and retention of seismic and other low bandwidth data. It accurately records FM data over a long period with very low power consumption. The Geostore tape recorder however differs from other FM recorders in that it contains no provision for frequency modulating a signal within itself, thus all inputs to this unit intended for the data channels must be FM signals, this however does not apply to an external 'Standard Radio Time Signal'. Eleven data channels are normally available, except in cases requiring the extended recording capability in the bi-directional mode, which doubles the recording time but reduces the number of signal channels from eleven to five. Recording speeds of $\frac{15}{160}$ to $\frac{15}{640}$ ips are provided, giving maximum recording times of 170 to 680 hours. Accuracy of recording speed is maintained by a phase-lock servo system referenced to a crystal oscillator. The 8" tape spool hold 2400 ft (730 m) of 1.0 to 1.2 mil, $\frac{1}{2}$in



P_0-P_5 = 0.8 sec. duration 10 sec. marks

Position Identifiers

R = 0.8 sec. duration - End of frame marks

Reference

R & P_0 denote 1 minute mark

Binary coded decimal bits - One = 0.5 sec
Zero = 0.2 sec

Unsued bits = 0.2 sec
Clock interval = 1 sec.
Time frame interval = 1 min.

Time Decoded reads:

Year = Zero

Day of year = 16

Hours = 8

Minutes = 1

Figure 4.4a. Vela - Standard Time Code used with the Geostore system.



Commencement of the first blip	055 sec
Duration of a short blip	100 msec
Duration of the long blip	500 msec

Figure 4.4b. Signature of the BBC World Service Radio Broadcast used in the present recordings.

tape.

The time encoder is an integral part of the recorder and provides time code (before recording data it is necessary to set the time code to zero,or to date and time), an accurate flutter compensation signal, and a capstan servo reference frequency. The timing signals from the encoder are accurate to one part in 10^6 over the full operating temperature ($-20^{o}C$ to $+50^{o}C$) range, and recording is in accordance with Vela Uniform Code for one minute time frames. Timing is in days, hours and seconds, which can be read numerically. The time decoded frame for one such unit is shown in Figure 4.4a. When the key operated security switch is turned,a push button associated with each digit enables the date/time to be updated. Facilities are also provided to allow the recording of a broadcast time code onto a data channel. The channel concerned may be used solely for the radio time code, solely for data, or in an automatic sequencing mode (radio recorded for every 40 sec every hour). The centre tracks on each record head are used to record a reference track which is used by the Base Reproducer (to be discussed later on) to improve the overall signal-to-noise ratio of the system. A 37-way socket is provided which, in conjunction with the Field Test Box (see 4), will monitor selected points within the recorder, in order to verify the correct functioning of the equipment.

A 12 volt power supply is required to operate the equipment, normally a car battery. Facilities are available

for changing batteries without disturbing recording or time.

(2) The Seismometers

Six Geospace HS 10 and six Willmore MK·II seismometers were available. The former has a natural frequency of 2 Hz, a coil resistance of 390 ohms and an intrinsic voltage sensitivity of 1.36 v/cm/sec, and a frequency response essentially flat between 2 and 50 Hz. The Willmore MK II seismometers have a natural frequency of 1 Hz, a coil resistance of 50 ohms, a sensitivity of 1.50 v/cm/sec, and a frequency response flat in the region between 0.3 and 1 Hz, beyond which it falls off sharply.

The six Willmore seismometers were used in pairs to record the two horizontal components at each of three of the stations, the HS 10's being used to record the horizontal components at the fourth station and the vertical component at all four.

(3) The Amplifier-Modulator

The seismometer is often situated at some distance from the recorder, and connected to it by long cable or radio link. The Amplifier-Modulator is intended to be installed close to the seismometer, and serves the dual function of pre-amplifier and frequency modulator, converting the amplitude modulated output of the seismometer into a frequency modulated signal for direct recording on the magnetic tape recorder. The carrier frequency is 676 Hz, and the maximum linear frequency deviation is 40% i.e. the maximum frequency

with which it can deal is 270 Hz.

The Amplifier-Modulator requires a single voltage supply in the range 10 - 18V d.c., which is normally fed along the signal lines but may be fed in locally through a separate connector. The typical power consumption at 12V is 75 mW. The Amplifier-Modulator has ten switched gain ranges so that 40% frequency deviation is produced by input voltages of 0.25 mV to 250 mV. The operating temperature of the unit is $-20^{o}C$ to $+50^{o}C$.

The Amplifier-Modulator is fitted with a socket for connection to the Field Test Box so that operational checks can be performed without disconnecting it from the system.

(4) The Field Test Box

The Geostore recorder, which is basically a magnetic tape recorder, contains no provision for monitoring what is being recorded, this function being provided by the Field Test Box. This consists of a strip chart recorder which can be used as a 'short-run' seismograph or it may be used to monitor any channel whilst the Geostore system is in use. It was not possible to carry this unit to Sicily because of excess weight problems. Instead,an alternative Field Test Box was carried that was much smaller in size and lesser in weight than the one mentioned above. This test unit however produced only audio signals when connected to the various recording channels in the Geostore system.

4.2.1 THE EQUIPMENT SETTING UP AND OPERATING PROCEDURE

Each individual site was carefully selected for freedom from traffic noise, ease of access, stability of bedrock,and for low background noise. A detailed survey conducted in the previous year with the Sprengnether MEQ 800 provided the necessary information.

A magnetic compass was used to align the horizontal seismometers so that they were in the geographical N-S and E-W directions. The seismometers were then emplaced by digging through the thin soil, so that their legs were firmly in contact with the bed rock. They were then connected to the three available data channels in the Geostore via three Amplifier-Modulators. External radio connections were made to a separate data channel. The time code,using the Vela-Standard,was recorded on a fixed channel. Power to the system was supplied by a heavy duty 12 volt, 54 AH battery.

Before recording any data,it was necessary to set the time code. The clock on the Geostore was set against a chronometer kindly made available by the personnel at the Astrophysical Observatory. The days and hours were set to their correct GMT values. In the present investigation one recording speed was used ($^{15}/_{320}$ ips), giving a d.c. to 16 Hz bandwidth in real time, and an effective -48 dB of signal-to-noise ratio. The overall magnification of the portable system depended on the gain level used in the field. Throughout the whole recording period an amplifier gain of 86 dB was

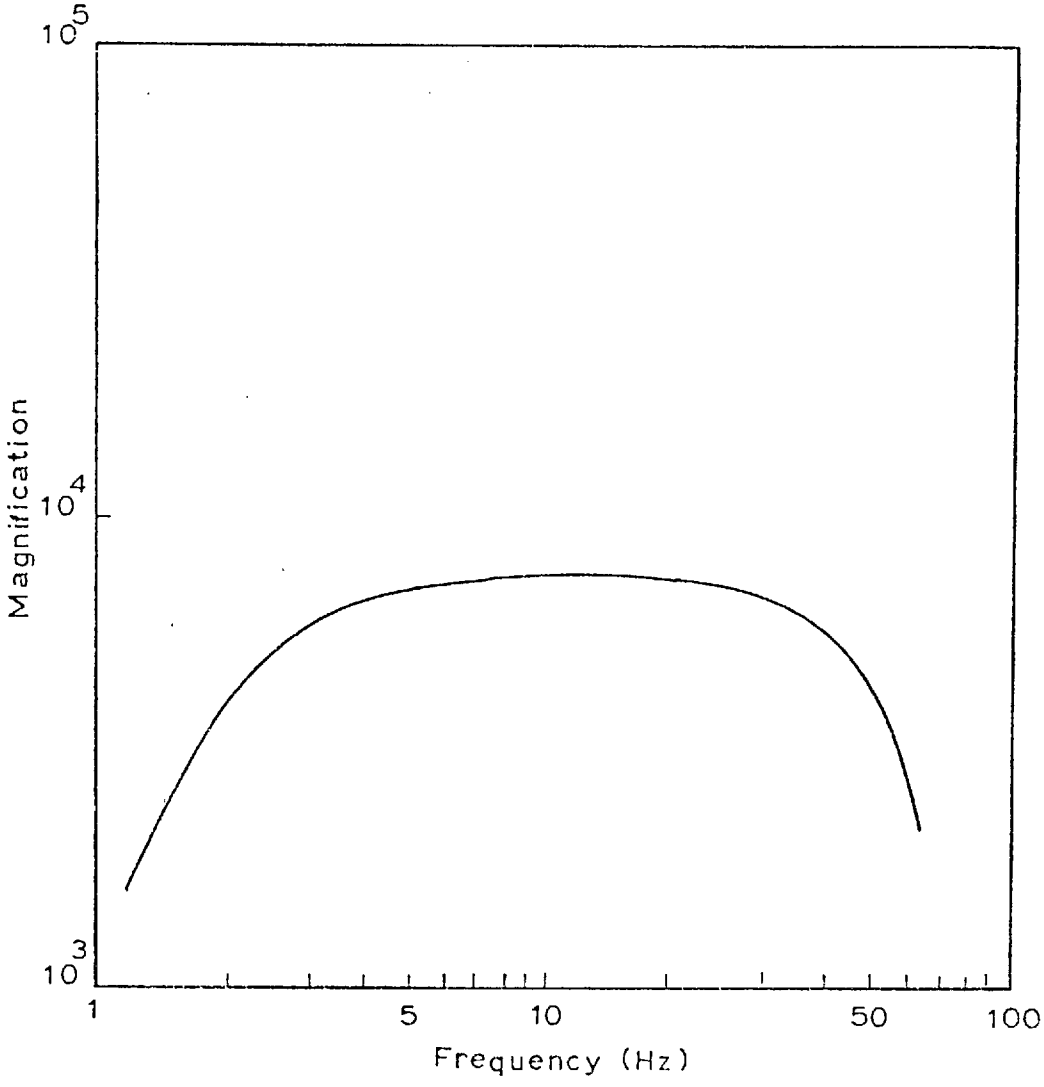


Figure 4.5. Response curve for the Geostore seismograph system.

used, giving a magnification of about 1 x 10^4. The approximate frequency versus magnification curve of the Geostore system operating at full gain is shown in Figure 4.5 (compare this response curve with that of the MEQ 800 given in Fig. 3.3).

An ordinary 'Zenith' radio receiver was used to pick up the BBC world service hourly broadcast signals. A played-back section of this time signal is shown in Figure 4.4b. Each tape on the seismograph provided from four to six days continuous record. The battery was replaced by a freshly charged one every three to four days, at which time routine maintenance was performed on the instrument. The whole Geostore system, whenever possible, was placed either in a shed or cave, and covered with plastic sheet.

After the termination of twenty recording days, nine magnetic tapes were brought back to London for further analysis.

4.2.2 THE ANALOGUE PLAYBACK SYSTEM

For selection of those parts of the tape suitable for detailed study it is necessary to have some means of displaying the record in analogue form. For this purpose 'The Geostore Base Reproducer' is available. In the present case the magnetic tapes were taken to the Eskdalemuir Seismological Observatory for transcription, as this was thought to be more convenient than transporting the equipment to Imperial College.

The Base Reproducer comprises a mains operated tape deck and an electronics unit,housed in separate cabinets. Two different head assemblies are available with the tape deck,the choice of which depends on whether uni- or bi-directional recording is employed in the field. For uni-directional recordings a full 14-track head assembly is used, and the tape replayed in one pass. In the case of bi-directional recording, the first replay run would reproduce half the tracks only. The take-up spool would then be transferred to the left hand side of the reproducer and a second run made for the remaining tracks.

A subtractive flutter compensation is used to reduce the base line noise and thereby improve the signal-to-noise ratio on all data channels. The compensated data outputs and the time code output are fed to a 15-way output socket. Additionally, a monitor switch enables any one channel to be switched independently to a separate BNC socket. From either of these outputs the final signals may be fed to a chart recorder (a Jet Pen Recorder in our case), computer or other analysing equipment.

4.2.3 PLAYING BACK GEOSTORE TAPES

Since a gain setting of 86 dB was used throughout, plenty of background noise was recorded on the tapes. It was thus essential to remove the background noise before any microearthquake could be well identified. From known work on volcanic background noise (Shimozuru, 1971; Schick and

Riuscetti, 1973; Lo Bascio et al., 1976; Guerra et al., 1976) it was decided to set the low-cut filter at 1 Hz and the high-cut filter at 30 Hz.

At first, it was intended to pick up events by playing the Geostore tapes on to an oscilloscope screen, but that proved difficult. It thus became necessary to play out the whole tape onto paper. The following steps were taken in order to ensure the best results.

(1) Five channels were selected on the Jet Pen Recorder and these were in turn connected to the Base Reproducer. The channels selected were as follows:

(i) The time signal.

(ii) The vertical HS 10 seismometer.

(iii) The horizontal (N-S) Willmore MK II or HS 10 seismometer.

(iv) The horizontal (E-W) Willmore MK II or HS 10 seismometer.

(v) The radio time signal.

(2) A time decoder unit was connected to channel (i) i.e. the time signal.

(3) A suitable combination of tape playback speed and chart recorder speed was first found. When searching for events, $3\frac{3}{4}$ ips playback speed and 10 mm per sec chart speed was found most suitable. After an event had been identified, a combination of $^{15}/_{16}$ ips tape playback and 100 mm per sec chart paper speed gives the best definition

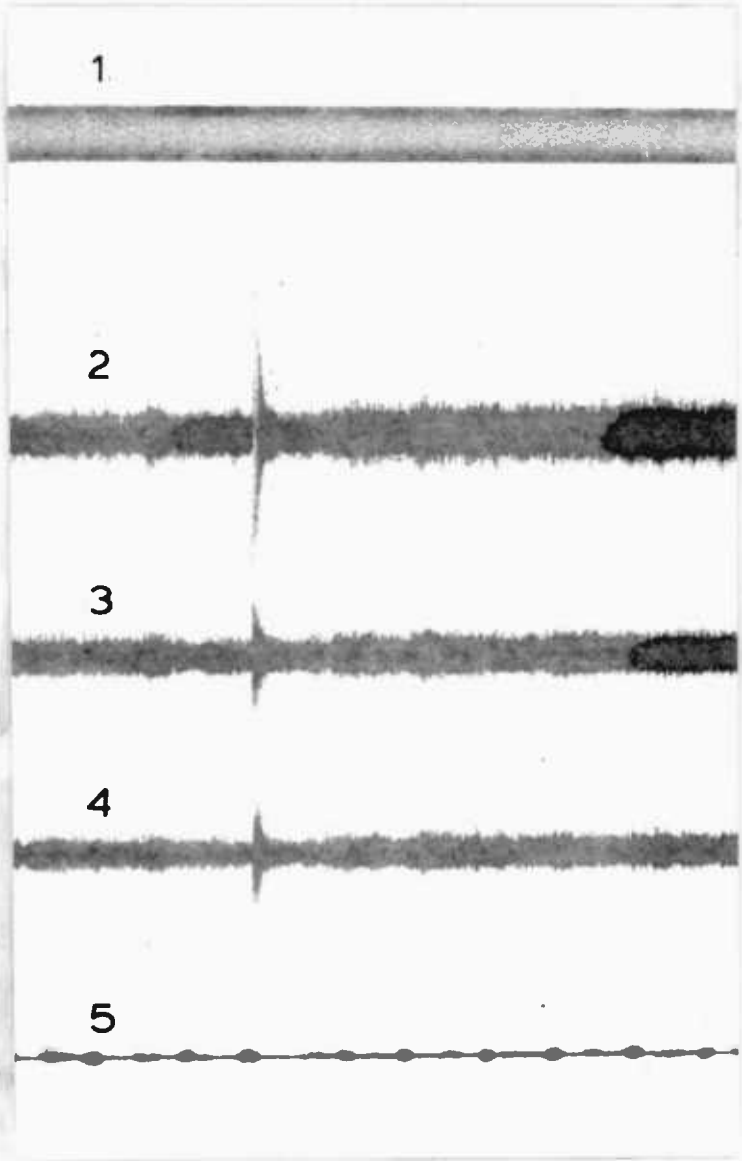


Figure 4.6. An example of a played back magnetic tape, using a playback speed of $3\frac{3}{4}$ ips (95 mm) and a chart speed of 10 mm per sec when searching for events. The channels from top to bottom are 1 : the time signal, 2 : Vertical, 3 : N-S, 4 : E-W components and 5 : the radio signal.

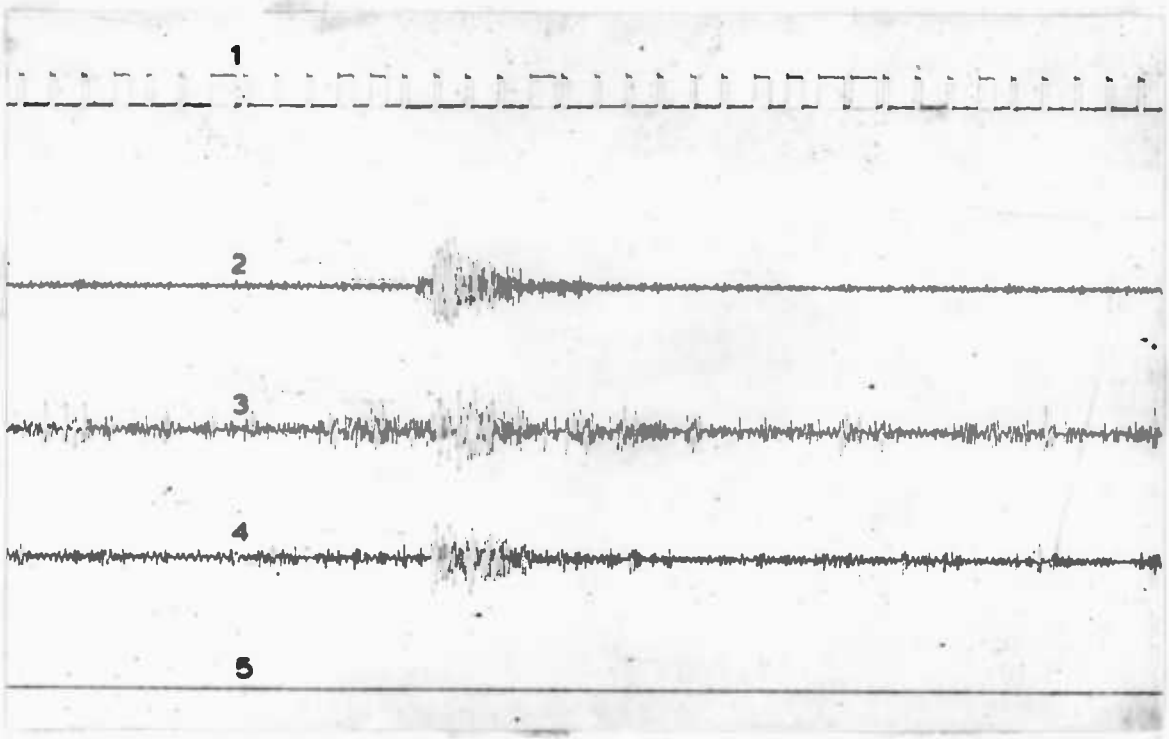


Figure 4.7a. Reproduction of an A-type microearthquake recorded by the Geostore using a playback speed of 15/16 ips (24 mm) and a chart speed of 100 mm per second. The channels indicated are the same as in Figure 4.6.

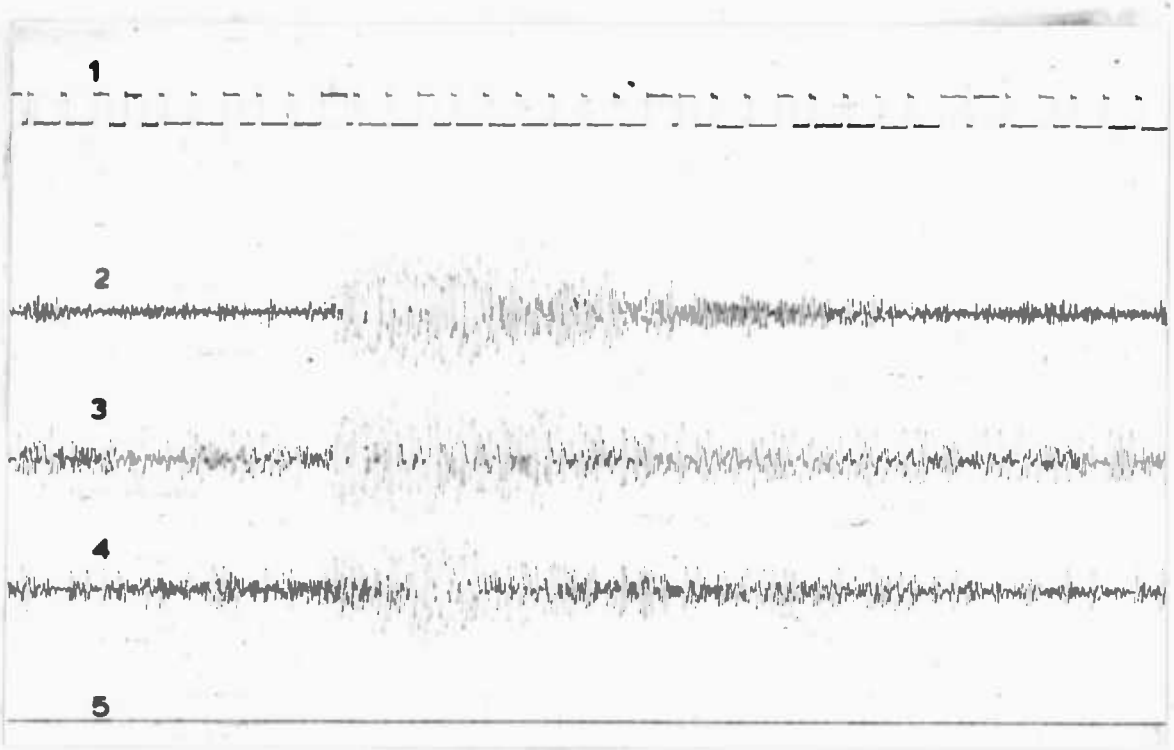


Figure 4.7b. Reproduction of a B- type microearthquake recorded by the Geostore using a playback speed of 15/16 ips (24 mm) and a chart speed of 100 mm per second. The channels indicated are the same as in Figure 4.6.

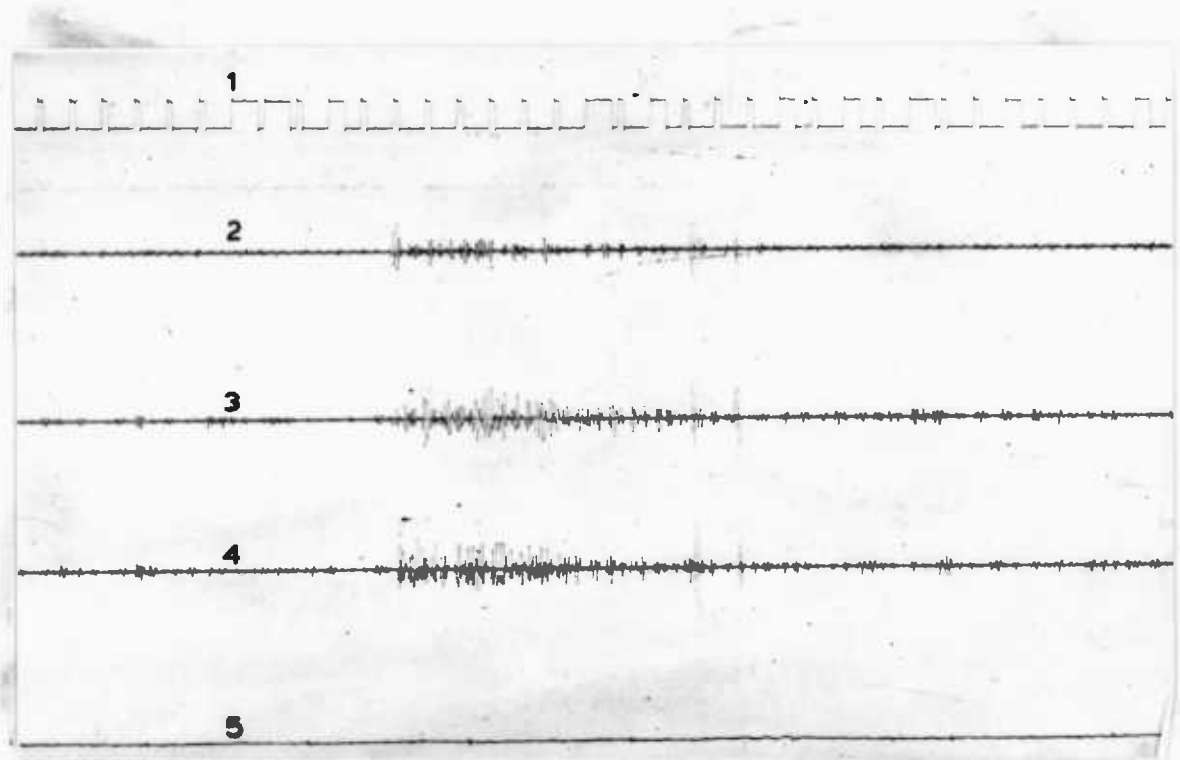


Figure 4.7c. Reproduction of a B-type microearthquake recorded by the Geostore using a playback speed of 15/16 ips (24 mm) and a chart speed of 100 mm per second . The channels indicated are the same as in Figure 4.6.

of onset time and first motion.

(4) The tapes were thus replayed at 80 times the recording speed using the first combination, and 20 times using the second.

(5) The low and high-cut filters were set to 80 and 2400 Hz on the first combination and 20 and 600 Hz on the second combination, respectively. This gave an effective passband of 1 and 30 Hz at the recording speed.

(6) The tape was started and played through the first combination ($3\frac{3}{4}$ and 10) until an event was found (Fig. 4.6). On finding the event, the time was noted from the time decoder unit, and the tape rewound a short way. It was then played back using the second combination ($^{15}/_{16}$ and 100). Figure 4.7a show the same event, and Figures 4.7b and 4.7c are two more examples, when played back using the second combination.

(7) The BBC radio signals were always played back using the second combination. A replayed version is shown in Figure 4.4b.

(8) As a second tape (from a different station) was replayed, care was taken to search the tape thoroughly at known times of events identified on the first tape.

(9) The same procedure was followed for all subsequent stations.

With practice, it is easy to pick out events from the background noise. Time marks are indistinguishable on the first combination but are legible on the second. It

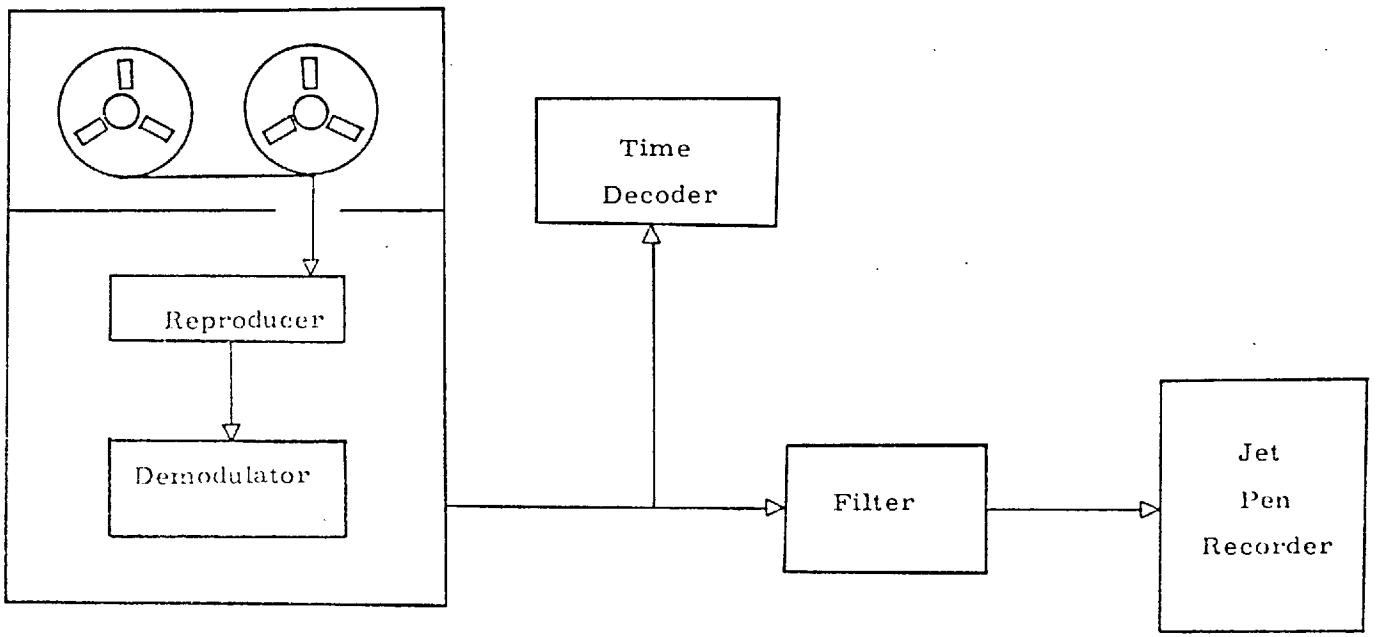


Figure 4.8. Block diagram of the replay system.

takes about 6 to 10 hours to go thoroughly over one tape, the time taken depending of course on the number of events.

Figure 4.8 is a schemmetic diagram of the replay system.

4.2.4 THE STORE-4 TAPE RECORDER

For the subsequent frequency analysis of the micro-earthquakes and volcanic background noise it was decided to transcribe the Geostore tapes on to the four channel $\frac{1}{4}$" tape of a Racal Thermionic Store-4 tape recorder. This was thought to be a more efficient course than to have to rely on the availability of the Geostore playback unit either for borrowing to use at Imperial College or for use elsewhere.

The Store-4 instrumentation recorder is designed to record four frequency modulated channels on 6.24 mm ($\frac{1}{4}$ in) magnetic tape. The recorder was used with instrumentation tape 35 μm thick (BASF, triple play) 2400 ft long and with a spool diameter of $6\frac{3}{4}$ in. Seven recording speeds are available from $\frac{15}{16}$ to 60 ips, selected by means of a rotary switch. The Geostore playback unit was run at a tape speed of $^{15}/_{16}$ ips, which is 20 times the original record speed. During transcribing on the Store 4, both the input and replay output signals were monitored by means of a signal monitor meter. The Store 4 was operated from the 230 V a.c. mains.

The four channels recorded were:

(i) The vertical component.

(ii) The horizontal (N-S) component.

(iii) The horizontal (E-W) component

(iv) The time signal.

In order to check the quoted figures of overall system linearity, ±0.3% deviation from best straight line through zero, and the harmonic distortion of < 1% at maximum modulation level, the following test was carried out. A small section of the output signal from the Geostore playback unit was centred around zero and stored on an oscilloscope screen. The same section was first recorded on the Store-4 recorder then played back and superimposed on the stored signal on the scope. From visual inspection of the records, no apparent distortion between the two signals could be seen. This test was carried out for a large number of tape sections recorded at different times and places.

It was thus concluded that the Store-4 reproduces the original signal faithfully to within the manufacturers specifications.

4.3 ANALYSIS OF DATA

Visual inspection of the records revealed the same three broad types of microearthquakes as were observed in the reconnaissance survey of 1974 and discussed in Section 3.4. Whenever an event was identified as an A-type microearthquake the horizontal component readings were used to facilitate the readings of S arrivals. The S-P intervals for the 1975 microearthquakes generally ranged from about

0.1 sec (in which case the epicentres are very near the recording station) to about 6 sec. The longer S-P intervals ($\gtrsim$ 3 sec), absent in 1974, might well arise from shocks associated with the local tectonic processes rather than with volcano-tectonic processes, as was the case in 1974.

The other two types of events (sharp impulsive arrival with no S-P phases, and emersion arrival, also with no S-P phase) defined as B-type microearthquakes in Section 3.4 produced similar kinds of traces on all three components. Both types will be discussed more fully in subsequent sections.

During interpretation of these played-back analogue records care was taken to avoid intervals with high background noise, and whenever possible the microearthquakes recorded at one station were compared with those recorded at the other stations. Primary timing pulses were provided by the Geostore clock, and these were checked against the standard BBC broadcast. Events could thus be read to an accuracy of about 0.05 sec.

Only three events provided seismic signals with sufficient signal-to-noise ratios at three stations to allow reasonable determination of their probable origin.

Two had identifiable phases and could be used for computer location by the programme HYPO developed in the Department. The third event had no clear phases (B-type shock) and a geometrical method was employed to locate the epicentre (Bath, 1973).

Apart from these microearthquakes, two other events with identifiable phases were recorded at two stations. A

crude method of locating their epicentres on the basis of their S-P intervals is given.

Bath (1973) discussed the possibility of crudely locating the epicentres of small events recorded at one station only on all three components. Epicentres for a few such well-recorded events were determined by this method. The procedure is discussed in detail in Section 4.4.3.

Volcanic tremors sometimes provide useful information about the volcano (see Chapters 1 & 5), and if intelligently monitored can be used for predicting eruptions. Continuous volcanic tremors were recorded throughout the whole recording period of observation. Their origin, mechanism and possible source are discussed in Chapter 6.

Preliminary selection of both the A and B-type microearthquakes for spectral analysis was also made at this stage, and the results are discussed in the second part of Chapter 5.

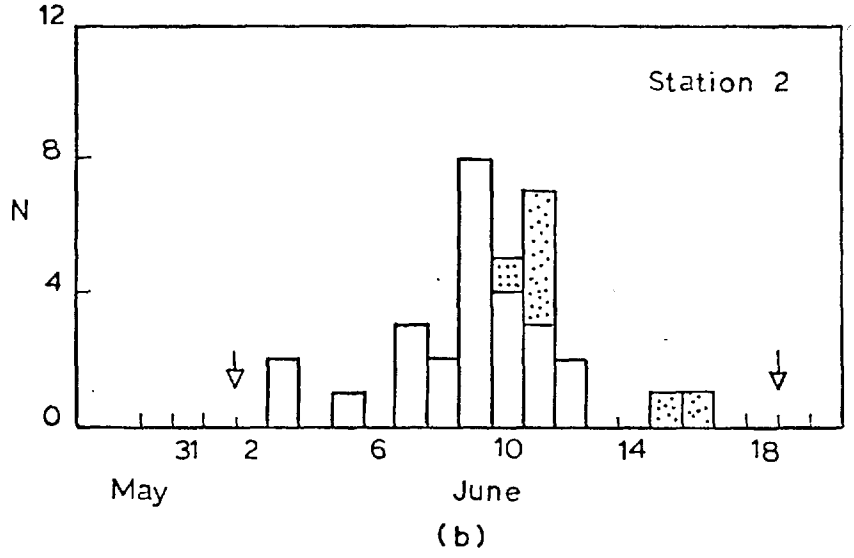
4.3.1 SEISMIC ACTIVITY OF THE VOLCANO

Statistics relevant to the occurrence rate of the A and B-type microearthquakes at the various stations are given in Table 4.2. Columns 1, 2, 3 and 8 of the table list the name of the stations, the total and useful hours of recording time and the total number of microearthquakes, respectively. The columns of particular interest are 4, 5, 6, 7 and 9. Columns 6 and 7 show the number of events that

Table 4.2

Microearthquake Activity

Station	Recording Time (hr)		Number of Events					
			A			B	Total	Per/Day
	Total	Usable	S-P(sec) ≤2.5	S-P(sec) >2.5	Total			
Serra La Nave	500.0	490.0	6	3	9	31	40	2
IC Bench Mark	384.0	380.0	7	4	12(1?)	24	36	2
Forestale Hut	24.0	22.0	2	0	2	3	5	5
Monte S. Maria	150.0	148.0	2	2	6(2?)	7	13	2



(a)

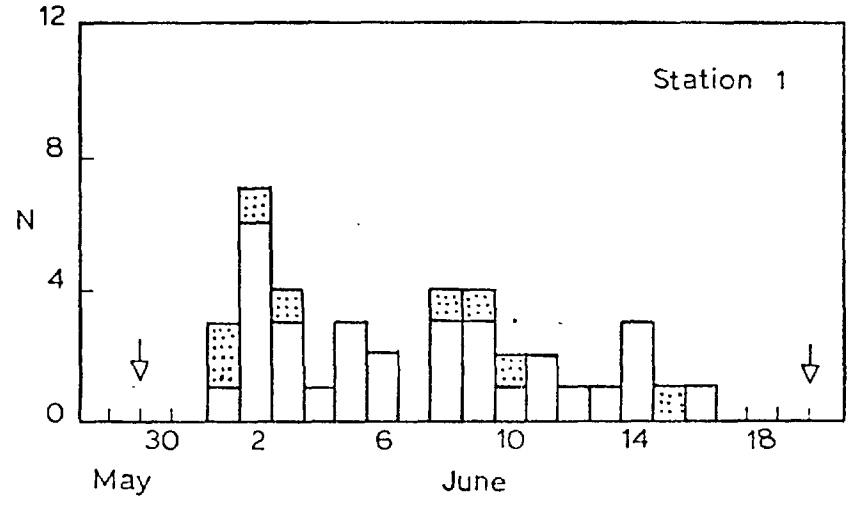
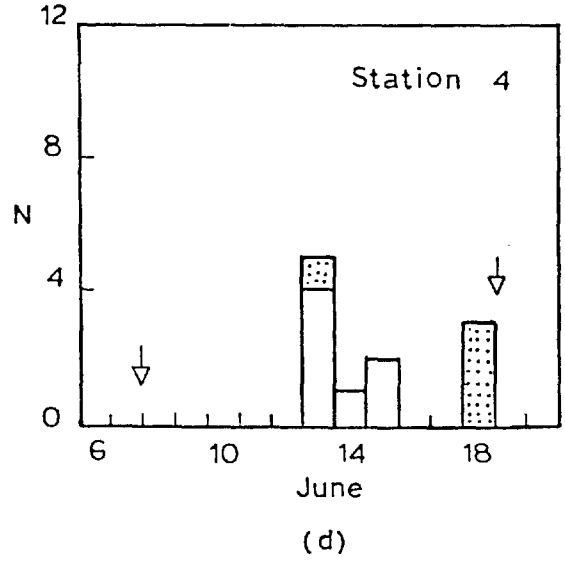


Figure 4.9(a-b). Graphs showing the total number of recorded events (N) plotted against the total recording interval (indicated by arrows). The dotted and blank area in each column indicate the number of volcano-tectonic and volcanic-microearthquakes respectively.



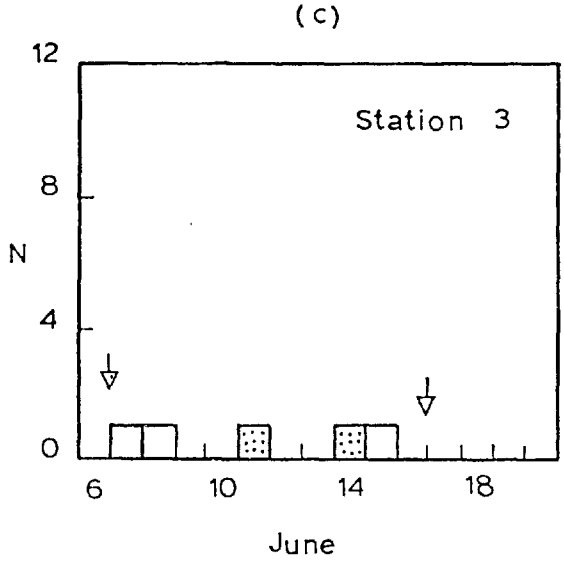


Figure 4.9(c-d). Graphs showing the total number of recorded events (N) plotted against the total recording interval (indicated by arrows). The dotted and blank area in each column indicate the number of volcano-tectonic and volcanic-microearthquakes respectively.

were broadly classified as A and B-type microearthquakes. The question mark against some of these numbers indicates their doubtful classification. The division of the A-type events (columns 4 and 5) into S-P times of 0 - 2.5 sec and 2.6 - 6.0 sec respectively were based on the 1974 results. The division is somewhat arbitrary but any events with S-P interval greater than 2.5 sec are thought not to be strictly volcano-tectonic microearthquakes, as they originate almost 20 km away from any recording stations (see Section 3.4.2), and possibly come from depths of >10 km, where the influence of the volcano in inducing events of this nature might be considered small. These type of events constitute about half the total A-type microearthquakes.

The figures in column 4 and 8 indicate that 20% of the total recorded events (excluding events with S-P > 2.5 sec) were of the A-type, while the figures in column 9 give the microearthquake occurrence rate (excluding any event with S-P > 2.5 sec).

Figure 4.9(a-d) shows the number of microearthquakes (excluding non-volcanic events) recorded at each station, plotted as histograms of the number of events per day. It is seen that there is no significant variation in the microearthquake occurrence rates (shocks/day) at the three recording stations. This is probably indicative of the volcano as a whole having reached some kind of 'seismic stability'. During this time no 'abnormal' movement of the magma took place, neither was any fumarolic activity above 'normal'

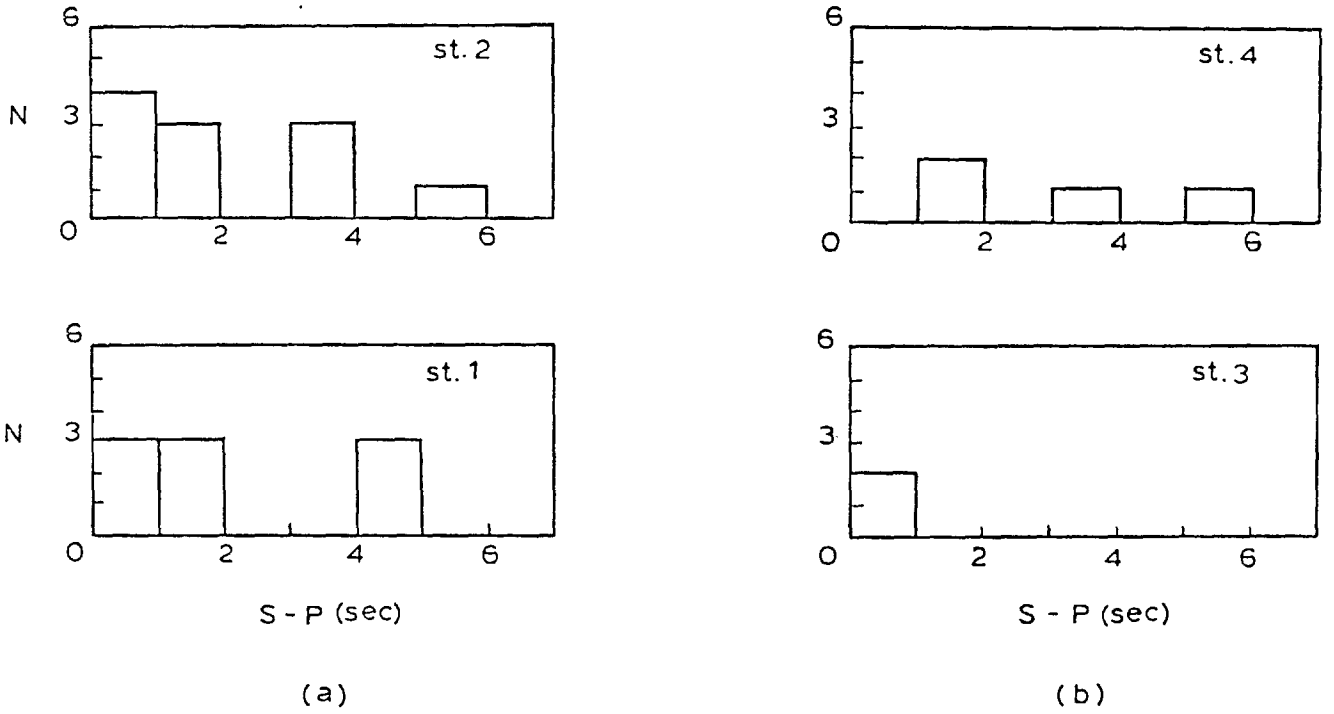


Figure 4.10(a-b). Graphs showing the frequency distribution of microearthquakes plotted against distances from the recording stations (in terms of S-P intervals).

noticed. These findings seem to be supported by Prof. Rittmann (verbal communication, '75) who described the volcano during the 1975 recording period as being "very quiet". An anomalous behaviour was however noticed at station 3, where the seismic activity level is more than double than that at the other stations. This difference, however, may not be significant, because of the short recording time, the microearthquake occurrence rate being based on only 22 hours of useful recordings.

It should be noted that during this short period of study no 'swarm type' bursts of energy, often seen elsewhere (Eaton, 1962; Robson et al., 1962; Matomuto and Ward, 1967; Mauk and Johnston, 1973), were observed, which further indicates the 'relative quiet' nature of the volcano during the 1975 recording period.

4.3.2 DISTRIBUTION OF S-P INTERVALS

Figures 4.10(a-b) show the distributions of S-P intervals for microearthquakes recorded at the four stations. At station 1, 2 and 3 the largest number of events fall in the S-P interval 0-2 sec, whereas at station 4 no events are found with an S-P interval of less than 1 sec. Some events are also distributed at the various stations with S-P intervals of 4, 5 and 6 sec. The distribution of the S-P times of all the recording stations taken together however seems to indicate a strong clustering of events. These groups have S-P values of 0-2 sec and 3-6 sec respectively.

If one assumes (see Section 4.4.3) an average P wave velocity of 5.0 km/sec,the first group involves activity at distances ranging up to 15 km, and the second group at distances of between 20 and 40 km from the recording stations.

These results suggests that the first group (0-2 sec) reflects adjustments to tectonic stresses within and around the volcano itself. Furthermore,the stress build-up appears to be concentrated in the area between stations 4, 1 and 2 (see Fig. 4.1). The second group (3-6 sec) appears to be associated with local tectonic forces much further away from the volcano.

4.3.3 MAGNITUDES

Estimation of Richter magnitudes was not possible in the present study as none of the Geostores could be calibrated in the field against magnitudes determined at permanent observatories. However,a rough estimate of the body-wave magnitude was made from the duration of the seismic signal using the values of R and β obtained from the 1974 results (see Section 3.4.7). Though the instruments used in the two years were quite different, there is no reason why the R and β values should be much different. Using the 1974 values of -0.08 and +0.62 for R and β respectively the body wave magnitude of the A-type microearthquakes appear to range between 0.4 and 1.5.

4.3.4 b-VALUES

The total number of events recorded during the 1975

survey was insufficient for determination of the b-value.

4.3.5 SEISMIC METHOD OF LOCATING MAGMA CHAMBERS

The finding of molten-pockets and considerations on their depth have so long been purely speculative. Recently,however,Gorshkov (1958) found that the waves from distant earthquake passing under a group of volcanoes in the Kamchatka suffered considerable weakening of the shear wave (S-wave). This attenuation was believed to have been caused by the presence of vast magma reservoirs in the upper part of the mantle, most probably at depths of between 50 and 70 km.

For a long time,this was the only available experimental evidence of shear wave attenuation by molten pockets of magma. Subsequently, many reports have been published of similar observations in other volcanic areas (e.g. Firstov and Shirokov, 1971; Farberov and Gorelchik, 1971; Kubota and Berg, 1967; Matumoto, 1971; Shimozuru, 1971a).

Kubota and Berg (1967), for instance, carried out several independent geophysical investigations looking for evidence for magma in the Katmai volcanic range. They observed a high value of 0.3 for Poisson's ratio, and the screening of the predominantly vertical component of the elastic shear waves. Local negative Bouguer anomalies also suggested the presence of low density material at shallow depths. The magma chambers were located using calculated wave paths for the rays exhibiting S-wave screening.

The most extensive investigation to date on the screening of S-waves was however carried out by Matumoto (1971) in the vicinity of Mount Katmai, Alaska. During an investigation extending from the summer of 1965 through 1967, as many as 40 to 50 events were recorded per day, the body wave magnitudes of which ranged from 0 to 3. Hypocentres were mostly shallow, < 10 km, although some occurred at depths ranging up to 150 km. Approximately 500 microearthquakes were simultaneously recorded at two stations. In some cases both P-and S-waves were recorded at one of the stations, but only P-waves and no, or very weak, shear waves at the other. The latter were also characterized by an increase in the apparent period of the P-waves, thought to be due to the absorbtion of higher frequencies.

The association of these two phenomena, the lack of an S-wave and the increase in the period of the P-wave, is not however very common throughout the whole area, but is confined rather to events originating from specific areas. Wave paths from hypocentres to recording stations plotted for twenty-five of these events strongly suggest that the disappearance of S-waves and probably the increase in the apparent period of P-waves are related directly to existing active volcanoes or possible magma chambers, magma pockets and zones of partial melting.

The phenomenon of partial or total screening of the shear waves by pockets of magma seems at the moment to be well established. As to the size and extent of these

pockets there is still a great deal of controversy. It is hoped that as more data becomes available these problems will be resolved.

One of the aims of the present project was to seek evidence for the existence of molten pockets by analysing S-wave attenuation and the increase in the apparent period of the P-waves, but approximately twenty days of recording did not provide suitable data for an analysis of this nature to be carried out.

It may not be out of place to mention here that the observation of shear wave attenuation and P-wave delays in local microearthquakes is one of the techniques being currently used to delineate liquid bodies in a geothermal environment. Local attenuation of shear waves from earthquakes have been observed in the geothermal areas in Yellowstone National Park (Eaton et al., 1975) and St. Lucia, West Indies (Aspinal et al., 1976).

Teleseismic P delays have also been observed in Yellowstone National Park and Long Valley Caldera, U.S.A. (Steeples and Iyer, 1975). These P velocity delays are consistent with their interpretation of an anamolous thermal zone, 300^{o} - 400^{o}C above normal. Combs and Ratstein (1975) also observed a decrease in the ratio of the P and S velocities, in the Coso geothermal area, California, U.S.A.. They interpreted this as due to the existence of a vapour-dominated reservoir where steam-filled voids cause a decrease in P

velocity.

4.4 REVIEW OF TECHNIQUES USED TO LOCATE LOCAL EARTHQUAKES

Any source of seismic disturbance, either an earthquake or an explosion, is defined by the following parameters:

(1) The time of the event, or the origin time of the seismic disturbance.

(2) The geographic latitude and longitude of the epicentre (point on the earth's surface vertically above the source).

(3) The depth of the source, or focal depth (the source is also known as the focus or hypocentre).

(4) The size of the event (expressed normally as the magnitude, or in terms of the energy released).

In order to calculate the various parameters in 1, 2 and 3, only time measurements are needed at the various seismograph stations, while the parameter in 4 requires measurements of amplitudes and periods. The location of an earthquake is thus concerned with the determination of a number of unknowns. Let us examine what is the least number of seismograph stations necessary for such a calculation.

To determine the focus of an earthquake requires the solution of a set of simultaneous equations, one for each station, of the form:

$$(\phi_i-\phi_o)^2 + (\lambda_i-\lambda_o)^2 + (z_i-Z_o)^2 = V_p^2(t_i-T_o)^2 \qquad (4.1)$$

where, ϕ_i, λ_i, z_i = co-ordinates of the stations,

ϕ_o, λ_o, Z_o = co-ordinates of the focus,

t_i = arrival time of the earthquake to station i,

T_o = origin time of the earthquake

V_p = propagation velocity of the P wave

As the arrival times of P are usually the primary data with which one has to work, a minimum of five recording stations are necessary to determine the five unknowns (ϕ_o, λ_o, Z_o, T_o, V_p) in the above equation. But if, in addition, information is available on azimuth, obtained from the horizontal components of the P wave, or on arrival times for other waves (for instance S), then the number of stations can be reduced correspondingly. The common practice today, however, is to base the determination on as many different stations as possible. Local deviations exist from assumed travel-time tables depending, for instance, on local structure, and therefore a least square calculation technique is applied. The error limits of the results obtained can then be estimated.

A number of computer programmes have been developed over the years, based on the least square iterative process, to locate near seismic events using readings from a net of local stations. Flinn (1960) used direct P and S arrival times to locate some of the local earthquakes recorded by the Australian National University network of nine seismic stations. Nordquist (1962) developed for the Pasadena network a programme for determining the source and origin time of a local earthquake, using the times of arrival of direct

and refracted P-waves. Considerable improvement upon the existing programmes have been achieved by Engdahl and Gunst (1966), whose single pass programme COAST computes a first approximation to the hypocentre using only five stations, subsequent to which it determines the refined hypocentre and earthquake magnitude. An improved hypocentral location can now be obtained by the crustal model programme HYPOLAR written by Eaton (1969), who takes as crustal model a uniform half-space overlain by a layer of constant velocity.

All these non-linear techniques calculate the four hypocentral parameters, latitude (ϕ_o), longitude (λ_o), depth of focus (Z_o), and origin time (T_o) but not independently. As James et al. (1969), pointed out, the four-parameter least-square approach gives solutions that depend upon the number and configuration of the observing stations, as well as the initial hypocentral approximation. For instance, an earthquake that occurred just outside the Arequipa network (in Central Peru) on Feb 6, 1965, and was recorded at all nine stations, provided a range of solutions that was dependent on which of the different subsets of the nine station data were used for the calculations. The total variation in origin time was more than 30 sec and in depth 110 km, and the position of the epicentre varied by more than 2^o.

One of the fundamental sources of instability in the least-square iterative process is the interdependence of the computed variables. In order to overcome these

problems, James et al. (1969) proposed using a three-parameter least-square method. The independent variables, ϕ_o, λ_o and Z_o are calculated by the usual least-square iterative process from the P arrivals, and S waves are used to calculate T_o from the relationship

$$T_o = T_p - \frac{V_k T_{sp}}{V_p} \tag{4.2}$$

where T_p = arrival time of P

T_{sp} = time interval between S and P wave arrivals

$$V_k = \frac{V_s V_p}{V_s - V_p} \text{ (S-P wave function)} \tag{4.3}$$

V_s = propagation velocity of S wave

and the other symbols have their usual meaning.

More recently, Crampin (1970), and Crampin and Willmore (1973), developed a programme (FAMG) that attempts to provide more stable and reliable solutions. Their improvement has been achieved by the addition of the time-term to the least-square iterative process described earlier. They argue that the previous programmes made no allowances for any variation of structure within the network, and are not adequate when the time-term is comparable to the total travel time.

The time-term, which depends on the velocity structure beneath the shot and recording point (Fig. 4.11), is given by the equation (Berry and West, 1966).

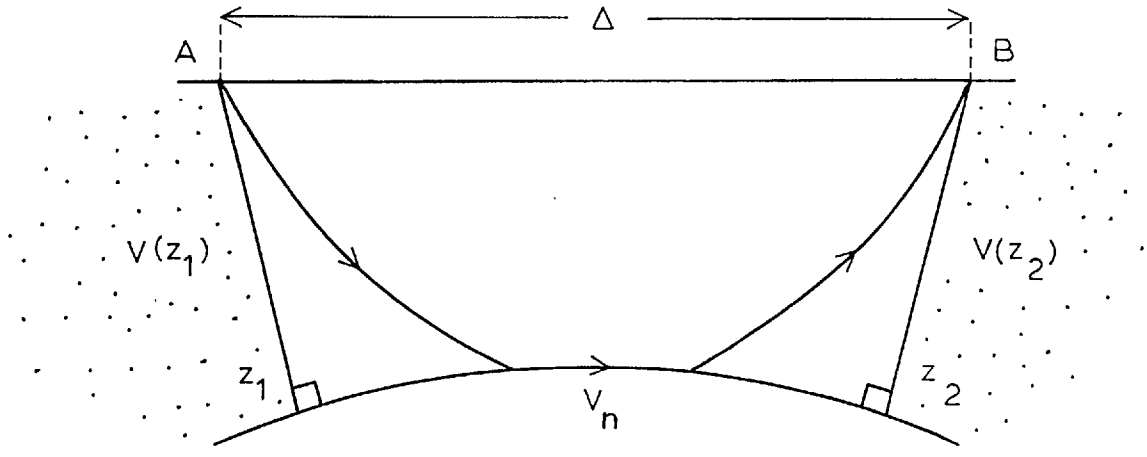


Figure 4.11. Raypath diagram of a wave travelling from the shot point (A) to recording station (B) at epicentral distance Δ from the shot point.

$$t = \frac{\Delta}{V_n} + \int_o^{z_1} \frac{\sqrt{V_n^2 - V(z_1)^2}}{V_n V(z_1)}\, dz_1 + \int_o^{z_2} \frac{\sqrt{V_n^2 - V(z_2)^2}}{V_n V(z_2)}\, dz_2 \qquad (4.4)$$

$$= \frac{\Delta}{V_n} + \text{Shot time-term} + \text{Station time-term}$$

where Δ = distance between shot point and station

$V(z)$ = velocity at depth z

V_n = velocity of the base refractor

z = depth to the refractor measured in a direction perpendicular to the refractor surface.

In practice, the restrictions that (1) velocity varies only with depth (perpendicular to refractor) within the critically refracted ray cone under the shot or station, (2) velocity of the base refractor is constant, and (3) slope

and curvature of the refracting surface is small, must be reasonably well satisfied for successful application of the above equation. The need for the addition of the time-term is well demonstrated by Berry and West (1966), while trying to explain the anomalous seismic velocity behaviour in the Canadian shield.

Crampin and Willmore's (1973) FAMG programme computes the hypocentral parameters of local earthquakes recorded within a small network where the travel-time equations are derived from the geometric ray paths in known geological structures, modified by the time-term at each point.

Thus the successful application of FAMG, and the determination of the focal position with the necessary degree of precision, depends upon the following conditions (1) the velocity structure in the area is assumed to be known accurately for a suitable time-term analysis (2) there exists a sufficient number of event arrivals with good azimuthal distribution, covering a wide range of distances.

4.4.1 OTHER LOCATION TECHNIQUES

Microearthquakes recorded at three or more stations with distinguishable P and S phases can be located using the techniques mentioned earlier. If, however, a B-type microearthquake is recorded at only three stations, the above method cannot be used.

The following section discusses the location tech-

nique for such microearthquakes when recordings are available from three (for B-type event) or from one station, with three-component recordings.

The first method to be discussed is the 'circle-method', which is suitable for locating B-type microearthquakes recorded at three stations.

For simplicity it is assumed that the wave velocity V is constant. It is also assumed that the arrival times t_1, t_2 and t_3 for the first arrivals at the three stations 1, 2 and 3 have been accurately measured, and that $t_3 < t_2 < t_1$. Next, with stations 1 and 2 as centres, circles are constructed with radii equal to $V(t_1-t_3)$ and $V(t_2-t_3)$ respectively. Then the epicentre 0 is the centre of a circle which passes through the station 3 and is tangential to the two above mentioned circles (Fig. 4.12).

In practical applications, it is possible to find the location of 0 after a few trials with no need to perform any calculations.

In order to determine the epicentre of a microearthquake recorded at only one station, we have to determine the distance and the direction from where it is coming. Of the two unknowns, the distance is the easier to calculate. It is usually obtained from the time-difference between the different phases, and in the case of microearthquakes it is generally S-P. The direction is more difficult to determine accurately because of the higher requirements on the quality

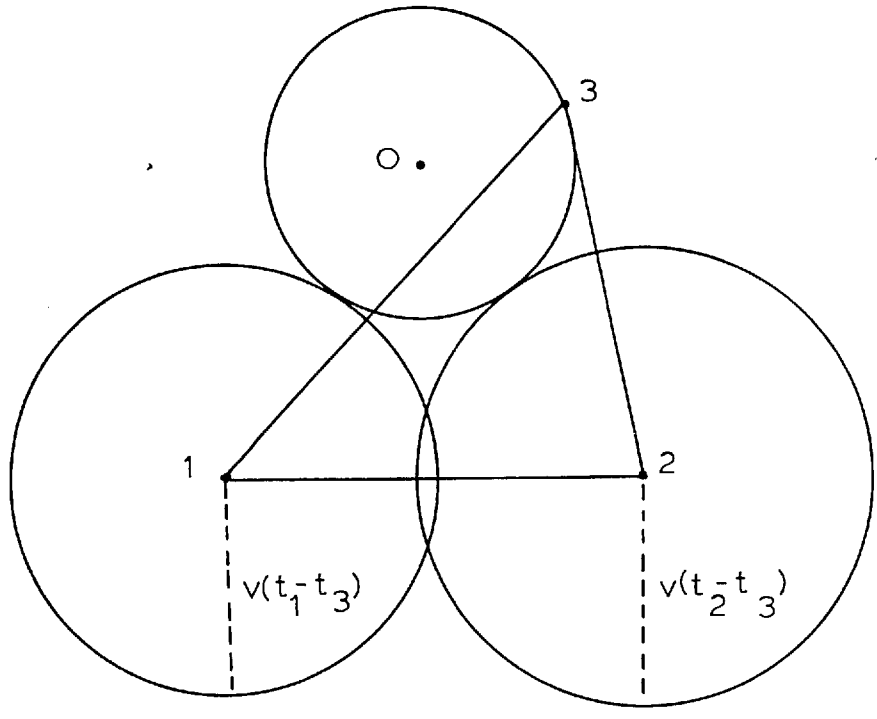


Figure 4.12. Determination of epicentre O, by the circle method. t_1, t_2 and t_3 are the first arrival times of a B-type microearthquake at the three stations 1, 2 and 3 respectively.

of the record. Thus if the amplitude of an event is available from the measurements of the three components, the resultant of these give the direction to the source. Figure 4.13 illustrates this procedure. It should however be remembered that the three components can only be combined vectorially if all the three seismometers have the same response curve. If this is not the case, then the trace amplitudes have first to be transformed into the corresponding ground amplitudes, and then combined to give the azimuth.

When in practice an epicentral distribution is obtained from the records of only one station, it is advisable

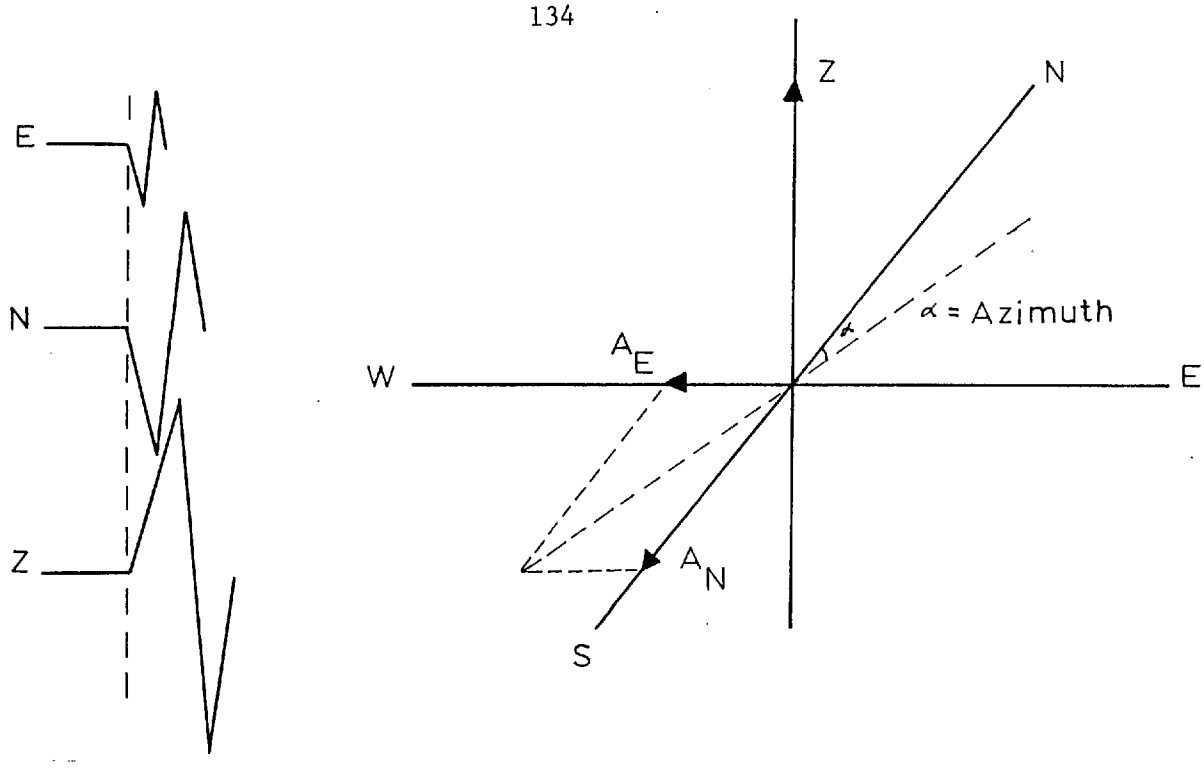


Figure 4.13. Sketch showing the direction to the epicentre determined from P amplitude measurements of the three components.

to use as many different phases as possible. If the amplitude measurements are correct, they should agree with one another within the limits of the error in the measurements.

Determinations of epicentres based on the principles outlined above have a number of limitations. In the 'circle-method', for instance, it was assumed that all the recording stations lie on the same plane, no corrections being applied for differences in elevation. In practice, especially in volcanic areas, the stations may not all lie on a plane. The second method assumes a straight ray path, which might only be true for a very shallow earthquake. Since ray paths are convex downwards, focal depth is liable to be overestimated.

The methods discussed above provide a rough estimation of the epicentre of local earthquakes, and thus have

very limited application.

4.4.2 A BRIEF DISCUSSION OF PROGRAMME HYPO

In the present investigation, as only two micro-earthquakes with identifiable P and S phases were recorded at as many as three stations, and the velocity structure is not known accurately enough for a time-term analysis, it was decided to develop the programme HYPO, mentioned earlier, taking the pecularities of the present situation into account. Programme HYPO, however, involves the following simplified assumptions:

(1) The structures are assumed to be isotropic and homogeneous with the velocities of P-and S-waves constant with depth.

(2) The average P-wave velocity V_p is taken as 5.25 km/sec (the actual value probably ranges between 5.0 and 5.50 km/sec).

Determination of the hypocentre requires solution of Eqn. (4.1). However, restriction to stations closer than 15 km allows the use of a rectangular co-ordinate system. Equation (4.1) can thus be re-written in the form

$$(x_i-X_o)^2 + (y_i-Y_o)^2 + (z_i-Z_o)^2 = V_p^2(t_i-T_o)^2 \qquad (4.5)$$

where i = 1, 2, 3 in the present case, and x_i, y_i, z_i are the co-ordinates of stations, and X_o, Y_o, Z_o are the co-ordinates of the focus, and the other symbols have their usual meaning.

As the ratio of S to P velocities is constant (assumed here as 0.59)* Eqn. (4.2) can be simplified to give

$$(T_o)_i = t_i - \frac{(T_{sp})_i}{0.7} \qquad (4.6)$$

Equation (4.5) is now solvable for X_i, Y_o by a second order determinant. Z_o is found by substituting these values into any of Eqn. (4.5).

As the assumed average velocity V_p is not well substantiated, three values of V_p (5.25, 5.0, 5.50 km/sec) were tried, to obtain a range of hypocentres for each event.

The programme is set up for rectangular co-ordinates, but it is desirable to feed in and read out locations in latitude and longitude. A mapping function was devised to convert geographical co-ordinates to rectangular co-ordinates (Hosmer, 1919).

Now $$x = N(\lambda-\lambda_o)\cos\phi$$

$$y = R_m(\phi-\phi_o) + (x^2/2N)\tan\phi_o \qquad (4.7)$$

whence $$\phi = \phi_o + y/R_m - (x^2/2NR_m)\tan\phi_o$$

$$\lambda = \lambda_o + (x/N)\sec\phi \qquad (4.8)$$

where λ = longitude

ϕ = latitude

λ_o = longitude of the origin of rectangular co-ordinates

*This corresponds to Poisson's ratio = 0.235, a representative value for rocks near the surface.

ϕ_o = latitude of the origin of rectangular co-ordinates

R_m = radius of curvature of the earth in the plane of the meridian, at the latitude of the origin of co-ordinates

N = radius of curvature of the earth in the prime vertical, at the latitude of the origin of co-ordinates.

Equations (4.7) and (4.8) are sufficiently accurate for the present purpose (for stations less than 150 km away from the origin of co-ordinates, the error involved is less than 0.1 km). The co-ordinates of Serra La Nave (37.69^o , 14.97^o) were taken as the origin, for which N = 6378.16 and R_m = 6335.47.

This method of locating hypocentres was successfully applied earlier by Westphal and Lang (1967) in monitoring the local seismic events at the Fairview Peak area in Nevada. More recently, Westhusing (1974) used the technique to locate microearthquakes in the volcanoes of the Cascade Range, Oregon.

4.4.3 LOCATION OF MICROEARTHQUAKES ON ETNA USING PROGRAMME HYPO

Two well defined shocks with identifiable P and S phases were located using the computer programme HYPO. Table 4.3 gives the average velocity models used in the present calculations and Table 4.4 gives the result in terms of latitude, longitude, depth and origin time. The epicentral distribution of the events corresponding to the three models are given in Figure 4.14 (indicated by crosses, and labelled,

Table 4.3

Average Velocity Model Used for Hypocentral Determination

Model	Depth (km)	P wave velocity (km/sec)	S wave velocity (km/sec)	Remarks
1	20	5.00	2.95	All models based on crustal structure given by Cassinis et al. (1969)
2	20	5.25	3.09	
3	20	5.50	3.25	

Table 4.4

Location of Microearthquakes Recorded
on Mount Etna

Date (d mon yr)	Origin Time (hr min sec)	Latitude (deg min sec)	Longitude (deg min sec)	Depth (km)
		MODEL 1		
11 06 75	19 58 28.45	37 48 32.02	15 00 12.70	7.793
12 06 75	19 27 11.89	37 46 28.51	15 09 20.50	19.030
		MODEL 2		
11 06 75	19 58 28.45	37 48 30.71	15 00 29.37	8.983
12 06 75	19 27 11.89	37 46 33.44	15 10 20.65	19.336
		MODEL 3		
12 06 75	19 58 28.45	37 48 27.63	15 00 47.43	10.137
12 06 75	19 27 11.89	37 46 40.29	15 11 47.42	18.600

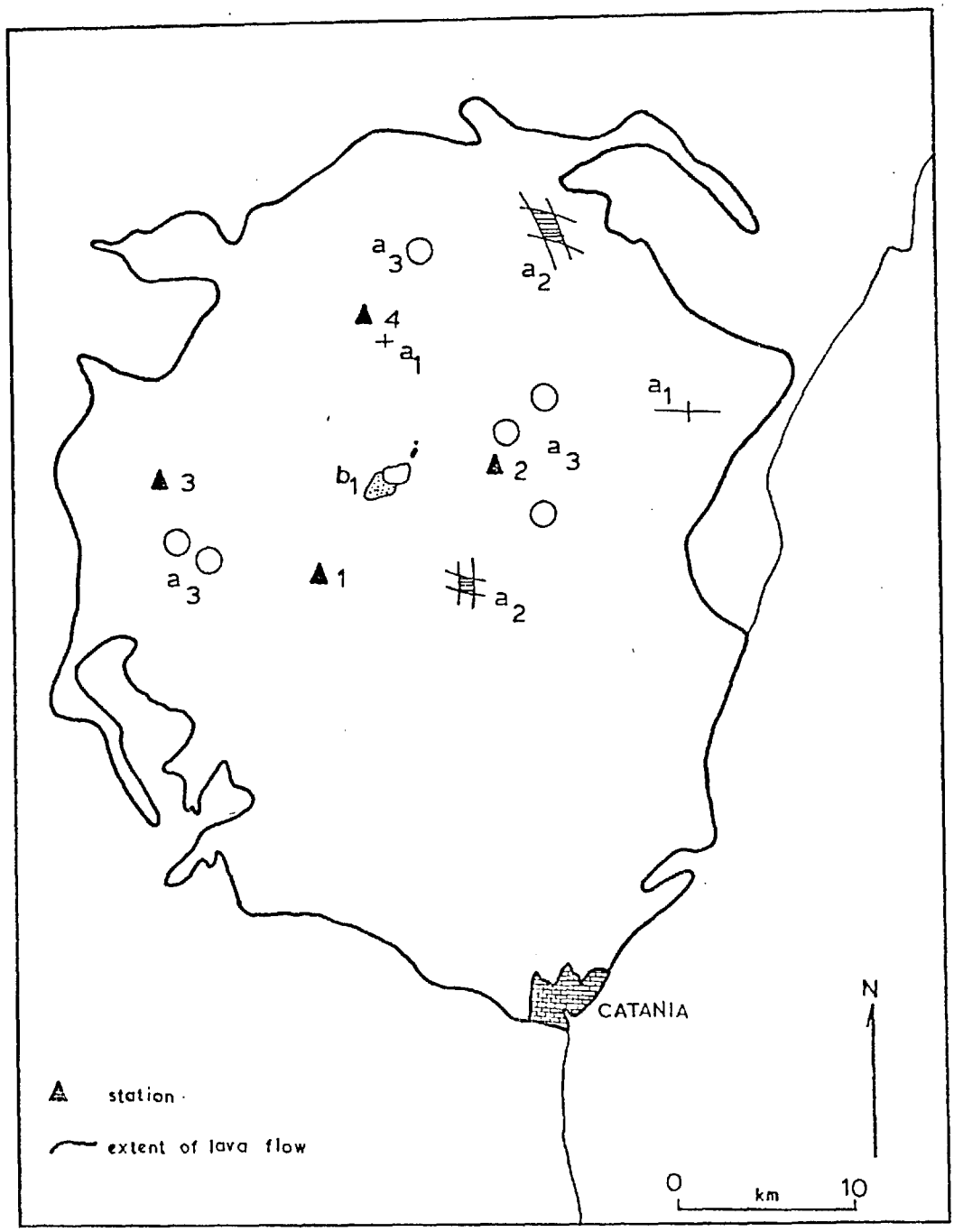


Figure 4.14. Map showing the epicentre of microearthquakes analysed in the present study. The crosses (a_1), the hatched area (a_2), and the open circles (a_3) are epicentres for A-type events and the dotted area (b_1) that of a B-type event. (For full explanation see text).

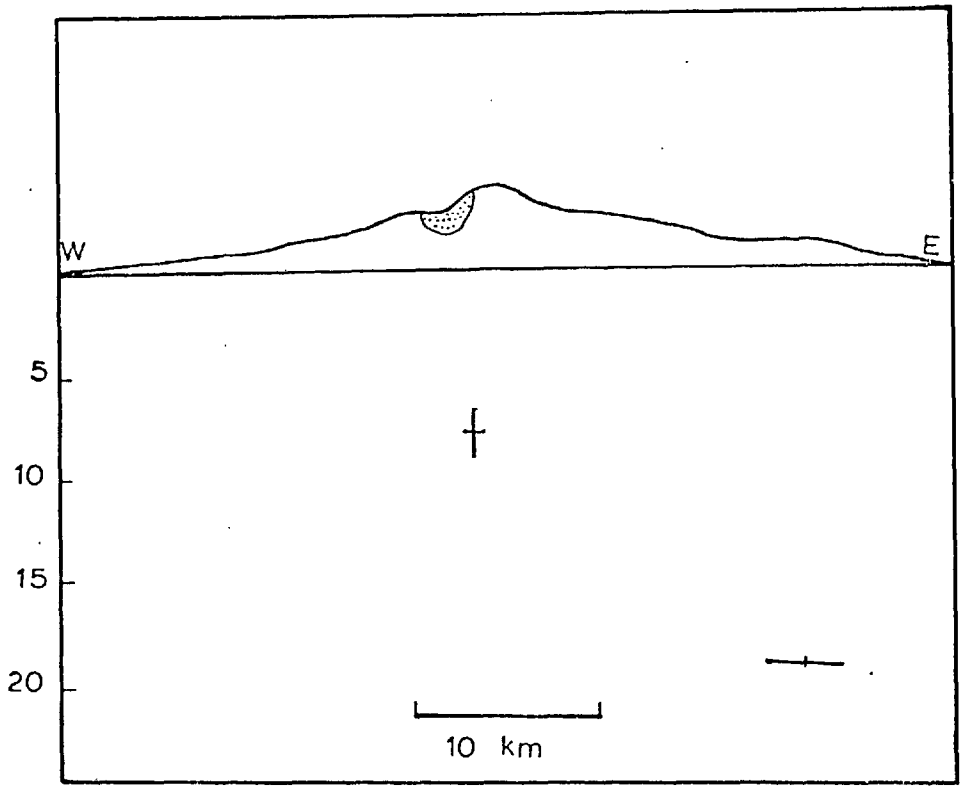


Figure 4.15. Depth of focus of two A-type (indicated by crosses) and a B-type event (indicated by the dotted area). For full explanation see text.

a_1). Figure 4.15 is an E-W cross-section through the centre of the volcano, showing the depth of focus of the above two events. These have been plotted only as a function of depth and of radial distance from the summit crater. The horizontal and vertical extent of the crosses in both the figures indicates the spatial uncertainty of the epicentres, as well as the foci of the events using the above models. It can be seen from the figures that for the shallow focus earthquake the epicentre is much better located than for the deeper earthquake, whereas the depth of the focus is much better controlled in the latter case.

The shallower of the two shocks lies at a depth of between about 7 and 10 km, and is probably related to the volcano-tectonics of Etna. These types of shocks are what Minakami (1960) described as A-type microearthquakes. The second, much deeper, shock is probably related to the non-volcanic tectonics of the area.

Proper epicentral location, as discussed earlier, requires the event to be recorded in at least three stations. Due to instrumental problems, as well as their small magnitudes, most of these microearthquakes were recorded at not more than two stations. Approximate locations were obtained for two shocks recorded in stations (2 & 1), and (2 & 4) using the relation

$$\Delta = V_k(t_s - t_p)\,\text{km}$$

where Δ = epicentral distance from recording stations,

and $$V_k = \frac{V_s V_p}{V_s - V_p}$$ (S-P wave function)

and the other symbols have their usual meaning. Both these

microearthquakes occur within 5 to 13 km of the recording stations, within the hatched area in Figure 4.14 (labelled, a_2).

As mentioned in Section 4.4.1, a B-type microearthquake was recorded in three stations (1, 2 & 4). A geometric method was used to locate its epicentre. The dotted area near the Central Crater (Fig. 4.14 & 4.15) seems to be the origin of this shock (labelled, b_1). The maximum apparent velocity which would be compatible with the observations of the first arrivals at the three stations is 1.09 km/sec. This low seismic wave propagation velocity can be explained as due to the presence of unconsolidated tuff and pumice in the top layers of the volcano.

It is interesting to note in this connection the findings of Latter (1971) on Vulcano, one of the islands of the Aeolian arc. In an investigation of the propagation velocities in the superficial rocks of the volcano he obtained a first P-wave arrival velocity range of 0.98 - 1.02 km/sec. This is in good agreement with the present result, probably because unconsolidated material on volcanoes have nearly the same propagation velocities.

Some very small magnitude microearthquakes were analysed by the technique mentioned in Section 4.4.1. These microearthquakes were recorded at only one station and thus the methods of Section 4.4 could not be used.

Obviously, three components are necessary and suffi-

cient for such a determination. If only two horizontal components were available and no vertical component, the determination of the direction would be ambiguous. In practice, however, it was found that the epicentre determination of these microearthquakes is very sensitive to amplitude estimates. Hence the technique should be used with reservation and only when the conventional techniques fail.

The open circles in Figure 4.14 show the epicentre of six of these microearthquakes (labelled, a_3). The diameters of the circles indicate the spatial uncertainty in their location, using the velocity models given in Table 4.3.

CHAPTER V

SPECTRAL CHARACTERISTICS OF MICROEARTHQUAKES AND BACKGROUND SEISMIC NOISE

5.1 INTRODUCTION

The importance of seismometric observation of volcanoes for predicting eruptions has been examined in Chapter I, and in Chapters III and IV the results of the 1974 and 1975 fieldwork on Mount Etna have been discussed, mainly in terms of the magnitude and recurrence frequency of the recorded microearthquakes. Information of a quite different kind can be obtained from spectral analysis, both of microearthquakes and of volcanic tremor, the background seismic noise of volcanic origin, as distinct from the normal microseismic background.

Spectral analysis provides information about the frequency content and the distribution of power, and thus enables changes in frequency content with time to be recognized. Such changes appear in some cases to be related to the eruptive state of a volcano, a matter that can be tested in the case of any particular volcano by observation over a prolonged period of time. Where found to exist, such changes have possible application in the prediction of eruptions.

The first seismometric observations of volcanic tremor possibly dates back to about 1910 when Omori (1911)

studied the eruption of Mount Usu in Japan. Many reports have been published since then of the eruptions of volcanoes, Mauna Loa and Kilauea in Hawaii by Jager (1920), Finch (1943, 1949), Eaton and Richter (1960); Vesuvius in Italy by Imbo (1935); Ruapehu in New Zealand by Dibble (1969); some Central African volcanoes by Berg and Janessen (1960); Meakan-dake in Japan by Sakuma (1957) etc.

Various types of volcanic tremor have been distinguished. For example, in the Strombolian and Hawaiian type eruptions, volcanic tremors are directly related to eruptions, whereas in others, tremors are not accompanied by simultaneous eruptive activity.

The individual waveforms or phases are difficult to identify for any type of volcanic tremor. However, they seem to share many characteristics, such as velocity of propagation, attenuation of wave energy etc, with seismic surface waves. As a result, many investigators think they are mainly composed of the latter kind of wave (Kubotera, 1974).

Spectral characteristics of volcanic tremor vary from volcano to volcano. They also vary with time, depending on the state of activity of the volcano. In practice, they are also influenced by factors external to the volcano, such as the nature of the propagation path and the frequency response of the seismograph. For instance, to study the short-period components of volcanic tremors, the seismographs employed

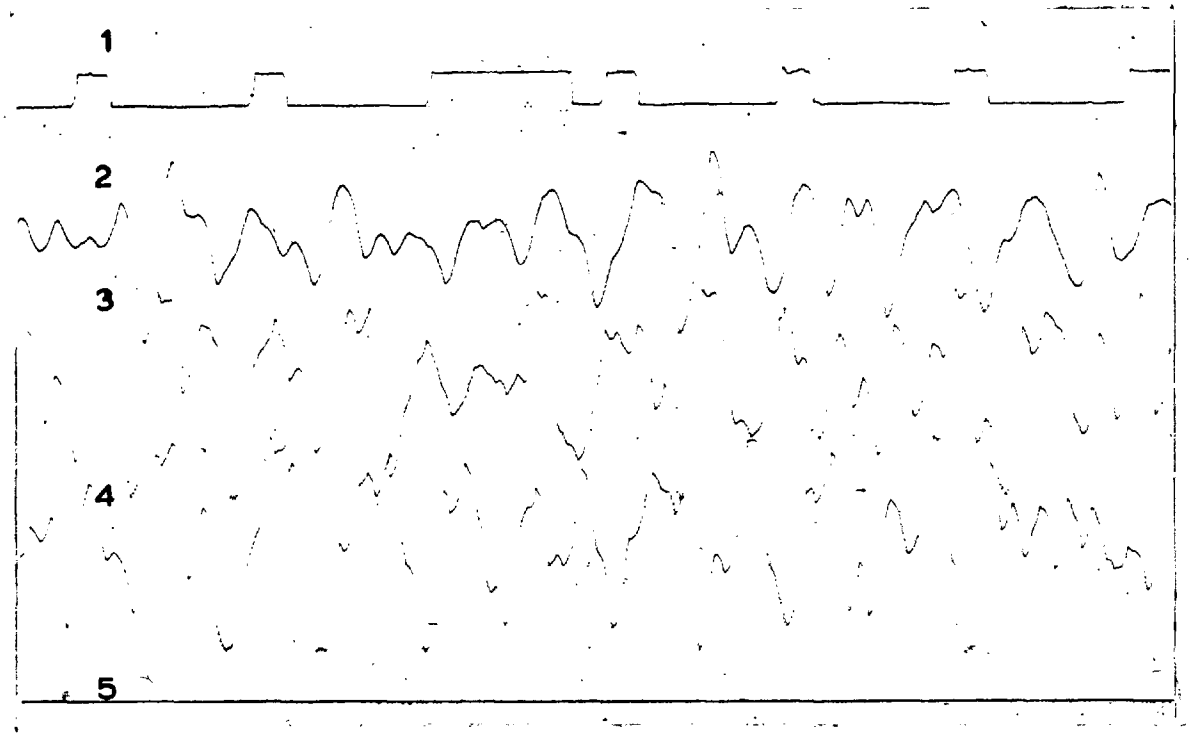


Figure 5.1. Examples of played back magnetic-tape record of volcanic tremor. The channels from top to bottom are, 1 : the time signal, 2 : Vertical, 3 : N-S, 4 : E-W components and 5 : the radio signal.

in the present investigation were adequate. However, volcanic tremors sometimes have long-period components (Minakami and Sakuma, 1953; Shimozuru, 1971; Kubotera, 1974). For the observation of these kinds of tremors, long-period seismographs are necessary, and it was not therefore possible to study the long-period components during the present investigation.

Examples of fast played-back magnetic tape record of volcanic tremor recorded during this investigation are shown in Figure 5.1.

Many suggestions have been made as to the origin of volcanic tremors. Most fall into one of two categories, (1) attributing them to the movement of magma, or (2) relating them to phenomena associated with gases.

The proponents of the first process believe that tremors are caused by the turbulent flow of magma or by the free oscillations of a hypothetical magma chamber within the volcano. Finch (1949) studied the seismograms of volcanic tremor (for Kilauea) recorded at the Hawaiian Volcano Observatory during various phases of its eruptive activity. He noticed, for instance, that the seismographs recorded small tremors almost continuously, and in general the tremors were most conspicuous when Kilauea was most active. He also noticed that when magmatic activity totally ceased, volcanic tremor also disappeared. Wood, as reported by Finch (1949), had previously suggested that these tremors were associated with the outbreak of fountains in an active lava lake

(Halemaumau). But Finch observed that there was no obvious connection between the two. For instance the 1922 eruption produced tremors at a time when no lava was visible at Halemaumau, although lava outpouring from a nearby rift (Puna) indicated underground movement of magma. The above observations lead him to suggest that volcanic tremors had a more "deep-seated origin" than envisaged by Wood. Thus Finch suggests that these tremors could be induced by the "vertical surgings of magma in the conduit under Halemaumau" or by "pulsating horizontal discharge" of magma.

During eruptions, or high volcanic activity, the processes suggested by Finch (1949) may be partly responsible for the observed volcanic tremor. It is however difficult to visualize (in the absence of further evidence) how such a physical process can be sustained for long periods (weeks and sometimes months) that is capable of producing volcanic tremor without any significant variation either in its period or amplitude.

Sassa (1936) made an extensive survey of Mount Aso, Japan (1929-1933) both during its active and its repose periods. He classified the recorded volcanic tremors into three distinct groups according to their wave characteristics. The first group had periods between 0.4 and 0.6 sec, the second group about 1 sec and the third group between 3.5 and 7.0 sec.

Volcanic tremors of the first kind (0.4-0.6 sec) were thought to be a kind of Rayleigh wave, generated by sur-

face eruptions and internal eruptions at very shallow places. The second kind (period 1 sec) was considered to be generated by "internal eruption of volcanic gases". Volcanic tremors of the third kind (3.5-7.0 sec) are believed to be generated by the oscillation of the magmatic chamber. The variation in periods are supposed to be related to the physical as well as to the chemical conditions both inside the chamber as well as in vents around the volcano.

If Sassa's (1936) explanation of the generation of volcanic tremor are accepted, the recording of three or even two types of wave group during a single survey probably indicates the complexity of volcanic processes, even for a small (in comparison with Etna) volcano such as Aso.

The above two broad categories of the origin of volcanic tremors, or a combination of both, appear to be accepted by seismologists as the primary cause of volcanic tremor in nearly all volcanoes (Omer, 1950; Sakuma, 1957; Steinberg and Steinberg, 1975). The degree of dominance depends, of course, on the particular volcano being investigated.

Among other processes thought to be responsible for volcanic tremors are continuous microfracturing of rocks combined with changes in temperature, discrete dislocation in rocks surrounding dykes while they are intruding, or the oscillation of water at temperatures above 600°C (the gas phase above the magma chamber is predominantly composed of water vapour), generally known as the 'Leidenfrost Effect'. The sinusoidal wave trains recorded by Latter (1971) on the

Aeolian Island of Vulcano are thought to be due to this effect.

In this chapter the spectral characteristics of some selected microearthquake and volcanic tremor records are studied, a tentative source location based on the attenuation of tremor amplitudes at the various stations is attempted, and finally a possible source mechanism is proposed for Mount Etna.

5.2 SELECTION OF DATA FOR DIGITIZATION

It would be prohibitively expensive and quite unnecessary to digitize the whole of the recorded data at the density required for useful analysis. It is necessary, therefore, to inspect the whole of the data and to select from it those portions containing interesting information. The procedure followed was to play back one of the recorded channels (from the Racal Store-4 instrumentation recorder, see Section 4.2.4), displaying the output on an oscilloscope screen, and to visually inspect the trace. Any sections contaminated by unwanted noise, or showing signal dropout due to malfunctioning of transducer etc, were rejected. The time of the selected portion was noted from the time decoder unit (the time decoder unit was connected to channel 4 of the Store-4, and displays hours and minutes) and the three channels of the appropriate time-span were then replayed in turn.

The analogue signal must now be converted into digital form. In doing this certain basic principles of

sampling theory must be followed, so that the reconstructed signal, obtained from the discrete signals $x(i\Delta t)$, where $i = 1,2,...N$ and Δt is the sampling interval, represents the original signal $x(t)$ with acceptable accuracy.

The process of analogue-to-digital (A/D) conversion is equivalent to a convolution of a continuous signal $x(t)$ with an infinite Dirac comb in the time domain,

$$\Delta(t,\Delta t) = \Delta t \sum_{n=-\infty}^{+\infty} \delta(t-n\Delta t)$$

Expressed mathematically, this becomes, (Kanasewich, 1975)

$$x(t)\nabla(t,\Delta t) = \sum_{n=-\infty}^{+\infty} x(t_n)\Delta t \,.\, \delta(t-n\Delta t) \qquad (5.1)$$

The right-hand side of the above equation, if expanded in a Fourier series, takes the simple form of the sampled signal as a series of amplitude modulated waves

$$\sum_{n=-\infty}^{+\infty} x(t_n)\Delta t \,.\, \delta(t-n\Delta t) = x(t) + 2\sum_{k=1}^{\infty} x(t_k)\cos(2\pi fk\Delta t) \qquad (5.2)$$

The 'd.c.' term $x(t)$ on the right-hand side of the above equation yields the correct spectrum of the designated signal. The second term, however, interferes constructively at frequencies $1/\Delta t$, $2/\Delta t$, $3/\Delta t$ and so on, producing 'side

lobes' all with the same strength as the 'd.c.' term. Thus, if the sampling frequency $\frac{1}{\Delta t}$ is much higher than the maximum frequency in x(t) Eqn. (5.2) will then yield the correct results over the frequency range of interest. In fact, the barest minimum is that $\frac{1}{\Delta t}$ must exceed twice the highest frequency in x(t).

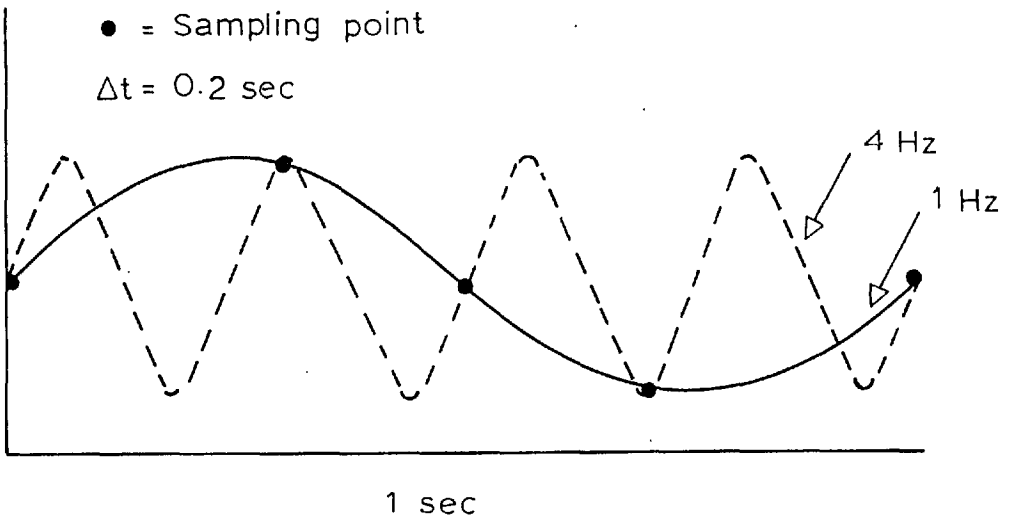


Figure 5.2. Two aliased sine waves displaying identical sample points. The 1 Hz signal is resolved but the 4 Hz is not.

One half the sampling frequency is called the Nyquist or folding frequency $f_N = \frac{1}{2\Delta t}$, and it must be greater than the highest frequency in x(t). Figure 5.2 illustrates the impossibility of resolving a frequency greater than the Nyquist frequency.

Thus if any signals are present with frequencies higher than f_N, their power will be reflected back or aliased into the power spectrum over the principal range. It is

therefore essential to filter out frequencies above f_N.

Aliasing is sometimes referred to as folding, as the frequency spectrum can be obtained by folding it back about the Nyquist frequency.

5.2.1 DIGITIZATION OF THE SEISMIC DATA

Suitable sections of the analogue record obtained from a playback of the magnetic tapes (described more fully in Section 4.2.3) were digitized using an Oscar-J Chart Measurer. This indirect method of digitizing the original data, by first converting it to an analogue strip-chart record and then manually digitizing, is extremely slow and inevitably downgrades the data. To digitize 40 sec of seismic signal, for instance, at a sampling interval of 0.02 sec would require about 3-4 days of work, and when one considers the vast amount of digitized data that was required for the analysis in this study it proved to be very time consuming.

A direct method in which the original tape-stored data is electronically digitized has the advantage of being fast and of avoiding the human factor involved in manual digitization. It was therefore decided to digitize the data electronically, using the A/D system of the Mechanical Engineering Department of Imperial College.

The hardware of this system has been described by Bloxham et al. (1972). It consists essentially of two

basic units (1) the playback and (2) the A/D converter.

The playback unit consists of a Racal Store-4 instrumentation recorder, a four channel amplifier (developed in the Department) to accomodate three unfiltered and one filtered seismic channel, the filter, a time decoder for enabling selected parts of the tape to be identified, an adjustable timing unit for controlling the signal sampling rate, and an oscilloscope for monitoring the amplifier outputs.

The A/D converter is an asynchronous multiplexed 10-bit converter. It has a core store of 8 K and is designed for an input voltage of 0-10. Four 5×10^{-4} sec pulses obtained from the timer unit connect it sequentially to the four amplifier outputs. The sampling frequency (for a group of four values) was set at 50 Hz for background seismic noise and 100 Hz for microearthquakes. With these sampling frequencies, seismic sections of 40 sec and 20 sec duration respectively could be digitized.

Prior to digitization, suitable sections were selected using the time decoder unit, and the playback gains were adjusted to give an optimum signal level of ~10V. The signals were monitored on the scope via the amplifier during digitization, as a check on the input signal to the converter.

The A/D converter operates in conjunction with a PDP-15 computer. The latter has a 256 K word disc, 18-bit



Figure 5.3. The digitization set up.

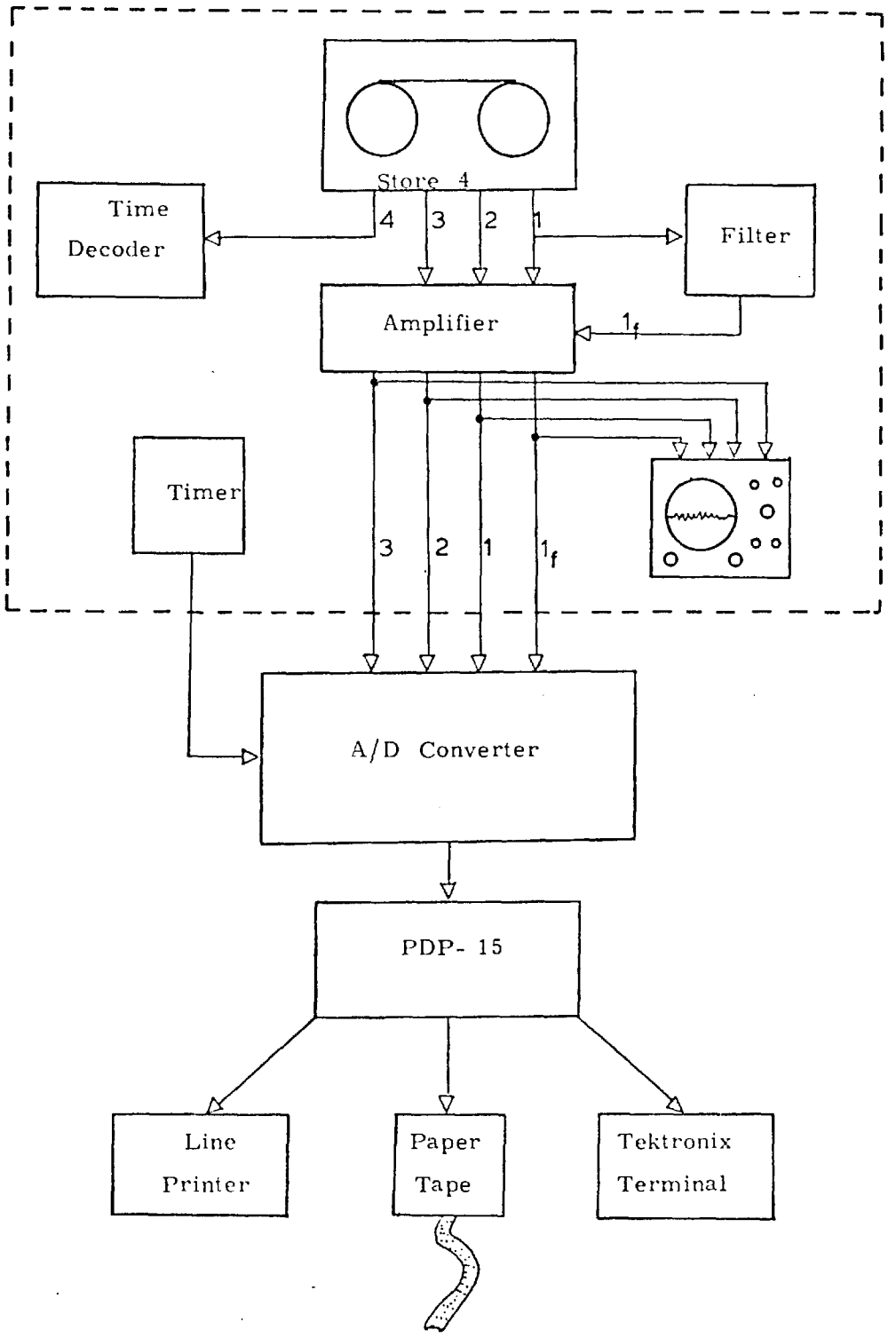


Figure 5.4. Block diagram of the digitization set up.

word length and a total core storage of 16 K. To digitize 20 sec or 40 sec lengths of record (depending on whether the section being digitized is a microearthquake or a background volcanic noise) a systems programme, called GE08, was developed by Dr. Wing of the Mechanical Engineering Department. The digitized data is first stored in the A/D unit in 10-bit words. It is next buffered into the PDP-15 computer where two 10-bit words are repacked into a new 18-bit word. The digitized signals were then dumped onto an 8-track paper tape in two separate 4 K sections.

Additional facilities incorportaed in the system were a Tektronix Terminal and a line printer output. Before producing any paper tape, the four digitized channels were in turn displayed in part on the terminal screen. If any or all of the channels were found unsatisfactory, the digitized data could be rejected. The line printer output produces hard copies, in two separate blocks, of the first two hundred values corresponding to the two 4 K sections. The digitization set-up is shown in Figure 5.3 and the various steps are illustrated diagramatically in Figure 5.4. The digitized values are dumped onto the paper tape in BCD. Each digitized value in the form of a three digit number represents in millivolts (x10) the location on the 0-10V converter range.

It is interesting to compare the time needed to digitize 40 sec data by this A/D system, with the Oscar J-Chart Measurer. The whole operation of digitization can

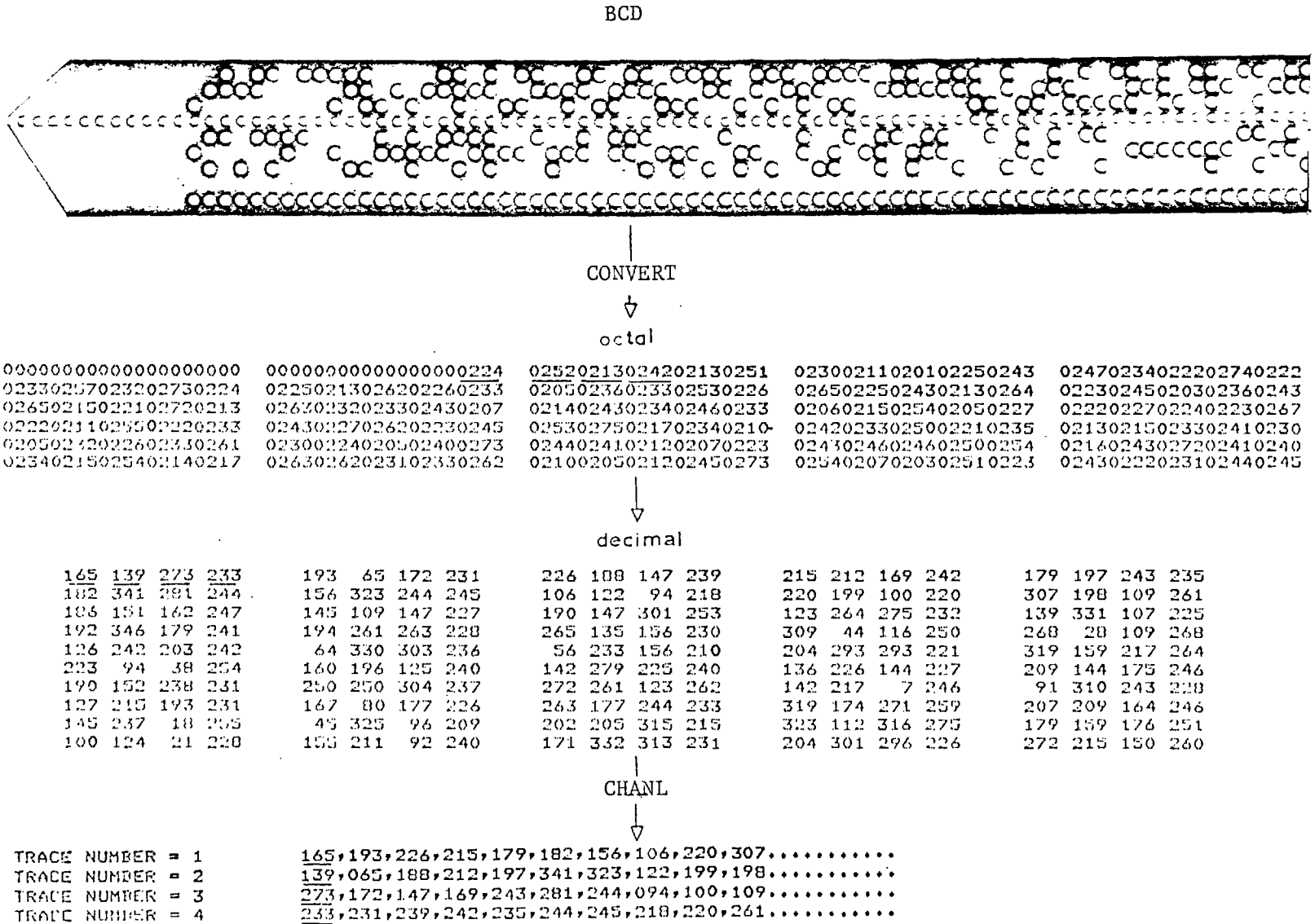


Figure 5.5. Paper - tape conversion diagram.

be accomplished in about 10 min, the bulk of which however is taken up in punching, rewinding and storing the paper tape.

5.2.2 CONVERSION OF PUNCHED PAPER TAPE

The digitized values as mentioned earlier are dumped onto the paper tape in BCD. In order to use these data for future analysis the BCD values must be converted to decimal values. This is achieved by the use of the computer programme CONVERT. CONVERT calculates the octal value of each frame, and converts them to decimal values. Programme CHANL next reassembles these mixed formated data into four separate channels and stores them as permanent files in the Imperial College CDC 6400 computer.

Figure 5.5 shows the paper tape output obtained from the A/D converter and punched in BCD. Also shown are the subsequent steps of conversion into octal, decimal values, and their final storage as permanent files. Details of the paper tape conversion procedure can be found in the ICCC handout entitled 'Batch Paper Tape Under Kronoss'. The paper tape data thus obtained can be checked by comparing it with the hard copy obtained previously from the line printer.

5.3 INTRODUCTION TO POWER SPECTRAL ANALYSIS

After the analogue data has been digitized and stored in permanent files, the next step is the analysis of

the data. Volcanic tremor data are generally described in terms of the power spectral density function (also called autospectral density function). The power spectral density function, which is the Fourier transform of the auto-correlation function, furnishes information about the seismic data in the frequency domain.

The basic concepts involved in the estimation of the power spectrum is that any signal X(t), arbitrary to within certain limits, can be represented as a continuous superposition of sine waves, with amplitudes and phases determined by the Fourier transform (FT) relationship (Richards, 1967).

$$X(t) = \int_{-\infty}^{+\infty} G(f) e^{2\pi i f t} \, df \tag{5.3}$$

$$G(f) = \int_{-\infty}^{+\infty} X(t) e^{-2\pi i f t} \, dt \tag{5.4}$$

G(f) is known as the FT of X(t), and X(t) is the inverse FT of G(f). The existence of the above equations for various classes of functions and conditions are discussed in Popoulis (1962), Bracewell (1965), Lanczos (1966) etc. Physically, the FT represents the distribution of signal strength with frequency i.e. it is a density-function. For example, if X is measured in volts and t in seconds, the dimensions of G(f) are 'volt-second'. The spectrum of G(f), as seen from

Eqn. (5.3), is generally a complex function, and extends over all frequencies from minus to plus infinity.

The power of the signal X(t) is defined by,

$$P = \lim_{T\to\infty}\left(\frac{1}{T}\int_{-T/2}^{+T/2} X(t)^2 dt \right) \tag{5.5}$$

and the corresponding power spectrum is given by,

$$P(f) = \lim_{T\to\infty}\left(|G(f)|^2 \right) \tag{5.6}$$

In practice, however, only records of finite length, T, are available. The finite length time series can be thought of as an infinite time series viewed through a time window of length T. Thus if X(t) is the signal in the range $-\infty \leq t \leq +\infty$ the signal actually measured in the finite interval can be written as,

$$x(t) = X(t)W(t) \tag{5.7}$$

When transformed into the frequency domain, the finite interval transform x(t) is the convolution of the transforms X(t) and the window W(t). The transform of the window W(t) is known as the spectral window. The spectral window of a rectangular wave function is shown in Figure 5.6,and is given by (Jenkins and Watts, 1969).

$$W(f) = T\,\frac{\sin \pi f T}{\pi f T} \tag{5.8}$$

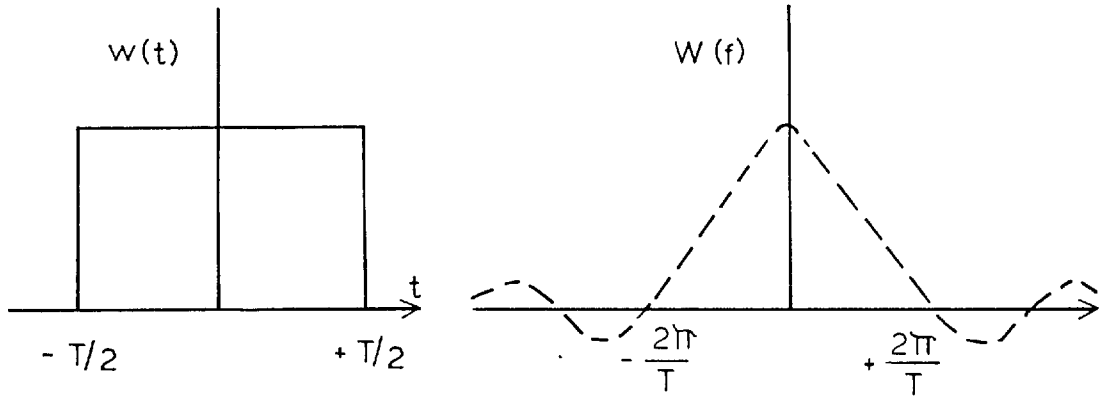


Figure 5.6. A rectangular wave function and it's Fourier transform.

Thus if a finite length of the record is available, the FT given by Eqn. (5.1) and (5.2) becomes

$$x(t) = \int_{-\infty}^{+\infty} g(f) e^{2\pi i f t} df \tag{5.9}$$

$$g(f) = \int_{-T/2}^{+T/2} x(t) e^{-2\pi i f t} dt \tag{5.10}$$

The power of the signal x(t) is

$$p = \frac{1}{T} \int_{-T/2}^{+T/2} x(t)^2 dt \tag{5.11}$$

and the corresponding power spectrum is given by

$$p(f) = \frac{1}{T} |g(f)|^2 \tag{5.12}$$

where the term $\frac{1}{T}$ is inserted to make p(f) independent of the duration of the data (Richards, 1967).

The requirement of any reliable power spectral analysis is thus to estimate the accuracy of various functions obtained from finite amounts of data, in our case to make p(f) a reliable estimate of P(f). This can only be achieved if x(t) does not vary with time, that is if x(t) is a stationary random time-series (Blackman and Tukey, 1958).

The calculation of the power-spectrum via Eqn. (5.12) (for any numerical computation, Eqn. (5.12) must however be replaced by a finite sum, see for instance Jenkins and Watts, 1969) gives a very erratic spectrum p(f), which fails to converge in any statistical sense to a limiting value, no matter how large T is made or how small the sampling interval (Δt) is chosen. A criterion that is often used to describe the reliability of the spectrum, is the error parameter

$$\varepsilon = \frac{\text{rms deviation of power from average power } (\Delta p)}{\text{average power } (p_{av})} \tag{5.13}$$

The error parameter, ε, associated with the power spectrum calculated by using Eqn. (5.10) has $\varepsilon \simeq 1$. That means the root mean square deviation of power from the average is equal to the average power itself. Clearly, this is not a satisfactory procedure for calculating the power spectrum. One way of getting round the problem would be to take M individual segments and then taking the average of the individual p(f). This would give an error parameter (Richards, 1967)

$$\varepsilon \simeq \left[\frac{1}{M}\right]^{\frac{1}{2}} \tag{5.14}$$

As can be seen from the above equation, increasing M decreases ε, but this unfortunately has the effect of broadening the individual peaks in p(f). M and T are, however, related to the spectral resolution (broadening) of the peaks in p(f) by

$$\Delta f = \frac{M}{T} \tag{5.15}$$

In practice, however, the error parameter can be more easily calculated from the formula (which follows from Eqn. (5.13))

$$\varepsilon \simeq \left[\frac{1}{T\Delta f}\right]^{\frac{1}{2}} \tag{5.16}$$

Equation (5.16) shows that decreasing the resolution, increasing Δf, gives a smaller value for ε. The same result can also be obtained by averaging or smoothing Eqn. (5.11) and (5.9) to obtain the power spectrum. A more efficient and reliable way of calculating the power spectrum is, however, via the autocorrelation function (Jenkins and Watts, 1969), details of which are given in the next section.

5.3.1 POWER SPECTRUM VIA THE AUTOCORRELATION FUNCTION

The autocorrelation function of a stationary series $X(t)$, $-\infty \leq t \leq +\infty$, is given by

$$R(u) = \lim_{T\to\infty}\left(\frac{1}{T}\int_{-T/2}^{+T/2} X(t)X(t+u)\,du\right) \tag{5.17}$$

which is normalized so that $\int_{-T/2}^{+T/2} X(t)^2 dt$ represents the total

power of the system. The autocorrelation function is a function only of the lag u, and under this condition $R(0) = 1$. The power spectrum can then be calculated by taking the Fourier transform of the autocorrelation function (Bracewell, 1965), i.e.

$$P(f) = \int_{-\infty}^{+\infty} R(u)e^{-2\pi ifu}du \tag{5.18}$$

The P(f) thus calculated is generally known as the power spectral density function. The power spectral density function not only gives information about the distribution of power with frequency but in addition provides means for comparing two time-series recorded, for example, by two different instruments.

For a continuous finite length of record, the auto-correlation function is given by (Blackman and Tukey, 1958).

$$r(u) = \frac{1}{T_n - |u|} \int_{-(T_n-|u|)/2}^{+(T_n-|u|)/2} x(t-\tfrac{u}{2})x(t+\tfrac{u}{2})du \tag{5.19}$$

where the lag $|u| \leq T_m < T_n$, where T_n is the length of the record and T_m is the maximum lag we want to use. The power spectrum is given by

$$p(f) = \int_{-T}^{+T} r(u)e^{-2\pi ifu}du \tag{5.20}$$

The spectral window corresponding to r(u) can be calculated from Eqn. (5.19) and is given by

$$r(u) = 2T \frac{\sin 2\pi fT}{2\pi fT} \tag{5.21}$$

It is seen that calculating the p(f) via the auto-correlation function decreases the error parameter by $\frac{1}{2}$. The resolution can, however, be controlled by changing the integration limits in Eqn. (5.20) from T to T_m

$$p(f) = \int_{-T_m}^{+T_m} r(u) e^{-2\pi i f u} du \tag{5.22}$$

The resolution then becomes $\frac{1}{2T_m}$. It must, however, be remembered that, if attempts were made to decrease ε too much by increasing m without increasing T, the resolution would become so poor as to render p(f) meaningless.

The spectrum calculated using the spectral window given by Eqn. (5.22) produces large sidelobes. These sidelobes result in an apparent shift of power from the mainlobe frequencies to the sidelobe frequencies. The sidelobes can be reduced by multiplying r(u) by some suitable lag window D(u) rather than truncating it with a rectangular function (Blackman and Tukey, 1958). The lag windows can be chosen so that the spectral resolution and the associated p(f) are satisfactory for the problem being investigated. Generally, in the design of any lag window the aim is to concentrate the main lobe of D(u) near f = 0, keeping the

Table 5.1

Lag and Spectral Windows

Description	Lag Window		Spectral Window
Rectangular or Box-Car	$D_R(u) = 1$	$\lvert u\rvert \leq T_m$	$D_R(f) = 2T_m \left(\frac{\sin \omega T_m}{\omega T_m} \right)$, $-\infty \leq f \leq +\infty$
	0	$\lvert u\rvert > T_m$	
Bartlett	$D_B(u) = 1 - \frac{\lvert u\rvert}{M}$	$\lvert u\rvert \leq T_m$	$D_B(f) = T_m \left(\frac{\sin \frac{\omega}{2} T_m}{\frac{\omega}{2} T_m} \right)^2$, $-\infty \leq f \leq +\infty$
	0	$\lvert u\rvert > T_m$	
Tukey	$D_T(u) = \frac{1}{2}(1+\cos \frac{\pi \lvert u\rvert}{T_m})$	$\lvert u\rvert \leq T_m$	$D_T(f) = T_m \left(\frac{\sin \omega T_m}{\omega T_m} \right) \left(\frac{1}{1-(\frac{\omega}{\pi} T_m)^2} \right)$, $-\infty \leq f \leq +\infty$
	0	$\lvert u\rvert > T_m$	
Parzen	$D_P(u)$ $1-6(\frac{\lvert u\rvert}{T_m})^2 + 6(\frac{\lvert u\rvert}{T_m})^3$	$\lvert u\rvert \leq \frac{T_m}{2}$	$D_P(f) = \frac{3}{4} T_m \left(\frac{\sin \frac{\omega T_m}{4}}{\frac{\omega T_m}{4}} \right)^4$, $-\infty \leq f \leq +\infty$
	$2(1 - \frac{\lvert u\rvert}{T_m})^3$	$T_m < \lvert u\rvert \leq T_m$	
	0	$\lvert u\rvert > T_m$	

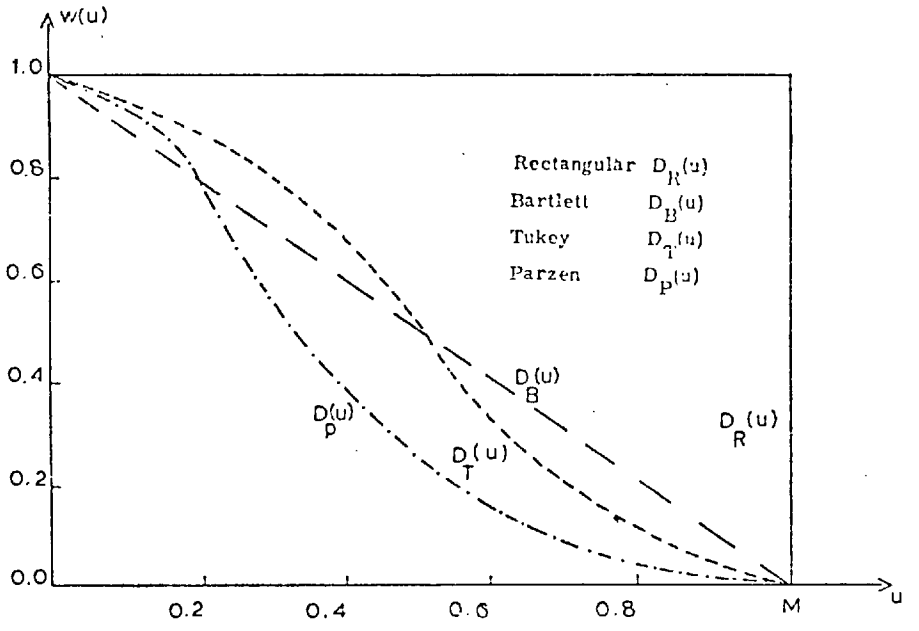


Figure 5.7. Some common lag windows.

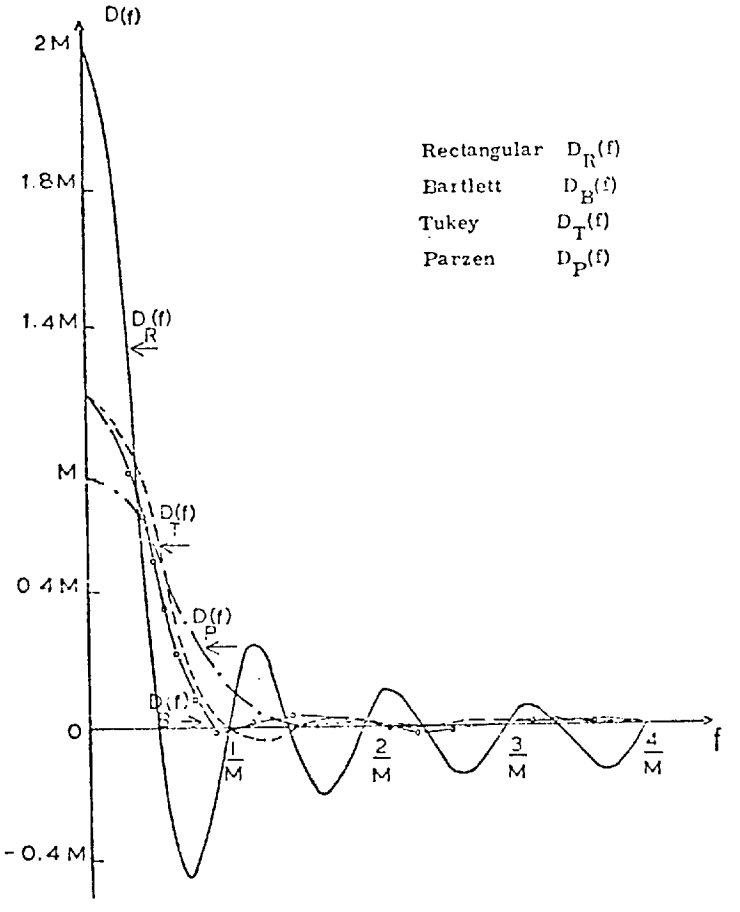


Figure 5.8. Spectral windows corresponding to the lag windows shown above.

sidelobes as small as possible. In order to concentrate the main lobe, D(u) has to be made flat. To reduce the sidelobes, however, D(u) has to be made smooth and gently changing, remembering that D(u) must vanish outside the limits $|T_m|$. Equation (5.22) then becomes,

$$p(f) = \int_{-T_m}^{+T_m} D(u)r(u)e^{-2\pi ifu}du \qquad (5.23)$$

Various lag windows have been suggested from time to time, to incorporate the various features discussed above. Table 5.1 lists those in common use, and Figures 5.7 and 5.8 are their diagrammatic representations.

The Parzen window was used here in the calculation of the power spectrum. One reason for choosing the Parzen window was the fact that it gives estimates of the power spectrum with extremely low side lobes.

5.3.2 PRE-WHITENING

Power spectral estimates are most precise when the power is evenly distributed over the whole range of frequencies. It sometimes happens that the power has one or more broad peaks. The average value of the power at any particular frequency, f, may be greatly distorted during computation, since the effect of the spectral window is to spread the power from the large peaks to adjacent frequencies. To avoid this, the data is first passed through a filter which

compensates or pre-emphasises the frequencies with lower amplitudes, and the spectrum then calculated in the usual way. This technique of bringing the resultant spectrum close to that of white noise is known as pre-whitening. However, after the spectrum has been obtained, an inverse pre-whitening filter has to be applied to remove the effect of the pre-whitening filter. For the present work, pre-whitening was not necessary. It must be remembered, though, that if the time series has a non-zero average, or a linear trend, a strong zero-frequency (d.c.) peak will be introduced in p(f). A zero-frequency peak also produces side-lobes, which distort the power spectrum and hence must be removed from the time series before any analysis. The d.c. level can be set to zero by subtracting the mean from the signal. The linear trend can be removed by fitting a straight line to the time series before the calculation of p(f). Removal of the d.c. level and the linear trend, before the analysis, are in fact special cases of the application of pre-whitening filters.

5.3.3 SOME PRACTICAL ASPECTS OF SPECTRAL ESTIMATION

The discussion of the previous sections related to estimation of the power spectra of continuous finite length analogue record. For a digitized time series the calculations are similar except that the integrals must be replaced by summations. In the present case the following procedure was adopted.

(1) The mean, square and variance of the samples were first calculated. These estimates are required to test for any trends and periodicities that may be present in the data (see for instance Bendat and Piersol, 1971).

(2) The data at this stage were transformed to have zero mean value. The new transformed data values are given by:

$$x_k = x(t)_i - \bar{x}(t)$$

where i, k = 1,2...K, the number of data points, and $\bar{x}(t)$ is the mean of the sample.

(3) The number of lags M for which the autocorrelations were to be computed was decided. The number of lags were chosen to be approximately K/4, K/5 and K/10 (Jenkins and Watts, 1965).

(4) Since the autocorrelation function is a symmetric function, only one half of it need be calculated. The digital formula is obtained by modifying Eqn. (5.19), and is given by:

$$r_m = \frac{1}{(K-m)} \sum_{m=0}^{K-m} x_k x_{k+m} \qquad m = 0,1,2...M$$

Plots of r_m for various lags assist in deciding what range of truncation values to use. The truncation point was decided by examining the chosen correlation function to see where it becomes negligible. A set of truncation values

M_1, M_2, M_3 was chosen, to cover a wide range.

(5) The power spectrum is calculated by taking the Fourier transform as is given in Eqn. (5.23). Since $D_m r_m$ is an even function of frequency, it is only necessary to calculate the cosine transform, which is given by, (Jenkins and Watts, 1969)

$$p(f) = 2\Delta t \left(r(o) + 2 \sum_{m=1}^{M} D_m r_m \text{Cos}(2\pi f m \Delta t) \right)$$

$$0 \leq f \leq \frac{1}{2\Delta t}$$

For purposes of computation, since $\Delta t = 1$, the smoothed power spectral density estimate is given by

$$p(f) = 2 \left(1 + 2 \sum_{m=1}^{M} D_m r_m \text{Cos}(2\pi f m) \right)$$

$$0 \leq f \leq \frac{1}{2}$$

In the present case, the points in the spectrum were calculated at every ℓ/M th interval. The final formula thus becomes

$$p(f) = 2 \left(1 + 2 \sum_{m=1}^{M} D_m r_m \cos(\pi \frac{\ell}{M} m) \right)$$

where $\ell = 0, 1, 2 \ldots M$

5.4 DATA ANALYSIS AND RESULTS

The analyses in this section were performed on the three unfiltered channels, all three channels being used for the volcanic tremor studies and the vertical component alone for the microearthquakes. The fourth, unfiltered, channel was primarily used for monitoring the output, using an oscilloscope, and also during the digitization of volcanic tremor as an anti-aliasing filter for the vertical component. This filtered channel, however, did not provide any additional information and hence is not included in the subsequent analysis.

For the convenience of discussion, this section has been divided into two parts. The first part deals with volcanic tremor and the second part with microearthquakes.

5.4.1 PART I: BACKGROUND SEISMIC RECORD

In order to study the spatial as well as the temporal variation in the background noise, selected portions of the recorded data were digitized according to the following scheme.

(1) For station 1 (Serra La Nave) the data were digitized every hour, approximately on the hour, for 40 sec. 12 sections of punched paper tape were obtained. Thus the first digitized section was for 40 sec after 13 June 12 hr 59 min, and so on.

(2) For station 2 (IC bench mark) and 4 (Monte S. Maria) the digitization was carried out from the 12 June 23 hr 59 min, but at every alternate hour. 12 punched paper tapes.

were thus obtained for each station. For station 3 (Forestale Hut) the digitization was carried out once only, because of the limited amount of data available.

All spectra are plotted as a function of the log power density against the log frequency (Hz). The spectrum of the vertical component was plotted first and whenever available was followed by the spectra of N-S and E-W components. Figures 5.9 to 5.16 show the spectra obtained at the various sites. The number against each curve indicates the time of the analysed signal (see Appendix 2A, 2B, 2C, 2D).

5.4.1.1 STATION 1: SERRA LA NAVE

A total of nine power spectra was utilized for the final analysis at this station. The N-S component seismometer was inoperative most of the time, due to mechanical failure. As none of the Geostores was calibrated in the field, it was not possible to calculate the power of the signal in absolute terms.

Relevant information as to the approximate time, bandwidth of the spectrum, distribution of total power in the various frequency bands etc., of the analysed signal are given in Appendix 2A.

It is seen from this table that the dominant frequency (defined as the frequency associated with the peak amplitude of the Fourier spectrum) is quite consistent and ranges between 1.18 and 1.76 Hz. In two instances, however,

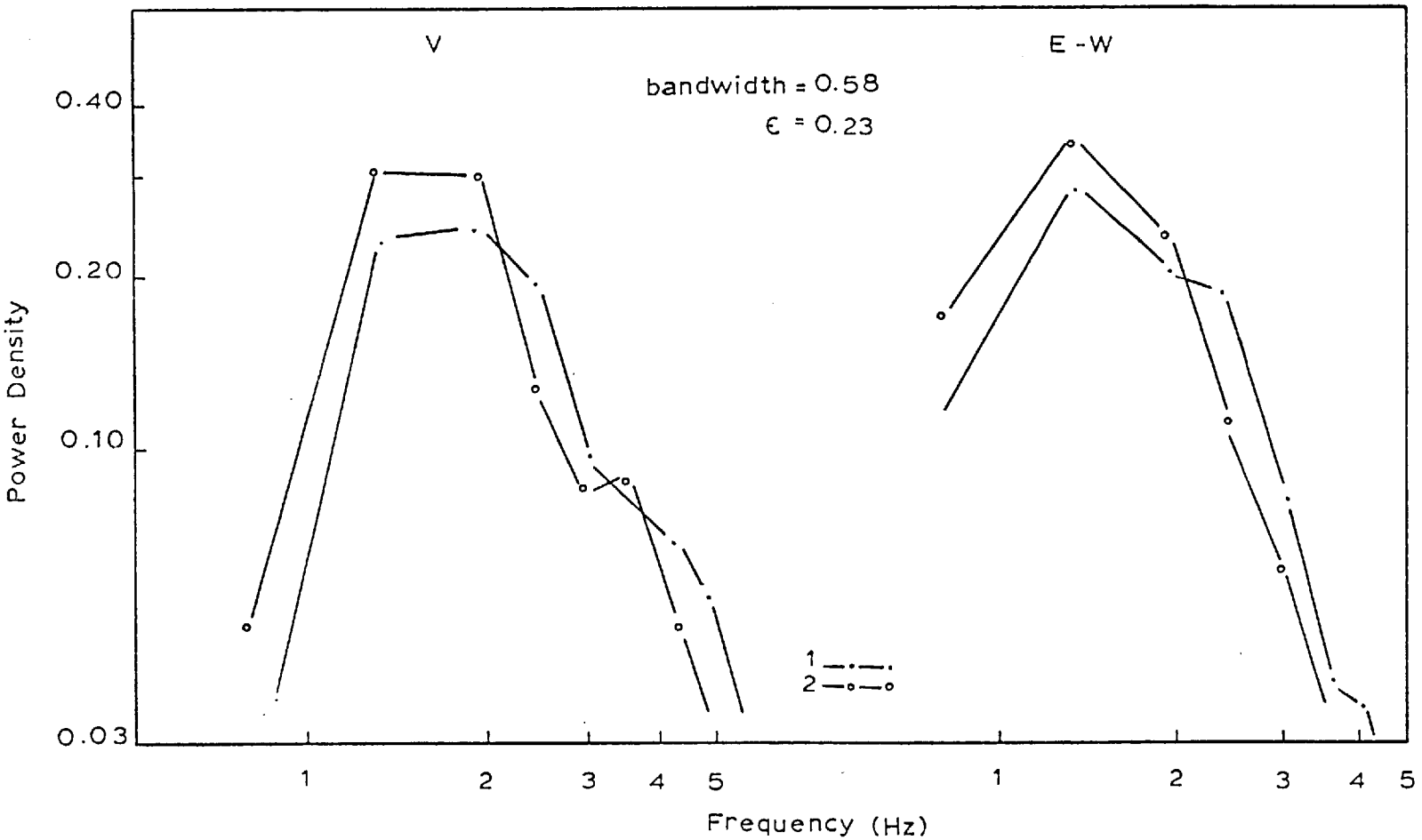


Figure 5.9. Plots of power density versus log frequency (Hz) for background seismic noise recordings obtained at Serra La Nave (station 1). The number associated with each curve indicates the hour of analysis in a 24 hour period (see Appendix 2A).

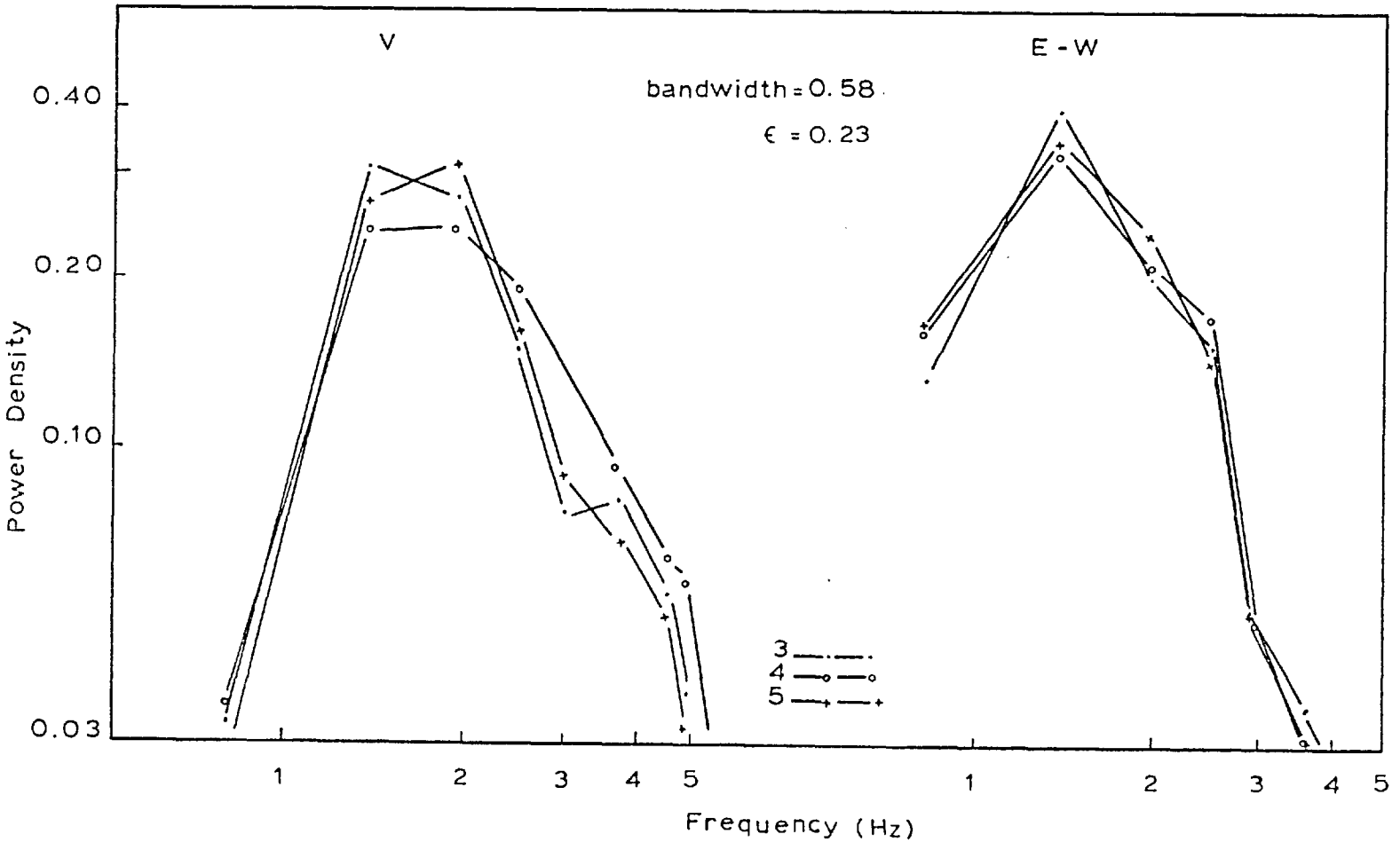


Figure 5.10. Caption as in Figure 5.9.

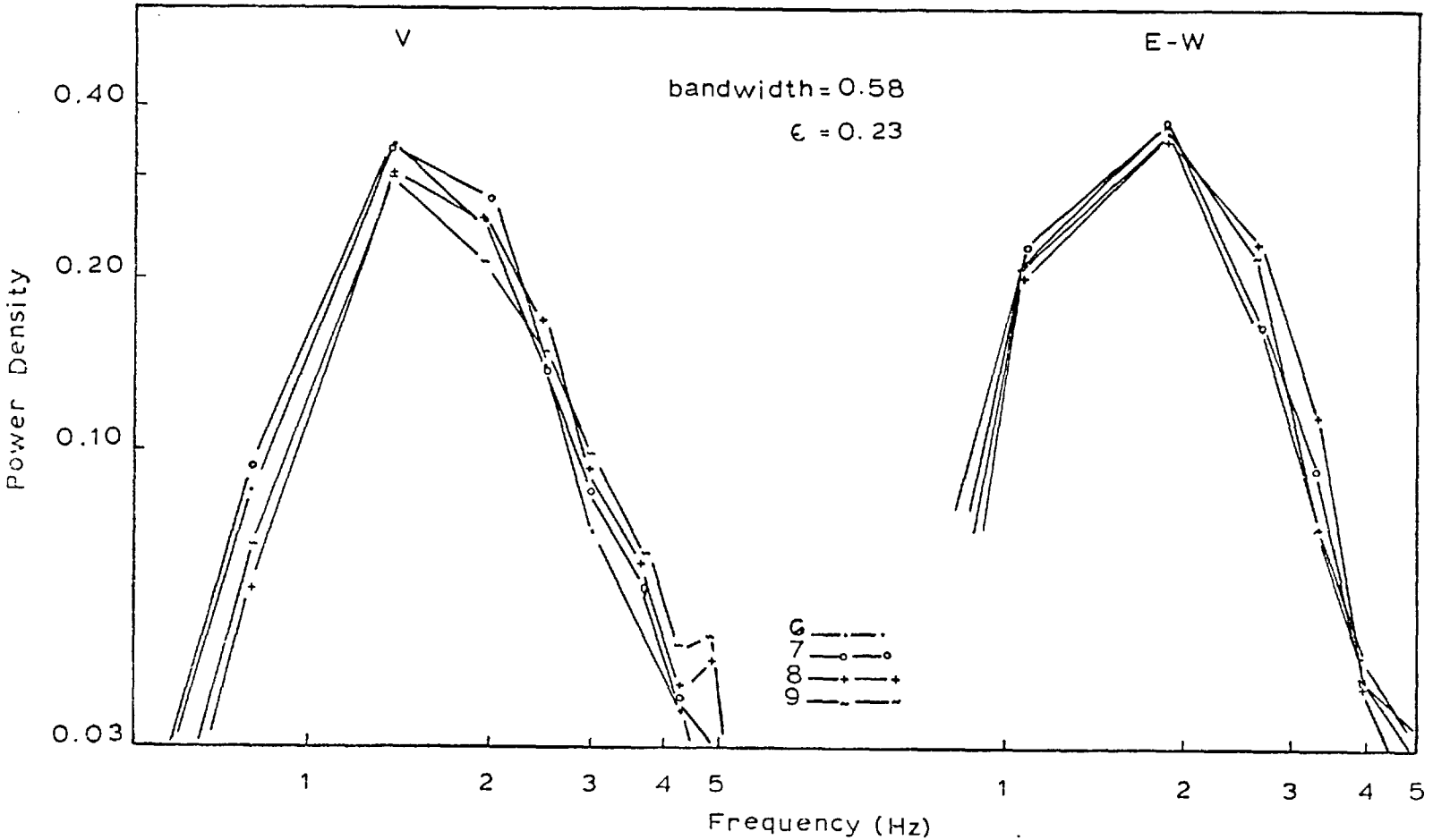


Figure 5.11. Caption as in Figure 5.9.

they range between 1.77 and 2.35 Hz. As we were interested in the 'gross-structure' of the spectrum, individual peaks were thus not resolved. These frequency ranges seem to be in good agreement with the volcanic tremor measurements carried out on Mount Etna by Shimozuru (1971), Schick and Riuscetti (1973), Lo Bascio et al. (1976), and Guerra et al. (1976).

An interesting feature of some of the power density plots, in addition to the dominant frequency, is the occurrence of a small peak between 3.54 and 4.12 Hz. This peak does not occur in the corresponding horizontal seismometer; the seismic signal cannot thus be associated with the volcanic activity. The spurious peak could be either of external origin, the nature of which is difficult to establish at this stage or more likely due to an error in the digitization process.

More than 60% of the total power in the vertical component is concentrated in the narrow frequency band of 1.18 to 2.94 Hz, whereas that in the E-W appears to range between 0.59 and 2.94 Hz.

The relative Fourier amplitude values associated with the dominant frequencies range between a maximum of 0.57 (arbitrary units) to a minimum of 0.48 (arbitrary units). The corresponding horizontal component values range between 0.61 and 0.53. No direct comparison can, however, be made between these two sets of values, as the horizontal and

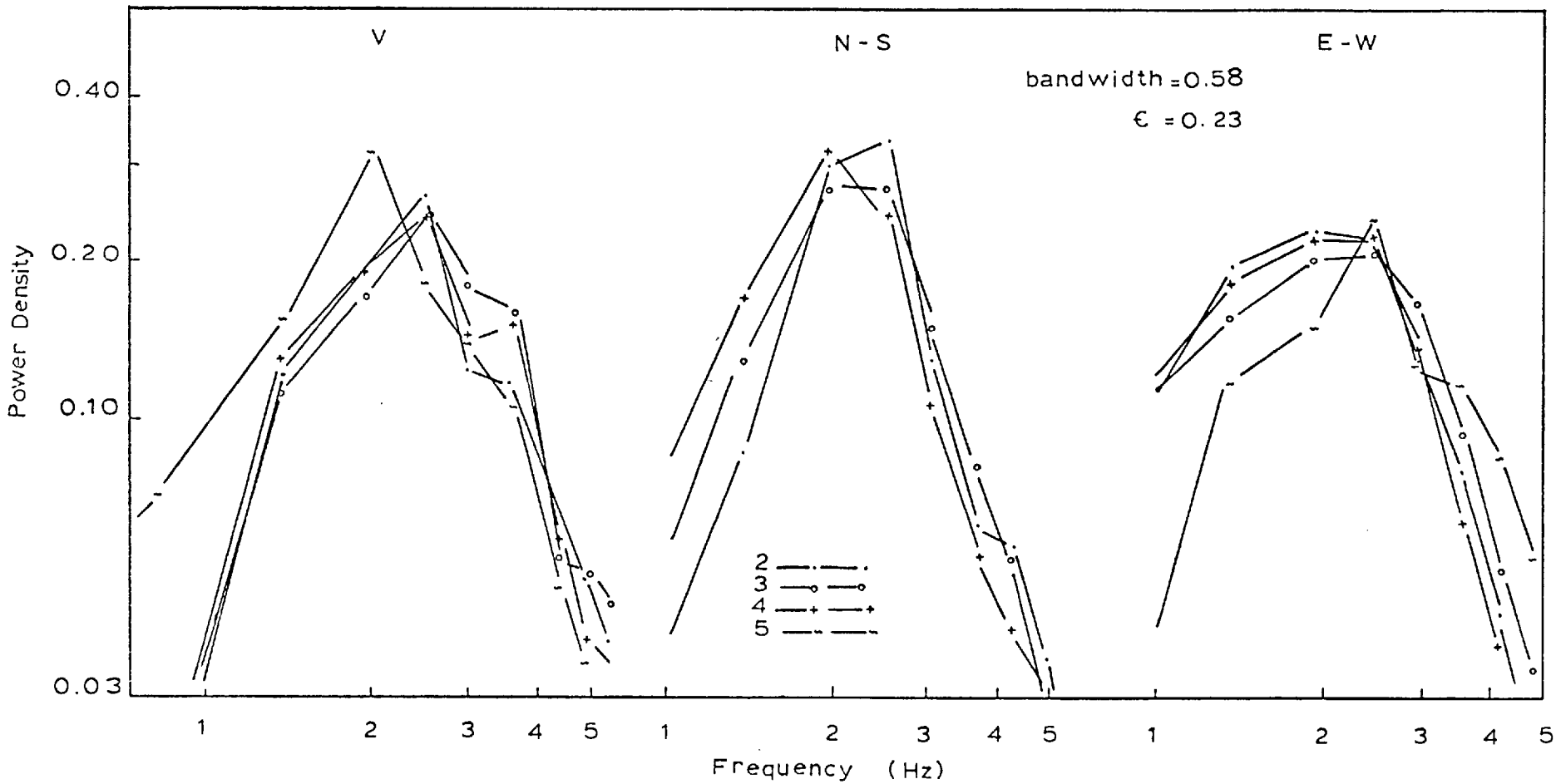


Figure 5.12. Plots of power density versus log frequency (Hz) for background seismic noise recordings obtained at IC bench mark (station 2). The number associated with each curve indicates the hour of analysis in a 24 hour period (see Appendix 2B).

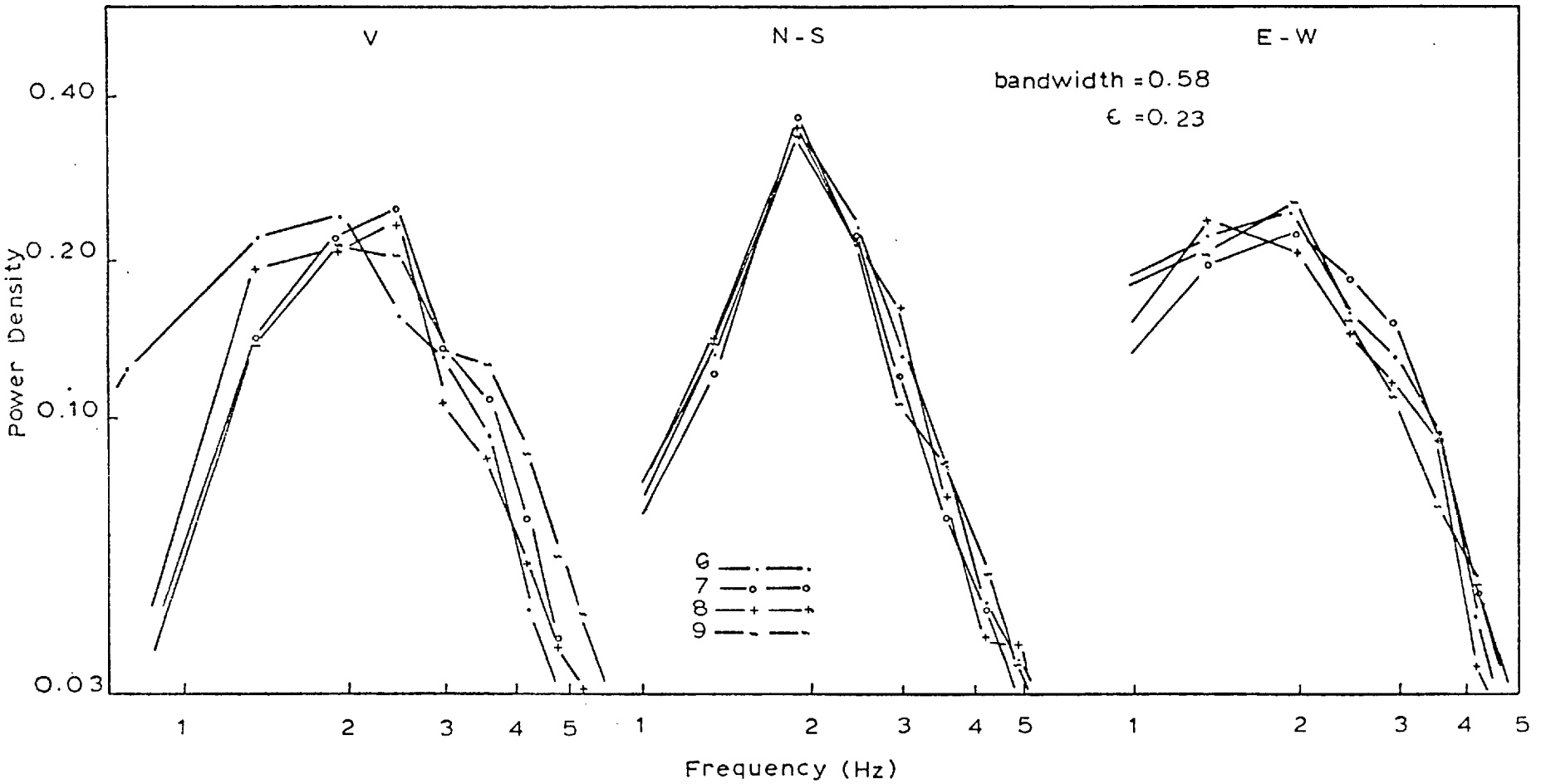


Figure 5.13. Caption as in Figure 5.12.

vertical seismometers had different frequency responses, but they will be used later for inter-station comparison (see Section 5.4.2).

The ratios of the various components are sometimes used to determine the nature of the seismic signal. The data from station 4 (Monte S. Maria), where similar seismometers were employed, will be used to discuss the nature of this wave.

5.4.1.2 STATION 2: IC BENCH MARK

Power density values at this station,with other relevant information,are listed in Appendix 2B. Figures 5.12 and 5.13 are plots obtained from such calculations. The shape of the power density curves are familiar bell-shaped, as at Serra La Nave. The dominant frequency is, however,slightly shifted towards higher values (2.36 - 2.94 Hz), except in two instances where they range between 1.77 and 2.35 Hz.

Power in the vertical component appears to be more spread out towards higher frequencies than at station 1. More than 60% of the total power lies between 1.18 and 3.53 Hz.

The relative Fourier amplitude values associated with the dominant frequencies range between a maximum of 0.54 and a minimum of 0.44 for the vertical, 0.56 and 0.44 for the N-S, and 0.43 and 0.37 for the E-W components,

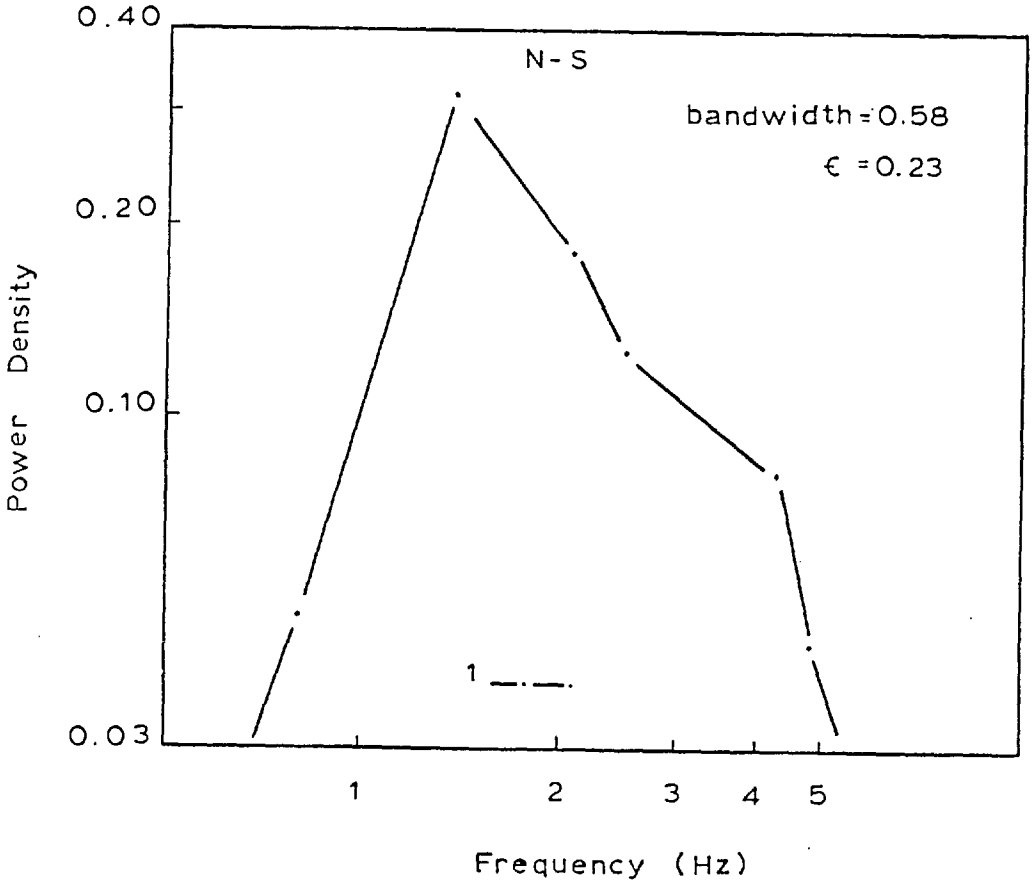


Figure 5.14. Plot of log power density versus log frequency (Hz) for background seismic noise recordings obtained at Forestale Hut (station 3). The number associated with the curve indicate the hour of analysis in a 24 hour period (see Appendix 2C).

respectively. As at station 1,no direct comparison can be made between the vertical and the other components, but the two horizontal recordings appear to indicate a higher (Fourier amplitude) value for the N-S component.

5.4.1.3 STATION 3: FORESTALE HUT

A small section of background noise data was analysed. The results are tabulated in Appendix 2C and shown in Figure 5.14. The dominant frequency range is 1.77 - 2.35. However,not enough reliable data is available in this station to define an accurate dominant frequency range.

5.4.1.4 STATION 4: MONTE S. MARIA

Seven digitized seismic sections were used for the spectral analysis at this station. Results of the calculation are tabulated in Appendix 2D and shown in Figures 5.15 and 5.16. The dominant frequency at this station appears to lie between 1.77 and 2.94 Hz, and more than 60% of the total power is confined within that limit. The relative Fourier amplitude values associated with the dominant frequencies range between a maximum of 0.62 and a minimum of 0.54.

In order to gain a better understanding of the nature of this background disturbance,relative average Fourier amplitude values were calculated for the 3-components. Table 5.2 gives the result.

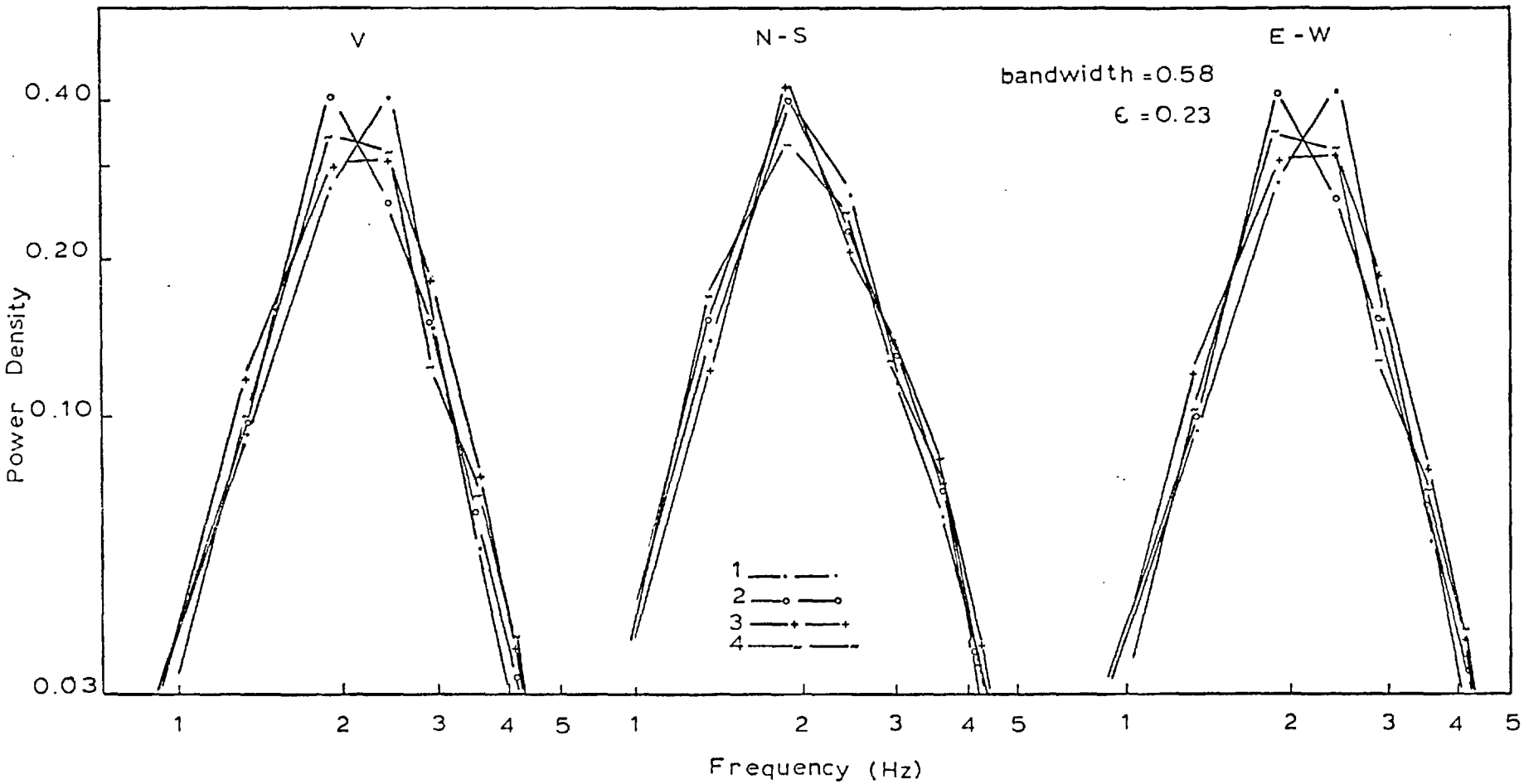


Figure 5.15. Plots of power density versus log frequency (Hz) for background seismic noise recordings obtained at Monte S. Maria (station 4). The number associated with each curve indicates the hour of analysis in a 24 hour period (see Appendix 2D).

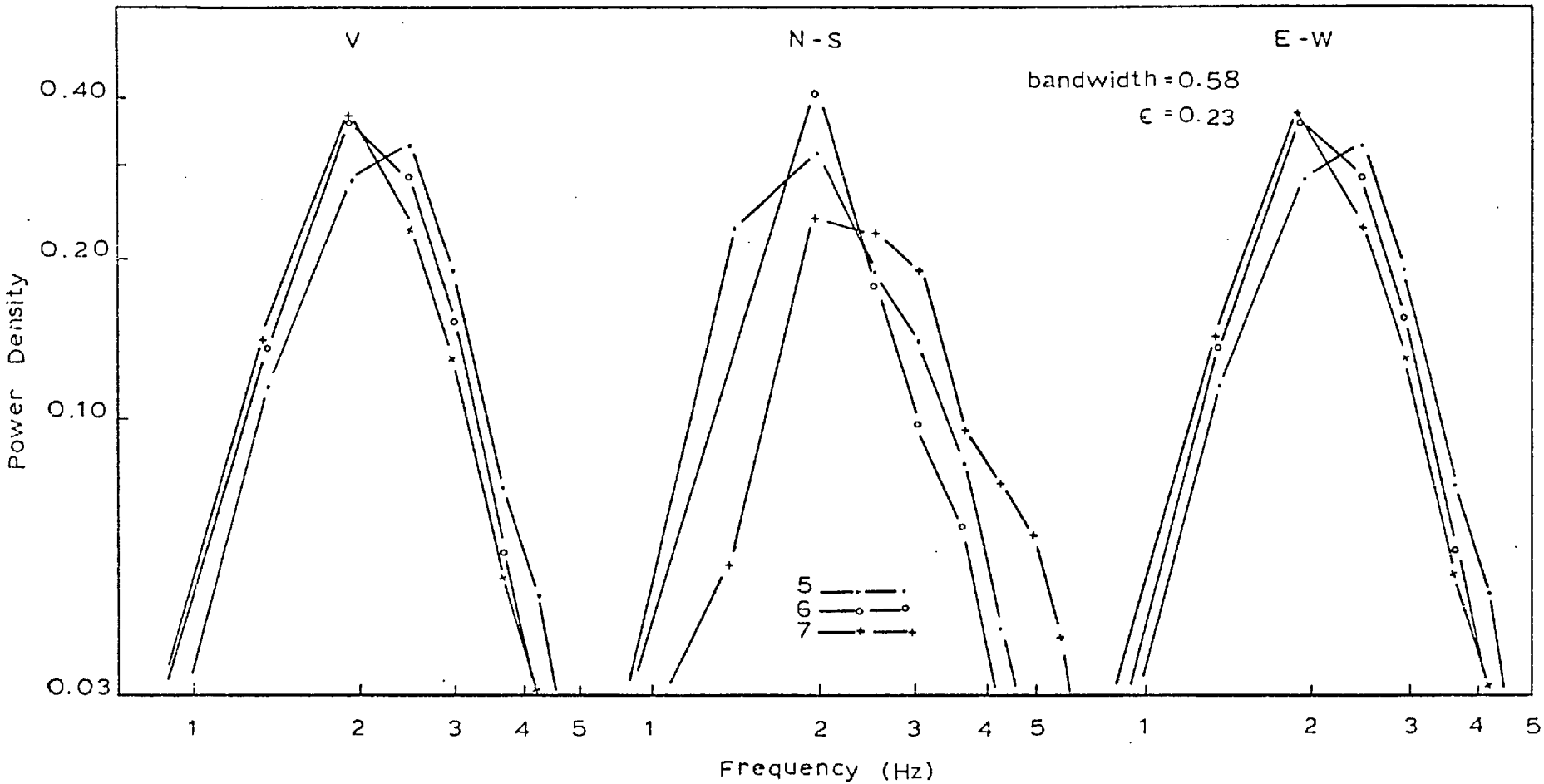


Figure 5.16. Caption as in Figure 5.15.

Table 5,2

Average Fourier Amplitude Estimates for
Monte S. Maria
(Arbitrary Units)

Frequency Interval	Component		
	V	N-S	E-W
0.0 - 0.58	0.08	0.07	0.05
0.59 - 1.17	0.13	0.13	0.13
1.18 - 1.76	0.35	0.38	0.39
1.77 - 2.35	0.57	0.58	0.55
2.36 - 2,94	0.51	0.45	0.49
2.95 - 3.53	0.38	0.36	0.36
3.54 - 4.12	0.24	0.27	0.25
4.13 - 4.71	0.18	0.19	0.19
4.72 - 5.30	0.12	0.15	0.14
5.31 - 5.89	0.11	0.13	0.13

It is seen from the table that at the dominant frequency the N-S component has the highest relative amplitude. Since this seismometer predominantly records the radial component of the shear wave, the recorded waves are probably of Rayleigh type. Kubotera (1974), while investigating Aso volcano in Japan, recorded volcanic tremors having periods of between 0.4 and 0.6 sec, i.e. frequencies of between 1.7 and 2.5 Hz. These, he thought, were of the Rayleigh type. Though no direct comparison exists between Etna and Aso volcanoes, the dominant periods of between 0.34 and 0.56 sec recorded at this station support the belief that they may be of the Rayleigh type as well.

5.4.2 INTER-STATION COMPARISON AND SOURCE LOCATION

In order to gain a better understanding of the nature and the source of the volcanic tremor, estimates of the average Fourier amplitudes (Table 5.3) were made at the various stations and plotted in Figure 5.17. Only the vertical components were used for the comparisons, as this was the only component for which the same type of seismometer (HS 10) was used at all four stations. Thus the plots in Figure 5.17 represent the mean spectrum obtained from the hourly samples for station 1, and two-hourly samples for stations 2 and 4, over the 12 hr period commencing at 13 June 13 hr 59 min.

In the frequency domain, each of the spectra $\phi(\omega)$,

Table 5.3

Average Fourier Amplitude Estimates
at the Various Stations
(Arbitrary Units)

Frequency Interval	Station		
	Serra La Nave	IC Bench Mark	Monte S. Maria
0.0 - 0.58	0.04	0.09	0.06
0.59 - 1.17	0.22	0.23	0.13
1.18 - 1.76	0.53	0.40	0.35
1.77 - 2.35	0.50	0.47	0.57
2.36 - 2.94	0.39	0.44	0.51
2.95 - 3.53	0.28	0.35	0.38
3.54 - 4.12	0.26	0.31	0.24
4.13 - 4.71	0.21	0.23	0.18
4,72 - 5.30	0.19	0.19	0.12
5.31 - 5.89	0.14	0.18	0.11

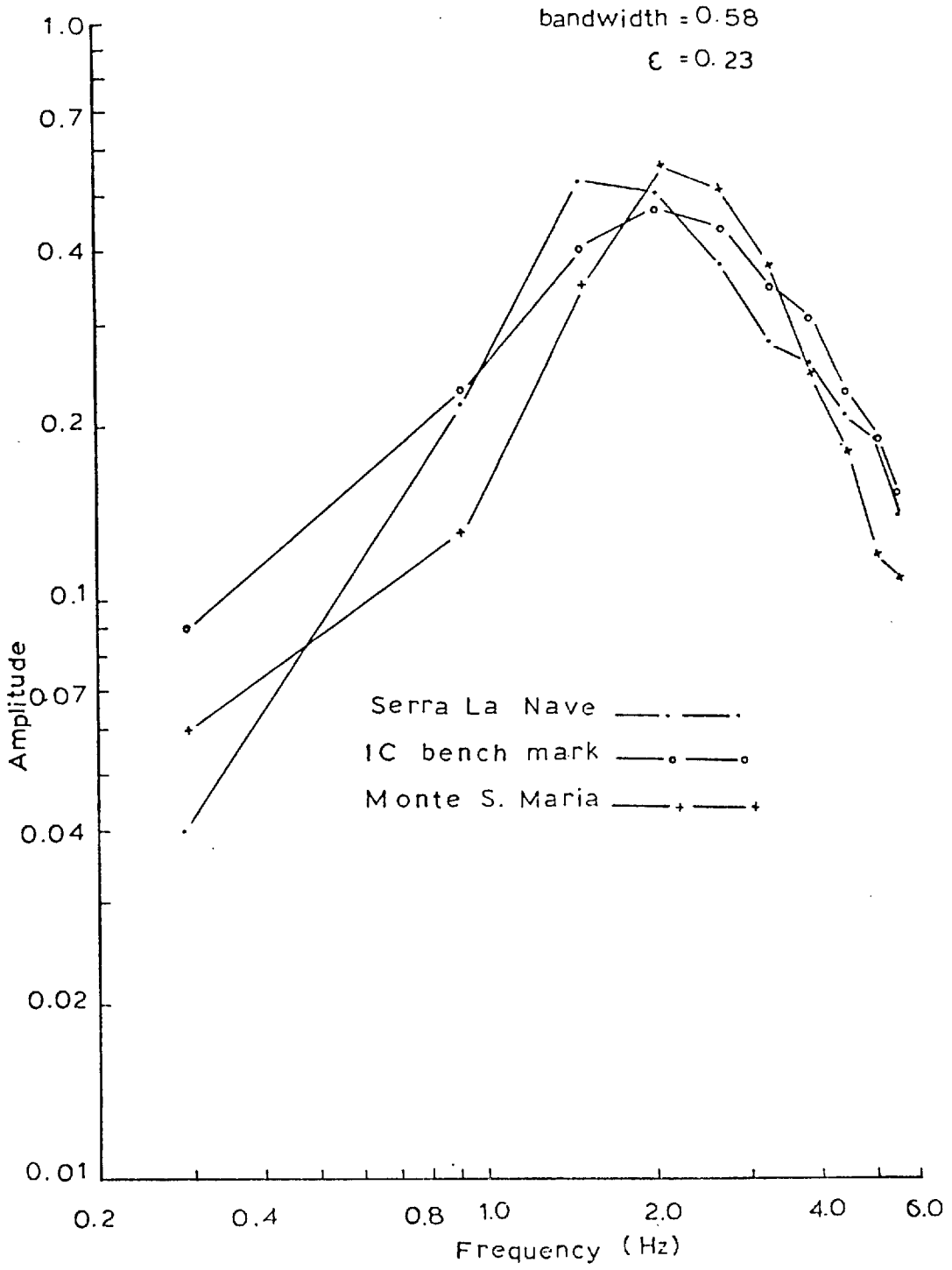


Figure 5.17. Average Fourier amplitudes of volcanic tremor obtained at the various stations and plotted as a function of frequency.

obtained from the recorded seismogram can be thought of as a seismic signal modified mainly by the source parameters $S(\omega)$ and the site geology $T(\omega)$,

or $$\phi(\omega) = S(\omega).T(\omega)$$

where $\omega = 2\pi f$ and f = frequency.

If we assume for simplicity that the signal recorded at the different stations is generated by the same source, and since all the seismographs have similar frequency response, the amplitude spectrum becomes a function of $T(\omega)$ only. $T(\omega)$ is often referred to as the transfer function and is dependent on the thickness, velocity and density of the medium through which the signal is travelling, as well as on the angle of incidence.

If the geological conditions were identical, the shape of the spectra would be similar. Figure 5.17 indicates a 'broad-similarity' between the shapes of the various spectra, implying, perhaps, the gross influence of the transfer function. A closer look at the various spectra, however, reveals local differences between the source and the station. Spectra obtained at Serra La Nave and Monte S. Maria are almost identical in shape between 1 and 3.2 Hz, although the shift to higher frequencies with a corresponding increase in amplitude at station 4 is obvious. Beyond those frequency limits, however, the similarities break down. At S. Maria the spectrum is flatter at the low frequency end than at Serra La Nave, although the opposite is true at higher fre-

quencies. These observations may imply preferential screening of frequencies from the source to the two stations. At the IC bench mark, however, the spectrum is much broader than at the other two stations and the dominant frequency appears to be around 2 Hz. The important question seems, however, how much of the spectra $\phi(\omega)$ are shaped by the source mechanism $S(\omega)$, and how much by the properties of the medium $T(\omega)$. With our present knowledge of Etna it is difficult to answer these questions satisfactorily.

Because of the non-impulsive character of volcanic tremor, it is not possible to apply the usual travel time techniques used to located microearthquakes. However, an approximate location of the source can sometimes be obtained by mapping the differences in amplitude of the seismic signal at the various locations. Seismic waves are reduced in amplitude as they propagate through the earth, due mainly to (1) absorption of energy in the medium of transmission and (2) geometrical spreading.

When a wave passes through a medium,the elastic energy associated with the wave motion is gradually absorbed by it, reappearing ultimately in the form of heat. This process is called absorption, and is responsible for the eventual complete disappearance of the wave motion. The mechanism by which the elastic energy is transformed into heat is not understood clearly. During the passage of a wave, heat is generated during the compressive phase and absorbed during the expansive phase. The process is not

perfectly reversible since, the heat conducted away during the compression is not equal to the heat flowing back during the expansion. Internal friction, and many other mechanisms, such as loss of energy involved in the creation of new surface (fracturing near an explosion) piezoelectric and thermoelectric effects, viscous losses in the fluid filling the rock pores, etc, contribute to the absorption of energy.

The attenuation of plane waves due to absorption of energy is of the familiar exponential form (Parasnis, 1972)

$$A = A_o \exp\left(-\frac{\delta f r}{V}\right)$$

where A = recorded amplitude

A_o = amplitude at source

δ = logarithmic decrement

f = frequency

r = distance in km

V = the velocity in km/sec.

The influence of the second factor (i.e. at large distances from the source waves are reduced in amplitude in inverse proportion to the distance travelled), combined with the first, can be written as

$$A = \frac{A_o}{r} \exp\left(-\frac{\delta f r}{V}\right)$$

The solid line in Figure 5.18 shows the relative values (A) plotted as a function of distance, using the above

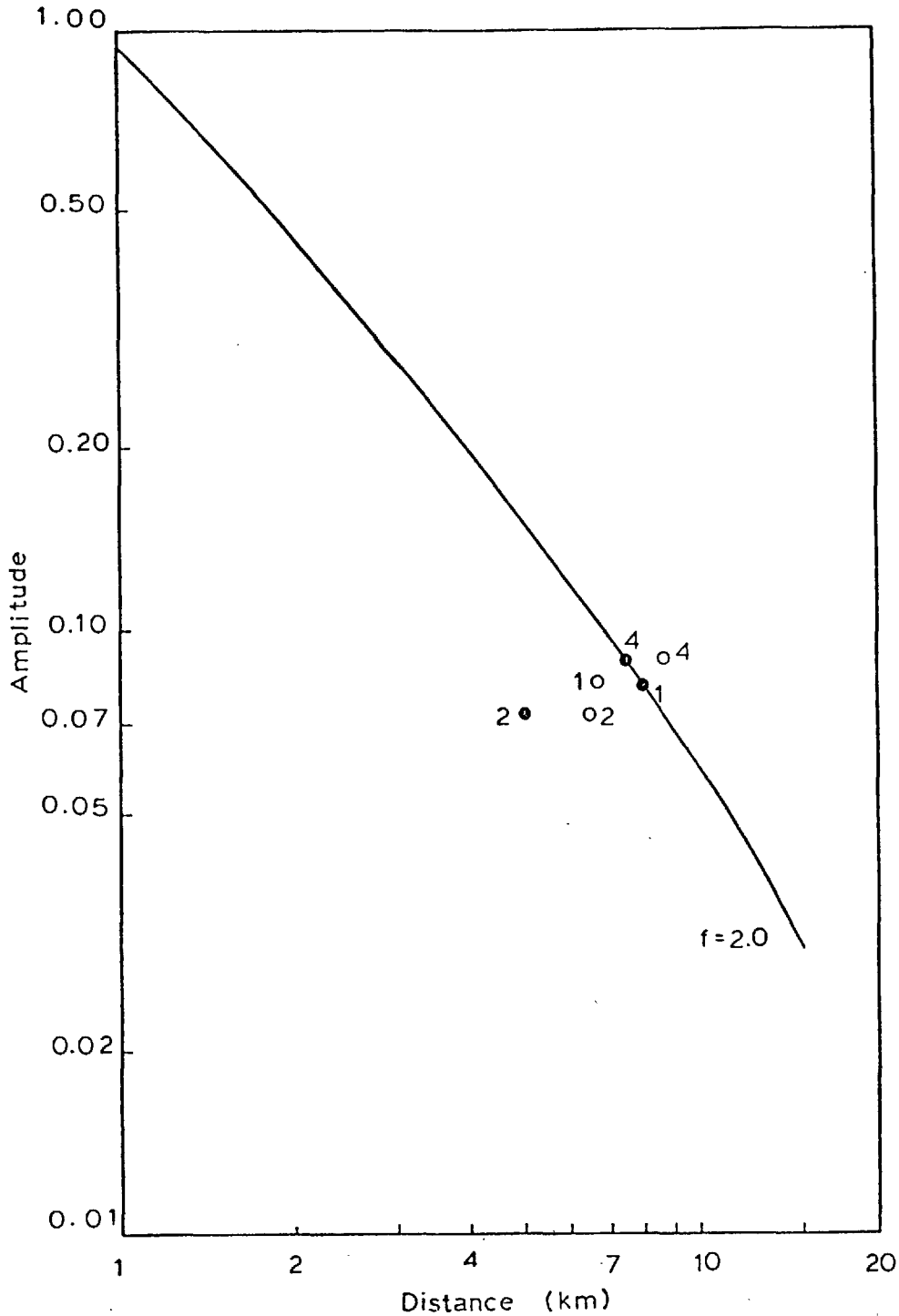


Figure 5.18. Relative amplitudes of the volcanic tremor (obtained at stations 1, 2 & 4) plotted as a function of distance from the Central Crater (open circles) and the Northeast Crater (solid circles).

relation. V, the velocity, was taken as 1 km/sec (corresponding to the surface wave velocity calculated in Section 4.4.3), δ as 0.025 (typical value of earth material in bulk) and f as 2.0 Hz (the dominant frequency recorded during this investigation). Also shown, by open and solid circles (numbers against them refer to the station) are the relative amplitudes, taking the origin of the tremors as the Central and the Northeast Crater respectively.

It is seen from Figure 5.18 that the amplitude values at Serra La Nave and S. Maria appear to follow the exponential law, when the Northeast Crater is taken as the seismic source, whereas at the IC bench mark it is about 29% short of the expected value. Two possible explanations of the low amplitudes at the IC bench mark site are that the Northeast Crater is not the source of the volcanic tremor, and that the tremors are highly attenuated between the Northeast Crater and the station, possibly due to the presence of very loose material, or less likely due to the presence of liquid bodies in the area.

Since only three stations are involved, it is possible to find, either formally or by trial and error, a unique location for the source that satisfies the observed relative amplitudes. The location is found to be about 3 km NW of the Central Crater. During the recording period, lava was erupting from new boccas 2 km to the north, at about 2,500 m (Murray et al. 1977), followed occasionally by Strombolian activity at the Northeast Crater.

Table 5.4

Dominant Period of Background Volcanic Tremor Obtained for Volcanoes in Various Parts of the World

Volcano	Period	Investigator
Hawaii (Kilauea)	0.10	Eaton et al.
(Kilauea)	0.50	Finch et al.
Sakurajima	0.40 - 0.80	Kagoshima Meteoral. Obs.
	0.33 - 0.40	Minakami et al.
	0.25 - 0.38	Watanbe
Aso	0.25	Minakami
	0.20	Shimozuru
Oosima	0.30	Takahashi et al.
	0.30 - 0.40	Minakami et al.
	0.50 - 0.60	Minakami et al.
Paricutin	0.10 - 0.20	Cavarrubias
	0.35 - 0.60	Cavarrubias
Vesuvius	0.63	Imbo
Nyiragongo	0.50 - 0.70	Shimozuru
Etna	0.10 - 0.44	Schick et al.
	0.33 - 0.50	Lo Boscio et al.
	0.50	Shimozuru
	0.35 - 0.83	Muniruzzaman
	0.55 - 0.66	Guerra et al.

The conclusion that can be drawn from the above observation is that, during the '75 investigation, the source of the seismic disturbance probably lies to the north of the Central Crater somewhere between the Northeast Crater and a point about 3 km northwest of the Central Crater.

The studies of the background seismic noise conditions at other volcanoes also indicate certain dominant periods - characteristic of each volcano. Table 5.4 lists the dominant period of volcanic tremor of some important volcanoes around the world, along with the present findings. It is seen from the table that there is a wide range of dominant periods even for the same volcano. For instance, the Hawaiian volcano appears to have frequencies whose periods range from 0.10 - 0.50 sec. This is, however, to be expected, as measurements were carried out by different investigators at different stages of the volcanic cycle. The present findings, however, seem to be in good agreement with those of other workers on Etna using similar kinds of instruments.

5.4.3 MECHANICS OF VOLCANIC TREMOR

The various theories that have been proposed from time to time to explain the causes of volcanic tremor have been discussed briefly in the introduction. In this section we shall take a closer look at one of these explanations, that appears to be favoured by seismologists working on Etna,

and examine how far it is successful in explaining our observations.

In the course of the present volcanic tremor survey we have established certain features that seem to characterize these processes:

(1) The presence of continuous volcanic tremor throughout the whole period of investigation (~ 20 days).
(2) The amplitudes and frequencies exhibit very little variation in space and time (at least over 24 hours).

Any proposed mechanism thus must be able to explain these features, taking the known geology of the area into account.

Possible sources of the kinetic energy released may be the continuous micro-fracturing, and dislocation of rocks surrounding dykes and sills. But Schick & Riuscetti (1973) in their analysis found that the vanishing seismic moment (defined as $\langle u \rangle = M_o/\mu A$, where $\langle u \rangle$ is the average dislocation or average slip over the fault surface, μ is the rigidity, M_o is the source moment, and A is the area of the fault slip, see for instance Brune, 1968) for these processes speak against such a source mechanism.

Volcanic tremors are thought to be generated by a physical process known as 'self-oscillation' (see for instance Andronov et al., 1960). The self-oscillations are,

however, characterized by certain features. The common feature is their ability to perform self-oscillations which do not depend, generally speaking, on the initial conditions but are determined by the properties of the system itself. Thus, whatever the initial conditions, undamped oscillations are established, and these undamped oscillations are stable. However, in any self-vibrating system, energy losses occur, and maintenance of the oscillations requires an input of energy. Thus there is bound to be a source of energy for this process. In other words a self-oscillating system is an apparatus which produces a periodic process at the expense of a non-periodic source of energy.

An analysis of volcanic tremor indicates the time constancy of its amplitude and period. Thus the properties of volcanic tremor and of a self-oscillator are quite similar. One possible source of the necessary energy that must be considered is the kinetic energy of gas flow.

A close look at the mechanics of gas flow through the magmatic channels will probably reveal more information about the conditions under which these oscillations are set up. The following analysis is due mainly to Steinberg and Steinberg (1975). To a first approximation, the motion of gases through the channels resembles the motion of viscous gases through a thermally insulated vertical cylindrical tube. Under these conditions, the equations of the flow may be written as

$$\frac{dW}{dZ} = \frac{k\lambda W}{2D\left(\frac{c^2}{W^2} - 1\right)} \qquad (5.24)$$

where,

$k = c^2/(RTg)$

Z = vertical distance along the tube

W = rate of gas motion

λ = co-efficient of tube resistance

R = gas constant

g = acceleration due to gravity

T = temperature

D = diameter of the tube

c = velocity of sound in the given medium

From the above equation, it is seen that $\frac{dW}{dZ} > 0$ if $c > W$, that is, when the gas is accelerated as it moves through the tube. Let us consider now the rate of gas motion W as an independent variable, and formulate the thermodynamic parameters as a function of W. Since the gas is viscous, friction against the wall will decrease its pressure as it moves up a distance dZ. This decrease in pressure is given by

$$P = \frac{W^2 \lambda}{2vgD} \cdot dZ \qquad (5.25)$$

where $\lambda = f(Re)$ and $Re = WD/\nu$

ν = kinematic viscosity of the gas

Re = Reynolds number

v = specific volume

This pressure decrease, however, means that the potential energy will also decrease. The energy loss will then manifest itself as frictional heat, given by

$$dQ = vdP = \frac{W^2\lambda}{2gD}\,dZ \tag{5.26}$$

The entropy of the system is given by

$$dS = \frac{dQ}{T} \tag{5.27}$$

So the vertical gradient of entropy is equal to

$$\frac{dS}{dZ} = \frac{W^2\lambda}{2gDT} \tag{5.28}$$

and since dW is an independent variable, Eqn. (5.28) can be written as

$$\frac{dS}{dW} = \frac{W^2\lambda}{2gDT} \cdot \frac{1}{dW/dZ} \tag{5.29}$$

Substituting the value of dW/dZ from Eqn. (5.24) into Eqn. (5.29) and simplifying we get,

$$\frac{dS}{dW} = R\left(\frac{W}{c}^2\right)(c^2-W^2) \tag{5.30}$$

Equation (5.30) thus is the equation that controls the flow of gas in a thermally insulated magmatic channel. It shows that the change of entropy with respect to the rate of gas motion depends on the three velocity ranges that W can attain.

(1) When W = c, i.e. the gas moves with the speed of sound, the function S(W) has its maximum value,

(2) when W < c i.e. the gas moves with speed less than the speed of sound, $\frac{dS}{dW} > 0$, and the gas entropy increases,

(3) and when W > c, i.e. the gas moves faster than

the speed of sound, $\frac{dS}{dW} < 0$, and the gas entropy decreases.

Experiments (as reported by Steinberg and Steinberg, 1975), however, have indicated that the transition from less than, through and greater than the velocity of sound is impossible when gas flowing along the tube encounters resistance. However, when the gas velocity W reaches the local sound velocity c (known as the critical value) intense vibrations are set up in the viscous gas. These vibrations impart large amounts of energy and (an increase in the gas entropy) to the volcanic edifice, which in turn is thought to give rise to volcanic tremor.

Measurements of gas velocities (as reported by Tazieff, 1972) were carried out on an eruptive vent in the Bouca Nova (Mount Etna) by a wheel anemometer. Velocities of about 160 m/sec were recorded (and the acceleration exceeded 10 g). If these velocities are regarded as typical gas velocities during volcanic paroxysms, it is unlikely that gas velocities exceed this value during repose periods (although data in this respect is very inadequate).

It thus appears, from a discussion of the current views on volcanic tremor, that no single process can satisfactorily explain the causes of volcanic tremor on Mount Etna. However, from the evidences gathered so far the most probable cause seems to be viscous gas flow*. This gas

*The magma of Etna normally contains 1-2% by weight of dissolved volatiles. These volatiles come out of solution when the pressure in the magma column drops below a critical value (Wadge, 1974).

originates by the degassing of magma in the upper part of the vent. The top of the central magma column of Etna is at atmospheric pressure most of the time, and Wadge (1974) suggests that degassing take place with the help of convection currents within the column, such as has been observed at several lava lakes. Whatever the physical process of degassing, it appears unlikely that the viscous gas always flows at supersonic speed on Etna to establish the 'self-oscillation', as has been envisaged by Steinberg & Steinberg (1975). It appears more likely that tremors are set up by the expanding gas front at places of widening vents. In our proposed model the frequencies and amplitudes of the volcanic tremor are thus determined by the parameters of the system , that is, to a first approximation, by the dimensions of the channels. And in a complex volcanic apparatus, such as Etna, it is thought that there are many channels through which volcanic gases may be released. The volcanic tremor recorded on a seismogram is thus the resultant of the sum of a number of harmonic oscillators (set up by the expanding gas front), the amplitudes of which appear to follow a Gaussian distribution.

5.4.4 PART 2: MICROEARTHQUAKE ANALYSIS

In order to investigate the spectral contents of microearthquakes, 13 selected events of both A and B-type were digitized at 100 samples/sec (giving a Nyquist frequency of 50 Hz), and analysed.

5.4.4.1 A-TYPE MICROEARTHQUAKES

Power density estimates for six A-type microearthquakes recorded at the various stations during the period of the investigation are tabulated in Appendix 3A, and Figures 5.19 to 5.22 are their power density versus frequency plots. All the microearthquakes have very small magnitudes, as none of them was recorded at more than one station.

Figures 5.19a and 5.19b show the spectral characteristics of two of these microearthquakes, recorded at station 2 (the IC bench mark site). Both these events have the first important peak between 1.39 and 1.85 Hz and the spectra in general have a rather smooth appearance. The dominant frequencies seem to range between 2.54 and 3.01 Hz for Figure 5.19a and between 2.08 and 2.54 Hz for Figure 5.19b. There is a remarkable similarity between the shape of the spectra, and both have three major peaks in the principal frequency range. The power of the microearthquakes effectively reduces to zero beyond about 6.50 Hz. Both these events appear to have originated from the same source and possibly by a similar mechanism.

Figures 5.20a and 5.20b are the spectra of a further two events recorded at station 2. These microearthquakes have dominant frequencies between 2.07 and 2.53 Hz (Fig. 5.20a) and between 3.27 and 3.73 Hz (Fig. 5.20b) respectively. The shape of the spectrum has a spikey appearance, and in general has a greater high frequency content than the two microearthquakes discussed earlier. Figure 5.21 is the

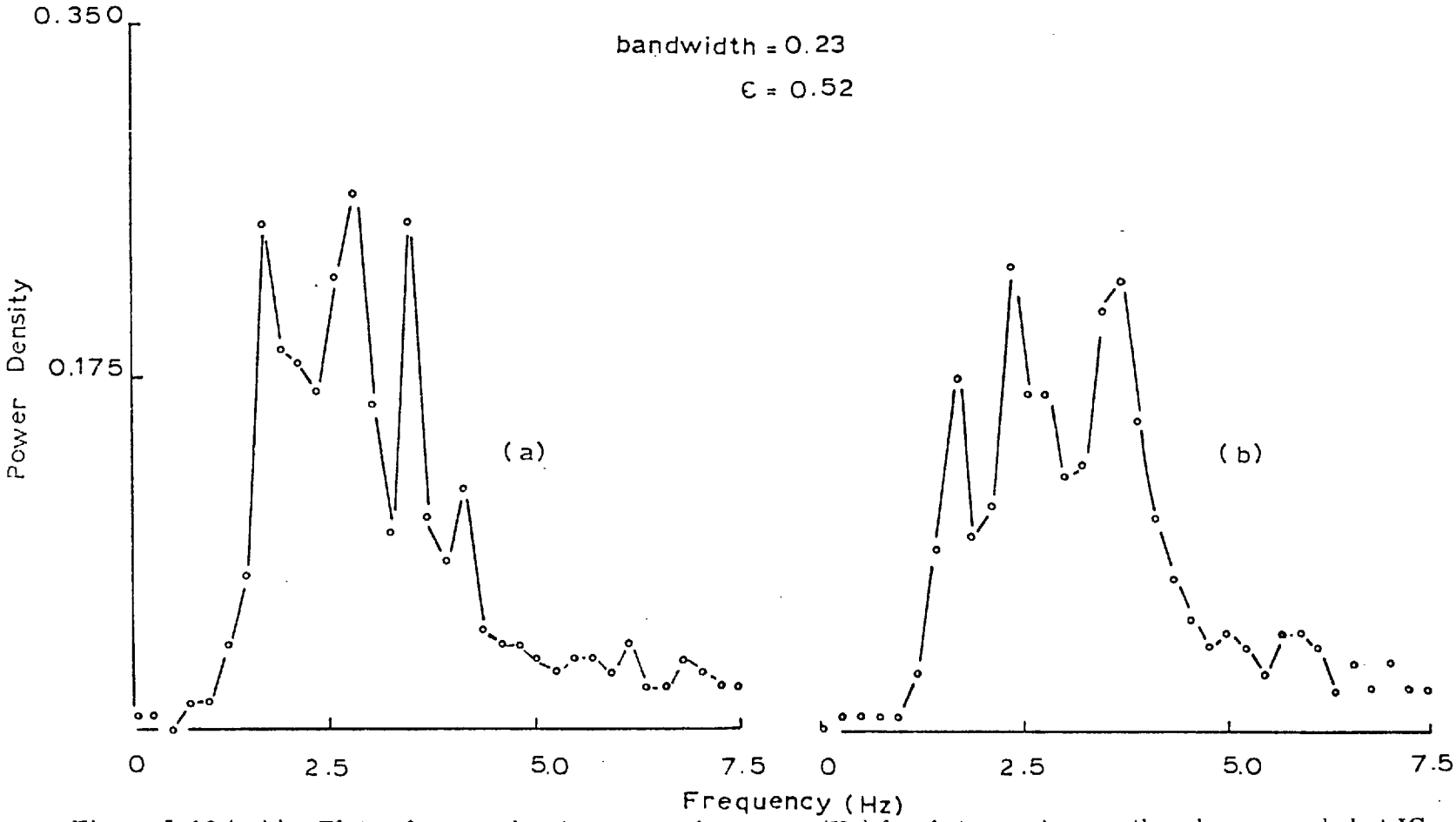


Figure 5.19 (a-b). Plots of power density versus frequency (Hz) for A-type microearthquakes recorded at IC bench mark (station 2).

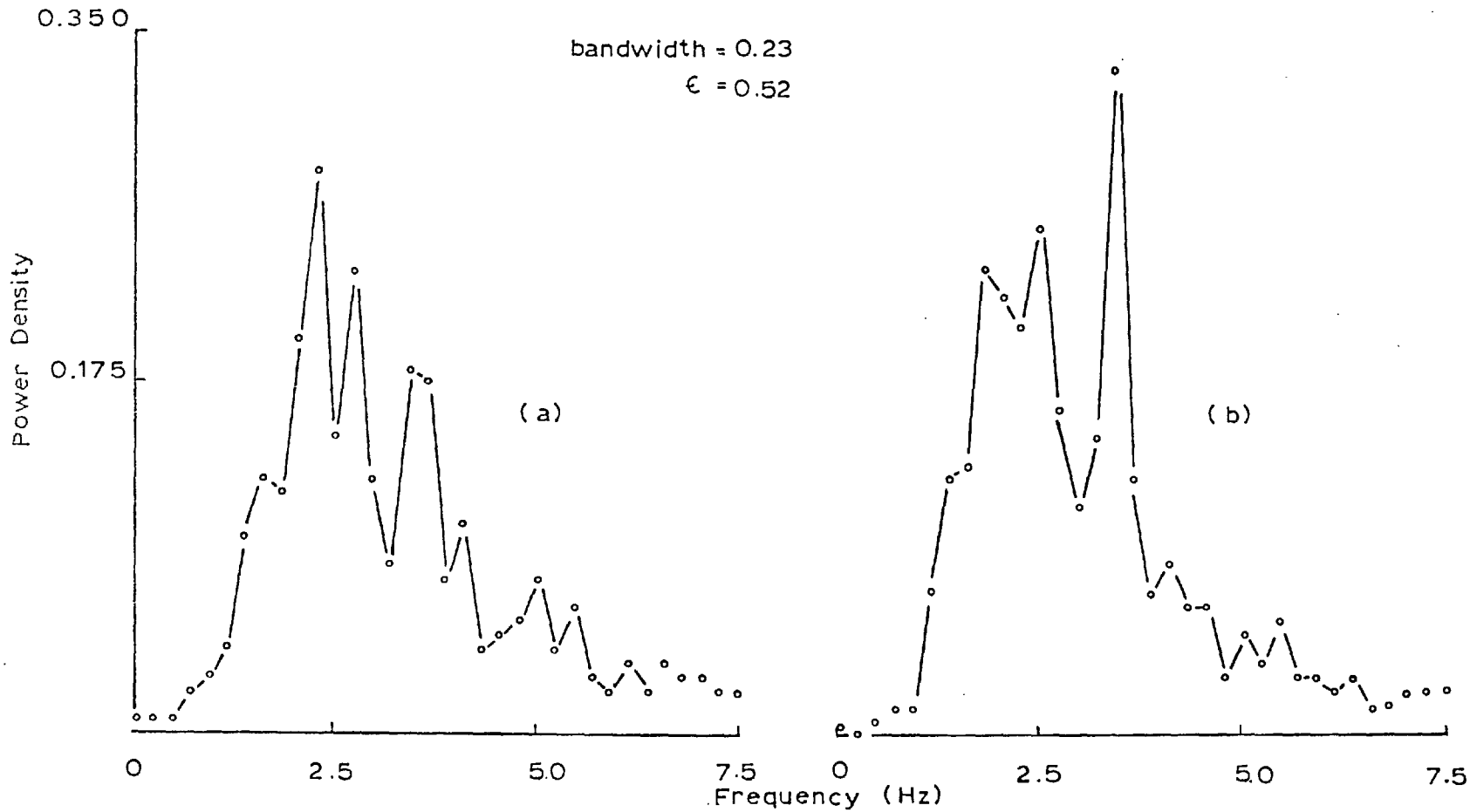


Figure 5.20 (a-b). Plots of power density versus frequency (Hz) for A-type microearthquakes recorded at IC bench mark (station 2).

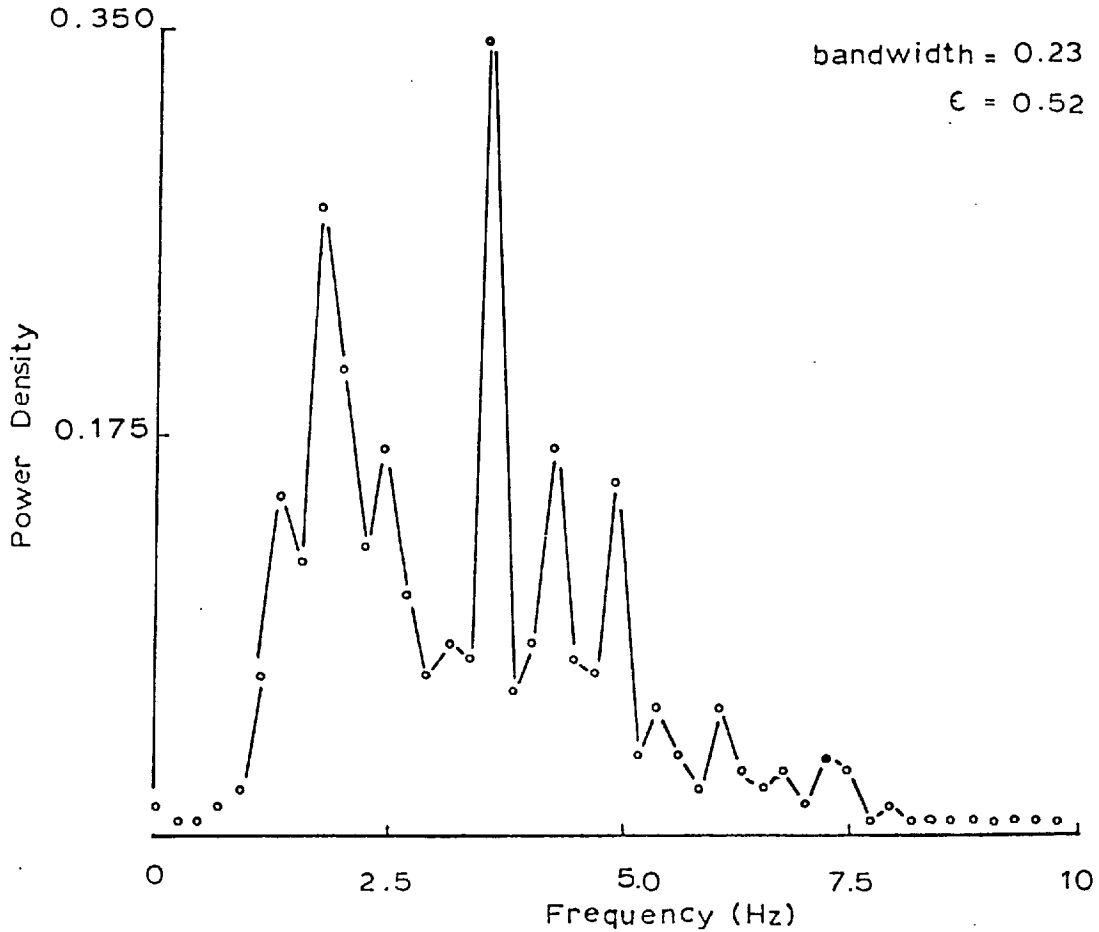


Figure 5.21. Plot of power density versus frequency (Hz) for an A-type microearthquake recorded at Serra La Nave (station 1).

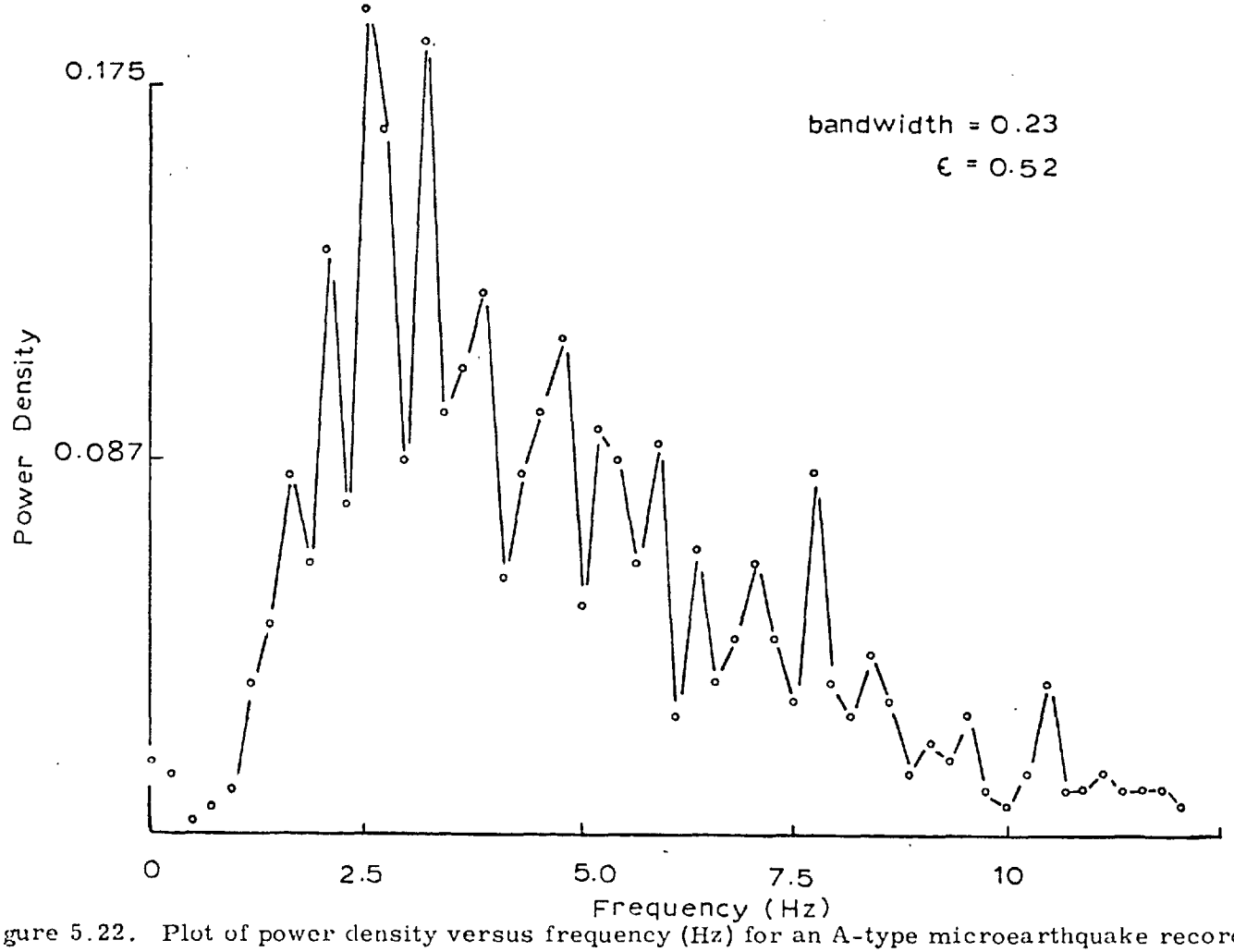


Figure 5.22. Plot of power density versus frequency (Hz) for an A-type microearthquake recorded at IC bench mark (station 2).

spectrum of a similar microearthquake recorded in station 1 (Serra La Nave). It has a dominant frequency between 3.47 and 3.93 Hz. The higher frequency components in this case extend to about 8.0 Hz.

In contrast to the spectrum discussed above, Figure 5.22 (recorded at station 2) has a very spikey appearance. The frequencies in Figure 5.22 converge to a maximum value of about 10.50 Hz with a dominant frequency between 2.32 and 2.78 Hz. The gradual transition (in the three groups) from a relatively smooth and lower frequency content to more spikey and higher frequencies are apparent.

The above observation would seem to imply that, other factors (like the transmission path, source mechanism, focal depth etc.) remaining constant, the frequencies of the microearthquakes appear to be a function of the magnitudes (proportional to the duration of the oscillation) though this is not a general rule.

5.4.4.2 B-TYPE MICROEARTHQUAKES

Power density estimates for seven B-type microearthquakes recorded at the various stations are tabulated in Appendix 3B, and Figure 5.23 to 5.26 gives their power density versus frequency plots. The seven selected microearthquakes cover a period of nine recording days, and each event is independent of the occurrence of the other.

The first four of the seven power density plots

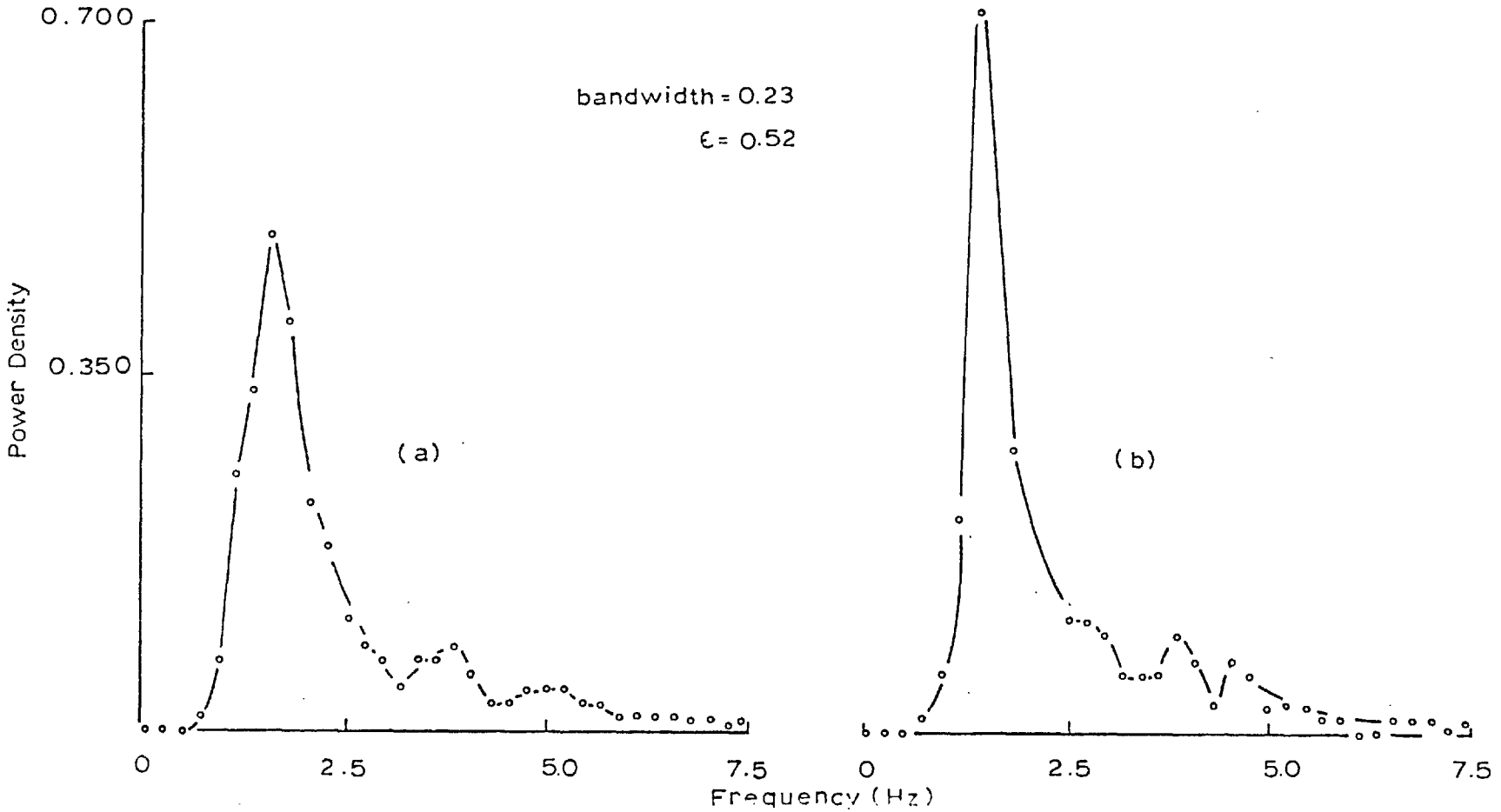


Figure 5.23 (a-b). Plots of power density versus frequency (Hz) for B-type microearthquakes recoeded at Serra La Nave (station 1).

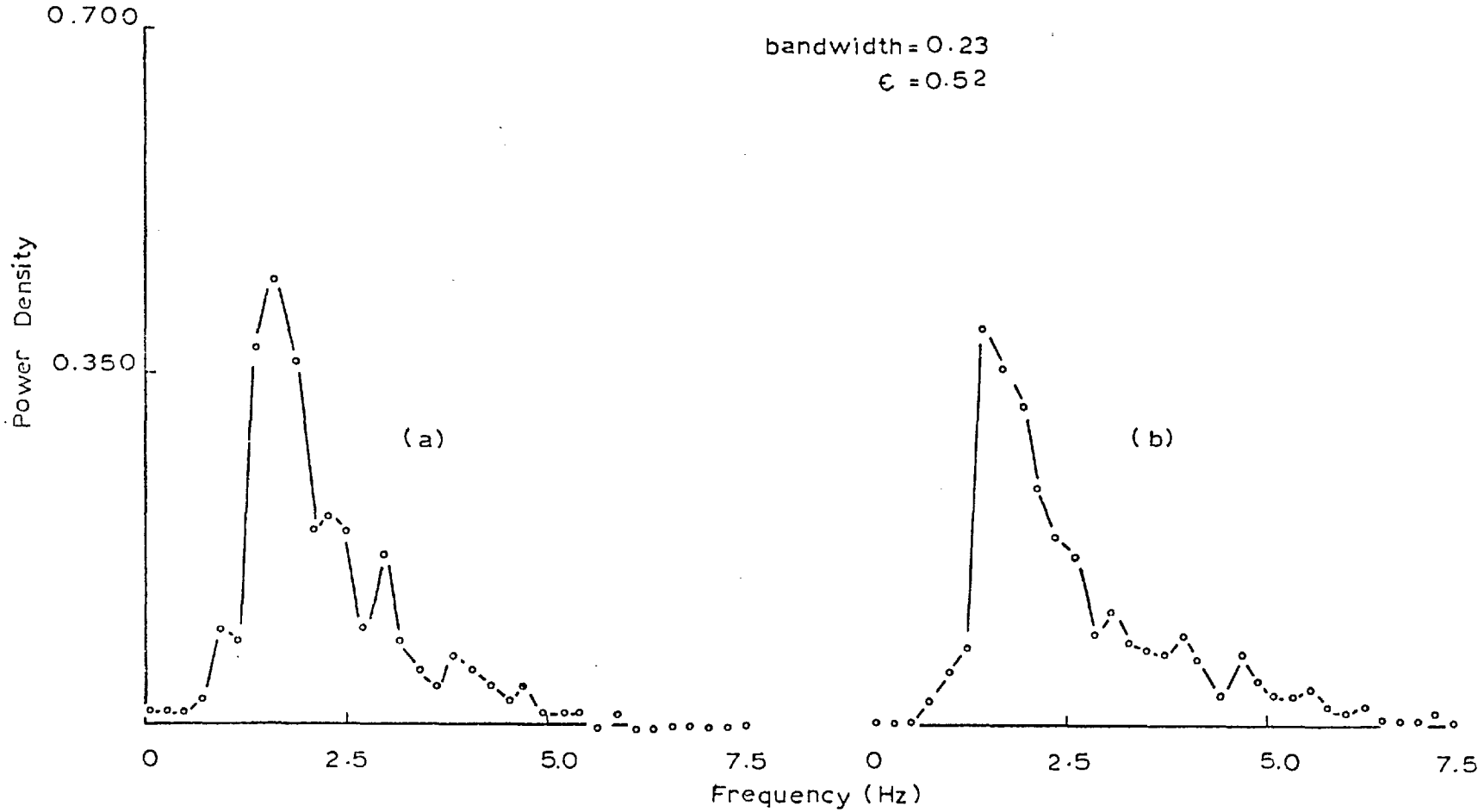


Figure 5.24 (a-b). Plots of power density versus frequency (Hz) for B-type microearthquakes recorded at Forestale Hut (station 3).

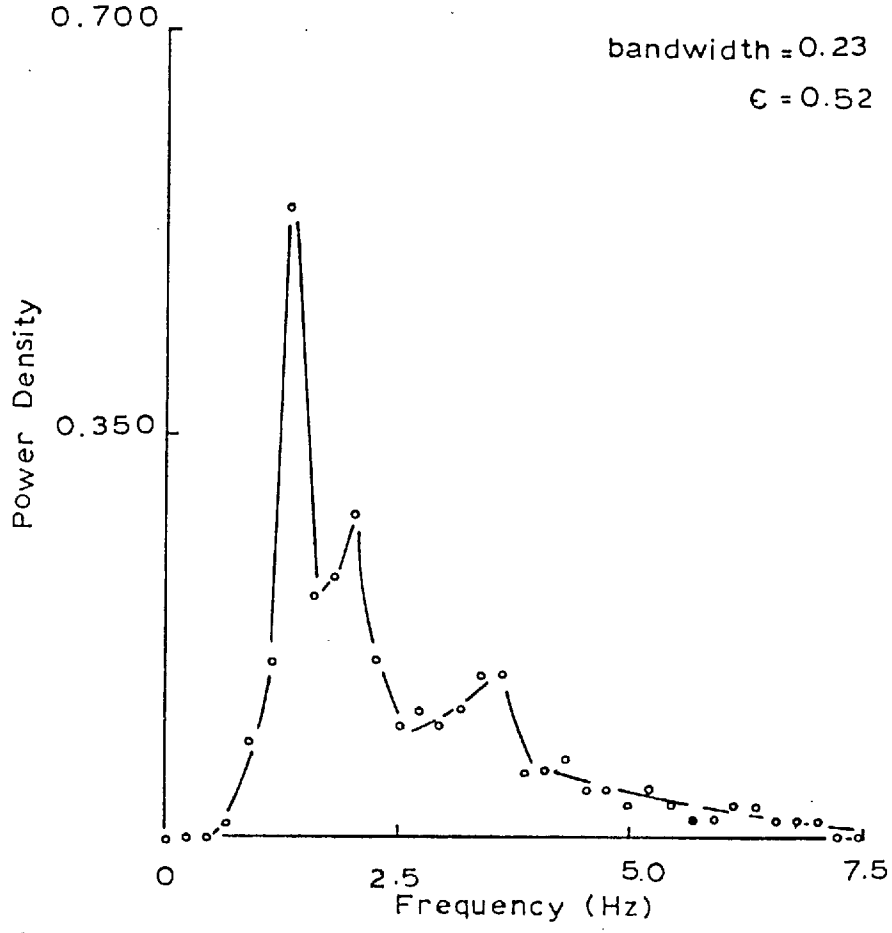


Figure 5.25. Plot of power density versus frequency (Hz) for a B-type microearthquake recorded at Serra La Nave (station 1).

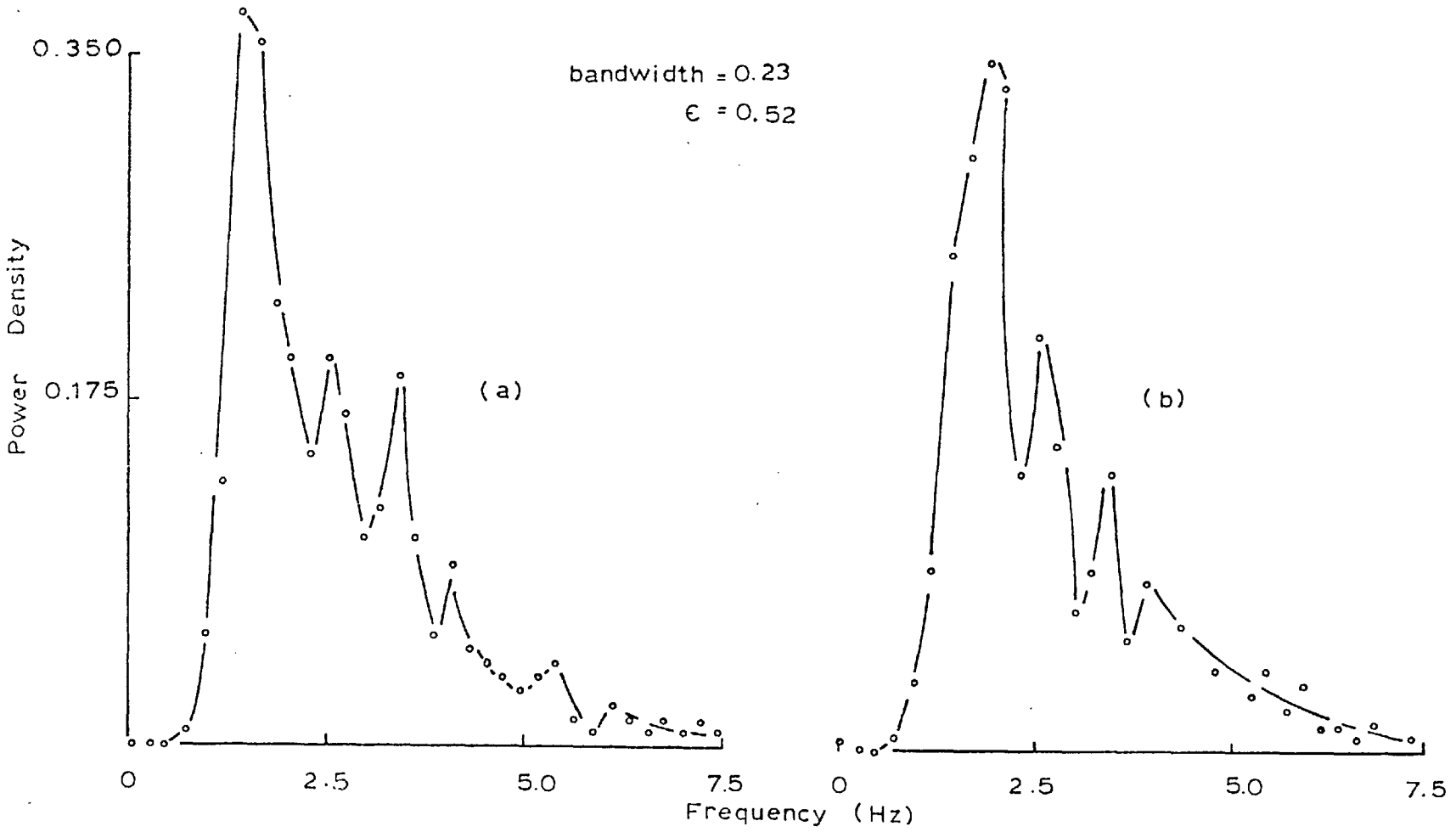


Figure 5.26 (a-b). Plots of power density versus frequency (Hz) for B-type microearthquakes recorded at Serra La Nave (station 1).

(Fig. 5.23 - 5.24) have very simple spectral diagrams. These microearthquakes are characterized by single dominant peaks between 1.16 and 1.85 Hz, and small amplitude peaks between 2.82 and 4.89 Hz. There is very little variation in the total power contents of the various spectra in the dominant frequency range and over 70% of the total power of the microearthquakes is concentrated in the narrow band between 0.71 and 3.54 Hz.

The next three spectral diagrams (Fig. 5.25 - 5.26) are not only characterized by single dominant peaks between 1.16 and 2.08 Hz, but in addition have pronounced peaks between 2.32 and 5.77 Hz. Unlike the first four spectra discussed above, power in these microearthquakes is distributed over the higher frequencies as well.

From the above discussion, it appears that all the analysed B-type microearthquakes are characterized by a low dominant frequency peak between 1.16 and 2.08 Hz. In some cases, high frequency peaks are also present between 2.32 and 5.77 Hz. Almost all the power of the events lies between 1 and 6 Hz.

Lo Bascio et al. (1976) analysed some similar microearthquakes on Etna and observed dominant spectral peaks around 2.0 and 6.0 Hz. Their findings seem to indicate slightly higher frequencies than in the present survey. However, the difference might be explained by the volcano being in a different state of activity at the two times.

It is interesting to note that some of the high frequency components of the spectrum discussed above are multiples of the fundamental frequency (e.g. 1.39 and 4.15 Hz). Probably, the fundamental frequency is related to the explosions in the vent, and under suitable conditions sets the higher frequency modes into oscillations.

5.4.5 COMPARISON BETWEEN THE TWO TYPES OF MICROEARTHQUAKES

The present study of the spectral characteristics of the two types of microearthquakes have revealed that A-type microearthquakes (small magnitude, shallow depth and originating within a few kilometers of the recording station) contain frequencies whose periods range up to about 0.09 sec. These figures, however, represent the average of both the P and S arrivals, as no facilities were available to analyse these separately. Unger (1969) reports a period of 0.06 to 0.15 sec for the P phase and 0.10 to 0.20 sec for the S phase for the microearthquakes recorded on Mt. Rainier, Washington. Though no direct comparison can be made between the two volcanoes, it seems that the volcano-tectonic shocks recorded on Etna are not fundamentally different from those recorded in other parts of the world.

The B-type microearthquakes, on the other hand, appear to have frequencies whose periods range up to a maximum of 0.15 sec. The spectra of these shocks look much simpler and do not exhibit the wide range of frequencies seen in the volcano-tectonic shocks. The power in all the analysed

events is concentrated in two frequency bands (1.16 to 1.85 Hz and 2.82 to 4.89 Hz) and there is little power beyond about 6.5 Hz.

It thus appears from the above, that it is difficult to differentiate A- and B-type events by their frequency content alone, however, the shape of the spectra, and the presence of a very dominant low frequency peak, might give us some indications as to which type they are.

CHAPTER VI

DISCUSSIONS

6.1 COMPARATIVE STUDY OF THE 1974 AND 1975 FIELD INVESTIGATIONS

The 1974 and 1975 field investigations of Mount Etna (as described in Chapters III and IV) were carried out at different times of their respective years, using two different recording instruments. The first (Aug. - Sept. 1974), conducted as a reconnaissance survey, was carried out using a high-gain, high-frequency portable seismograph producing visual smoked paper records. The second (May - June 1975), intended as a more detailed study, was carried out using 4 Geostore magnetic tape recorders, each connected to three seismometers.

During the first survey an average of 7 microearthquakes were recorded per day. This is about 3.5 times the daily rate during the second period. These results are based on a total of 486 hours of useful recording for the first, and a maximum of 490 hours (at Serra La Nave) for the second. Thus the two surveys covered roughly equal lengths of time. During the reconnaissance survey approximately 18% of the total recorded events were of the A-type and 20% during the second survey (these percentages, however, exclude any A-type events with S-P > 2.5 sec). The proportion of B-type events, on the other hand, showed an overall decrease

of about 2% between 1974 and 1975.

As regard the types of microearthquakes being recorded at any one station, only at Serra La Nave (station 1) was enough data obtained for a meaningful analysis to be possible. During the first survey, 17% were A-type and during the second, 19% (these percentages again exclude events with S-P > 2.5 sec).

It may be recalled that no event with an S-P > 2.5 sec were recorded during the'74 survey, whereas during the second they numbered as many as nine. Why tectonic microearthquakes with S-P > 2.5 sec should have been recorded only during the second survey is difficult to say. The only conclusion that can be drawn is that the more distant, tectonic,faults were inactive during 1974.

As data from only one station was available, it was not possible to locate foci in 1974. With the four instruments available in 1975, depth estimates were possible for two A-type events. The first (depth ~ 10 km) is probably related to volcano-tectonic processes and the second (depth ~ 20 km) to tectonic forces. The depth of the other six (A-type) events are not available. The B-type microearthquakes, as expected, originate from within 1 km of the Central Crater.

From visual inspection, the volcanic tremor on the smoked paper record appears to contain frequencies below about 5.0 Hz. Detailed analysis (from '75 recordings), however,

indicates that the dominant frequencies ranged between 1.20 and 2.90 Hz. A tentative source location indicated the origin of these disturbances in between the Northeast Crater and 3 km NW of the Central Crater. Spectral analysis of micro-earthquakes, on the other hand, appears to indicate lower frequencies for the B-type events, but this again is not a general rule.

An interesting feature of the '75 investigations is that if an arbitrary north-south line is drawn through the volcano via the Central Crater, most of the microearthquake activity is found to be concentrated on the eastern half of the volcano.

Before we attempt an explanation of these findings, let us take a look at the 'state of the volcano' during those two periods.

6.2 A BRIEF DESCRIPTION OF THE ACTIVITY OF MOUNT ETNA DURING THE TWO RECORDING PERIODS

Before the start of the 1974 field investigations Mount Etna had remained dormant since the eruption of 1971. It resumed its activity again on the 28 September 1974 (Murray et al. 1977) in the Northeast Crater. This, Strombolian, activity lasted for about five months, after which lava flowed out from new boccas 2 km to the north at an altitude of about 2500 m. The rate of eruption was estimated to be upto 1.5 m^3/sec during this phase. Figure 6.1 shows the approximate location of this flow.

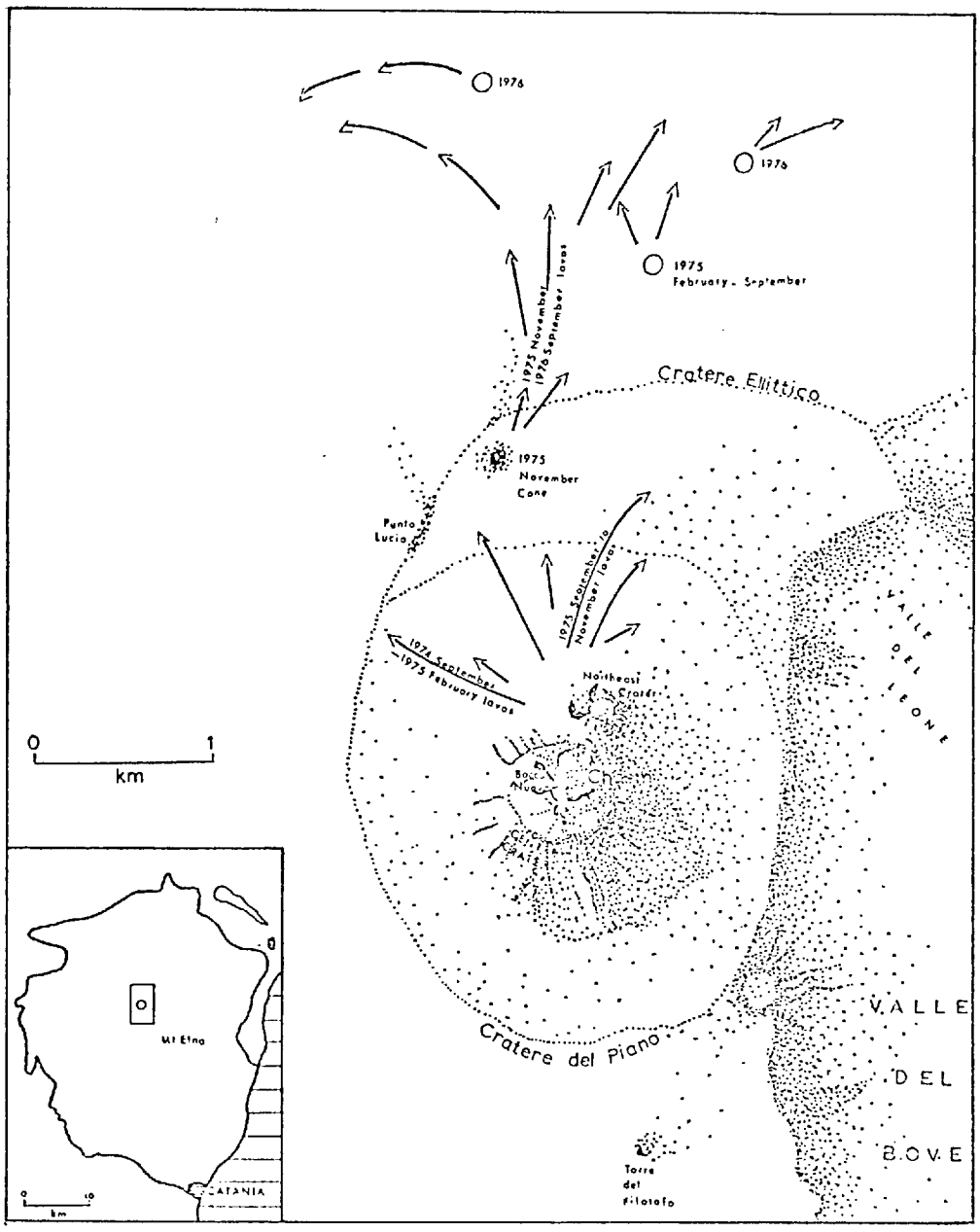


Figure 6.1. Map showing the centres of eruptive activity on Mount Etna from September 1974 until the beginning of 1976. (After Murray et al., 1977)

The state of the volcano during 1975 seems to have alternated between emission of lava flow on the north flank and activity at the Northeast Crater. The emission of lava that started around 23/24 February continued intermittently until 12 September, 1975, after which effusion stopped in the north flank and Strombolian activity accompanied by lava flow erupted from the Northeast Crater. Rates of eruption were measured upto 0.9 m^3/sec during this period, which terminated on 28 November 1975. On November 29 a fissure 450 m long opened east-northeast of Punta Lucia, at an elevation of 2900 m. This was accompanied by an intense Strombolian activity, that resulted in the formation of a 40 m high cone (Murray et al., 1977). Figure 6.1 also shows these new eruption sites. In the early parts of 1976, a collapse pit approximately 170 m x 70 m was formed on the west flank of the Northeast Crater. This was accompanied by the emission of ash and the onset of intense sulphur-bearing fumarolic activity.

With the activity of the volcano during those two periods in mind, attempts are made in the following sections to explain the results of the present findings.

6.3 SIGNIFICANCE OF THE PRESENT FINDINGS

It will be seen from the preceding description of the activity of Etna that the 1974 survey commenced about seven weeks prior to the resumption of volcanic activity on the 28th of September of that year. During the first three days of observations, only a few microearthquakes were

recorded. From the 10th to the 14th August, however, about 4 events were recorded per day (a mixture of both A and B-type events), almost a four-fold increase on the previous days recordings. From the 15th to the 17th August the seismograph was installed at three new sites (see Table 3.2), and seismograms obtained during that period proved to be so noisy that it was not possible to pick out microearthquakes from the background. On the afternoon of the 17th, however, the seismograph was moved to near the IC bench mark site, and during the next 44 hours, 55 B-type microearthquakes were recorded. The instrument was then moved again to two new sites. From the 23rd onwards until the 30th August, the seismograph was installed near Monte Nero, and on the average about 4 events were recorded each day (again a mixture of both A and B-type microearthquake), after which until the termination of the recording period, about 10 events were recorded every day, at Serra La Nave. In this case, as well, the recorded events were a mixture of both A and B-type microearthquakes.

Figure 6.2 illustrates the noticeable increase in the number of microearthquakes about a month and a half prior to the outbreak of the September 1974 eruption. The exceptionally high number of B-type microearthquakes recorded at the IC bench mark might have been due to an appreciable movement of magma during that particular period, and this movement might have taken place from or via the Rifugio Citelli area.

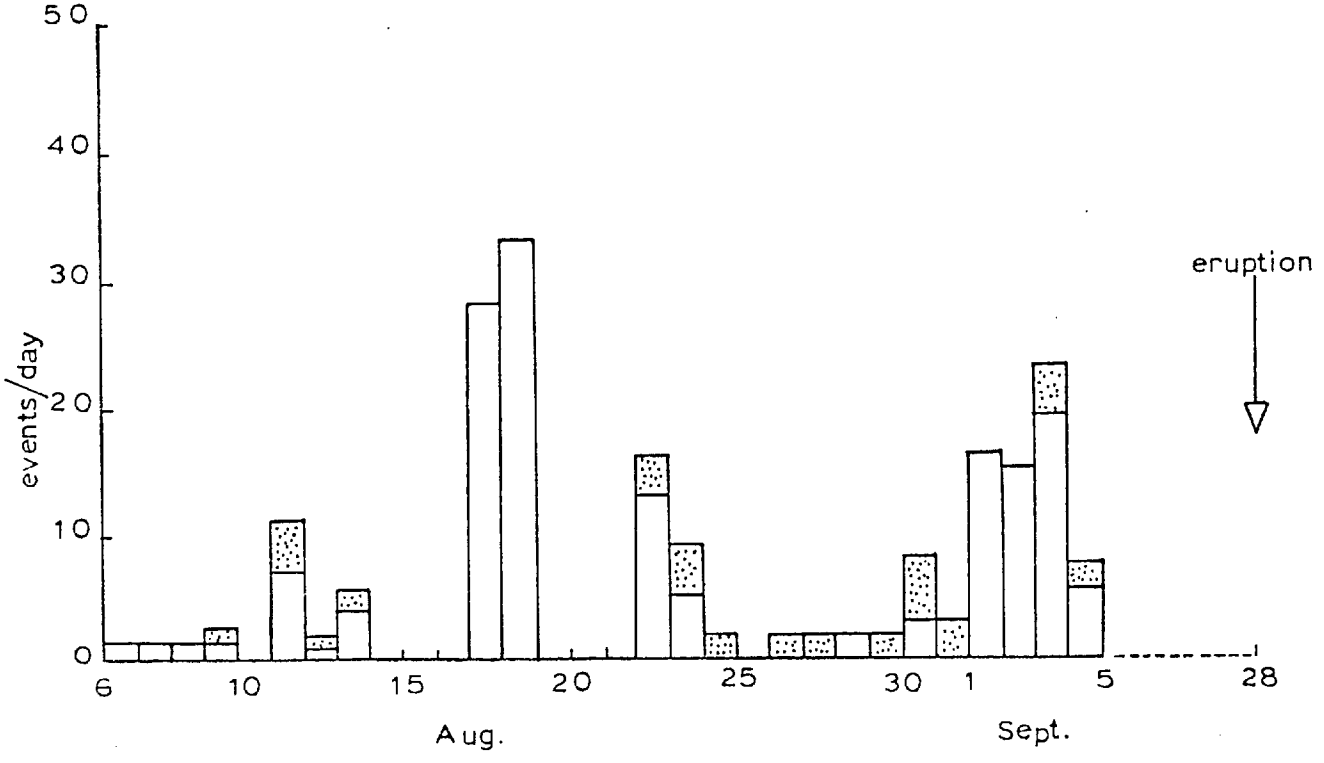


Figure 6.2. Plot of daily frequency of microearthquakes recorded on Mount Etna during Aug. - Sept. 1974. In each column the dotted area represents A-type and the blank area B-type events respectively.

These findings appear to be in agreement with investigators working on other volcanoes. In fact, one of the methods often used to predict eruptions on volcanoes is by observing this increased seismicity. Prediction will be discussed further in the next section.

During the second occupation the volcano was in a state of 'quiet effusion'. Throughout the whole recording period the seismic activity level was more or less constant (see Section 4.3.1 and Fig. 4.9 a-d).

It has been mentioned briefly in Section 3.4.1 that one of the critical criteria used to distinguish between A- and B-type microearthquakes is their respective b-values. Let us take a look at these values and examine how they are related to the activity of the volcano during those two periods.

It is known that shallow earthquakes occur as a result of fracture in the earth's crust, and that the larger the earthquake's magnitude,the smaller is its chance of occurrence. This simple relationship between the cumulative frequency and magnitude was put into its present mathematical form by Gutenberg and Richter (1954). However, many investigators today suggest much wider implications of the relationship than was previously thought to exist (Mogi, 1962, 1962a, 1963, 1967; Minakami, 1960).

In a number of experiments performed under controlled laboratory conditions, Mogi (1962, 1962a) thoroughly investigated the b-values of events due to microfacturing of

various materials subjected to stresses under conditions thought to exist in the crust of the earth. His results on various samples such as homogeneous brittle material (pine resin), brittle material of heterogeneous structure (pine resin including mechanical irregularities) and heterogeneous brittle material in a granular state (granular pumice or coal) indicated that the b-value increased as the specimens became weaker and less homogeneous. He thus concluded that the variation in the b-values from region to region can be attributed to the mechanical structure of the medium and the spatial distribution of external stress.

Scholz (1968, 1968a) similarly studied the magnitude/frequency relation of microfracturing of rocks under uniaxial and triaxial loading. His laboratory experiments differ from Mogi's in that he used a much higher frequency component of the microfracturing energy. He was thus able to record events several orders of magnitude greater from a single specimen. He showed that the b-value of these microfractures depends primarily on stress, and that variations in the local stress field may cause observed variations in the b-value. His investigations further confirmed that under a given condition the constants 'a'* and 'b' in the Gutenberg-Richter's recurrence curve depend on the fracture mechanism and transmission properties of the medium as well as on the response characteristics of the instrument.

---

*Note also that the 'a' value is proportional to the total number of earthquakes recorded and is hence related to the duration of the observing period.

It appears from these experiments that the mechanism of the generation of earthquakes and the formation of fractures during simulated laboratory tests are very similar. The experiments have further confirmed that different b-values found under different conditions are a direct result of the stress concentration in the area,and to a lesser extent on the type of rocks present.

This naturally raises the question of the A- and B-type microearthquakes recorded in these surveys. Since the b-values of A-type microearthquakes closely resemble those of tectonic shocks, it appears that they both originate from similar mechanisms inside the earths crust. The local stress build up is due to changes within the volcano, and this results in tectonic faulting. Thus A-type microearthquakes originate primarily from faulting along planes of failure in the rocks surrounding the volcano. This failure might have been brought about by volcanic processes where the stress concentration is sufficient to cause a rupture in the rocks. When considered in this fashion, the A-type microearthquakes are seen to be associated with the volcano in an indirect way. In order to investigate this mechanism more fully it is necessary to study the geographic distribution of the initial motion of the microearthquakes, but unfortunately this was not possible in the first survey as only one seismograph was available, or during the second, because of the paucity of microearthquakes. (It is hoped that in future more data will be available to enable a study of this nature.)

The B-type microearthquakes are unique in that they are only recorded in a volcanic region. They have no analogy in the microearthquakes generated by tectonic faulting. The high b-value in the first survey indicates a localized stress concentration, probably in and around the Northeast Crater region, where the rocks are weak and heterogeneous. Unfortunately, no b-value is available for the second survey. The localized stress build-up, mentioned above, is possibly due to the expansion in volume of the magma as it rises near the Crater bottom. This upward movement of the column results in a separation of the volatiles, and a new stress distribution. This excess stress is later on released as small earthquakes.

Some investigators, e.g. Craig et al. (1976), have shown the existence of B-type microearthquakes under very different circumstances. In their investigation of Mount Saint Helens, a strato-volcano in the Cascade Range of Washington State, they found B-type microearthquakes associated with the glaciers on the mountains. This, however, can not be the cause of B-type microearthquakes on Mount Etna.

Thus we have seen that the b-values associated with the cumulative frequency versus magnitude (or amplitude in the present case) of the microearthquakes provided some very interesting information about the origin of these events. However, longer recording periods are necessary if we are to understand the volcano-seismic activity of Mount Etna more fully.

It has been proposed earlier (see Section 5.4.3) that

volcanic tremor on Mount Etna is the resultant of the sum of a number of harmonic oscillators set up by the expanding gas front. In this section it was seen that the volcanic microearthquake is a consequence of the release of excess localized stress concentration, brought about by the upward movement of the magma. In addition, both the volcanic tremor and volcanic microearthquakes were found to have low frequencies (below about 5 Hz, in the 1975 survey). The location of both the source of volcanic tremor and the epicentre of at least one B-type event indicate their association with the active part of the volcano.

It appears from the above analysis that volcanic tremor and B-type microearthquakes are two different manifestations of the same physical process. Under 'suitable conditions' of the movement of the magma, one process is favoured over the other. Just what these 'suitable conditions' are is difficult to say. This is particularly so for Etna, where so little geophysical data is available.

It is worth finishing this chapter with a discussion of the influence of what has been said so far on the possibility of predicting eruption on Mount Etna. In the following section some of these aspects, e.g. microearthquake occurrence rate, seismicity and volcanic tremor analysis that are relevant to predicting eruptions will be discussed.

6.4 PREDICTING ERUPTIONS ON MOUNT ETNA

To be able to predict volcanic eruptions, a relation-

ship has first to be found between the eruption and the various phenomena preceding it, and for the forecast to be useful this relationship must enable the date or time, place or magnitude (or intensity), of the eruption to be predicted within certain defined limits. Unfortunately, the peculiarities of the connection between seismic and volcanic activity are so specific to each volcano that so far no common formula has evolved for predicting the precise time of an eruption with any degree of certainty. Nevertheless, useful methods have been developed in specific cases, based on the results of instrumental observations of earthquakes, crustal movements, and other phenomena, originating from the volcano itself.

It has been found, for example, that certain types of microearthquakes are more directly related to volcanic processes than others. Microearthquakes, capable of being detected by a sensitive short-period seismograph, occur at all stages of the eruptive cycle at all active volcanoes. However, prior to an eruption significant changes have been noticed in the frequency of volcanic microearthquakes. Thus prediction involves essentially the monitoring of microearthquakes and the comparison of day-to-day occurrence rates. However, there are difficulties. Firstly, there appear to be large variations with time in the background level of seismicity at most volcanoes. Secondly, and perhaps more important, criteria have to be established for judging the significance of changes in the occurrence rate.

Figures 6.3 and 6.4 are examples gathered from volcanoes in different parts of the world, which show changes

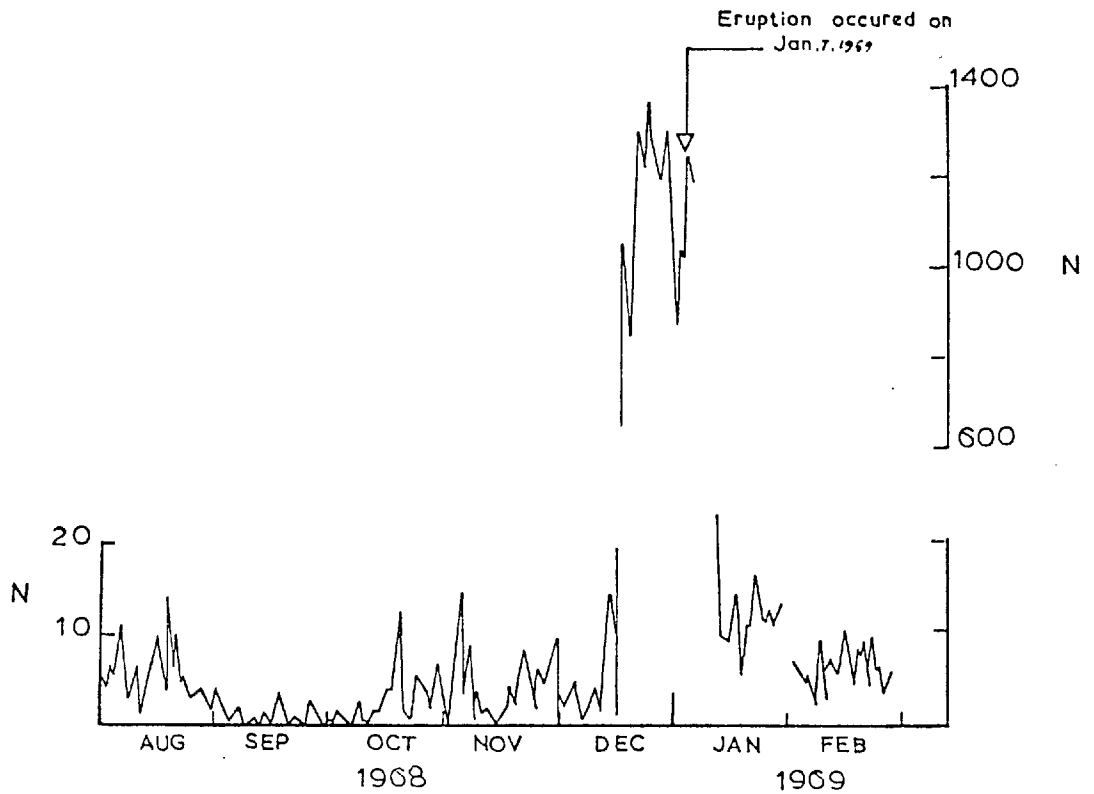


Figure 6.3. Plot of daily frequency of microearthquakes (N) recorded at Merapi volcano, Indenesia prior to an eruption. Note change of scale from mid - December to mid - January. (After Shimozuru et al., 1969).

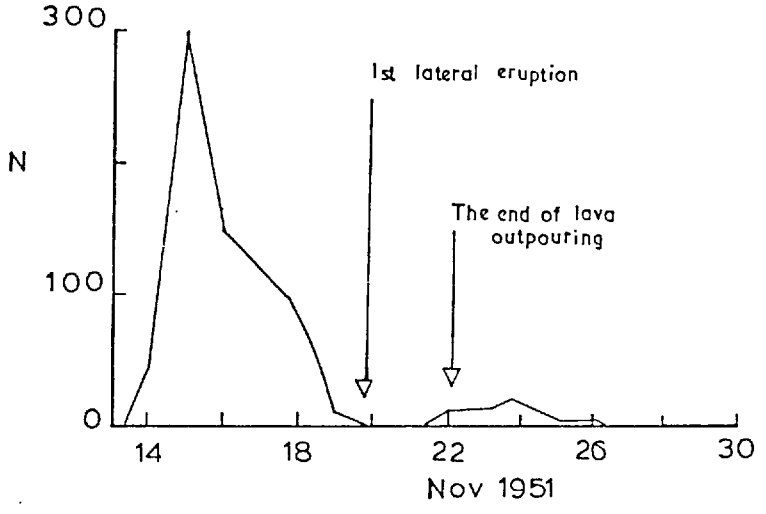


Figure 6.4. Number of microearthquakes (N) recorded per day by the seismograph at Kliuchevskai volcano Kamchatka prior to the first lateral eruption, Novemver, 1951. (After Gorshkov, 1960).

of more than one hundred times in the background level of seismicity prior to an eruption. However, this is not a general rule. Harlow, as reported by Decker (1973), studied the relationship between earthquakes and volcanic eruptions for 71 cases and found that for 58% there was an increase in the number of earthquakes before an eruption, while in 38% there was an increase in earthquakes without any eruption, and in 4% there was an eruption without any increase in earthquakes.

As mentioned previously, very little seismic data exists for Mount Etna. In spite of its reconnaissance nature, this investigation forms one of the major studies yet carried out in the area, and thus serves as a guide to future work. In hindsight, it appears that the increased seismicity recorded about forty-five days prior to the 28 Sept. 1974 eruption was indeed a precursory event. It was unfortunate that we had to stop recording about 24 days before this eruption.

In addition to the microearthquake studies, continuous monitoring of volcanic tremor on Mount Etna might provide valuable information about the state of activity of the volcano. In fact, during the monitoring of volcano Aso in 1932 - 1933, Sassa (1936) observed that prior to an eruption the amplitude of the volcanic tremor increased suddenly and remained constant for a short period. This was then followed by a rapid decay in amplitude, and then a period of quiescence, followed finally by an explosive eruption. In Hawaii, high amplitude volcanic tremor is the most diagnostic index that an eruption has begun or is about to begin (Decker, 1973). In

New Zealand, the volcanic tremor has been successfully used to forecast eruptions from between 10 hours and 7 days in advance.

Unfortunately, analysis of volcanic tremor was not possible during the first survey, and no significant variation in the tremor amplitudes was observed in 1975.

CHAPTER VII

SUMMARY OF CONCLUSIONS AND RECOMMENDATIONS FOR FURTHER STUDY

7.1 SUMMARY OF CONCLUSIONS

This project has demonstrated clearly that it is possible to investigate the seismic activity of Mount Etna in a relatively short period of time, using simple instrumentation and recording sites without the normal observatory facilities.

Below is a summary of the most important conclusions reached from this investigation, and recommendations for further study.

(1) Microearthquake activity exceeding 7 events per day was recorded on Mount Etna during the reconnaissance survey of Aug. - Sept. 1974. The volcano displayed 'low to moderate seismicity' during that period, a result arrived at by comparing the microearthquake activity of Mount Etna with that of other active volcanoes around the world.

(2) The signature and characteristics of these microearthquakes were similar to those recorded on other active volcanoes. Firstly were the volcano-tectonic microearthquakes (classified as A-type) which had an impulsive first arrival and a distinguishable P-S phase. Secondly, the volcanic microearthquakes (classified as B-type), which had an impulsive or an emersion type arrival and no distin-

guishable P-S phase. About 82% of the total recorded events were of this type.

(3) The S-P distribution of the A-type microearthquakes showed their origin to be about 20 km from the recording stations.

(4) Plots of microearthquakes in space and time indicated that the seismic activity was not a constant in time. Certain intervals of time appeared more active than others. Seismically, the IC bench mark site (near Rifugio Citelli) was found to be most active. It is believed that the movement of magma took place via or from below this site prior to the 1974 eruption.

(5) The b-values for A-type (0.99) and B-type (1.78) microearthquakes, obtained in the present survey, are consistent with those obtained in other parts of the world.

By analogy with laboratory studies of various rock samples, the high b-value (1.78) of B-type microearthquake appears to be due to inhomogenity and localized stress concentration in the crateral region of the volcano.

(6) The energy of the largest microearthquake recorded during this survey appears to be approximately 6×10^{13} ergs.

(7) Results from the second field survey (May-June 1975) showed the volcano to be in a seismically 'quiet state', with only about 2 recordable events per day. This is in agreement with observation of the active craters at that time. Both A- and B-type microearthquakes were recorded during this time, the former constituting about 20% of the total and the

latter about 80%.

(8) The S-P distribution of these microearthquakes indicates two distinct groupings, the first group being at an epicentral distance of about 15 km and the second at about 40 km from the recording stations.

Only two events were recorded at more than two stations during the whole period and it was therefore not possible to look for evidence of shear wave screening.

(9) Using P- and S-wave velocities of 5.25 $\pm$ 0.25 km/sec and 3.10 $\pm$ 0.15 km/sec respectively, and the standard S-P technique, these two events appear to have originated at depths of about 10 km and 20 km respectively. The first is thought to be related to volcano-tectonic processes and the second to local tectonic forces.

Six other A-type events were located using the three components recorded at a single station, together with the S-P travel time.

In general, it was not possible to locate the B-type microearthquakes, because of their small amplitudes. However one such event was located using the arrival times at three stations. The data is consistent with an origin within the crateral region of the volcano and an average surface wave velocity of 1.09 km/sec.

(10) Spectral analysis of the background seismic noise shows a dominant frequency of between 1.2 and 2.9 Hz. Hourly samples over 24 hour periods do not indicate any significant variation in either the frequency or the amplitude of these tremors, at any given station.

From an analysis of the attenuation of the amplitude of volcanic tremor, at the various stations, it was found that the source of disturbance was between the Northeast Crater and 3 km NW of the Central Crater.

(11) The volcanic tremors are thought to originate from oscillations induced by degassing processes, the tremor recorded on a seismogram being the resultant of a number of random harmonic oscillators set up by the expanding gas front.

(12) Location, as well as the frequency contents, of the B-type microearthquakes and the volcanic tremors support the view that they originate from similar source mechanisms inside the volcano.

(13) A-type microearthquakes appear to have a frequency range from about 1.40 Hz to above 10.00 Hz. The B-type microearthquakes, on the other, hand seem to have dominant frequencies in the range 1.0 and 5.0 Hz. It is concluded from these observations that it is difficult to classify events on their frequency contents alone.

7.2 RECOMMENDATIONS FOR FURTHER STUDY

Attention has been drawn in various sections of this thesis to the lack of geophysical data available for Mount Etna. Seismic investigations on Etna have so far been limited to either microearthquake or volcanic tremor studies for short intervals of time. These surveys, though useful in providing short term information about the present day activity of the volcano, do not give much idea about the structure of the volcano, mechanism of the generation of microearthquakes, or

even the variation in activity throughout the year.

In order to understand these more fully, studies of the volcano on the following lines are recommended:

(1) Seismic velocity studies (e.g. by refraction techniques or otherwise) of the volcano itself, and also the deep basement structure. It may be mentioned here that little data exists in this respect.

(2) Mapping pockets of liquid bodies by S-wave screening of local or distant earthquakes by suitably placed recording instruments.

(3) Extensive studies of both the microearthquake and volcanic tremor by continuously monitoring them throughout the year. These studies are necessary if we are to understand how the volcano behaves during various phases of its eruptive cycle.

(4) Efforts should be made to study the mechanism of their generation as well as their distribution in space and time.

It is hoped that the present findings, along with the above suggestions, will serve as the basis for further seismic work in the area.

REFERENCES

Andronov, A.A., Vitt, A.A. and Khaikin, S.E. 1966. Theory of oscillations. Pergamon Press Ltd. Oxford.

Asada, T. 1957. Observations of nearby microearthquakes with ultra-sensitive seismometers. J. Phys. Earth. 5, 83-113.

Asada, T., Suyehiro, S. and Akamatu, K. 1958. Observations of nearby microearthquakes with ultra-sensitive seismometers at Matsushiro, Japan. J. Phys. Earth. 6, 23-33.

Asada, T., Suzuki, Z. and Tomoda, Y. 1951. Notes on the energy and frequency of earthquakes. Bull. Earthq. Res. Inst. 29, 289-293.

Aspinal, W.P., Michael, M.O. and Tomblin, J.F. 1976. Evidence for fluid bodies beneath the Sulphur Springs geothermal region, St. Lucia, West Indies. Geophys. Res. Lett. 3(2), 89-90.

Barberi, F., Civetta, L., Gasparini, P., Innocenti, F., Scandone, R. and Villari, L. 1974. Evolution of a section of the Africa-Europe plate boundary. Paleomagnetic and volcanological evidence from Sicily. Earth Plan. Sci. Lett. 22, 123-132.

Barberi, F., Ferra, G., Keller, J., Innocenti, F. and Villari, L. 1974a. Evolution of Eolian arc volcanism. Earth Plan. Sci. Lett. 21, 269-276.

Barberi, F., Gasparini, P. and Villari, L. 1973. Volcanism of South Tyrrhenian Sea and its geodynamic implications. J. Geophys. Res. 78, 5221-5232.

Bath, M. 1973. Introduction to Seismology. Halstead Press, New York.

Belderson, R.H., Kenyon, N.H. and Stride, A.H. 1974. Calabrian ridge, a newly discovered branch of the Mediterranean ridge. Nature, 274, 453.

Bendat, J.S. and Piersol, A.G. 1971. Random Data: Analysis and Measurement Procedures. Wiley Interscience, New York.

Berg, E. and Jenessen, 1960. Microseismes et seismes precedant l'eruption du Nyamuragira-Kitzimbanyi (Afrique Central) 1958. Bull. Volc. 23, 63-68.

Berry, M.J. and West, G.F. 1966. An interpretation of the first arrival data of the Lake Superior experiment by the time term method. Bull. Seism. Soc. Am. 56, 141-171.

Blackman, R.M. and Tukey, J.W. 1958. The measurement of power spectra. Dover Publications, New York.

Bloxham, R.D. and others, 1972. Computer control for Imperial College engines development. C.M.E. 19(9), 58-61.

Bottari, A. and Riuscetti, M. 1967. La statzione sismica di Serra La Nave Sull' Etna. Annali di Geofisica. 22, 243-264.

Bracewell, R. 1965. The Fourier transform and its applications. McGraw-Hill, New York.

Brune, J.N. 1968. Seismic moment, seismicity and rate of slip along major fault zones. J. Geophys. Res. 73, 777-784.

Bullard, E.C. 1965. Concluding remarks, symposium on continental drift. Phil. Trans. R. Soc. A. 258, 322.

Caire, A. 1970. Sicily in its Mediterranean setting. Geology and history of Sicily. Petroleum Expl. Soc. of Libya, Tripoli, 145-170.

Caputo, M., Folloni, G., Pieri, L. and Unguendoli, M. 1974. Geodimetric control across the Straits of Messina. Geophys. J.R. Astr. Soc. 38, 1-8.

Caputo, M., Panza, G.F. and Postpischl, D. 1972. New evidence about the deep structure of the Lipari arc. Tectonophysics, 15, 1-13.

Cassinis, R., Finetti, I., Giese, P., Morelli, C., Steinmetz, L. and Vecchia, O. 1969. Deep seismic refraction research on Sicily. Boll. di Geofis. XI, 43-44, 140-160.

Clacy, G.R.T. 1972. Analysis of seismic events recorded with a slow motion tape recorder near Chateau Tongariro, New Zealand, during Feb. 18, 1966 to Dec. 31, 1966. Bull. Volc. 36, 20-28.

Combs, J. and Rotstein, Y. 1975. Microearthquake studies at the Coso geothermal area, China Lake, California. Second UN Symposium on the development and use of geothermal resources, San Francisco, Proceedings, 2, 909-916.

Craig, S.W. and Malone, S.D. 1976. Mt. Saint Helens seismic events: Volcanic earthquakes or glacial noises? Geophys. Res. Lett. 3(3), 197-200.

Crampin, S. 1970. A method for the location of near seismic events using travel-times along ray paths. Geophys. J.R. Astr. Soc. 21, 535-539.

Crampin, S. and Willmore P.L. 1973. Small earthquakes observed with local seismometer networks. Phil. Trans. R. Soc. London, A. 274, 383-387.

Cristofolini, R. 1973. Recent trends in the study of Etna. Phil. Trans. R. Soc. London, A. 274, 17-35.

Crosson, R. 1972. Small earthquakes, structure and tectonics of Puget Sound region. Bull. Seis. Soc. Am. 62, 1133-1173.

Decker, R.W. 1973. State of art in volcano forecasting. Bull. Volc. 37, 372-393.

Del Pezzo, E., Guerra, I., Lo Bascio, A., Luongo, G., Nappi, G. and Scarpa, R. 1974. Microtremors and volcanic explosions at Stromboli - Part 2. Bull. Volc. 38, 1023-1036.

Dibble, R.R. 1969. Seismic power recordings during hydrothermal eruptions from Ruapehu crater lake in April, 1968. J. Geophys. Res. 74, 6545-6551.

Douze, E.Y. and Sorrells, G.G. 1972. Geothermal ground noise surveys. Geophys. 37, 813-824.

Eaton, G.P., Christiansen, R.L., Iyer, H.M., Pitt, A.M., Mabey, D.R., Blank, H.R., Zietz, I. and Gettings, M.E. 1975. Magma beneath Yellowstone National Park. Science, 188, 787-796.

Eaton, J.P. 1962. Crustal structure and volcanism in Hawaii, crust of the Pacific basin. Geophys. Mono. 6, 13-29.

Eaton, J.P. 1969. HYPOLAR - a computer program for determining hypocentres of local earthquakes in an earth consisting of uniform flat layers over a half space. U.S. Geol. Sur. Open file report.

Eaton, J.P. and Richter, D.H. 1960. The 1959 eruption of Kilauea. Geotimes, IV, 5, 24-27.

Engdahl, E.R. and Gunst, R.H. 1966. Use of a high speed computer for the preliminary determination of earthquake hypocentres. Bull. Seism. Soc. Am. 56, 325-336.

Farberov, A.I. and Gorelchik, V.I. 1971. Anomalous seismic effects under volcanoes and some features of deep seated structure of volcanic area. Bull. Volc. 35, 212-224.

Finch, R.H. 1943. The seismic prelude to the 1942 eruption of Mauna Loa. Bull. Seism. Soc. Am. 33, 73-78.

Finch, R.H. 1949. Volcanic tremor. Bull. Seism. Soc. Am. 39, 73-78.

Firstov, P.P. and Shirokov, V.A. 1971. Seismic investigation of the root of the Kliuchevskaya group volcanoes, Kamchatka. Bull. Volc. 35, 164-172.

Flinn, E.A. 1960. Local earthquake location with an electronic computer. Bull. Seism. Soc. Am. 50, 467-470.

Francaviglia, A. 1959. L'imbasamento sedimentario dell'Etna e il golfo pre-Etneo. Boll. Serv. Geol. Ital. 81, 4-5, 583-684.

Giese, P., Morelli, C. and Steinmetz, L. 1973. Main features of crustal structure in western and southern Europe based on data of explosion seismology. Tectonophysics, 20, 367-379.

Goforth, T.T., Douze, E.J. and Sorrells, G.G. 1972. Seismic noise measurements in a geothermal area. Geophys. Prosp. 20, 76-82.

Gorshkov, G.S. 1958. On some theoretical problems in volcanology. Bull. Volc. 19, 103-114.

Gorshkov, G.S. 1960. Some results of seismometric investigations at the Kamchatka Volcanological Station. Bull. Volc. 23, 121-128.

Grindley, G.W. 1973. Structural control of volcanism at Mt. Etna. Phil. Trans. R. Soc. A. 274, 165-175.

Guest, J.E. 1973. The summit of Mt. Etna prior to the 1971 eruption. Phil. Trans. R. Soc. A. 274, 63-78.

Guerra, I., Lo Bascio, A., Luongo, G. and Scarpa, R. 1976. Seismic activity accompanying the 1974 eruption of Mt. Etna, J. Vol. Geoth. Res. 1, 347-362.

Gutenberg, B. and Richter, C.F. 1954. Seismicity of the earth and associated phenomena. Princeton University Press, Princeton, New Jersey.

Hadley, D. and Combs, J. 1974. Microearthquake distribution and mechanism of faulting in the Fontana , SanBernardino area of Southern California. Bull. Seism. Soc. Am. 64, 1477-1499.

Hedayati, A. 1976. Microearthquakes, seismicity and tectonics of the north-central Persian plateau. Ph.D. Thesis. University of London.

Hosmer, G.L. 1919. Geodesy. John Wiley and Sons Inc. New York.

Imbo, G. 1935, Agitazione asmonica Vesuviano. Annali Osserv. Vesuviano, Napoli, 163.

Isacks, B. and Oliver, J. 1964. Seismic waves with frequencies from 1 to 100 cps recorded in a deep mine in Northern New Jersey. Bull. Seism. Soc. Am. 54, 1941-1979.

Ishimoto, M. and Iida, K. 1939. Observations sur les seismes enregistres par la microseismographe construit dernierement (1). Bull. Earthq. Res. Inst. 17, 443-478.

Iyer, H.M. and Hitchcock, T. 1974. Seismic noise measurements in Yellowstone National Park Geophys. 39, 4, 389-400.

Jagger, T.A. 1920. Seismometric investigations of the Hawaiian lava column. Bull. Seism. Soc. Am. 10, 204.

James, D.E., Sacks, I.S., Lanzol, E. and Aparicio, P.G. 1969. On locating local earthquakes using small networks. Bull. Seism. Soc. Am. 59, 1201-1212.

Jenkins, G.M. and Watts, D.G. 1969. Spectral analysis and its applications. Holden-Day, San Francisco.

Kanasewich, E.R. 1975. Time Sequence Analysis in Geophysics. The University of Alberta Press, Alberta.

Kieffer, G. 1969. Origine explosive de la Valle del Bove (Etna Sicilie). C.R. Acad. Sci. Paris, 269, 1938-1941.

Klerkx, J. 1968. Etude Geologique et petrologique del la Valle del Bove (Etna). Thesis. University de Liege.

Klerkx, J. and Evrard, P. 1970. Les anomalies gravimetriques del'Etna (Sicile) et l'evolution du Trifoglietto. Ann. Soc. Geol. Belg. 93, 145-147.

Koyanagi, R.Y. 1968. Earthquakes from common sources beneath Kilauea and Mauna Loa volcanoes in Hawaii from 1962-1965. U.S. Geol. Survey Prof. Paper 600-C, 120-125.

Koyanagi, R.Y. and Endo, E.T. 1965. Hawaii seismic events during 1963. U.S. Geol. Survey Prof. Paper 625-B, 13-16.

Kubota, S. and Berg, E. 1967. Evidence for magma in Katmai Volcanic Range. Bull. Volc. 31, 175-214.

Kubotera, A. 1974. Volcanic tremors at Aso volcano. Physical Volcanology. Edited by Civetta et al. Elsevier Sci. Pub. Co. Amsterdam, 29-47.

Kubotera, A. and Yosikawa, K. 1963. Prediction of volcanic eruption from Aso and Sakurazima and some related geophysical problems. Bull. Volc. 26, 297-317.

Lanczos, C. 1966. Discourse on Fourier series. University Mathematical Monographs, London.

Langenkamp, D.F. and Combs, J. 1974. Microearthquake study of the Elsinore fault zone, Southern California. Bull. Seism. Soc. Am. 64, 187-203.

Latter, J.H. 1966. The relationship between seismicity and volcanism in the Sicilian volcanoes. Proc. Geol. Soc. London, 1637, 58-59.

Latter, J.H. 1971. Near surface seismicity of Vulcano, Aeolian Islands, Sicily. Bull. Volc. 35, 117-126.

Lee, W.H., Bennet, R.E. and Meagher, K.L. 1972. A method of estimating the magnitude of local earthquakes from signal duration. U.S. Geol. Surv. Open file report.

Lo Bascio, A., Nappi, G. and Scarpa, R. 1976. Seismicity of Etna during November 1973. Boll. di Geofisica, 70, 92-97.

Matumoto, A. 1971. Seismic body waves observed in the vicinity of Mount Katmai, Alaska, and evidence for the existence of molten chambers. Geol. Soc. Am. Bull. 82, 2905-2920.

Matumoto, A. and Ward, P. 1967. Microearthquake study of Mt. Katmai and vicinity, Alaska. J. Geophys. Res. 72, 2557-2568.

Mauk, F.J. and Johnston, M.J.S. 1973. On triggering of volcanic eruptions by earth tides. J. Geophys. Res. 78, 3356-3362.

Mauk, F.J. and Kienle, J. 1973. Microearthquakes at St. Augustine Volcano, Alaska, triggered by earth tides. Science, 182, 386-389.

McKenzie, D.P. 1970. The plate tectonics of the Mediterranean region. Nature, 226, 239-245.

McKenzie, D.P. 1972. Active tectonics of the Mediterranean region. Geophys. J.R. Astr. Soc. 30, 109-185.

McDonald, G.A. 1972. Volcanoes, Prentice-Hall, New Jersey.

Minakami, T. 1960. Fundamental research for predicting volcanic eruptions. Bull. Earthq. Res. Inst. 38, 497-544.

Minakami, T. and Sakuma, S. 1953. Reports on volcanic activities and volcanological studies concerning them in Japan during 1948-1951. Bull. Volc. 14, 79-130.

Mogi, K. 1962. The magnitude frequency relation for elastic shocks accompanying fractures for various materials and some related problems in earthquakes. Bull. Earthq. Res. Inst. 40, 831-853.

Mogi, K. 1962a. The fracture of a semi-infinite body caused by an inner stress, origin and its relation to earthquake phenomenon. Bull. Earthq. Res. Inst. 40, 815-829.

Mogi, K. 1963. The fracture of semi-infinite body and its relation to the earthquake phenomenon. Bull. Earthq. Res. Inst. 41, 595-615.

Mogi, K. 1967. Regional variation in magnitude frequency relation of earthquakes. Bull. Earthq. Res. Inst. 45, 313-325.

Mohajer-Asjhai, A. 1975. Recent and contemporary crustal deformation in Eastern Iran. Ph.D. Thesis. University of London.

Moore, J.G. and Krivoy, H.L. 1964. The 1962 flank eruptions of Kilauea volcano and the structure of East Rift Zone. J. Geophys. Res. 69, 2033-2045.

Murray, J.B., Guest, J.E. and Butterworth 1977. A large ground deformation on Mount Etna Volcano. Nature, 266, 338-340.

Murray, J.B., Wright, M., Foster, J.H. and Baker, A. 1974. Map of summit area of Mount Etna in 1973.United Kingdom Research on Mount Etna. R. Soc. London.

Nicholls, H.R. and Rinehart, J.S. 1967. Geophysical studies of the geyser action in Yellowstone National Park. J. Geophys. Res. 72, 4651-4663.

Ninkovich, D. and Hays, J.D. 1972. Mediterranean island arcs and the origin of high potash volcanics. Earth Plan. Sci. Lett. 16, 331-345.

Nordquist, J.M. 1962. A special purpose program for earthquake location with an electronic computer. Bull. Seism. Soc. Am. 52, 431-437.

Ogniben, L. 1966. Lineamenti idrogeologici dell' Etna. Riv. Min. Sicil. 24, 100-102.

Oliver, J., Ryall, A., Brune, J.N. and Slemmons, D.B. 1966. Microearthquake activity recorded by portable seismographs of high sensitivity. Bull. Seism. Soc. Am. 56, 899-924.

Omer, G.C. 1950. Volcanic tremor. Bull. Seism. Soc. Am. 40, 175-194.

Omori, F. 1911-1918. The Usu-San eruption and the earthquakes and elevation phenomena. I, II. Bull. Imp. Earthq. Invest. Comm. 5, 1-38; 101-107.

Papoulis, A. 1962. The Fourier integral and its applications. McGraw-Hill Book Comp. Inc. New York.

Parasnis, D.S. 1972. Principles of applied Geophysics, Chapman & Hall Ltd. London.

Real, C.R. and Teng, T.L. 1974. Local Richter magnitude and total signal duration in Southern California. Bull. Seism. Soc. Am. 63, 1809-1827.

Richards, P.I. 1967. Computing reliable power spectra. IEEE Spectrum, 83-90.

Richter, C.F. 1935. An instrumental earthquake scale. Bull. Seism. Soc. Am. 25, 1-32.

Richter, C.F. 1958. Elementary Seismology. Freeman and Comp. San Francisco.

Rinehart, J.S. 1965. Earth tremors generated by Old Faithful Geyser. Science, 150, 494-496.

Ritsema, A.R. 1969. Seismic data of the Western Mediterranean and the problem of oceanization. Verhand. Kon. Ned. Geol. Mijn. XXVI, 105-120. (Symposium on the problem of oceanization in the Western Mediterranean).

Rittmann, A. 1962. Volcanoes and their activity. John Wiley & Sons, New York.

Rittmann, A. 1963. Vulcanismus und tektonick der Atna. Geol. Rund. 53, 788-800.

Rittmann, A. 1973. Structure and evolution of Mt. Etna. Phil. Trans. R. Soc. London, A. 274, 5-16.

Rittmann, A. 1975. (Personal Communication). Intern. Inst. Volc. Catania, Sicily.

Riuscetti, M. and Schick, R. and Seidl, D. 1977. Spectral parameters of volcanic tremors at Etna. J. Volc. Geoth. Res. 2, 289-298.

Robson, G.R., Barr, K.G. and Smith, G.W. 1962. Earthquake series in St. Kitts-Nevis, 1961-1962. Nature, 195, 972-974.

Romano, R. 1970. Tectonic control on magmatic differentiation; an example. Bull. Volc. 34, 823-832.

Sakuma, S. 1957. Volcanic tremor at eruption of Meakandake. J. Fac. Sci. Hokkaido Univ. 7, I(1).

Sassa, K. 1936. Micro-seismometric study on eruptions of volcano Aso. Mem. Coll. Sci. Kyoto Univ. 19, 11-56.

Schick, R. and Riuscetti, M. 1973. An analysis of volcanic tremors at South Italian volcanoes. Zeitschrift für Geophys. 39, 247-262.

Scholz, C.H. 1968. Micro-fracturing and the inelastic deformation of rock in compression. J. Geophys. Res. 73, 1417-1432.

Scholz, C.H. 1968a. The frequency magnitude relation of micro-faulting in rock and its relation to earthquakes. Bull. Seism. Soc. Am. 58, 399-415.

Shimozuru, D. 1971. A seismological approach to the prediction of volcanic eruption. UNESCO, Earth Sci. Mono. 8, Paris, 19-45.

Shimozuru, D. 1971a. Geophysical evidences for suggesting the existence of molten pockets in the earth's upper mantle. Geol. Soc. Am. Bull. 82, 181-195.

Shimozuru, D., Miyazaki, T., Gyoda, N. and Matahelumual, J. 1969. Volcanological survey of Indonesian volcanoes. Bull. Earthq. Res. Inst. 47, 969-990.

Stacy, F.D. 1969. Physics of the earth. John Wiley & Sons Inc. New York.

Steeples, D.W. and Iyer, H.M. 1975. Teleseismic P wave delays in geothermal exploration. Second UN Symposium on the Development and Use of Geothermal Resources, San Francisco. Proceedings 2, 1199-1206.

Steinberg, G.S. and Steinberg, A.S. 1975. On possible causes of volcanic tremor. J. Geophys. Res. 80, 1600-1604.

Suzuki, Z. 1953. A statistical study on the occurrence of small earthquakes. I. Sc. Rep. Tohuku Univ. 5, 177-182.

Suzuki, Z. 1954. A statistical study on the occurrence of small earthquakes. II. Sc. Rep. Tohoku Univ. 6, 105-118.

Suzuki, Z. 1958. A statistical study on the occurrence of small earthquakes. III. Sc. Rep. Tohoku Univ. 10, 15-27.

Suzuki, Z. 1959. A statistical study on the occurrence of small earthquakes. IV. Sc. Rep. Tohoku Univ. 11, 10-54.

Sykes, N.R. 1970. Earthquake swarms and sea-floor spreading. J. Geophys. Res. 75, 6598-6611.

Tsumura, K. 1967. Determination of earthquake magnitude from total duration of oscillation. Bull. Earth. Res. Inst. 15, 7-18.

Tazieff, H. 1971. A dynamic approach to the problem of forecasting volcanic paroxysms. UNESCO, Earth Sci. Mon. 8, Paris, 127-130.

Unger, J. 1969. The microearthquake activity of Mt. Rainier, Washington. Ph.D. Thesis. Dartmouth College.

Wadge, G. 1974. Volcanic deformation and the eruptive mechanisms of Mt. Etna. Ph.D. Thesis. London University.

Ward, P.L., Palmason, G. and Drake, C. 1969. Microearthquake survey of the mid-Atlantic ridge in Iceland. J. Geophys. Res. 74, 665-685.

Westhusing, J.K. 1974. Reconnaissance surveys of near-event seismic activity in the volcanoes of the Cascade Range, Oregon. Bull. Volc. 37, 258-286.

Westphal, W.H. and Lange, A.L. 1967. Local seismic monitoring - Fairview Peak Area, Nevada. Bull. Seism. Soc. Am. 57, 1279-1298.

Wilcoxson, K. 1967. Volcanoes. Cassell & Comp. Ltd. London.

Wood, R. 1974. Microearthquakes at Central American volcanoes. Bull. Seism. Soc. Am. 64, 275-277.

Yokoyama, I. 1963. Structure of caldera and gravity anomaly. Bull. Volc. 26, 67-72.

APPENDIX 2A

POWER DENSITY ESTIMATES FOR VOLCANIC TREMOR
STATION : SERRA LA NAVE

SAMPLING INTERVAL = 0.02 SEC BANDWIDTH = 0.58 HZ
TOTAL POWER UNDER ANY CURVE ≅ 1

TIME (GMT) D/HR/MIN & CURVE NO.	FREQUENCY INTERVAL (HZ)	FRACTION OF TOTAL POWER V N - S E - W
44 13 59 (1)	0.00 - 0.58	0.002 - 0.017
	0.59 - 1.17	0.021 - 0.109
	1.18 - 1.76	0.255 - 0.288
	1.77 - 2.35	0.233 - 0.203
	2.36 - 2.94	0.183 - 0.182
	2.95 - 3.53	0.093 - 0.078
	3.54 - 4.12	0.081 - 0.036
	4.13 - 4.71	0.065 - 0.033
	4.72 - 5.30	0.051 - 0.020
	5.31 - 5.89	0.029 - 0.018
44 14 59 (2)	0.00 - 0.58	0.001 - 0.023
	0.59 - 1.17	0.045 - 0.161
	1.18 - 1.76	0.294 - 0.330
	1.77 - 2.35	0.292 - 0.255
	2.36 - 2.94	0.114 - 0.101
	2.95 - 3.53	0.074 - 0.056
	3.54 - 4.12	0.078 - 0.031
	4.13 - 4.71	0.040 - 0.021
	4.72 - 5.30	0.028 - 0.019
	5.31 - 5.89	0.017 - 0.016
44 16 59 (3)	0.00 - 0.58	0.001 - 0.018
	0.59 - 1.17	0.030 - 0.123
	1.18 - 1.76	0.294 - 0.357
	1.77 - 2.35	0.263 - 0.188
	2.36 - 2.94	0.141 - 0.143
	2.95 - 3.53	0.073 - 0.047
	3.54 - 4.12	0.076 - 0.033
	4.13 - 4.71	0.053 - 0.022
	4.72 - 5.30	0.035 - 0.017
	5.31 - 5.89	0.018 - 0.018
44 17 59 (4)	0.00 - 0.58	0.004 - 0.024
	0.59 - 1.17	0.033 - 0.152
	1.18 - 1.76	0.299 - 0.310
	1.77 - 2.35	0.228 - 0.198
	2.36 - 2.94	0.181 - 0.161
	2.95 - 3.53	0.081 - 0.047
	3.54 - 4.12	0.087 - 0.029
	4.13 - 4.71	0.060 - 0.025
	4.72 - 5.30	0.055 - 0.021
	5.31 - 5.89	0.024 - 0.017

44 18 59 (5)	0.00 - 0.58	0.002	-	0.168
	0.59 - 1.17	0.026	-	0.153
	1.18 - 1.76	0.256	-	0.326
	1.77 - 2.35	0.298	-	0.231
	2.36 - 2.94	0.153	-	0.130
	2.95 - 3.53	0.086	-	0.048
	3.54 - 4.12	0.065	-	0.030
	4.13 - 4.71	0.047	-	0.020
	4.72 - 5.30	0.032	-	0.020
	5.31 - 5.89	0.020	-	0.018
44 19 59 (6)	0.00 - 0.58	0.002	-	0.021
	0.59 - 1.17	0.079	-	0.206
	1.18 - 1.76	0.325	-	0.346
	1.77 - 2.35	0.261	-	0.225
	2.36 - 2.94	0.133	-	0.072
	2.95 - 3.53	0.068	-	0.041
	3.54 - 4.12	0.052	-	0.030
	4.13 - 4.71	0.033	-	0.021
	4.72 - 5.30	0.029	-	0.155
	5.31 - 5.89	0.012	-	0.012
44 21 59 (7)	0.00 - 0.58	0.002	-	0.020
	0.59 - 1.17	0.089	-	0.207
	1.18 - 1.76	0.319	-	0.364
	1.77 - 2.35	0.258	-	0.211
	2.36 - 2.94	0.132	-	0.071
	2.95 - 3.53	0.064	-	0.038
	3.54 - 4.12	0.054	-	0.029
	4.13 - 4.71	0.035	-	0.017
	4.72 - 5.30	0.028	-	0.016
	5.31 - 5.89	0.011	-	0.013
44 22 59 (8)	0.00 - 0.58	0.002	-	0.018
	0.59 - 1.17	0.054	-	0.191
	1.18 - 1.76	0.288	-	0.355
	1.77 - 2.35	0.242	-	0.221
	2.36 - 2.94	0.162	-	0.113
	2.95 - 3.53	0.088	-	0.038
	3.54 - 4.12	0.060	-	0.024
	4.13 - 4.71	0.037	-	0.018
	4.72 - 5.30	0.040	-	0.018
	5.31 - 5.89	0.017	-	0.013
44 23 59 (9)	0.00 - 0.58	0.002	-	0.023
	0.59 - 1.17	0.065	-	0.219
	1.18 - 1.76	0.288	-	0.364
	1.77 - 2.35	0.205	-	0.162
	2.36 - 2.94	0.145	-	0.091
	2.95 - 3.53	0.095	-	0.039
	3.54 - 4.12	0.063	-	0.032
	4.13 - 4.71	0.043	-	0.021
	4.72 - 5.30	0.044	-	0.020
	5.31 - 5.89	0.013	-	0.016

APPENDIX 2B

POWER DENSITY ESTIMATES FOR VOLCANIC TREMOR
STATION : IC BENCH MARK

SAMPLING INTERVAL = 0.02 SEC BANDWIDTH = 0.58 HZ
TOTAL POWER UNDER ANY CURVE = 1

TIME (GMT) D/HR/MIN & CURVE NO. C	FREQUENCY INTERVAL (HZ)	FRACTION OF TOTAL POWER V	N-S	E-W
43 23 59 (1)	0.00 - 0.58	-	0.044	-
	0.59 - 1.17	-	0.049	-
	1.18 - 1.76	-	0.091	-
	1.77 - 2.35	-	0.237	-
	2.36 - 2.94	-	0.297	-
	2.95 - 3.53	-	0.161	-
	3.54 - 4.12	-	0.058	
	4.13 - 4.71	-	0.044	-
	4.72 - 5.30	-	0.040	-
	5.31 - 5.89	-	0.048	-
44 01 59 (2)	0.00 - 0.58	0.006	0.013	0.018
	0.59 - 1.77	0.015	0.019	0.073
	1.18 - 1.76	0.117	0.080	0.188
	1.77 - 2.35	0.168	0.280	0.216
	2.36 - 2.94	0.258	0.312	0.207
	2.95 - 3.53	0.120	0.122	0.123
	3.54 - 4.12	0.151	0.059	0.076
	4.13 - 4.71	0.050	0.054	0.041
	4.72 - 5.30	0.048	0.033	0.022
	5.31 - 5.89	0.038	0.030	0.019
44 07 59 (3)	0.00 - 0.58	0.005	0.012	0.012
	0.59 - 1.17	0.016	0.028	0.079
	1.18 - 1.76	0.106	0.121	0.142
	1.77 - 2.35	0.161	0.254	0.188
	2.36 - 2.94	0.227	0.254	0.206
	2.95 - 3.53	0.167	0.138	0.156
	3.54 - 4.12	0.153	0.076	0.089
	4.13 - 4.71	0.052	0.050	0.050
	4.72 - 5.30	0.058	0.029	0.032
	5.31 - 5.89	0.042	0.018	0.022
44 09 59 (4)	0.00 - 0.58	0.006	0.015	0.024
	0.59 - 1.17	0.017	0.050	0.089
	1.18 - 1.76	0.125	0.160	0.171
	1.77 - 2.35	0.182	0.288	0.207
	2.36 - 2.94	0.229	0.228	0.209
	2.95 - 3.53	0.138	0.101	0.130
	3.54 - 4.12	0.147	0.052	0.061
	4.13 - 4.71	0.058	0.038	0.036
	4.72 - 5.30	0.037	0.027	0.029
	5.31 - 5.89	0.034	0.026	0.025

44 13 59	0.00 - 0.58	0.016	-	0.007
(5)	0.59 - 1.17	0.068	-	0.016
	1.18 - 1.76	0.141	-	0.110
	1.77 - 2.35	0.294	-	0.257
	2.36 - 2.94	0.170		0.230
	2.95 - 3.53	0.132	-	0.121
	3.54 - 4.12	0.100	-	0.112
	4.13 - 4.71	0.045	-	0.082
	4.72 - 5.30	0.033	-	0.052
	5.31 - 5.89	0.028	-	0.046
44 15 59	0.00 - 0.58	0.014	0.010	0.014
(6)	0.59 - 1.17	0.114	0.035	0.117
	1.18 - 1.76	0.200	0.133	0.200
	1.77 - 2.35	0.224	0.310	0.224
	2.36 - 2.94	0.144	0.211	0.144
	2.95 - 3.53	0.120	0.121	0.120
	3.54 - 4.12	0.080	0.078	0.086
	4.13 - 4.71	0.040	0.041	0.040
	4.72 - 5.30	0.021	0.032	0.021
	5.31 - 5.89	0.020	0.022	0.020
44 19 59	0.00 - 0.58	0.006	0.014	0.017
(7)	0.59 - 1.17	0.026	0.041	0.101
	1.18 - 1.76	0.129	0.114	0.180
	1.77 - 2.35	0.193	0.314	0.206
	2.36 - 2.94	0.253	0.197	0.170
	2.95 - 3.53	0.124	0.114	0.141
	3.54 - 4.12	0.101	0.061	0.094
	4.13 - 4.71	0.059	0.041	0.044
	4.72 - 5.30	0.035	0.023	0.029
	5.31 - 5.89	0.046	0.029	0.030
44 21 59	0.00 - 0.58	0.008	0.013	0.017
(8)	0.59 - 1.17	0.029	0.042	0.102
	1.18 - 1.76	0.126	0.151	0.218
	1.77 - 2.35	0.233	0.252	0.177
	2.36 - 2.94	0.224	0.176	0.139
	2.95 - 3.53	0.105	0.141	0.123
	3.54 - 4.12	0.083	0.065	0.086
	4.13 - 4.71	0.052	0.035	0.032
	4.72 - 5.30	0.036	0.034	0.021
	5.31 - 5.97	0.029	0.021	0.016
44 23 59	0.00 - 0.58	0.005	0.017	0.019
(9)	0.59 - 1.17	0.024	0.039	0.151
	1.18 - 1.76	0.130	0.130	0.184
	1.77 - 2.35	0.194	0.315	0.233
	2.36 - 2.94	0.189	0.192	0.139
	2.95 - 3.53	0.130	0.092	0.103
	3.54 - 4.12	0.121	0.096	0.063
	4.13 - 4.71	0.081	0.047	0.045
	4.72 - 5.30	0.041	0.033	0.028
	5.31 - 5.89	0.041	0.024	0.024

APPENDIX 2C

POWER DENSITY ESTIMATES FOR VOLCANIC TREMOR
STATION : FORESTALE HUT

SAMPLING INTERVAL = 0.02 SEC BANDWIDTH = 0.59 Hz
TOTAL POWER UNDER ANY CURVE = 1

TIME (GMT) D/HR/MIN & CURVE NO C	FREQUENCY INTERVAL (HZ)	FRACTION OF TOTAL POWER V	N-S	L-U
49 10 00 (1)	0.00 - 0.58	-	0.012	-
	0.59 - 1.17	-	0.039	-
	1.18 - 1.76	-	0.149	-
	1.77 - 2.35	-	0.311	-
	2.36 - 2.94	-	0.193	-
	2.95 - 3.53	-	0.118	-
	3.54 - 4.12	-	0.075	-
	4.13 - 4.71	-	0.043	-
	4.72 - 5.30	-	0.032	-
	5.31 - 5.89	-	0.025	-

APPENDIX 2D

POWER DENSITY ESTIMATES FOR VOLCANIC TREMOR
STATION : MONTE S. MARIA

SAMPLING INTERVAL = 0.02 SEC BANDWIDTH = 0.56 HZ
TOTAL POWER UNDER ANY CURVE ≃ 1

TIME (GMT) D/HR/MIN & CURVE NO	FREQUENCY INTERVAL (HZ)	FRACTION OF TOTAL POWER V	N-S	E-W
43 23 59 (1)	0.00 - 0.58	0.003	0.003	0.004
	0.59 - 1.17	0.018	0.021	0.011
	1.18 - 1.76	0.086	0.131	0.104
	1.77 - 2.35	0.267	0.363	0.317
	2.36 - 2.94	0.385	0.246	0.310
	2.95 - 3.53	0.139	0.108	0.124
	3.54 - 4.12	0.053	0.063	0.065
	4.13 - 4.71	0.022	0.031	0.028
	4.72 - 5.30	0.093	0.017	0.016
	5.31 - 5.89	0.006	0.012	0.014
44 01 59 (2)	0.00 - 0.58	0.001	0.004	0.004
	0.59 - 1.17	0.011	0.015	0.010
	1.18 - 1.76	0.092	0.156	0.149
	1.77 - 2.35	0.324	0.299	0.268
	2.36 - 2.94	0.294	0.222	0.287
	2.95 - 3.53	0.142	0.119	0.143
	3.54 - 4.12	0.068	0.069	0.060
	4.13 - 4.71	0.037	0.031	0.030
	4.72 - 5.30	0.012	0.016	0.015
	5.31 - 5.89	0.007	0.013	0.016
44 03 59 (3)	0.00 - 0.58	0.002	0.004	0.003
	0.59 - 1.17	0.019	0.020	0.016
	1.18 - 1.76	0.094	0.142	0.184
	1.77 - 2.35	0.379	0.368	0.306
	2.36 - 2.94	0.241	0.204	0.213
	2.95 - 3.53	0.142	0.122	0.121
	3.54 - 4.12	0.063	0.067	0.066
	4.13 - 4.71	0.030	0.034	0.036
	4.72 - 5.30	0.017	0.016	0.019
	5.31 - 5.89	0.001	0.014	0.019
44 05 59 (4)	0.00 - 0.58	0.002	0.002	0.003
	0.59 - 1.17	0.015	0.017	0.013
	1.18 - 1.76	0.110	0.115	0.098
	1.77 - 2.35	0.280	0.389	0.278
	2.36 - 2.94	0.288	0.191	0.223
	2.95 - 3.53	0.170	0.133	0.136
	3.54 - 4.12	0.072	0.078	0.075
	4.13 - 4.71	0.034	0.034	0.043
	4.72 - 5.30	0.015	0.019	0.022
	5.31 - 5.89	0.009	0.014	0.021

44 13 59 (5)	0.00 - 0.58	0.005	0.004	0.004
	0.59 - 1.17	0.013	0.019	0.017
	1.18 - 1.76	0.108	0.212	0.193
	1.77 - 2.35	0.362	0.276	0.249
	2.36 - 2.94	0.292	0.177	0.213
	2.95 - 3.53	0.173	0.133	0.139
	3.54 - 4.12	0.069	0.077	0.069
	4.13 - 4.71	0.043	0.038	0.055
	4.72 - 5.30	0.017	0.022	0.032
	5.31 - 5.89	0.011	0.015	0.022
44 15 59 (6)	0.00 - 0.58	0.008	0.003	0.002
	0.59 - 1.17	0.016	0.020	0.016
	1.18 - 1.76	0.128	0.211	0.215
	1.77 - 2.35	0.330	0.390	0.293
	2.36 - 2.94	0.267	0.169	0.219
	2.95 - 3.53	0.143	0.094	0.113
	3.54 - 4.12	0.052	0.060	0.062
	4.13 - 4.71	0.026	0.027	0.036
	4.72 - 5.30	0.011	0.012	0.019
	5.31 - 5.89	0.007	0.008	0.015
44 23 59 (7)	0.00 - 0.58	0.005	0.015	0.002
	0.59 - 1.17	0.021	0.017	0.027
	1.18 - 1.76	0.139	0.051	0.122
	1.77 - 2.35	0.360	0.227	0.380
	2.36 - 2.94	0.221	0.215	0.236
	2.95 - 3.53	0.126	0.184	0.133
	3.54 - 4.12	0.049	0.092	0.045
	4.13 - 4.71	0.030	0.073	0.027
	4.72 - 5.30	0.017	0.058	0.016
	5.31 - 5.89	0.016	0.037	0.009

APPENDIX 3A

POWER DENSITY ESTIMATES FOR A-TYPE MICROEARTHQUAKE

SAMPLING INTERVAL = 0.01 SEC BANDWIDTH = 0.23 HZ
TOTAL POWER UNDER ANY CURVE = 1

FREQUENCY INTERVAL (HZ)	MEQ 1 (5.19A)	MEQ 2 (5.19B)	MEQ 3 (5.20A)	MEQ 4 (5.20B)	MEQ 5 (5.21)	MEQ 6 (5.22)
0.00-0.70	0.004	0.005	0.005	0.010	0.008	0.011
0.71-1.41	0.021	0.015	0.031	0.031	0.036	0.017
1.42-2.12	0.172	0.122	0.155	0.155	0.182	0.066
2.13-2.83	0.190	0.171	0.210	0.225	0.167	0.139
2.84-3.54	0.174	0.140	0.146	0.142	0.097	0.149
3.55-4.25	0.148	0.196	0.147	0.177	0.163	0.112
4.26-4.96	0.071	0.080	0.065	0.070	0.111	0.081
4.97-5.67	0.034	0.044	0.058	0.040	0.087	0.089
5.68-6.38	0.033	0.043	0.040	0.038	0.034	0.031
6.39-7.09	0.028	0.032	0.027	0.020	0.063	0.043
7.10-7.80	0.027	0.028	0.026	0.017	0.026	0.055
7.81-8.51	0.016	0.029	0.022	0.013	0.017	0.055
8.52-9.22	0.011	0.025	0.020	0.014	0.003	0.004
9.23-9.93	0.009	0.020	0.018	0.011	0.008	0.018
9.94-10.64	0.007	0.018	0.015	0.009	0.006	0.015
10.65-11.35	0.005	0.014	0.013	0.007	0.007	0.020
11.36-12.06	0.004	0.012	0.011	0.005	0.009	0.012
12.07-12.77	0.001	0.009	0.007	0.005	0.008	0.009

APPENDIX 3B

POWER DENSITY ESTIMATES FOR S-TYPE MICROEARTHQUAKE

SAMPLING INTERVAL = 0.01 SEC BANDWIDTH = 0.23 HZ
TOTAL POWER UNDER ANY CURVE = 1

FREQUENCY INTERVAL (HZ)	MEQ 1 (5.23A)	MEQ 2 (5.23B)	MEQ 3 (5.24A)	MEQ 4 (5.24B)	MEQ 5 (5.25)	MEQ 6 (5.26A)	MEQ 7 (5.26B)
0.00-0.70	0.002	0.002	0.004	0.009	0.003	0.003	0.003
0.71-1.41	0.114	0.093	0.057	0.073	0.068	0.045	0.088
1.42-2.12	0.406	0.432	0.368	0.419	0.323	0.297	0.333
2.13-2.83	0.173	0.158	0.192	0.216	0.182	0.277	0.177
2.84-3.54	0.067	0.084	0.102	0.130	0.135	0.103	0.109
3.55-4.25	0.077	0.062	0.085	0.061	0.120	0.091	0.144
4.26-4.96	0.039	0.057	0.056	0.049	0.063	0.061	0.053
4.97-5.67	0.043	0.039	0.038	0.023	0.034	0.044	0.040
5.68-6.38	0.023	0.018	0.024	0.009	0.022	0.032	0.020
6.39-7.09	0.014	0.006	0.013	0.006	0.015	0.013	0.023
7.10-7.80	0.011	0.007	0.011	0.005	0.011	0.017	0.010
7.81-8.51	0.005	0.008	0.011	0.005	0.007	0.018	0.006